ICRR
Institute for Cosmic Ray Research
University of Tokyo

Scientific Activities

Institute for Cosmic Ray Research, The University of Tokyo

Report to the Review Committee

14 May 2025

CONTENTS

OVERVIEW 1

NEUTRINO AND ASTROPARTICLE DIVISION 8

Super-Kamiokande
T2K Experiment
XMASS / XENON Experiments
Hyper-Kamiokande Experiment

HIGH ENERGY COSMIC RAY DIVISION 53

CTAO: Cherenkov Telescope Array
TA: Telescope Array Observatory
Tibet AS γ Project
ALPACA
High Energy Astrophysics Group

ASTROPHYSICS AND GRAVITY DIVISION 105

KAGRA Group
Observational Cosmology Group
Theory Group

FACILITIES 141

KAMIOKA Observatory
KAGRA Observatory
High Energy Astrophysics facility in Canarias
Research Center for Cosmic Neutrinos
NORIKURA Observatory
AKENO Observatory
Low-Level Radioisotope Measurement Facility

APPENDIX 162

A.1: Organization
A.2: ICRR Staff (2024)
A.3: Budget (FY2018-2023)
B.1: Agreements of International Academic Cooperation
B.2: International Meetings
B.3: Inter-University Collaborative Researches
B.4: Educational Activities
B.5: Public Relations

OVERVIEW

The Institute for Cosmic Ray Research (ICRR) has its origin at a lodge for research, called Asahi Hut, built on Mt. Norikura based on Asahi Academic Grant. In 1953, it was established as the Cosmic Ray Observatory of the University of Tokyo. This Observatory was Japan's first research facility for nationwide joint use. In 1976, the Cosmic Ray Observatory was reorganized into the Institute for Cosmic Ray Research (ICRR) of the University of Tokyo. Since the era of Cosmic Ray Observatory, ICRR has been functioning as "Inter University Research Institution", where researchers in Japan in the field of cosmic rays carry out diverse researches using various facilities in ICRR.

In 2004, the Japanese National Universities, including the University of Tokyo, became independent administrative agencies (National University Corporations). The concept was to strengthen the Universities through mutual competition. At that time, the concept of "independent administrative agencies" and "Inter University Research Institution" did not go along well.

This problem was recognized by the Ministry of Education, Culture, Sports, Science and Technology (MEXT) in Japan. A new system, called "Joint Usage / Research Center", was established. ICRR was selected as one of these Centers in 2010. Since then, ICRR's research style as "Inter University Research Institution" has been officially re-recognized by the Japanese government.

In 2018 MEXT established "International Joint Usage / Research Center" which can play a central role in international research activity and promote world-class research. ICRR was selected as one of the six International Joint Usage / Research Centers.

The external review panel of ICRR has been organized approximately every six years since 1994, the last one having been held on 15-17 May, 2019. This report provides the material prepared for the External Review Panel to be held on 14-16 May, 2025 to examine the research activity of the ICRR. The prime purposes of the present Review are:

(1) to give oversight to the institute's scientific activities between 2018 and 2024, whether they meet the international scientific standard and have given sufficient impacts on the community,

(2) to assess the scientific merits of individual research activities and make recommendations about future support,

(3) to assess the technical competence of the proponents and the feasibility of the R&D experiments or projects,

(4) to assess the Institute's policy and its role in the scientific community.

At present, ICRR consists of 27 faculties, 1 project professor[1], 1 project associate professor[2], 19 assistant professors, 12 project assistant professors[3], 18 post-doctoral fellows and 22 supporting technical staff, and consists of three divisions — Neutrino and Astroparticle Division, High-Energy Cosmic Ray Division, and Astrophysics & Gravity Division. They are further subdivided into thirteen research groups. Most of the activities receive participation by other university members that partially offset small numbers of staff of the ICRR. Most of the faculties are counted as members of the Faculty of Science of the Graduate School and are engaged in the teaching of graduate students of this university, jointly with those who belong to the Department of Physics in the Hongo campus.

ICRR runs 10 facilities (6 domestic and 4 overseas) to perform its research projects. The overseas facilities are operated jointly in collaboration with academic institutions of respective countries under memoranda of understanding. The Institute also supports, directly or indirectly, some of cosmic-ray-related research activities of research scientists in this country. More information as to the structure of ICRR is given in Appendix A.1.

Divisions

Neutrino and Astroparticle Division

This division is focused on particle and astroparticle physics with primary interests in the physics of neutrinos, proton decay, and dark matter using underground experimental detectors at Kamioka Observatory. The primary detector is the Super-Kamiokande (SK), which is a 50,000-ton water Cherenkov detector that studies neutrino physics and proton decay. The Tokai-to-Kamioka (T2K) long-baseline neutrino experiment is also a focus project of this division. A liquid xenon detector (XMASS) had been operated with the aim of direct detection of dark-matter interactions, and the project was completed in 2023. Some of the XMASS members joined the XENON and XLZD collaborations and have continued their research activity. The construction of a larger water Cherenkov detector, Hyper-Kamiokande (HK), started with the approval of the first-year construction budget by the Japanese Diet and is ongoing toward its completion in 2027.

High Energy Cosmic Ray Division

This division is devoted to the study of astroparticle physics with very high-energy cosmic rays and cosmic gamma rays, consisting of four major research activities, TA, Tibet ASγ, ALPACA, and CTAO, with one theoretical group.

The Telescope Array (TA) Collaboration operates TA, TA Low-Energy extension (TALE) including TALE infill, and TAx4 in the Northern Hemisphere (Utah in the USA). The experiment consists of air shower arrays of plastic scintillator

[*1] fixed-term professor
[*2] fixed-term associate professor
[*3] fixed-term assistant professors

surface detectors and fluorescence telescopes to measure the energy spectrum, mass composition, and arrival direction distributions of cosmic rays with energies from 10^{15} to over 10^{20} eV, and explore their origin and nature.

The Tibet ASγ Collaboration operates a surface air shower array of scintillation detectors, underground water Cherenkov muon detectors and air shower core detectors at high altitude (4300m) in Yangbajing, Tibet, China realizing high statistics studies of cosmic rays with energies $10^{12} - 10^{17}$ eV sensitive for both charged cosmic rays and gamma rays in the northern sky.

ALPACA is a joint research project between Bolivia, Mexico, and Japan to construct a surface air shower array and underground water Cherenkov muon detectors at high altitudes in Bolivia. A partial surface air shower array started operation in 2023.

CTAO is an international project to construct the next-generation large-scale imaging atmospheric Cherenkov Telescope Array Observatory to explore the high-energy Universe with an order of magnitude better sensitivity, higher angular resolution, and wider energy coverage. CTAO-Japan is leading the construction of four large-size telescopes (LSTs) in La Palma, Spain.

A theoretical group, High Energy Astrophysics group, aims at revealing violent astrophysical phenomena, in which non-thermal particles are accelerated. The group promotes the theoretical study on multi-messenger astronomy.

Astrophysics and Gravity Division

This division consists of the KAGRA Group, the Observational Cosmology Group, and the Theory Group.

KAGRA aims to conduct gravitational wave physics and astrophysics through the observation of gravitational waves. KAGRA performed its first international joint observation with GEO600 in 2020. In May-June 2024, KAGRA performed an observing run during the LVK's 4th Observing run.

The Observational Cosmology Group is conducting an optical sky survey with prime interests in cosmology and extragalactic astrophysics. The group participates in the Subaru Hyper Suprime-Cam (HSC) and Prime Focus Spectrograph (PFS) surveys in parallel with leading various observational projects with James Webb Space Telescope.

The Theory group is making theoretical studies on phenomenology-oriented particle physics, astro/cosmoparticle physics and cosmology.

Facilities

ICRR has four domestic observatories, one center, one facility, and three overseas observatories, and one facility. These facilities are all open to researchers, and the use will be admitted after a proper review process.

Domestic

- Kamioka Observatory.

  This observatory is located 1000 m underground (2700 m.w.e.) in the Kamiokande Moumi Mine, Gifu prefecture. The SK water Cherenkov detector is located in this observatory. The observatory offers a well-developed and maintained, low vibration and low radioactivity environment. Therefore, it is used by a number of research groups both inside and outside ICRR, including the CANDLES double beta decay experiment led by Osaka University, the NEWAGE dark matter experiment led by Kobe University, and a cryogenic test experiment for gravitational wave detection (CLIO: Cryogenic Laser Interferometer Gravitational Wave Observatory) run by ICRR, seismic and geophysical experiments performed by the Earthquake Research Institute of the University of Tokyo, as well as the AXEL double beta decay experiment led by Tohoku University, and others. It was used for the XMASS experiment as well.

  The observatory will expand its experimental space in the Tochibora Mine (600-meter depth), 8 km south of the Kamioka Mozumi Mine for HK after the completion of the water tank construction.

- Akeno Observatory.

  The Akeno Observatory is located in Akeno of Hokuto in Yamanashi Prefecture. It was used for a giant-air-shower-array experiment, AGASA. Now it is used for small-scale observations, research and development including the multicolor imager (MITSuME) led by Tokyo Institute of Technology, large area muon telescope by Chubu University et al. and a small atmospheric Cherenkov telescope by ICRR et al. It is also used occasionally for detector assembly including the surface detectors of the Telescope Array extension.

- Norikura Observatory (at 2770m altitude).

  This observatory, located close to the summit of Mt. Norikura, was historically a very important station of ICRR. This is now used for long-term monitors of cosmic ray muons and solar neutrons, mainly by teams from Shinshu University and from Chubu University. It is occasionally used for various types of research (not necessarily cosmic ray proper) that require the high altitude environment, as it now offers a unique high altitude facility in Japan.

- KAGRA Observatory.

  KAGRA observatory was established in 2016 for the operation of the large-scale cryogenic gravitational wave telescope, KAGRA, and the research of gravitational wave physics and astronomy. It is located in Kamioka, Hida City, Gifu prefecture.

- Research Center for Cosmic Neutrinos.

  This was established in 1999 primarily to promote research of neutrino physics. This center has been organizing neutrino meetings and neutrino public lectures. It also acts as a body for accepting ICRR's inter-university programs related to Low-Level Radioisotope Measurement Facility and is in charge of the computer system of the institute.

- Low-Level Radioisotope Measurement Facility.

This is located underground in the Kashiwa building and is used for measurements of the concentration of natural radioisotope by interested researchers in the country.

Overseas

ICRR operates three overseas observatories and one facility, which play central roles in carrying out its research projects, jointly with various academic institutions in respective countries:

- The Tibet ASγ Observatory, Yangbajing, Tibet, China
- Observatory for Highest Energy Cosmic Rays, Utah, U. S. A.
- Chacaltaya Observatory of Cosmic Physics, Mt. Chacaltaya, Bolivia
- High Energy Astrophysics Facility in Canarias.

  This facility was established on April 1, 2019, in La Palma, Canary Islands, Spain. It is an actual base of international collaborations on CTAO (Cherenkov Telescope Array Observatory) project co-hosted by the CTAO group of ICRR.

Historical Remarks and Funding Sources

Brief histories are described for each group, including the financial viewpoint. In general, there are two channels for funding: the use of Grants-in-Aid from the Japan Society for the Promotion of Science (JSPS) by individual scientists, and the fund from the government revenue directly to the Institute through the University finance. The former applies to short-term projects, say for 5 years with no guarantees beyond, and the latter to long-term projects that usually cost more than that defrayed by the former. The square parentheses indicate the present institute's personnel of each group. The current status and scientific goals of the projects are summarized in the table.

- Super-Kamiokande

  The detector was constructed from 1991 to 1996, and data acquisition began in April 1996. Construction and operation costs are covered by funds provided by the government. Super-Kamiokande discovered atmospheric neutrino oscillations in 1998 and solar neutrino oscillations in 2001. The K2K (KEK to Kamioka) long-baseline accelerator experiment, operated from 1999 to 2004, confirmed the existence of atmospheric neutrino oscillations. Since full reconstruction work was performed in 2005 and 2006, the detector has been running stably, and high-precision oscillation studies have been performed. The readout electronics and online data acquisition system were updated in 2008 to ensure stable operations over the long term. The detector was refurbished in 2018 to prepare for gadolinium (Gd) loading. In 2020 and 2022, progressive Gd loading steps were taken up to 0.01% and 0.03% Gd concentrations, respectively. [9 faculties + 1 project associate professor + 7 assistant professors + 7 project assistant professors + 1 project academic specialist + 3 postdoctoral fellows]

- T2K

  The Tokai-to-Kamioka (T2K) long-baseline accelerator neutrino experiment started in 2009. The SK detector functions as the far detector of the T2K experiment and ICRR is responsible for operating the far detector. Host institutes of the T2K experiment are KEK and ICRR. Based on data taken up until March 2011, the T2K collaboration announced an indication of electron neutrino appearance, and therefore non-zero θ_{13}, with a statistical significance of 2.5σ in June 2011. After the recovery of the J-PARC accelerator site from damage sustained in the earthquake, the T2K experiment resumed operations in March 2012. The observed number of electron neutrino candidates is now 117 while the observed number of the anti-electron neutrino candidate is 16. The expected numbers of the electron neutrino and anti-electron neutrinos without CP violation are 104 and 20 and thus, they found a larger number of the electron neutrino candidates but a smaller number of the electron anti-neutrino candidates. As a result, they excluded some parameter space of δ_{CP} at more than 3σ and the CP conserving points at 90% C.L. level. Regarding the mass hierarchy, the data prefers normal ordering and upper θ_{23} octant. The first joint analysis of Super-Kamiokande atmospheric and T2K accelerator neutrino data was conducted and the CP-conserving value ($J_{CP} = 0$) was excluded at a 1.9 to 2.0σ level. [9 faculties + 1 project associate professor + 7 assistant professors + 3 project assistant professors + 1 project academic specialist + 3 postdoctoral fellows]

- XMASS/XENON

  The XMASS project started in 2000 and after its R&D study, the XMASS-I detector construction started in 2007. It was completed in 2010 and the subsequent commissioning run until 2012 enabled us to conduct various dark matter and new physics searches. The detector refurbishment in 2012 succeeded in reducing the impact of surface background by an order of magnitude and data taking with the lower background continues through the end of the fiscal year 2018. The detector operation continued until Feb. 2019, when the Super-Kamiokande refurbishment work was completed, so as not to miss a possible supernova burst signal. Finally, the whole data set over the five-year operation was analyzed and the results were published as the summary of the collaboration.

  A planned future detector, XMASS1.5, became uncompetitive as other large-scale liquid-xenon detectors became operational first. Participation in a second-generation experiment, the XENONnT experiment, started in 2017. ICRR group introduced technologies originating from XMASS and Super-Kamiokande and contributed to the WIMP search and other new physics

searches. In 2024, the group also joined the XLZD collaboration toward further future studies.

The project is supported by Grant-in-Aids of the Ministry of Education, Culture, Sports, Science and Technology. [2 faculties + 1 assistant professor + 1 post-doctoral fellow]

- Hyper-Kamiokande

  The Hyper-Kamiokande (also referred to as Hyper-K or HK) will provide major new capabilities for making discoveries in particle and astroparticle physics. The project consists of the Hyper-K detector, which has an 8.4 times larger fiducial mass than its predecessor, Super-Kamiokande, equipped with newly developed high-sensitivity photosensors and a high-intensity neutrino beam produced by an upgraded J-PARC accelerator facility. The construction of the Hyper-K detector began in 2020, aiming to start observations in 2027. [9 faculties + 7 assistant professors + 1 project associate professor + 7 project assistant professors + 2 post-doctoral fellow]

- TA

  The TA project received a fund by Grant-in-Aid for Scientific Research in Priority Areas (2003 - 2008) for its construction and commissioning. A continued fund for 5 years of operation (2009-2013) was granted as a Grant-in-Aid for the Specially Promoted Research. The TA consists of a ground array of scintillation counters and fluorescence telescopes. The hybrid observation of cosmic ray air showers with TA started in May 2008 and has been maintained by the contributions of Japan, USA, Korea, Russia, and Belgium. The TA collaboration confirmed the cutoff at the highest energies. The mass composition of cosmic rays above $10^{18.2}$ eV is consistent with light composition. The Grant-in-Aid for the Specially Promoted Research (2015-2019) was obtained for the TAx4 project to quadruple the aperture of the TA surface detector for its construction and commissioning to explore the origin and nature of the highest energy cosmic rays, especially to confirm the anisotropies such as the TA hotspot. The TA Low-Energy extension studies the transition from galactic to extra-galactic cosmic rays. Its telescopes were completed in 2013 and have been operational by the US fund. For the completion of the TALE surface detectors and their operation in addition to TA, the Grand-in-Aid for Scientific Research (S) was funded in 2015-2018. For their continuation, and the construction and operation of the TALE infill surface detector array that extends the energy threshold down to $\sim 10^{15}$ eV, the Grand-in-Aid for Scientific Research (S) was obtained in 2019-2023. The deployment of the TALE surface detectors was completed in 2017 and has been in operation. [2 faculties + 2 assistant professors + 1 project assistant professor + 1 post-doctoral fellow + 1 senior fellow + 1 technical specialist + 1 skilled assistant]

- Tibet ASγ

  The Tibet air shower array was constructed with gradual upgrades from 1988 to 2014, by the funds from Grants-in-Aid and from the government. As an upgrade, new air shower core detectors were added for the next-step measurement of the chemical composition in the knee energy region, while large ($\sim$4,000 m^2) muon detectors aiming at higher-sensitivity gamma-ray observation in the 100 TeV region were constructed under the Tibet air shower array. The muon detectors also play an important role in measuring the chemical composition of cosmic rays in the knee energy region. The hybrid experiment (air shower array + muon detectors + air shower core detectors) started data-taking in 2014. The Tibet ASγ Collaboration found that yearly variation in depth of the Sun shadow in cosmic rays was sensitive to the coronal magnetic field in the Sun in 2013 and that the average interplanetary magnetic field employed in a popular solar magnetic field model was underestimated by approximately 50 % in 2018. Using the air shower array and muon detectors, the Tibet ASγ Collaboration successfully detected gamma-rays beyond 100 TeV from the Crab Nebula in 2019. Detection of diffuse gamma-rays beyond 398 TeV along the galactic plane was also reported in 2021. [1.5 faculties + 1.5 assistant professors + 3 post-doctral fellow]

- ALPACA

  The ALPACA, a joint project between Bolivia, Mexico, and Japan, will be composed of an 83,000 m^2 surface air shower array and a 3,600 m^2 underground muon detector array to make wide field-of-view (2 sr) high-sensitivity observation of high-energy cosmic rays/cosmic gamma rays on the highland, 4,740 m above sea level near Mount Chacaltaya, of Bolivia. ALPACA-Japan will make a major contribution to the construction of the surface array and the muon detector array. The initial R&D program was financed by TORAY science foundation and now the ALPACA project is funded by the Grants-in-Aid. Approximately 20 % of the surface array of ALPACA has been constructed and operated since April 2023. The construction of the first muon detector is planned to start in 2024. [1.5 faculties + 1.5 assistant professors + 3 post-doctral fellows]

- CTAO

  CTAO R&D program had been financed by a Grant-in-Aid for Specially Promoted Research (2012-2016). Four CTAO Large Size Telescopes (LSTs) with a 23m dish on La Palma have been under construction with the budget for the facility development from the Japanese Government MEXT (2016-2018), in cooperation with Germany, Spain, France, and Italy. The first LST (LST-1) was inaugurated in 2018 October, and the total observation time has exceeded 2000 hours. OP 313, a distant Flat Spectrum Radio Quasar (FSRQ) located at redshift z=0.997, was detected with LST-1 in 2023, following the gamma-ray flare detection by *Fermi*-LAT. This detection makes this source the 10th FSRQ, the

furthest AGN in the VHE gamma-ray sky, and the second furthest VHE source after GRB 201216C. Three more LSTs (LST 2-4) will be completed in 2026. The array of four LSTs is planned to start the scientific operation in 2026. A significant part of the operation and maintenance of LST 1-4 and CTAO North site is financed by a Grant-in-Aid for scientific research (S) (2017-2021, 2023-2027) and a specific research budget from MEXT since 2018. The CTAO LST Collaboration is planning the LST extension to CTAO-South in Chile after the completion of CTAO-North to make CTAO an all-sky observatory. [3 faculties + 4 assistant professors + 1 project professor + 1 project assistant professor + 3 post-doctral fellows]

- High Energy Astrophysics

  This group was established in December 2009 with one faculty member. In April 2013 an assistant professor joined, but the original faculty member retired in March 2016. Until June 2017, only the assistant professor had acted as a permanent member. From July 2017, the group was reconstructed with one faculty member. One assistant professor joined in March 2018, which stimulated the activity of the group again. He has studied kilonova emissions as counterparts of GW events. Another assistant professor joined in January 2020. His research theme is GW astronomy. The two assistant professors moved to other institutes in April 2023. However, a project assistant professor joined in June 2023. He has aimed to promote multi-messenger astronomy in the context of the Galaxy evolution. The group is currently pursuing the theoretical study of high-energy astronomical phenomena based on multi-messenger astronomy, collaborating with the other groups in ICRR. [1 faculty + 1 project assistant professor]

- KAGRA

  The first medium-scale laser interferometric gravitational wave detector in Japan was the TAMA 300 detector which was built in NAOJ, Mitaka, The main objective was to detect gravitational waves (GW) from our Galaxy and nearby region and was operated at the highest sensitivity with the stable operation in 2000. To achieve the direct detection of GW signals with a more sensitive detector, the Large-scale Cryogenic Gravitational wave Telescope (LCGT) was planned for GW events within 200 Mpc. As a prototype of LCGT, a laser interferometer with 100m arm length and with cryogenic mirrors, the CLIO detector, was built. A sensitivity of CLIO with cryogenic mirrors was demonstrated in 2010. In 2010, partial funding of LCGT was approved by the government under a new category of the funding of MEXT, "Leading-edge Research Infrastructure Program", for the period from 2010 to 2012. The tunnel excavation at the Kamioka site was started in May 2012 by using additional funding from MEXT. Further funding for installing the core optics including sapphire mirrors was approved by MEXT later. In the meantime, the new name for LCGT was decided to be KAGRA through a public call. The construction of KAGRA with the designed configuration was mostly finished in the spring of 2019 after several operations as an interferometer with simpler configurations from 2016 to 2018. In October 2019, KAGRA signed an MoA with LIGO and Virgo, and the framework of the LIGO-Virgo-KAGRA (LVK) Collaboration was established. After the commissioning works, KAGRA achieved an observable distance for binary neutron stars of 1 Mpc in March 2020. KAGRA performed its first international joint observation with GEO600 in April 2020 which is called O3GK. In May-June 2024, KAGRA performed an observing run for one month at the beginning of the first half of the fourth observing run (O4a) of LVK.

  The annual operation costs of KAGRA are covered by the MEXT budget. [8 faculties + 3 assistant professors + 3 project assistant professors + 3 postdoctoral fellows + 1 project staff + 13 technical staff(3 tenured + 10 project-oriented)]

- Observational Cosmology

  Japanese Sloan Digital Sky Survey (SDSS) key members moved to ICRR in 1996 with a Grant-in-Aid for Specially Promoted Area, forming the observational cosmology group. SDSS-I and II programs were completed by 2008 with additional support from JSPS and RESCUE at the Department of Physics. After the completion of the SDSS programs, the group has started new programs mainly for Subaru HSC and PFS surveys since July 2010, winning multiple grants of Grant-in-Aid for Scientific Research (A) seamlessly for 2011-2014, 2015-2019, 2019-2024, and 2024-2028 as well as various notable research prizes. The headquarters of the University of Tokyo approved a proposal requesting an assistant professor twice, in 2014 and 2020. With the addition of two more assistant professors, the group expanded and became a group of one faculty and two assistant professors. The HSC survey observations were completed in 2020, while the PFS commissioning observations are going on for the scheduled start of the PFS survey in early 2025. In parallel, the group has conducted diverse projects of JWST observations since the launch of JWST in 2022. [1 faculty + 2 assistant professors]

- Theory

  The theory group has a long history, but there was a reset of the group in April 2001 owing to the retirement of the first group leader. A new group was established in 2002 with two faculty members, and one of the members served as the Director of the Institute for three years (2001-2004). Although one faculty member moved in June 2010, the group had a new faculty and recovered its full activity in February 2011. Research highlights include work on theories beyond the Standard Model, with applications to the early universe to explore the origins of matter and fluctuations. Key areas

include supersymmetric theory, grand unified theory, axion models, dark matter models, primordial black holes, Big Bang nucleosynthesis, gravitational waves, and extended objects like Q-balls, I-balls/oscillons, cosmic strings, and magnetic monopoles. This broad research scope reflects the group's commitment to advancing theoretical physics and cosmology. [2 faculties + 2 post-doctoral fellows]

Summary of 2018-2024 Activities

Important events related to the ICRR's activity in 2018-2024 since the previous external review in 2018 is summarized below.

- The Institute for Cosmic Ray Research was certificated as an "International Joint Usage / Research Center" in 2018.
- The tank open work of Super-Kamiokande (SK) in 2018 successfully stopped the leak.
- The first LST (LST-1) of CTAO was inaugurated in 2018.
- The operation of the XMASS-I detector was completed in Feb. 2019.
- The TAx4 is a project to quadruple the TA experiment, with the goal of detecting the highest energy cosmic rays. Half of the planned additional surface detectors were deployed in 2019 and are in operation. The TAx4 fluorescence telescopes were constructed by the US fund and are in operation.
- The Tibet ASγ Collaboration discovered a gamma-ray emission from the Crab Nebula above 100 TeV in 2019.
- According to the recommendation from the 2019 External Review Committee, ICRR Young Researchers' Workshop for young researchers and graduate students has been held once a year since 2020.
- The Hyper-K project and its construction started in 2020 with the aim of starting data-taking in 2027.
- Science runs of LST-1 started in 2020, and the total observation time exceeded 2000 hours in Jan. 2024.
- KAGRA's first solo observation was done in February 2020.
- KAGRA performed O3GK observation with GEO600 in April 2020.
- The International Laboratory for Astrophysics, Neutrinos and Cosmology Experiments(ILANCE) was established by CNRS/IN2P3 and four divisions of the University of Tokyo in 2021.
- The Tibet ASγ Collaboration discovered a diffuse gamma-ray emission along the galactic plane above 398 TeV in 2021, which reveals the existence of PeV cosmic-ray accelerators in our galaxy.
- Gd was loaded in SK in 2020 and 2022. Gd concentration of 0.03%, which corresponds to 50% neutron capture efficiency was achieved. The neutron tagging capability of SK significantly improved the sensitivity for supernova neutrino searches.
- Construction of LST-2,-3,-4 started in 2022, and will be completed in 2026.
- Construction of the TA Low-Energy extension (TALE) surface detector array was completed in 2017, and the array is now operational. The TALE infill surface detectors, which further lower the detection energy threshold, were deployed in 2022 and have been in operation since October 2023.
- NNSO was reorganized into the "Next-Generation Neutrino Science and Multi-messenger Astronomy Organization" to expand our research activities into the field of multi-messenger astronomy in 2023.
- The whole data set for the XMASS-I was analyzed and the results were published in 2023 as the summary of the collaboration.
- In 2021, the TA experiment recorded an extremely energetic particle by the surface detector in the direction of a void in the large-scale structure of the Universe. Its energy was 244 EeV, comparable to the energy of the Oh-My-God particle recorded by the Fly's Eye experiment about 30 years ago. This result was published in 2023.
- The ALPACA Collaboration constructed a partial air shower array in Bolivia and has operated it since 2023.
- KAGRA performed O4a observation with LIGO and Virgo in May and June 2023.
- In 2017 and 2024, some of the XMASS members joined the XENON collaboration and the XLZD collaboration for further study on dark matter, respectively.
- The TA experiment found an isotropy feature in the distribution of arrival directions of cosmic rays above 10^{20} eV. The result published in 2024 favors their heavy mass composition by comparing their distribution with the large-scale structure of the local Universe.
- The Noto-peninsula earthquake on January 1st, 2024 damaged KAGRA mainly in mirror suspension and isolation systems.

Details of the above activities related to the research are described in the following sections.

Project status and main scientific goals

Neutrino and Astroparticle Division

Project	Status	Main Scientific Goals
Super-Kamiokande	running	Study of neutrino oscillations, proton decay, and astrophysical objects with neutrino emission such as Sun and supernova
T2K	running	Precise measurement of neutrino oscillation parameters using SK with accelerator neutrino beam
XMASS	completed	Direct detection of dark matter particles and search for new physics with liquid xenon detectors
XENON	running	
XLZD	planned/ R&D	
Hyper-Kamiokande	under construction	Study of neutrino CP violation, proton decays and supernova neutrinos with a megaton water Cherenkov detector

High Energy Cosmic Ray Division

Project	Status	Main Scientific Goals
Telescope Array	running	Study of extremely-high energy cosmic rays; their origin, propagation and interaction
Tibet ASγ	running	Study of origin, acceleration mechanism and modulation of high-energy cosmic rays
ALPACA	partially running	Study of cosmic-ray origin, Ultra-high energy gamma-astronomy
CTAO	under construction	VHE Gamma Ray Astronomy, the study of the cosmic-ray origin, particle acceleration and indirect search for dark matter

Astrophysics and Gravity Division

Project name	Status	Main Scientific Goals
KAGRA	GW observation and commissioning	Through the detection of gravitational wave, study physics of gravitational waves and open gravitational wave astronomy
Subaru PFS	commissioning	Uncovering physical processes and history of cosmic reionization and early galaxy formation

NEUTRINO AND ASTROPARTICLE DIVISION

SUPER-KAMIOKANDE

Introduction

Super-Kamiokande(SK, Super-K) is a 50 kton water Cherenkov detector studying the physics of neutrinos, proton decay, and neutrinos from astrophysical phenomena such as supernovae. Data taking started in April 1996. Atmospheric neutrino oscillations were discovered by SK in 1998, and solar neutrino oscillations were discovered by comparing SK solar neutrino data with SNO-charged current data in 2001. The first data phase of Super-K, SK-I, ran until July 2001. Due to an accident in 2001, about 60% of the photomultipliers (PMTs) in the detector were destroyed, and the detector was reconstructed in 2002 using the remaining PMTs with PMT cases which prevents shock-wave production even if a single PMT implodes. The second data phase, SK-II, ran from December 2002 to October 2005 after the recovery. The missing PMTs were reproduced, and full reconstruction of the detector was performed from October 2005 to July 2006. The third data phase, SK-III, lasted from July 2006 to August 2008. The readout electronics system was fully upgraded in September 2008. Since this upgrade the fourth data phase, SK-IV, ran until May 2018.

Regarding preparation for loading gadolinium (Gd) into the SK tank to enhance the anti-electron neutrino detection efficiency, the detector was refurbished from June 2018 to January 2019 to repair the leak in the Super-K water tank and improve the water piping in the tank to double the water flow rate. The fifth data phase, SK-V, ran from January 2019 to June 2020 with pure water. 13 tons of $Gd_2(SO_4)_3{\cdot}8H_2O$ was loaded to the SK tank in July/August 2020, which corresponds to 0.01% Gd concentration and 50% neutron capture efficiency. The sixth data phase, SK-VI, ran from August 2020 to May 2022 with this Gd concentration. An additional 26 tons of $Gd_2(SO_4)_3{\cdot}8H_2O$ was loaded to the SK tank in June / July 2022, increasing the concentration of Gd to 0. 03% and the neutron capture efficiency to 75 %. The seventh data phase, SK-VII, has been running since then. Table 1 summarizes all phases of SK data collection.

During the period of this external review, the upgrade of the Super-K detector was performed successfully, and initial results from the Gd-loaded data were obtained. In addition, the results of high-precision neutrino oscillation analysis of atmospheric and solar neutrinos have been obtained, and significant progress in the study of proton decay, supernova physics, and other physics targets have been achieved.

Summary from 2018 to 2024

Here we summarize the notable achievements during the period of this review, that is, after 2018.

- One of the most significant achievements during this period was the start of the Gd loaded Super-K detector. In order to load Gd to the SK tank, the water leak had to be repaired. The tank open work in 2018 successfully stopped the leak, and no water leak has been observed since then. The Gd was loaded in 2020 to 0.01% concentration and increased to 0.03% in 2022. Water transparency has been as good as about 80 m even after the Gd-loading and that has been enough for performing various physics at Super-K.

- The Diffuse Supernova Neutrino Background (DSNB) was searched using SK-Gd data (SK-VI and SK-VII). The sensitivity of the search has entered the range predicted by modern DSNB theoretical predictions above 17 MeV in neutrino energy. The SK-Gd results gave the world's best flux upper limit above 12 MeV.

- The neutron tagging with Gd significantly improved the performance of the real-time supernova monitor. That enabled automatic alert of galactic supernova to GCN Notice within 1.5 minutes after the neutrino signals in SK. Pointing accuracy has been improved to $\sim$3.7 degrees for a 10 kpc supernova.

- In order to enhance the sensitivity of the atmospheric neutrino oscillation analysis, the fiducial volume was enlarged from 22.5 kton to 27.2 kton and now includes the volume of water between 1 and 2 m from the wall. All 6,511 days of Super-K purewater data (SK-I through SK-V) was reanalyzed. The data disfavor the Inverted Hierarchy with a significance of 92.3% and favor $\delta_{CP} \sim -\pi/2$.

- High-quality solar neutrino data were taken during the SK-IV phase because of the improved water circulation system, which reduced the radon background, and the lowered energy threshold of the data acquisition system. The method to estimate the energy of each event and various systematic errors have been improved and careful analysis of the SK-IV data has been performed. As a result, the energy spectrum upturn which is expected from the matter effect in the Sun has been favored with 1.5 σ. In addition, the combined data of all SK phases give 3.2σ of the day/night asymmetry which is expected from the matter effect of the earth. The apparent difference in Δm_{12} between the solar global and the KamLAND reactor result has been reduced to $\sim 1.5\sigma$ level.

- Searches for nucleon decays have been performed with the enlarged fiducial volume of 27.2 ktons for $p \to e^+\pi^0$ and $p \to \mu^+\pi^0$ decay modes. With 450 kton·yrs of exposure a lifetime lower limit has been obtained to be $> 2.4 \times 10^{34}$ years for $p \to e^+\pi^0$ and $> 1.6 \times 10^{34}$ years for $p \to \mu^+\pi^0$. With 365 kton·yrs of exposure a lifetime lower limit of $p \to \bar{\nu}K^+$ is obtained to be $> 0.82 \times 10^{34}$

phase	SK-I	SK-II	SK-III	SK-IV	SK-V	SK-VI	SK-VII
start	Apr. 1996	Sep. 2002	Jul. 2006	Sep. 2008	Jan. 2019	Jul. 2020	Jun. 2022
end	Jul. 2001	Oct. 2005	Aug. 2008	May 2018	Jun. 2020	May 2022	Running
ID PMTs	11,146	5,182	11,129	11,129	11,129	11,129	11,129
(photo coverage)	(40%)	(19%)	(40%)	(40%)	(40%)	(40%)	(40%)
OD PMTs	1,885	1,885	1,885	1,885	1,885	1,885	1,885
Electronics	ATM	ATM	ATM	QBEE	QBEE	QBEE	QBEE
Water	pure	pure	pure	pure	pure	0.01% Gd	0.03% Gd

Table 1. Data taking phases of Super-Kamiokande. ID stands for the Inner Detector of SK, while OD refers to the Outer Detector of SK. The front-end electronics used until SK-III was the ATM (ADC/TDC data recording Module). Starting with SK-IV, it was replaced by QBEE (QTC-Based Electronics with Ethernet), an improved version of the front-end electronics.

years. Searches for other decay modes were also performed and we obtained the most stringent limits on nucleon lifetime in the world.

Tank Open Work 2018–2019

From May 31, 2018 to January 29, 2019, the tank open work to refurbish the SK detector was performed after 12 years of continuous operations. The main tasks of the works are as follows:

- Fix a small water leak in the Super-K tank.
- Clean any rust and other dirt accumulated in the detector since its original completion in 1996.
- Install additional water piping to increase the total water flow for increased water purification and to enable better control of the flow direction in the tank.
- Replace the PMTs that have failed (a few hundred out of 13,000) since the previous in-tank refurbishment in 2006.

The leak fix

During this phase of the refurbishment effort, we drained two meters of water from the tank every three days and worked to seal potential water leakage points on the outer wall and replace those failed PMTs that we could reach from the floor. The Super-K tank is 40 m in diameter and 42 m in height and contains 50,000 tons of pure water. Its sides form an icosagon comprised of 400 pieces of 4 mm thick stainless steel plates and able to withstand external stretching forces with the support of backup concrete and rock. It had to meet requirements regarding small elution into water, low natural radioactivity, long-time stability during water exposure, and sufficient attachment strength to stainless steel plates. Figure 1 shows the actual sealant work. Workers put thick tape along both sides of the welding line to hold the sealant material on the line. They used trowels and paint brushes to spread the sealant material over the weld with the same thickness as the surrounding tape. A double sealant layer was required to allow for unexpected gaps or pinholes in one of the two layers.

After filling the tank with pure water, a water leakage measurement was conducted. The method monitors the water level to 0.1 mm precision while water circulation is stopped. We could not see any decrease in the water level and concluded that the SK water leakage has been reduced to less than 1/200 of the rate during the period before the tank upgrade work.

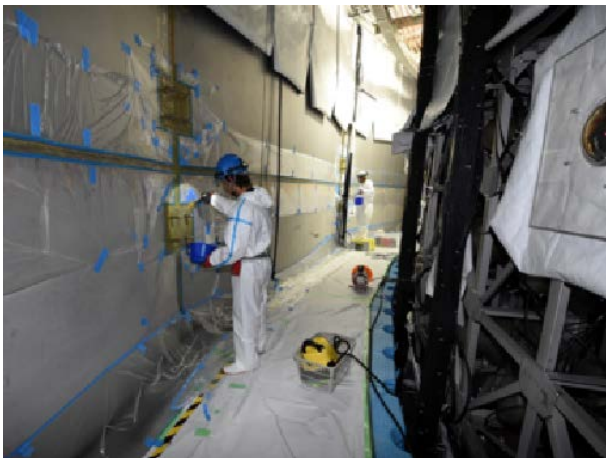

Fig. 1. Sealant work on the SK tank wall conducted from the floating floor

Cleaning and rust removal

The dirty walls and structures inside the Super-K tank required much personpower to clean up. In particular, the top and outermost structures were covered by a heavy residue of exhaust gas and dust left over from when we constructed the detector in 1991-1996. We also aimed to remove the most potential sources of rust during the cleaning work. As for tools, it was dangerous to choose arbitrary ones since most of them leave other types of dust, which may then degrade the water after restarting the operation of Super-K. The water team tried, investigated, combined, and developed many tools. We maintained the excellent quality of sealant attachment and removed a large amount of radioactivity; according to a germanium detector measurement, at least 100 Bq of radium was removed during the cleanup. As the radon gas emitted from this radium is comparable to that arising from the PMTs themselves, the in-tank shift workers contributed to lowering the background for future solar neutrino observations.

Water piping upgrade

The water purification system was originally designed with a supply of 30 m^3/h and circulation of 60 m^3/h, and the piping inside the tank was made without separate lines for the inner detector (ID) and the outer detector (OD). This time, we decided to improve the water flow in the tank by separating the pipes of the inner volume and the outer volume and the pipes on the side, top, and bottom of the outer volume so that all the flow rates could be adjusted independently. The effective detector volume for the solar neutrino analysis had been limited by the inflow of radon background, but this plumbing improvement makes it possible to control and optimize the water flow in the tank.

PMT exchange and other work

During this tank open period, dead PMTs were also exchanged in parallel with sealing work. In total, 136 ID PMTs and 224 OD PMTs were exchanged. For ID PMT replacement, new PMTs under development for Hyper-Kamiokande (HK) were used. In addition to the recovery of SK performance, another purpose of this exchange is to check the performance and long-term stability of HK PMTs in the expected operating environment. Similarly to other SK ID PMTs, shift workers attached anti-implosion covers made of fiber-reinforced plastic (FRP) and acrylic to these PMTs. The exchange of ID and OD PMTs, including cable connections inside the tank and the following signal checks, was also performed by shift workers with a well-coordinated schedule to avoid interference with the sealant work, as shown in Figure 2. Another important task carried out during the tank open work

Fig. 2. Exchange work of the ID (top two panels) and OD (bottom two panels) PMTs.

is related to the calibration system inside the tank and studies for more precise detector understanding, such as the replacement of laser injectors and optical fibers, installation of a new light injection system, precise magnetic field mapping, and recording all PMTs dynode directions. The installation work of the white Tyvek® sheet that covers the OD region for high light detection efficiency was also a significant job. With much effort from many workers, all the sheets covering the tank wall were removed for sealant work and reinstalled afterwards as shown in Figure 3.

Fig. 3. OD Tyvek® installation work

SK-Gd

Diffuse supernova neutrino background search

Diffuse Supernova Neutrino Background (DSNB) is a neutrino radiation background emitted from past supernova explosions that have occurred since the early universe after the Big Bang, as shown in Figure 4. If we can obtain information about DSNB, we can study the history of supernova explosions, such as when many supernova explosions have occurred in the universe. A search for DSNB has been performed using

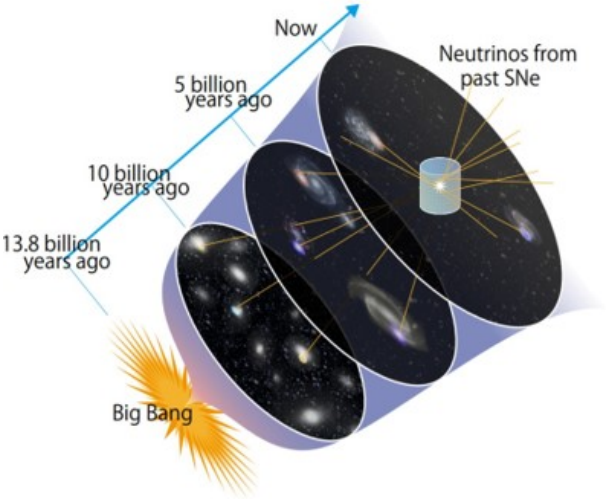

Fig. 4. Diffuse Supernova Neutrino Background

data obtained to date with SK in the pure water phase, including all 2970 days of SK-IV data, and the results have been published in [99]. In this analysis, the neutron capture events by hydrogen nuclei in pure water were used to reduce the background events by identifying neutrons with a detection efficiency of 20-30% and to limit the flux of DSNB with the world's highest sensitivity in the region below 31.3 MeV. The 2.2 MeV gamma rays emitted when neutrons are captured by hydrogen nuclei are extremely weak signals, averaging about 7 photoelectrons in SK.

The Gd loading

Anti-electron neutrinos from supernovae interact with protons in water, and positrons and neutrons are produced. By

loading Gd into pure water, neutrons are captured by Gd, emitting gamma rays with a total energy of 8 MeV. These gamma rays can be detected with much higher efficiency than the 2.2 MeV gamma rays from proton captures, which are just above SK's detection threshold.

In the process of loading Gd and conducting research, we have taken the utmost care to prevent Gd from leaking into the natural environment. As already explained in the previous section, in 2018, before loading Gd, we carried out refurbishment work on the SK tanks.

The first step was to develop Gd itself for loading into the pure water. Since Gd alone is not soluble in water, it was necessary to dissolve a Gd compound, and gadolinium sulfate octahydrate ($Gd_2(SO_4)_3{\cdot}8H_2O$) was selected because of its less-corrosiveness to stainless steel and its small effect on light transmission when dissolved. Because SK is conducting the world's most precise solar neutrino measurement, it must be extremely low in radioactive impurities to maintain its performance. We have developed such ultrapure gadolinium sulfate in collaboration with a rare earth company. We also developed a system to recirculate and purify water while retaining the gadolinium sulfate. After the refurbishment, the tank was filled with pure water by the end of 2019. Through February 2020, a series of tests were conducted to treat the water using the newly developed purification system. These tests confirmed that the transparency of the pure water in the tank could be maintained at the same level as with the original purification system. The most crucial element here is a special ion exchange resin that removes other ions while retaining Gd^{3+} and SO_4^{2-}, developed jointly with the water purification system company. We decided to load Gd in two steps. First, 13 tons of $Gd_2(SO_4)_3{\cdot}8H_2O$ was dissolved starting July 14, 2020 [100]. This is a $Gd_2(SO_4)_3{\cdot}8H_2O$ concentration of 0.026% by weight for 50,000 tons of pure SK water, which is a Gd concentration of 0.01% by weight (Gd neutron capture efficiency of 50%). To introduce Gd during one circulation of the tank water (about 35 days), pure water was sent from the top of the tank to the gadolinium sulfate dissolving system, and water containing Gd was sent to the bottom of the tank so that the Gd concentration would quickly become uniform over the tank. In fact, it proceeded stably, and the gadolinium sulfate loading was completed on August 17, 2020.

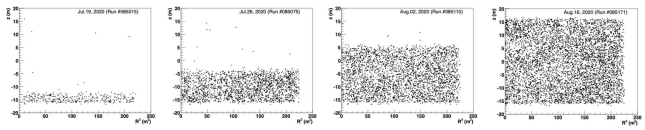

Fig. 5. The time evolution of neutron capture events by Gd over 35 days during the first gadolinium loading. The horizontal axis is the square of the radius of the cylindrical detector [m^2]. The Vertical axis is the height position [m]

Figure 5 shows the position of the neutrons produced by the high energy muon-induced hadron reaction and captured by Gd during loading of $Gd_2(SO_4)_3{\cdot}8H_2O$ to SK. It shows how the Gd concentration in the tank changed on a daily basis, and it can be seen that the Gd was introduced from the bottom of the tank as planned. The Gd concentration in the tank was measured using an Am/Be neutron source and a BGO scintillator. The gamma rays are replaced by scintillation light from BGO crystals to simulate the anti-electron neutrino signal. Figure 6 shows the distribution of the time difference be-

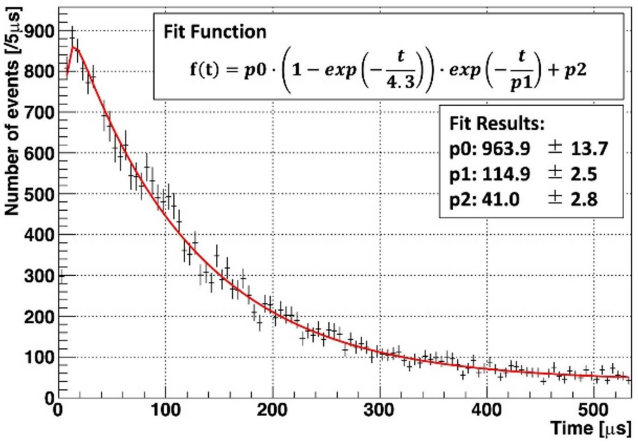

Fig. 6. Distribution of the time difference between scintillation event and neutron capture event by Gd in SK-VI

tween scintillation events and neutron capture events by Gd in Am/Be and BGO measurements after the loading of Gd. The analysis shows that the neutron capture time constant for Gd, calculated from a Gd concentration of 0.01%, is 110 μs, as expected. The spatial uniformity of the Gd concentration was also confirmed by changing the source location. This phase of 0.01% Gd concentration was designated as SK-VI, the sixth physical analysis period of SK.

The second Gd loading was conducted from June 1 to July 5, 2022, to triple the Gd concentration to 0.03% and increase the neutron capture efficiency to 75% by dissolving an additional 26 tons of $Gd_2(SO_4)_3{\cdot}8H_2O$ in the SK tank. As with the first Gd loading, water with a concentration of 0.03%Gd was introduced from the bottom of the tank during one circulation of the tank water, and Figure 5 shows how the Gd concentration became uniform immediately after completion, as shown by the neutron capture event. This phase of 0.03%Gd concentration was designated as SK-VII, the seventh physical analysis period of SK.

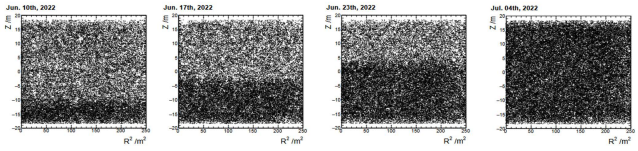

Fig. 7. The time evolution of neutron capture events by Gd over 35 days during the second gadolinium loading.

Figure 8 shows the results of periodic measurements of the neutron capture time constant of Gd since the first Gd loading. It can be seen that the neutron capture time constants of Gd at the top, center, and bottom of the detector are uniform and stable with time for SK-VI and SK-VII, respectively. The Gd concentration obtained from the time constants is also consistent with the amount dissolved $Gd_2(SO_4)_3{\cdot}8H_2O$, confirming that the data are stable and ready for physics analysis.

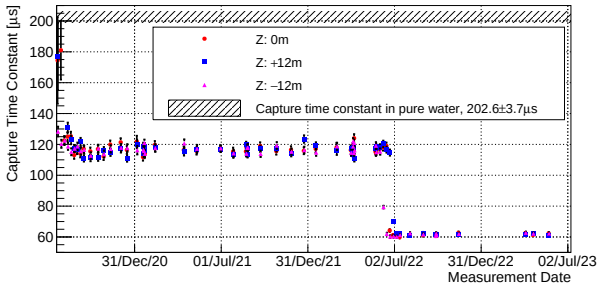

Fig. 8. The history of the neutron capture time constant in SK since July 2020, obtained from the analysis of Am/Be neutron source data.

Diffuse supernova neutrino background search after Gd loading

First, a DSNB search was performed on the SK-VI data using the conventional method. As shown in Figure 9, this method selects neutron capture events by applying various cuts, such as cut on the energy of the events, to the detected events and achieves a final signal identification efficiency of about 36%. The energy spectrum of the final events is shown

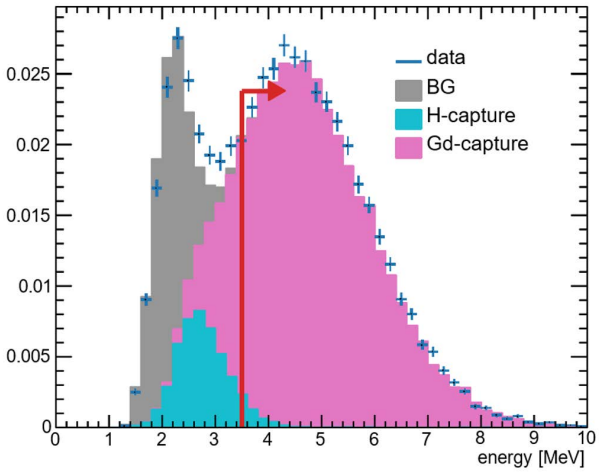

Fig. 9. Selection of neutron capture events (delayed events) by energy cut for the calibration data and its MC simulation with Am/Be neutron source. The vertical axis is normalized to be 1 when integrated over the entire region, i.e. it is normalized by the number of prompt events.

in Figure 10. 16 events are in the 7.5 MeV–29.5 MeV range, which is consistent with the expected background, and the number of accidental coincidence events is significantly reduced compared to the SK-IV results. The number of backgrounds is as expected. Figure 11 shows the limits on the flux of DSNB obtained from this SK-VI analysis. This result, with only 552 days of data, is comparable to that of SK-IV, which has five times the live time data, and shows that this is the most sensitive detector in the world above 13 MeV with the power of the 0.01% Gd [108].

Next, we improved the analysis method to reduce the background further by incorporating machine learning methods. Specifically, we developed a method to efficiently identify neutrons using a neural network, and at the same time, we

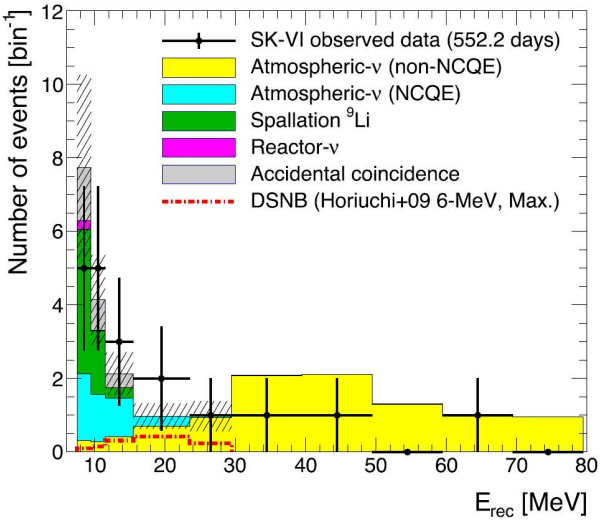

Fig. 10. Energy distribution of events remaining in the final sample in the SK-VI DSNB search using conventional cut-based analysis

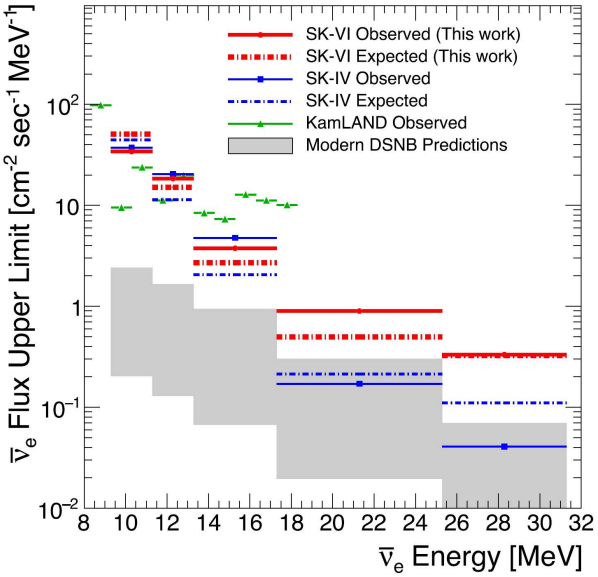

Fig. 11. Sensitivity of the DSNB flux of SK-VI (red dashed line) and the upper limit obtained (red solid line)

investigated a method to reduce NCQE reaction events caused by atmospheric neutrinos, which are the largest background source of DSNB (for evaluation of the machine learning, we also performed an analysis using independent Boosted Decision Tree analysis to confirm similar results). The neural network was trained with 12 variables as input, including the number of PMT hits and the hit time. As a result, in addition to the capture by Gd, the capture by protons was efficiently identified, and the neutrino detection efficiency was 1.3 times higher than that of the conventional method. The method developed for reducing the low-energy radioactive background in solar neutrino observations was found to be effective for reducing the NCQE background and was applied to reduce the background. The resulting energy spectrum is shown in Figure 12. Compared to Figure 10, the NCQE background is significantly reduced and the expected signal is increased.

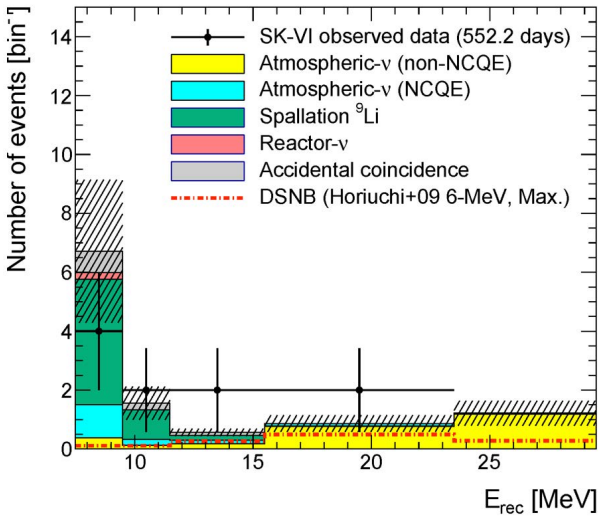

Fig. 12. Energy distribution of events remaining in the final sample in the SK-VI DSNB search using improved neural network analysis

The method developed above was then applied to SK-VII at 0.03% Gd concentration, and the results of the energy spectra obtained as SK-Gd until September 2023, including data from SK-VI, are shown in Figure 13. The resulting sensitivity to the DSNB flux is also shown in Figure 14. These are sta-

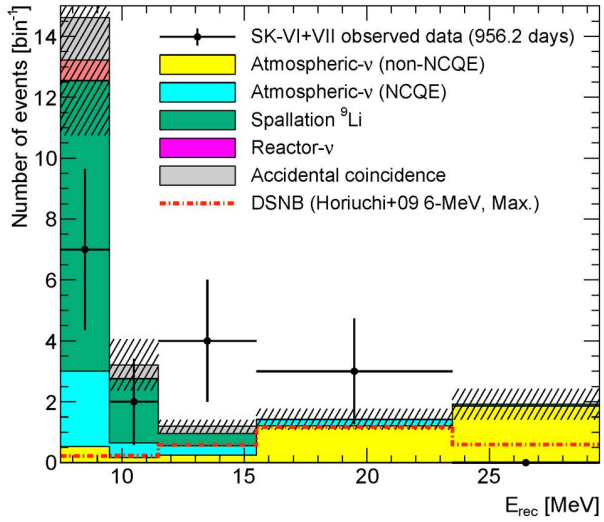

Fig. 13. Energy distribution of events remaining in the final sample in the SK-VI + SK-VII DSNB search using improved neural network analysis

tistically limited, and further improvements are expected, but it can be seen that we have already reached the range expected from the theoretical model above 13 MeV. Future observations with SK-Gd will aim to detect the signal of the DSNB.

Supernova burst monitoring

Core-collapse supernovae (supernovae after that) are cataclysmic explosions of massive stars ($> 8M_{\odot}$) due to the gravitational collapse of the star materials at the end of their life. More than 99.9% of the energy released by this event is expected to be through neutrino emission. If the supernova burst

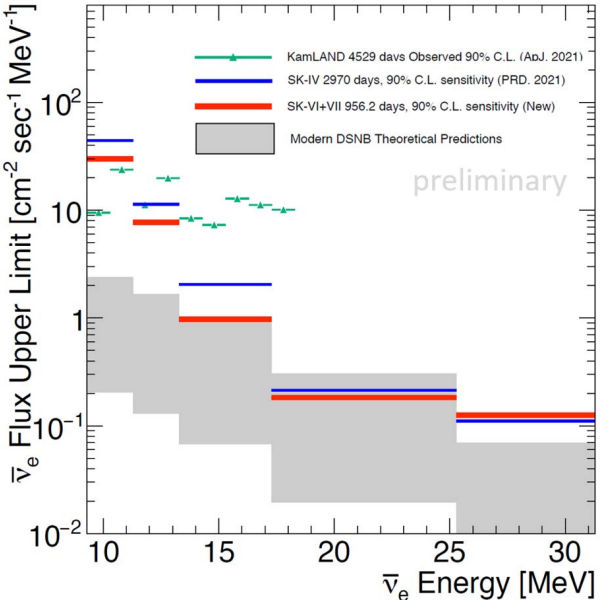

Fig. 14. SK-VI + SK-VII sensitivity of the DSNB flux(red)

occurs at the distance of the galactic center ($\sim$ 10-kpc), about 3000 inverse β decay events (IBD; $\bar{\nu}_e + p \rightarrow e^+ + n$), 200 electron scattering events (ES; $\nu + e^- \rightarrow \nu + e^-$), and about 100 charged current reaction (CC) with oxygen nucleus (^{16}O) events are expected assuming a Nakazato model (20 M_{solar}, metallicity $Z = 0.02$, shock revival time t_{revive} = 200ms case, as an example) [114] . ES interactions conserve the direction from the neutrino, thus, reconstructing the direction of these events enable the possibility to reconstruct the direction from the supernova.

When a supernova happens, theories predict that the electromagnetic signal from the explosion arrives several minutes to a dozen hours after the neutrinos burst arrival. Neutrinos propagate from the collapsing iron core to the surface of the exploding star at the speed of light, while the electromagnetic shock wave propagates through the outer layers of the star at about 1/30th the speed of light ($\sim$100 km/sec) due to the high matter density. In order to allow telescopes to observe the first electromagnetic signal from the supernova, it is necessary to quickly inform the astronomer community around the world of the direction of the neutrino flux. Without Gd in the detector, identifying the supernova neutrino burst signal was ambiguous and required expert analysis and judgment, which was expected to take about an hour before transmitting the alert to the world. After the loading of Gd, the characteristic delayed coincidence of the IBD signal can be used to identify IBD events, providing a clear signal for the supernova burst, as well as improving the capability of SK to separate IBD events from the other supernova neutrino burst interactions in the detector. Thus, allowing us to release a fast automated alarm, as well as improving our supernova direction reconstruction performances.

We developed the first version of an IBD tagging algorithm in 2021, with an IBD tagging efficiency of $33.10 \pm 1.05\%$. Following this, we implemented an automated supernova alarm in case of detection of a 10-second cluster of 60

or more events spread uniformly within the fiducial volume and including at least 10 IBD tagged events. These criteria were selected to ensure full coverage of the Large Magellanic Cloud (LMC) with 0.01% Gd loading. The automated alarm would be released through the GCN notice network [115].

Following the increase of the Gd loading to 0.03% in summer 2022, the IBD tagging performance was improved to $46.86 \pm 0.04\%$. These initial results with 0.03% were published in [117].

Further improvements were achieved on the supernova neutrino signal selection, as well as on the supernova reconstruction fitter. A new fitter was developed, using an HEALPix method [118] as a primer to estimate the direction of the supernova, our maximum-likelihood fitter, presented in [116] and improved in [117] is used to provide the final supernova direction. It was re-written to use better performances CPU access methods. These improvements allowed to reduce the supernova direction reconstruction's processing time from ~ 5 minutes to few seconds for a 10kpc-supernova. The current time between the supernova neutrino burst arrival in the detector and the alarm release is about 1.5 minute for a 10kpc-supernova.

On the signal algorithm selection, the method used to select neutron capture events was improved, allowing to reduce the BG contamination in the final "non-IBD tagged" sample from $5.72 \pm 0.04\%$ to $1.11 \pm 0.01\%$. This improvement allowed us to reduce the energy threshold of the online analysis from 7 to 6 MeV, increasing the BG contamination to $2.70 \pm 0.01\%$ but allowing to increase the ES event selection efficiency from $40.46 \pm 0.04\%$ to $46.27 \pm 0.03\%$.

Figure 15 shows the supernova direction's angular resolution using the lastest fitter version for the different gadolinium loading. Table 2 shows the performance of the SK supernova burst monitoring system over time.

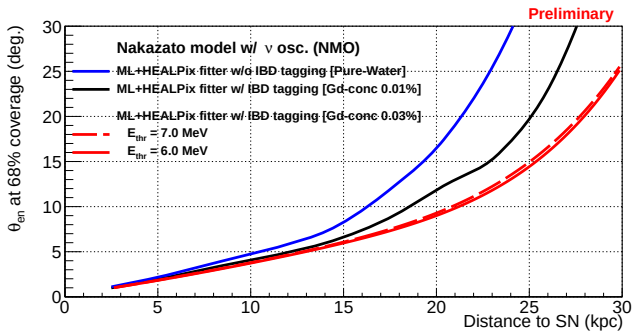

Fig. 15. Supernova direction reconstruction's angular resolution at 1σ. Assuming Nakazato model (20 M_{solar}, z=0.02, $t_{revive} = 200$ms) with Normal Mass Ordering (NMO). The distortion visible around 20kpc for the pure-water and 0.01% Gd curves are due to the limited statistics used for these cases to estimate the angular resolution in the 10 to 30 kpc range.

Pre-supernova burst monitoring

In addition to supernova neutrino burst, SK with Gd can detect neutrino signals from the pre-supernova star before the gravitational collapse of the iron core, making it possible to "predict supernova explosions". Massive stars undergo a silicon (Si) burning process just before they collapse under gravity and go into a supernova explosion. This process emits low energy antielectron neutrinos, called pre-supernova neutrinos, which are too low energy to be observed because they are obscured by the background. We have built a system that monitors the number of antielectron neutrino events in real time and issues a supernova explosion prediction alarm when it observes a significant excess over the background level. SK can issue a supernova explosion prediction for about 20 supernova candidates, including Betelgeuse, up to 500 pc (with an average about 150 pc) a few hours before the explosion. In addition, in collaboration with the KamLAND experiment, we have developed a combined monitoring system for SK and KamLAND, which is available on [119].

Atmospheric Neutrinos

Super-Kamiokande's atmospheric neutrino data provided the first evidence for $\nu_\mu \to \nu_\tau$ neutrino oscillations in 1998 [5] with the observation of a significant deficit of upward-going ν_μ-induced interactions. Though that discovery spawned an entire industry of neutrino oscillation experiments, the atmospheric neutrino data themselves still offer one of the most robust probes of this phenomenon. Indeed, despite impressive constraints on most of the standard PMNS mixing parameters by accelerator and reactor neutrino experiments, the nature of the neutrino mass ordering (MO) and whether or not neutrinos posess CP-violating oscillations are two open questions that can be probed with atmospheric neutrinos. Going beyond this now-standard framework, the long baselines and wide range of energies carried by these neutrinos coupled with SK's low thresholds and precision resolution make it possible to probe exotic scenarios such as tests of additional interactions, additional sterile neutrinos, or other symmetry-breaking oscillations.

With a data set spanning more than 6,500 live days and a total exposure of 484.2 kton-years, SK's atmospheric neutrino sample has been used over the last six years to provide the strongest constraints on unknown mixing parameters and to search for indications of new physics ahead of the start of next-generation experiments.

PMNS Oscillation Analysis

Matter effects along the trajectory of Earth-core-crossing neutrinos coming up into the detector imbue atmospheric neutrinos with sensitivity to the MO. Importantly, either only neutrinos or only antineutrinos experienced enhanced oscillations depending upon where the MO is normal (NO) or inverted (IO). At the same time, the impact of the CP-violating oscillation parameter δ_{CP} has an asymmetric effect on neutrinos and antineutrinos at lower energies. Enabling maximal sensitivity to both of these open questions then relies critically on SK's ability to distinguish CP sign (and flavor) of atmospheric neutrino interactions.

Since 2008 SK has the ability to identify neutrons capturing on hydrogen nuclei via the resulting 2.2 MeV gamma ray emitted during the process with an efficiency of approximately 25%. With the addition of gadolinium in 2020 and again in 2022 this efficiency has increased 50%. This provides

	Gd concentration	IBD tagging eff.	$\Delta\theta_{SN}$ (for 10kpc)	Ref
2016	-	-	5.22 ± 0.16	[116]
2022	0.01%	33.10 ± 1.05 %	4.17 ± 0.13	
2023	0.03%	46.86 ± 0.04 %	4.00 ± 0.10	[117]
2024	0.03%	51.27 ± 0.01 %	3.68 ± 0.04	

Table 2. SK supernova burst monitoring performance over time. Results are assuming Nakazato model (20 M_{solar}, z=0.02, $t_{revive} = 200$ms) with Normal Mass Ordering (NMO)

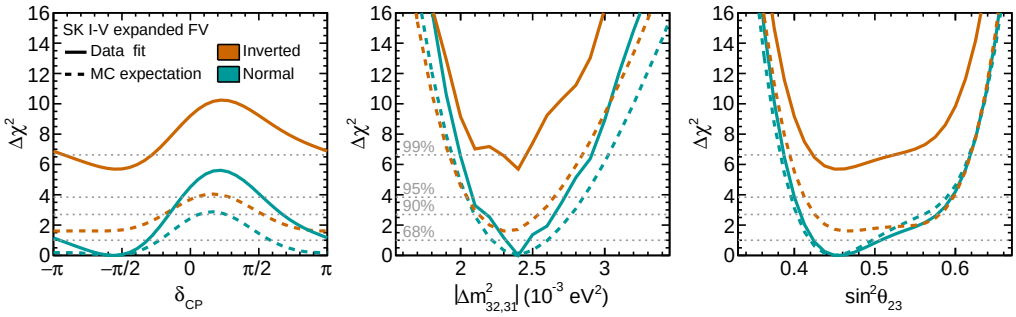

Fig. 16. Measured $\Delta\chi^2$ distributions for the $\Delta m^2_{23,31}$, $\sin^2\theta_{23}$, and δ_{cp} oscillation parameters for the Super-K only fit with $\sin^2\theta_{13}$ constrained to the value preferred by reactor measurements.

an important tool for separating neutrinos from antineutrinos in that the latter produces final states with more neutrons than the former, the neutron multiplicity is now utilized to separate these two species. Since 2020 the atmospheric neutrino analysis at SK has adopted neutron tagging in the pure-water SK-IV phase to purify its single-ring samples in neutrino and antineutrino components. With the selection samples whose hierarchy-sensitive electron neutrino component is more than 60% pure in ν_e interactions and others that are more than 46% pure in $\bar{\nu}_e$ interactions. The CP-sensitive samples are now separated into similar pieces with 80% and 36% purities, respectively. With this revised event selection the sensitivity to the MO has improved by roughly 10%.

At higher energies the neutron multiplicity for both neutrinos and antineutrinos becomes too large to separate them. Instead a boosted decision tree has been newly introduced for this purpose. Finally, the MO sensitivity is currently statistically limited, such that reconstruction improvements aimed at increasing the size of the usable dataset are essential for this analysis. As discussed in detail below such improvements have resulted in a 20% increase in the available data set. The results of the latest oscillation analysis using all pure-water data are shown in Figure 16 with the best fit parameter valuse shown in Table 3. With these improvements the analysis indicates a NO preference of of between 78% and 96.7% for atmospheric mixing parameters allowed at the 90% confidence level. At the best fit of the analysis, which is consistent with worldwide measurements, the preference is 92.3%. Further, the updated analysis shows no strong preference for the octant of $\sin^2\theta_{23}$ and has a weak preference for a non-zero CP-violating phase. These results have now been published in Ref. [110].

Despite the successful introduction of neutron-tagged analysis samples to purify the atmospheric neutrino samples, uncertainties surrounding the number of neutrons produced in neutrino interactions hinder the oscillation measurements. Indeed, the presence of intranuclear hadronic interactions between a generated neutron and the surrounding nuclear medium (Final State Interactions, or FSI) as well as interactions between escaping hadrons and external nuclei (Secondary Interactions, or SI) can dramatically impact the number of observed neutrons. Energetic hadrons may produce additional neutrons or be absorbed during these processes. Data are lacking on these interactions, so currently it is not well known how much they impact the final observation. With SK's neutron tagging, however, it is now possible to measure in-situ the number of neutrons generated in atmospheric neutrino interactions as has been done in Figure 17. The data in-

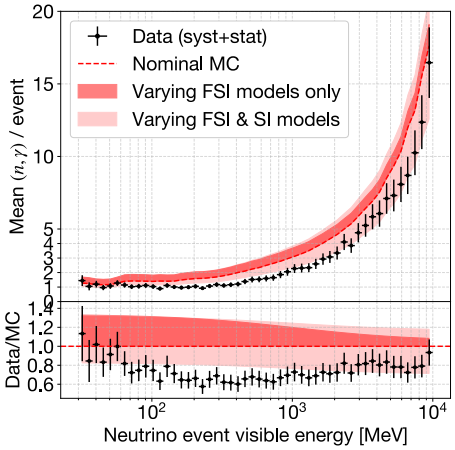

Fig. 17. Measured average neutron multiplicity as a function of visible energy for atmospheric neutrino interactions. Data are compared against a variety of FSI+SI models shown by the colored bands.

dicate clearly that modern models do not predict the neutron multiplicity well.

Smoking gun evidence for neutrino oscillations comes in the form of detecting the appearance of a neutron flavor amidst a pure beam of some other flavor. For the SK atmospheric neutrinos, such evidence comes in the form of ν_τ appearance in the detector. Indeed, the contribution of ν_τ to the atmospheric neutrino flux is negligible at energies probed by SK. Though few-GeV ν_μ (and below) oscillate most readily into ν_τ, their energy is often too small to overcome the τ lepton production threshold of ~ 3.5 GeV. As a result, many neutrinos that have oscillated into ν_τ escape unobserved and those with enough energy to interact produce complicated event topologies that must be extracted using a novel neural network technique. Despite these difficulties, using the entire purewater data set the ν_τ signal has now been observed at 4.8σ. Further, a flux-averaged measurement of the tau neutrino interaction cross section has been measured as $(0.94 \pm 0.2) \times 10^{-38}\mathrm{cm}^{-2}$[88].

Solar neutrino

By April 2024, we completed a precise analysis of solar neutrino oscillations using data from all periods of SK-IV observations and published a paper [111]. In this analysis, we used 2970 days of SK-IV data from October 2008 to May 2018, bringing the total solar neutrino observation time at SK to 5805 days. A new energy reconstruction method was developed and applied to reduce the uncertainty of solar neutrino observations, and a more efficient method to reduce spallation background events. With these improvements, we reduced the systematic error for solar neutrino flux from 2.2% in SK-III to 1.4% in SK-IV. The most accurate solar neutrino oscillation analysis results in SK were obtained.

As an example of the main results, figure 18 shows the annual average of solar neutrino fluxes observed in SK; no significant correlation between solar neutrino fluxes and sunspot numbers was found during the approximately 22-year observation period in SK. A more detailed analysis of the periodic

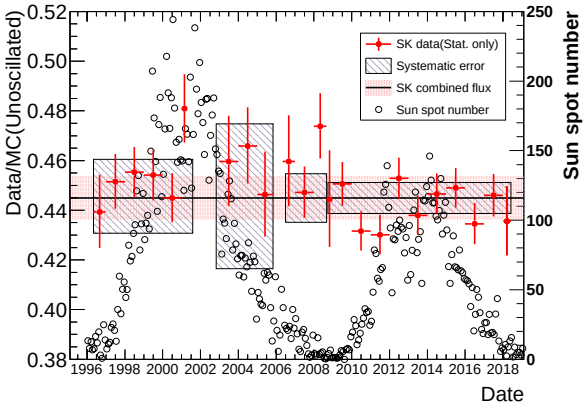

Fig. 18. Red plots are the observed annual average flux of solar neutrinos. White circles are the number of sunspots. The black-shaded region is the systematic uncertainty.

time variation of solar neutrino flux was also performed and no significant periodic modulation, except for the earth's orbit, was reported in a separate paper [113]. Figure 19 shows the results of the updated solar neutrino oscillation analysis. The restrictions on the solar neutrino oscillation parameters

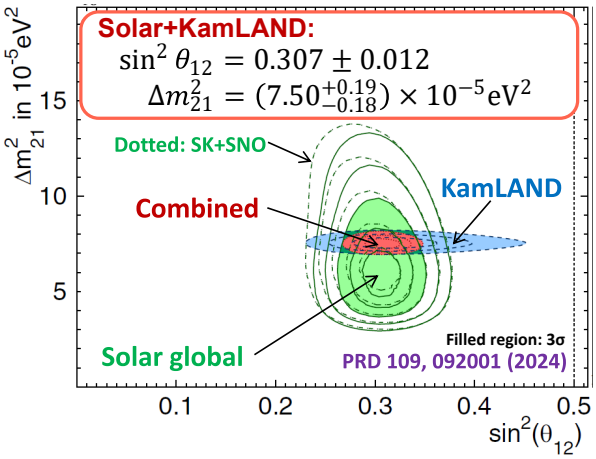

Fig. 19. Comparison of the oscillation parameter results from the solar neutrino experiment (green) with the KamLAND results (blue) and their combined results (red).

obtained in SK are particularly significant for θ_{12}, resulting in more accurate values of $\sin^2\theta_{12}$ than the value in the current Particle Data Group summary table. We also obtained the energy spectrum upturn which is expected from the matter effect in the Sun has been favored with 1.5 σ. In addition, the combined data of all SK phases give 3.2 σ of the day/night asymmetry which is expected from the matter effect of the earth. The apparent difference in Δm_{12} between the solar global and the KamLAND reactor result has been reduced to $\sim$1.5 σ level.

For SK-V, VI, and VII, we are verifying the quality of the low-energy observation data acquired so far and developing solar neutrino analysis tools for the SK-Gd phase. Figure 20 compares the solar neutrino signal and background levels between SK-IV and VII. In both phases, the observed solar neutrino fluxes are consistent with those observed in SK-IV, although the errors are large. In SK-V, the radon background was successfully reduced compared to SK-IV by precise water flow control in the SK detector, and in SK-VI and VII, the quality of the solar neutrino data above 6.49 MeV was confirmed to be comparable to that of SK-IV. In the future, we will analyze the solar neutrino oscillation including the solar neutrino data acquired after SK-V, especially to further improve the accuracy of the θ_{12} parameter.

Nucleon decay

Nucleon decay search gives us a unique window to test Grand Unified Theories (GUTs) of elementary particles. Super-Kamiokande (SK) is the world's largest detector to search for nucleon decays. Various nucleon decay modes have been searched for in SK, but no significant signal has been seen so far. The proton decay into one charged lepton and one neutral pion ($p \to e^+\pi^0$ and $p \to \mu^+\pi^0$) are the one that occurs in a large number of theoretical models.

Fit	Hierarchy	$\sin^2\theta_{23}$	$\lvert\Delta m^2_{32,31}\rvert$ [$\times 10^{-3}$ eV^2]	δ_{CP}	$\sin^2\theta_{13}$	$\delta\chi^2$ (IO-NO)
			ordering0.8pt			
SK only	NO	0.45	2.40	-1.89	0.020	–
	IO	0.48	2.40	-1.89	0.010	5.23
SK, θ_{13} constrained	NO	0.45	2.40	1.75	–	–
	IO	0.45	2.40	-1.75	–	5.69

Table 3. Best fit oscillation parameters obtained by the three flavor oscillation analysis. Fits are conducted for both the normal (NO) and inverted (IO) ordering assumptions The fit was performed assuming $\sin^2\theta_{13}$=0.0218, which is taken from the PDG.

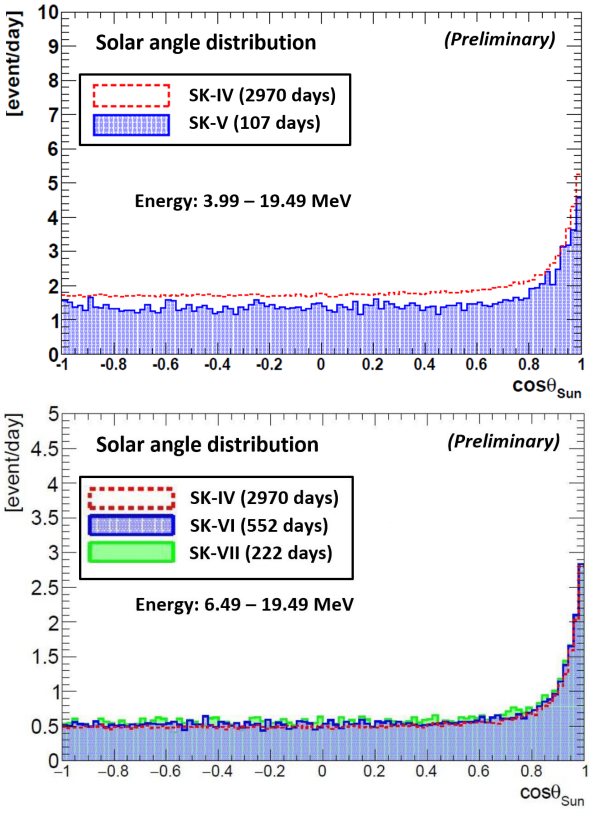

Fig. 20. Comparison of solar neutrino signal and background levels in SK-IV to VII. the peak near $\cos\theta_{\rm sun}$ is the solar neutrino signal and the background component is around -1 to 0.6.

To discriminate the signal from atmospheric neutrino background, we reconstruct the total invariant mass and total momentum corresponding to the parent proton mass and the proton's Fermi momentum in oxygen, respectively. The detector's fiducial volume is defined by using distance between the reconstructed vertex of the event and the nearest inner detector wall (dwall). After several careful check of external background like cosmic-ray muons or noise events from erroneous discharges in a PMT dinode, we decided to expand the fiducial volume for these modes from dwall $>$ 200 cm (22.5 kton) to dwall $>$ 100 cm (27.2 kton). We analyzed data from SK-I through SK-IV, in total 450kton·years. Figures 21 shows scatter plots of total invariant mass and total momentum for conventional and additional fiducial volume for $p \to e^+\pi^0$. As shown in Table 4, there were no candidate events observed for $p \to e^+\pi^0$ with 0.6 expected background. One event observed for $p \to \mu^+\pi^0$ but it is consistent with expected background (0.9 events). Thus we set lower limit of proton lifetime with 90% confidence level as 2.4×10^{34} and 1.6×10^{34} years for $p \to e^+\pi^0$ and $p \to \mu^+\pi^0$, respectively [95], which have exceeded the original goals written in the SK proposal.

$p \to \bar{\nu}K^+$ is also important because it is a dominant mode in SUSY-GUTs. In this mode, most of K^+ stops in water and decays into two particles, $\nu\mu^+$ or $\pi^+\pi^0$, which have monochromatic momentum and are back-to-back each other. For $K^+ \to \nu\mu^+$ case, we looked for single muon ring events with 236 MeV/c. Another important feature is that the remaining nuclei may emit de-excited gamma rays after the proton decay and this γ should be emitted before $K^+ \to \nu\mu^+$ (lifetime: 12 nsec). Thus we looked for the prompt gamma rays in the single muon ring sample. For $K^+ \to \pi^+\pi^0$, the momentum of charged pion is just above the Cherenkov threshold and it doesn't make clear Cherenkov ring. We searched for monochromatic π^0s which have PMT activities in the backward. Table 4 summarizes efficiencies and expected backgrounds for each methods. Search for $p \to \bar{\nu}K^+$ mode was carried out with 365kton·years data. We didn't find any proton decay candidates and calculated partial lifetime limits, taking into account systematic uncertainties. The obtained limits are 8.2×10^{33}years at 90% confidence level.

The another dominant decay mode which SUSY-GUTs predict is $p \to \mu^+K^0$ which is expected to have comparable, or even shorter lifetime of $p \to \bar{\nu}K^+$. We have analyzed this mode using data from SK-I to SK-III, and recently SK-IV data were added resulting 373 kton·year in total exposure. Furthermore, there was improvement in the event reconstruction algorithm. K^0 is a composite status of K^0_S and K^0_L. K^0_L has longer lifetime (51 nsec) and its decay products make another vertex far from the primary one. The conventional event reconstruction tool assumes one vertex per one event, thus the performance to reconstruct such multi-vertices events was poor. The new event reconstruction algorithm based on the maximum likelihood method enable to reconstruct muon from proton decay and decay products from K^0_L separately. The total observed events in SK-IV data was one, which was consistent with expected background, 3.1 events. By combining from SK-I to SK-IV, 3.6×10^{33} years was obtained for $p \to \mu^+K^0$ as a lower lifetime limit with 90% confidence level [103].

As described in above, still we don't observe major decay modes like $p \to e^+\pi^0$. If the usual lower dimensional operators responsible these modes are suppressed, then different proton decay channels can dominate from higher dimensional operators. This can naturally occur when considering lepton flavor symmetries. In this case, trilepton nucleon decay channels, such as $p \to \mu^-e^+e^-$ or $p \to e^-\mu^+\mu^+$ can be dominant. We searched for all combination of proton decays into three charged leptons with 373 kton·year data. Similar analy-

mode	exposure $(kt \cdot yr)$	εB_m (%)	observed event	B.G.	τ/B limit $(10^{34} yrs)$
$p \to e^+\pi^0$	450	36-39	0	0.6	2.4
$p \to \mu^+\pi^0$	450	30-37	1	0.9	1.6
$p \to \bar{\nu}K^+$	365				0.8
$-\mu^+$ spec.		31-37	–	–	
– prompt γ		7-9	0	0.4	
$-\pi^+\pi^0$		7-10	0	0.6	

Table 4. Summary of major nucleon decay search results in Super-Kamiokande.

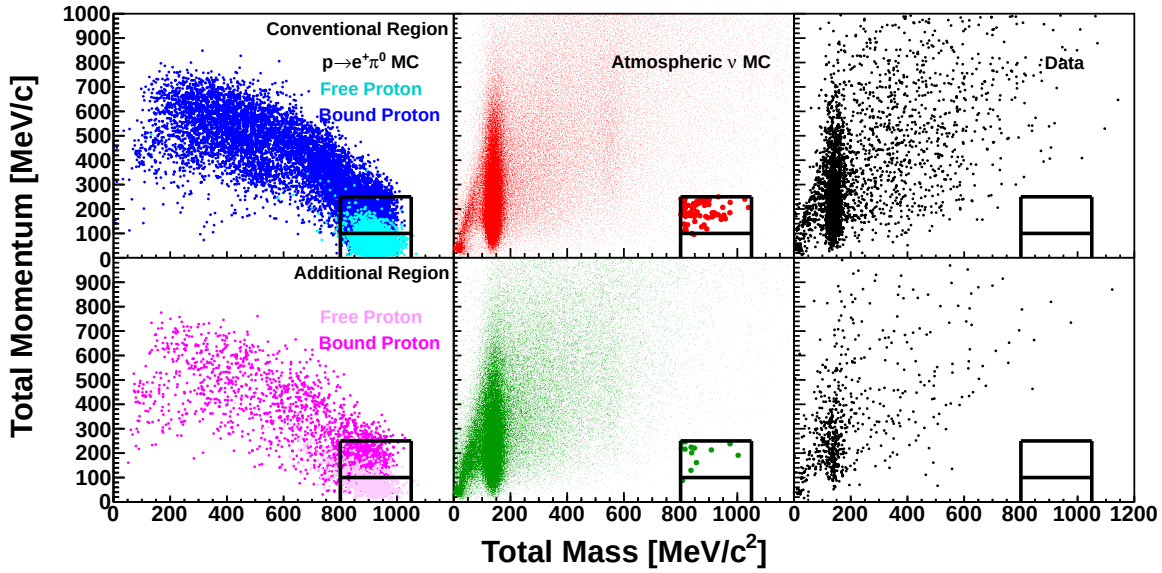

Fig. 21. Reconstructed total mass shown against the total momentum distributions for $p \to e^+\pi^0$ after all cut except those on these variables. The top panel shows the conventional (dwall $>$ 200 cm) and the bottom corresponds to additional (100 cm $<$ dwall $<$ 200 cm) fiducial volume. The left plots show the signal MC, where lighter colors show free protons and dark colors show bound protons. The middle panel show atmospheric neutrino MC. The right panel shows SK-I to SK-IV data. The boxes show signal regions.

sis method as $p \to e^+\pi^0$ was applied to events which has three Cherenkov rings. One candidate is observed in one e-like and two mu-like sample and three mu-like sample, but they were consistent with expected backgrounds. Obtained lower limits of proton lifetime range between (0.9 - 3.4) $\times 10^{34}$ years [93].

Super-Kamiokande also looked for the other various nucleon decay modes and Figure 22 shows summary of the lower limit of the nucleon lifetime. We have obtained the world's strongest nucleon lifetime limits for most of the modes.

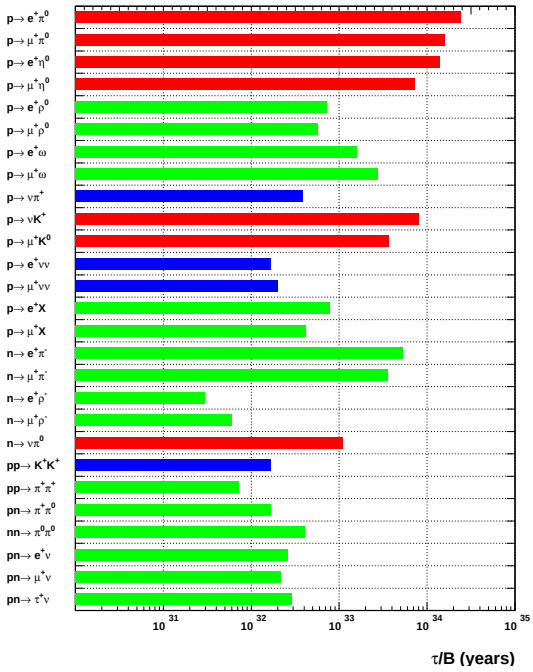

Fig. 22. Summary of lower limits of nucleon with 90% CL studied by Super-Kamiokande. Red color shows proton decay modes which were analyzed with more than 365kton· data and green are with 350kton· years data. Modes in blue color were results of SK I-III data.

Super-Kamiokande Collaboration

Spokesperson : Masayuki Nakahata (Kamioka Observatory, ICRR, The University of Tokyo)

Institute	Country	(*)
ICRR, Univ. of Tokyo	Japan	36
Boston Univ.	USA	4
California State Univ.	USA	1
Chonnam Univ.	Korea	5
Duke Univ.	USA	3
Ecole Polytechnique	France	8
Gifu Univ.	Japan	1
Gwangiu Institute of Science and Technology	Korea	1
IFIRSE	Viet Nam	1
ILANCE	France	3
Imperial College London	UK	5
INFN Sezione di Bari and Universite Politecnico di Bari	Italy	4
INFN Sezione di Napoli and Universite di Napoli	Italy	2
INFN Sezione di Padova and Universite di Padova	Italy	3
INFN Sezione di Roma and Universite La Sapienza	Italy	1
Institute for Basic Science	Korea	2
Keio Univ.	Japan	6
KEK	Japan	12
Kings College London	UK	8
Kobe Univ.	Japan	5
Kyoto Univ.	Japan	11
Miyagi Kyoiku Univ.	Japan	1
Nagoya Univ.	Japan	3
National Centre for Nuclear Research	Poland	4
Okayama Univ.	Japan	6
Osaka Electro-Communication Univ.	Japan	1
Rutherford Appleton Laboratory	UK	2
Seoul National Univ.	Korea	2
Shizuoka Univ. of Welfare	Japan	1
Stony Brook Univ.	USA	2
SungKyunKwan Univ.	Korea	4
Tohoku Univ.	Japan	2
Tokyo Institute of Technology	Japan	3
Tokyo Univ. of Science	Japan	6
TRIUMF.	Canada	7
Tsinghua University	China	5
Univ. of Autonoma Madrid	Spain	4
Univ. of California, Irvine	USA	8
Univ. of California, Davis	USA	1
Univ. of Glasgow	UK	2
Univ. of Hawaii	USA	1
Univ. of Minnesota	USA	1
Univ. of Liverpool	UK	3
Univ. of Oxford	UK	4
Univ. of Sheffield	UK	4
Univ. of Silesia	Poland	1
Univ. of Tokyo	Japan	7
Univ. of Tokyo, Kavli IPMU	Japan	8
Univ. of Toyama	Japan	1
Univ. of Warwick	UK	6
Univ. of Winnipeg	Canada	2
Yokohama National Univ.	Japan	5
Total		234

(*) Number of collaborators.

Members

Staff

Kamioka Observatory

Masato Shiozawa, Professor
Masayuki Nakahata Professor
Shigetaka Moriyama, Professor
Yoshinari Hayato, Assoc. Professor
Yasuhiro Kishimoto, Assoc. Professor (till Mar. 2019)
Hiroyuki Sekiya, Assoc. Professor
Shoei Nakayama, Assoc. Professor
Atsushi Takeda, Assoc. Professor (from Feb. 2020)
Atsushi Takeda, Research Associate (till Jan. 2020)
Yoichi Asaoka, Assoc. Professor (from Jun. 2023)
Katsuki Hiraide, Project Assoc. Professor (from May 2020)
Makoto Miura, Research Associate
Jun Kameda, Research Associate
Ko Abe, Research Associate
Motoyasu Ikeda, Research Associate
Yasuhiro Nakajima, Research Associate (till Mar. 2021)
Hidekazu Tanaka, Research Associate (from Feb. 2019)
Hidekazu Tanaka, Project Research Associate (till Jan. 2019)
Kei Ieki, Research Associate (from Nov. 2021)
Kei Ieki, Project Research Associate (Apr. 2021 - Oct. 2021)
Lluis Magro Marti, Project Research Associate (till Aug. 2020)
Koichi Ichimura, Project Research Associate (till Mar. 2019)
Yo Kato, Project Research Associate (till Mar. 2019)
Christophe Bronner, Project Research Associate (till Apr. 2022)
Christophe Bronner, Project Research Associate (from Apr. 2023)
Yosuke Kataoka, Research Associate (from Jun. 2020)
Yosuke Kataoka, Project Research Associate (till May 2020)
Takatomi Yano, Project Research Associate (from Dec. 2017)
Yasuhiro Takemomo, Project Research Associate (from Apr. 2019)
Guillaume Pronost, Project Research Associate (Jul. 2019 - Mar. 2022, from Apr. 2024)
Yuki Nakano, Project Research Associate (Sep. 2021 - Mar. 2024)
Kazufumi Sato, Project Research Associate (from Sep. 2021)
Keishi Hosokawa, Project Research Associate (from Sep. 2021)
Shunichi Mine, Project Academic Specialist (from Apr. 2022)

Research Center for Cosmic Neutrinos

Takaaki Kajita, Professor (till Mar. 2024)
Kimihiro Okumura, Assoc. Professor
Yasuhiro Nishimura, Research Associate (till Mar. 2019)
Takuya Tashiro, Project Research Associate (from Oct. 2019)

Institute for Comic Ray Research

Takaaki Kajita, Professor (from Apr. 2024)

Postdoctorial Fellows

Kamioka Observatory

Yuuki Nakano (till Mar. 2019)
Kazufumi Sato (till Mar. 2019)
Guillaume Pronost (till Jun. 2019)
Hiroshi Ito (Apr. 2019 - Mar. 2021)
Kiseki Nakmura (Apr. 2020 - Mar. 2021)
Yohei Noguchi (from Apr. 2022)
Seisho Abe (from Apr. 2023)
Masayuki Harada (from Apr. 2024)

Graduate students

Three students were awarded doctor degrees and thirteen students earned master degrees during 2018–2024, supervised by ICRR staff members.

Bibliography

Before Year 2018

[1] "Measurement of a small atmospheric ν_μ/ν_e ratio", Super-Kamiokande Collaboration (Y. Fukuda et al.), Phys. Lett. B **433**, 9 (1998), **Cited 997 times.**

[2] "Study of the atmospheric neutrino flux in the multi-GeV energy range", Super-Kamiokande Collaboration (Y. Fukuda et al.), Phys. Lett. B **436**, 33 (1998), **Cited 938 times.**

[3] "Measurements of the solar neutrino flux from Super-Kamiokande's first 300 days", Super-Kamiokande Collaboration (Y. Fukuda et al.), Phys. Rev. Lett. **81**, 1158 (1998) [Erratum-ibid. **81**, 4279 (1998)], **Cited 1087 times.**

[4] "Search for proton decay via $p \to e^+\pi^0$ in a large water Cherenkov detector", Super-Kamiokande Collaboration (M. Shiozawa et al.), Phys. Rev. Lett. **132**, 3319 (1998), **Cited 209 times.**

[5] "Evidence for oscillation of atmospheric neutrinos", Super-Kamiokande Collaboration (Y. Fukuda et al.), Phys. Rev. Lett. **81**, 1562 (1998), **Cited 8061 times.**

[6] "Calibration of Super-Kamiokande using an electron linac", Super-Kamiokande Collaboration (M. Nakahata et al.), Nucl. Instrum. Meth. A **421**, 113 (1999), **Cited 189 times.**

[7] "Constraints on neutrino oscillation parameters from the measurement of day-night solar neutrino fluxes at Super-Kamiokande", Super-Kamiokande Collaboration (Y. Fukuda et al.), Phys. Rev. Lett. **82**, 1810 (1999), **Cited 533 times.**

[8] "Measurement of the solar neutrino energy spectrum using neutrino electron scattering", Super-Kamiokande Collaboration (Y. Fukuda et al.), Phys. Rev. Lett. **82**, 2430 (1999), **Cited 553 times.**

[9] "Measurement of the flux and zenith-angle distribution of upward through-going muons by Super-Kamiokande", Super-Kamiokande Collaboration (Y. Fukuda et al.), Phys. Rev. Lett. **82**, 2644 (1999), **Cited 930 times.**

[10] "Observation of the east-west anisotropy of the atmospheric neutrino flux", Super-Kamiokande Collaboration (Y. Futagami et al.), Phys. Rev. Lett. **82**, 5194 (1999), **Cited 133 times.**

[11] "Search for proton decay through $p \to \bar{\nu}K^+$ in a large water Cherenkov detector", Super-Kamiokande Collaboration (Y. Hayato et al.), Phys. Rev. Lett. **83**, 1529 (1999), **Cited 202 times.**

[12] "Neutrino-induced upward stopping muons in Super-Kamiokande", Super-Kamiokande Collaboration (Y. Fukuda et al.), Phys. Lett. B **467**, 185 (1999), **Cited 320 times.**

[13] "N-16 as a calibration source for Super-Kamiokande", Super-Kamiokande Collaboration (E. Blaufuss et al.), Nucl. Instrum. Meth. A **458**, 638 (2001), **Cited 58 times.**

[14] "Tau neutrinos favored over sterile neutrinos in atmospheric muon-neutrino oscillations", Super-Kamiokande Collaboration (S. Fukuda et al.), Phys. Rev. Lett. **85**, 3999 (2000), **Cited 992 times.**

[15] "Detection of accelerator produced neutrinos at a distance of 250-km", K2K Collaboration (S.H. Ahn et al.), Phys. Lett. B **511**, 178 (2001), **Cited 394 times.**

[16] "Solar B-8 and hep neutrino measurements from 1258 days of Super-Kamiokande data", Super-Kamiokande Collaboration (S. Fukuda et al.), Phys. Rev. Lett. **86**, 5651 (2001), **Cited 1484 times.**

[17] "Constraints on neutrino oscillations using 1258 days of Super-kamiokande solar neutrino data", Super-Kamiokande Collaboration (S. Fukuda et al.), Phys. Rev. Lett. **86**, 5656 (2001), **Cited 919 times.**

[18] "Search for neutrinos from gamma-ray bursts using Super-Kamiokande", Super-Kamiokande Collaboration (S. Fukuda et al.), Astrophys. J. **578**, 317 (2002), **Cited 48 times.**

[19] "Determination of solar neutrino oscillation parameters using 1496 days of Super-Kamiokande I data", Super-Kamiokande Collaboration (S. Fukuda et al.), Phys. Lett. B **539**, 179 (2002), **Cited 1141 times.**

[20] "Search for supernova relic neutrinos at Super-Kamiokande", Super-Kamiokande Collaboration (M. Malek et al.) , Phys. Rev. Lett. **90**, 061101 2003), **Cited 287 times.**

[21] "Indications of neutrino oscillation in a 250 km long baseline experiment", K2K Collaboration (M.H. Ahn et al.), Phys. Rev. Lett. **90**, 041801 (2003), **Cited 1330 times.**

[22] "Search for anti-nu(e) from the sun at Super-Kamiokande I", Super-Kamiokande Collaboration (Y. Gando et al.), Phys. Rev. Lett. **90**, 171302 (2003), **Cited 82 times.**

[23] "The Super-Kamiokande detector", Super-Kamiokandecollaboration (Y. Fukuda et al.), Nucl. Instrum. Meth. A **501**, 418 (2003), **Cited 1182 times.**

[24] "Development of super-high sensitivity radon detector for the Super-Kamiokande detector", C. Mitsuda, T. Kajita, K. Miyano, S. Moriyama, M. Nakahata, Y. Takeuchi, S. Tasaka, Nucl. Instrum. Meth. A **497**, 414 (2003), **Cited 37 times.**.

[25] "A search for periodic modulations of the solar neutrino flux in Super-Kamiokande I", Super-Kamiokande Collaboration (J. Yoo et al.), Phys. Rev. D **68**, 092002 (2003), **Cited 102 times.**

[26] "Precise measurement of the solar neutrino day / night and seasonal variation in Super-Kamiokande-1", Super-Kamiokande Collaboration (M.B. Smy et al.), Phys. Rev. D **69**, 011104 (2004), **Cited 318 times.**

[27] "Limits on the neutrino magnetic moment using 1496 days of Super-Kamiokande-I solar neutrino data", Super-Kamiokande Collaboration (D.W. Liu et al.), Phys. Rev. Lett. **93**, 021802 (2004), **Cited 102 times.**

[28] "Search for electron neutrino appearance in a 250 km long baseline experiment", K2K Collaboration (M.H. Ahn et al.), Phys. Rev. Lett. **93**, 051801 (2004), **Cited 102 times.**

[29] "Search for dark matter wimps using upward through-going muons in Super-Kamiokande", Super-Kamiokande Collaboration (S. Desai et al.), Phys. Rev. D **70** 083523 (2004) [Erratum-ibid. D **70** 109901 (2004)], **Cited 465 times.**

[30] "Evidence for an oscillatory signature in atmospheric neutrino oscillation", Super-Kamiokande Collaboration (Y. Ashie et al.), Phys. Rev. Lett. 93: 101801, 2004, **Cited 1086 times.**

[31] "Measurement of single pi0 production in neutral current neutrino interactions with water by a 1.3-GeV wide band muon neutrino beam", K2K Collaboration (S. Nakayama et al.), Phys. Lett. B **61**, 255 (2005), **Cited 128 times.**

[32] "Evidence for muon neutrino oscillation in an accelerator-based experiment", K2K Collaboration (E. Aliu et al.), Phys. Rev. Lett. **94** 081802 (2005), **Cited 640 times.**

[33] "A measurement of atmospheric neutrino oscillation parameters by Super-Kamiokande I", Super-Kamiokande Collaboration (Y. Ashie et al.) et al., Phys. Rev. D71: 112005, 2005, **Cited 1258 times.**

[34] "Search for nucleon decay via modes favored by supersymmetric grand unification models in Super-Kamiokande-I", Super-Kamiokande Collaboration (K. Kobayashi et al.), Phys. Rev. D **72**, 052007 (2005), **Cited 181 times.**

[35] "An improved search for $\nu_\mu \to \nu_e$ oscillation in a long-baseline accelerator experiment", K2K Collaboration (S. Yamamoto et al.), Phys. Rev. Lett. **96**, 181801 (2006), **Cited 105 times.**

[36] "Measurement of Neutrino Oscillation by the K2K Experiment", K2K Collaboration (M. H. Ahn et al.), Phys. Rev. D **74** 072003 (2006), **Cited 1275 times.**

[37] "Observation of the Anisotropy of 10 TeV Primary Cosmic Ray Nuclei Flux with the Super-Kamiokande-I Detector", The Super-Kamiokande Collaboration (G. Guillian et al.), Phys. Rev. D **75**, 062003 (2007), **Cited 196 times.**

[38] "Solar neutrino measurements in Super-Kamiokande-I", The Super-Kamiokande Collaboration (J. Hosaka et al.), Phys. Rev. D **73**, 112001 (2006), **Cited 756 times.**

[39] "Three flavor neutrino oscillation analysis of atmospheric neutrinos in Super-Kamiokande", The Super-Kamiokande Collaboration (J. Hosaka et al.), Phys. Rev. D **74**, 032002 (2006), **Cited 286 times.**

[40] "Search for Diffuse Astrophysical Neutrino Flux Using Ultra-High Energy Upward-Going Muons in Super-Kamiokande I", The Super-Kamiokande Collaboration (M. E. C. Swanson et al.), Astrophys.J. **652** 206 (2006), **Cited 26 times.**

[41] "High energy neutrino astronomy using upward-going muons in Super-Kamiokande-I", The Super-Kamiokande Collaboration (K. Abe et al.), Astrophys.J. **652**, 198 (2006), **Cited 37 times.**

[42] "A Measurement of Atmospheric Neutrino Flux Consistent with Tau Neutrino Appearance", The Super-Kamiokande Collaboration (K. Abe et al.), Phys. Rev. Lett. **97**, 171801 (2006), **Cited 184 times.**

[43] "Search for Neutral Q-balls in Super-Kamiokande II", The Super-Kamiokande Collaboration (T. Takenaga et al.), Phys. Lett. B **647**, 18 (2007), **Cited 49 times.**

[44] "Search for Supernova Neutrino Bursts at Super-Kamiokande", The Super-Kamiokande Collaboration (M. Ikeda et al.), Astrophys J. **669**, (2007) 519, **Cited 195 times.**

[45] "Study of TeV Neutrinos with Upward Showering Muons in Super-Kamiokande", The Super-Kamiokande Collaboration (S. Desai et al.), Astropart. Phys. **29**, 42 (2008), **Cited 82 times.**

[46] "Search for Matter-Dependent Atmospheric Neutrino Oscillations in Super-Kamiokande", The Super-Kamiokande Collaboration (K. Abe et al.), Phys. Rev. D **77**, 052001 (2008), **Cited 28 times.**

[47] "Solar neutrino measurements in Super-Kamiokande-II", The Super-Kamiokande Collaboration (J. P. Cravens), Phys. Rev. D **78**, 032002 (2008), **Cited 431 times.**

[48] "First Study of Neutron Tagging with a Water Cherenkov Detector", The Super-Kamiokande Collaboration (H. Watanabe et al.), Astropart. Phys. **31**, 320 (2009), **Cited 141 times.**

[49] "Search for Proton Decay via $p \to e^+\pi^0$ and $p \to \mu^+\pi^0$ in a Large Water Cherenkov Detector", The Super-Kamiokande Collaboration (H. Nishino et al.), Phys. Rev. Lett. **102**, 141801 (2009), **Cited 291 times.**

[50] "Kinematic reconstruction of atmospheric neutrino events in a large water Cherenkov detector with proton identification", The Super-Kamiokande Collaboration (M. Fechner et al.), Phys. Rev. D **79**, 112010 (2009), **Cited 36 times.**

[51] "Search for Neutrinos from GRB 080319B at Super-Kamiokande", The Super-Kamiokande Collaboration (E. Thrane et al.), Astophys. J. **697**, 730 (2009), **Cited 11 times.**

[52] "Search for Astrophysical Neutrino Point Sources at Super-Kamiokande", The Super-Kamiokande Collaboration (E. Thrane et al.), Astrophys. J. **704**, 503 (2009), **Cited 50 times.**

[53] "Atmospheric neutrino oscillation analysis with subleading effects in Super-Kamiokande I, II and III", The Super-Kamiokande Collaboration (R. Wendell et al.), Phys. Rev. D **81**, 092004 (2010), **Cited 410 times.**

[54] "Solar neutrino results in Super-Kamiokande-III", The Super-Kamiokande Collaboration (K. Abe et al.), Phys. Rev. D **83**, 052010 (2011), **Cited 569 times.**

[55] "Study of Non-Standard Neutrino Interactions with Atmospheric Neutrino Data in Super-Kamiokande I and II", The Super-Kamiokande Collaboration (G. Mitsuka et al.), Phys. Rev. D **84**, 113008 (2011), **Cited 141 times.**

[56] "An Indirect Search for WIMPs in the Sun using 3109.6 days of upward-going muons in Super-Kamiokande", The Super-Kamiokande Collaboration (T. Tanaka et al.), Astrophys. J. **742**, 78 (2011), **Cited 233 times.**

[57] "Search for Differences in Oscillation Parameters for Atmospheric Neutrinos and Antineutrinos at Super-Kamiokande", The Super-Kamiokande Collaboration (K. Abe et al.), Phys. Rev. Lett. **107**, 241801 (2011), **Cited 127 times.**

[58] "Supernova Relic Neutrino Search at Super-Kamiokande", Super-Kamiokande Collaboration (K. Bays et al.), Phys. Rev. D. **85**, 052007 (2012), **Cited 268 times.**

[59] "Search for Nucleon Decay into Charged Anti-lepton plus Meson in Super-Kamiokande I and II", The Super-Kamiokande Collaboration (H. Nishino et al.), Phys. Rev. D. **85**, 112001 (2012), **Cited 150 times.**

[60] "Search for GUT monopoles at Super-Kamiokande", The Super-Kamiokande Collaboration (K. Ueno et al.), Astropart. Phys. **36**, 121 (2012), **Cited 46 times.**

[61] "Search for proton decay via $p \to \mu + K^0$ in Super-Kamiokande I, II, and III", Super-Kamiokande Collaboration (C. Regis et al.), Phys. Rev. D. **86**, 012006 (2012), **Cited 94 times.**

[62] "Search for Nucleon Decay into Charged Anti-lepton plus Meson in Super-Kamiokande I and II (H. Nishino et al.)", Phys. Rev. D **85**, 112001 (2012), **Cited 150 times.**

[63] "Evidence for the Appearance of Atmospheric Tau Neutrinos in Super-Kamiokande", Super-Kamiokande Collaboration (K. Abe et al.), Phys. Rev. Lett. **110**, 181802 (2013), **Cited 172 times.**

[64] "Calibration of the Super-Kamiokande Detector", Super-Kamiokande Collaboration (K. Abe et al.), Nucl. Instrum. Meth. A **737**, 253 (2014), **Cited 75 times.**

[65] "First Indication of Terrestrial Matter Effects on Solar Neutrino Oscillation", Super-Kamiokande Collaboration (A. Renshaw et al.), Phys. Rev. Lett. **112**, 091805 (2014), **Cited 139 times.**

[66] "Search for Dinucleon Decay into Kaons in Super-Kamiokande", Super-Kamiokande Collaboration (M. Litos et al.), Phys. Rev. Lett. **112**, 131803 (2014), **Cited 36 times.**

[67] "Search for Nucleon Decay via $n \to \nu\pi^0$ and $p \to \nu\pi^0$ in Super-Kamiokande", Super-Kamiokande Collaboration (K. Abe et al.), Phys. Rev. Lett. **113**, 121802 (2014), **Cited 98 times.**

[68] "Search for Trilepton Nucleon Decay via $p \to e + \nu\nu$ and $p \to \mu + \nu\nu$ in the Super-Kamiokande Experiment", Super-Kamiokande Collaboration (V. Takhistov et al.), Phys. Rev. Lett. **113**, 101801 (2014), **Cited 36 times.**

[69] "Search for proton decay via $p \to \nu K^+$ using using 260 kiloton · year data of Super-Kamiokande", Super-Kamiokande Collaboration (K. Abe et al.), Phys. Rev. D **90**, 072005 (2014), **Cited 237 times.**

[70] "Supernova Relic Neutrino Search with Neutron Tagging at Super-Kamiokande-IV", Super-Kamiokande Collaboration (H. Zhang et al.), Astropart. Phys. **60**, 41 (2015), **Cited 155 times.**

[71] "Test of Lorentz invariance with atmospheric neutrinos", Super-Kamiokande Collaboration (K. Abe et al.), Phys. Rev. D **91**, 052003 (2015), **Cited 109 times.**

[72] "Limits on sterile neutrino mixing using atmospheric neutrinos in Super-Kamiokande", Super-Kamiokande Collaboration (K. Abe et al.), Phys. Rev. D **91**, 052019 (2015), **Cited 198 times.**

[73] "Search for Neutrinos from Annihilation of Captured Low-Mass Dark Matter Particles in the Sun by Super-Kamiokande", Super-Kamiokande Collaboration (K. Choi et al.), Phys. Rev. Lett. **114**, 141301 (2015), **Cited 368 times.**

[74] "Search for n - nbar oscillation in Super-Kamiokande", Super-Kamiokande Collaboration (K. Abe et al.), Phys. Rev. D **91**, 072006 (2015), **Cited 163 times.**

[75] "Search for dinucleon decay into pions at Super-Kamiokande", Super-Kamiokande Collaboration (J. Gustafson et al.), Phys. Rev. D **91**, 072009 (2015), **Cited 50 times.**

[76] "Search for Nucleon and DiNucleon Decays with an Invisible Particle and a Charged Lepton in the Final State at the Super-Kamiokande Experiment", Super-Kamiokande Collaboration (V. Takhistov et al.), Phys. Rev. Lett. **115**, 121803 (2015), **Cited 41 times.**

[77] "First measurement of radioactive isotope production through cosmic-ray muon spallation in Super-Kamiokande IV", Super-Kamiokande Collaboration (Y. Zhang et al.), Phys. Rev. D **93**, 012004 (2016), **Cited 74 times.**

[78] "Real-Time Supernova Neutrino Burst Monitor at Super-Kamiokande", Super-Kamiokande Collaboration (K. Abe et al.), Astropart. Phys. **81**, 39 (2016), **Cited 94 times.**

[79] "Solar Neutrino Measurements in Super-Kamiokande-IV", Super-Kamiokande Collaboration (K. Abe et al.), Phys. Rev. D **94**, 052010 (2016), **Cited 410 times.**

[80] "Measurements of the atmospheric neutrino flux by Super-Kamiokande: Energy spectra, geomagnetic effects, and solar modulation", Super-Kamiokande Collaboration (E. Richard et al.), Phys. Rev. D **94**, 052001 (2016), **Cited 156 times.**

[81] "Search for Neutrinos in Super-Kamiokande associated with Gravitational Wave Events GW150914 and GW151226", Super-Kamiokande Collaboration (K. Abe et al.), Astrophys. J. Lett. **830**, 1 (2016), **Cited 44 times.**

[82] "Search for proton decay via $p \to e + \pi^0$ and $p \to \mu + \pi^0$ in 0.31Megaton·years exposure of the Super-Kamiokande water Cherenkov detector", Super-Kamiokande Collaboration (K. Abe et al.), Phys. Rev. D **95**, 012004 (2017), **Cited 318 times.**

[83] "Search for nucleon decay into charged antilepton plus meson in 0.316 megaton·years exposure of the Super-Kamiokande water Cherenkov detector", Super-Kamiokande Collaboration (K. Abe et al.), Phys. Rev. D **96**, 012003 (2017), **Cited 57 times.**

[84] "Search for an Excess of Events in the Super-Kamiokande Detector in the Directions of the Astrophysical Neutrinos Reported by the IceCube Collaboration", Super-Kamiokande Collaboration (K. Abe et al.), Astrophys. J. **850**, 166 (2017), **Cited 9 times.**

[85] "Atmospheric neutrino oscillation analysis with external constraints in Super-Kamiokande I-IV", Super-Kamiokande Collaboration (K. Abe et al.), Phys. Rev. D **97**, 072001 (2018), **Cited 318 times.**

[86] "Search for Neutrinos in Super-Kamiokande associated with the GW170817 neutron-star merger", Super-Kamiokande Collaboration (K. Abe et al.), Astrophys. J. Lett. **857**, L4 (2018), **Cited 54 times.**

[87] "Search for Boosted Dark Matter Interacting With Electrons in Super-Kamiokande", Super-Kamiokande Collaboration (C. Kachulis et al.), Phys. Rev. Lett. **120**, 221301 (2018), **Cited 71 times.**

After Year 2018

[88] "Measurement of the tau neutrino cross section in atmospheric neutrino oscillations with Super-Kamiokande", Super-Kamiokande Collaboration (Z. Li et al.), Phys. Rev. D **98**, 052006 (2018), **Cited 97 times.**

[89] "Atmospheric Neutrino Oscillation Analysis With Improved Event Reconstruction in Super-Kamiokande IV", Super-Kamiokande Collaboration (M. Jiang et al.), Prog. Theor. Exp. Phys. **2019**, 053F01 (2019), **Cited 92 times.**

[90] "Measurement of the neutrino-oxygen neutral-current quasielastic cross section using atmospheric neutrinos at Super-Kamiokande", Super-Kamiokande Collaboration (L. Wan et al.), Phys. Rev. D **99**, 032005 (2019), **Cited 30 times.**

[91] "Sensitivity of Super-Kamiokande with Gadolinium to Low Energy Antineutrinos from Pre-supernova Emission", Super-Kamiokande Collaboration (C. Simpson et al.), Astrophys. J. **885**, 133 (2019), **Cited 47 times.**

[92] "Search for Astronomical Neutrinos from Blazar TXS0506+056 in Super-Kamiokande", Super-Kamiokande Collaboration (K. Hagiwara et al.), Astrophys. J. Lett. **887**, L6 (2019), **Cited 7 times.**

[93] "Search for proton decay into three charged leptons in 0.37 megaton-years exposure of the Super-Kamiokande", Super-Kamiokande Collaboration (M. Tanaka et al.), Phys. Rev. D **101**, 052011 (2020), **Cited 24 times.**

[94] "Indirect search for dark matter from the Galactic Center and halo with the Super-Kamiokande detector", Super-Kamiokande Collaboration (K. Abe et al.), Phys. Rev. D **102**, 072002 (2020), **Cited 50 times.**

[95] "Search for proton decay via $p \to e + \pi^0$ and $p \to \mu + \pi^0$ with an enlarged fiducial volume in Super-Kamiokande I-IV", Super-Kamiokande Collaboration (A. Takenaka et al.), Phys. Rev. D **102**, 112011 (2020), **Cited 124 times.**

[96] "Neutron-Antineutron Oscillation Search using a 0.37 Megaton·Year Exposure of Super-Kamiokande", Super-Kamiokande Collaboration (K. Abe et al.), Phys. Rev. D **103**, 012008 (2021), **Cited 44 times.**

[97] "Search for neutrinos in coincidence with gravitational wave events from the LIGO-Virgo O3a Observing Run with the Super-Kamiokande detector", Super-Kamiokande Collaboration (K. Abe et al.), Astrophys. J. **918**, 78 (2021), **Cited 21 times.**

[98] "Search for Tens of MeV Neutrinos associated with Gamma-Ray Bursts in Super-Kamiokande", Super-Kamiokande Collaboration (A. Orii et al.), Prog. Theor. Exp. Phys. **2021**, 103F01 (2021), **Cited 3 times.**

[99] "Diffuse supernova neutrino background search at Super-Kamiokande", Super-Kamiokande Collaboration (K. Abe et al.), Phys. Rev. D **104**, 122002 (2021), **Cited 100 times.**

[100] "First Gadolinium Loading to Super-Kamiokande", Super-Kamiokande Collaboration (K. Abe et al.), Nucl. Instrum. Meth. A **1027**, 166248 (2022), **Cited 102 times.**

[101] "Search for solar electron antineutrinos due to spin-flavor precession in the Sun with Super-Kamiokande-IV", Super-Kamiokande Collaboration (K. Abe et al.), Astropart. Phys. **139**, 102702 (2022), **Cited 14 times.**

[102] "Pre-supernova Alert System for Super-Kamiokande", Super-Kamiokande Collaboration (L. N. Machado et al.), Astrophys. J. **935**, 40 (2022), **Cited 12 times.**

[103] "Search for proton decay via $p \to \mu + K^0$ in 0.37 megaton-years exposure of Super-Kamiokande", Super-Kamiokande Collaboration (R. Matsumoto et al.), Phys. Rev. D **106**, 072003 (2022), **Cited 24 times.**

[104] "Searching for Supernova Bursts in Super-Kamiokande IV", Super-Kamiokande Collaboration (M. Mori et al.), Astrophys. J. **938**, 35 (2022), **Cited 9 times.**

[105] "Neutron tagging following atmospheric neutrino events in a water Cherenkov detector", Super-Kamiokande Collaboration (K. Abe et al.), JINST **17**, P10029 (2022), **Cited 8 times.**

[106] "Search for Cosmic-Ray Boosted Sub-GeV Dark Matter Using Recoil Protons at Super-Kamiokande", Super-Kamiokande Collaboration (K. Abe et al.), Phys. Rev. Lett. **130**, 031802 (2023), **Cited 28 times.**

[107] "Measurement of the cosmogenic neutron yield in Super-Kamiokande with gadolinium loaded water", Super-Kamiokande Collaboration (K. Abe et al.), Phys. Rev. D **107**, 092009 (2023), **Cited 7 times.**

[108] "Search for astrophysical electron antineutrinos in Super-Kamiokande with 0.01wt% gadolinium-loaded water", Super-Kamiokande Collaboration (M. Harada et al.), Astrophys. J. Lett. **951**, L27 (2023), **Cited 31 times.**

[109] "Measurement of the neutrino-oxygen neutral-current quasielastic cross section using atmospheric neutrinos in the SK-Gd experiment", Super-Kamiokande Collaboration (S. Sakai et al.), Phys. Rev. D **109**, L011101 (2023), **Cited 3 times.**

[110] “Atmospheric neutrino oscillation analysis with neutron tagging and an expanded fiducial volume in Super-Kamiokande I–V”, Super-Kamiokande Collaboration (T. Wester et al.), Phys. Rev. D **109**, 072014 (2024), **Cited 9 times.**

[111] “Solar neutrino measurements using the full data period of Super-Kamiokande-IV”, Super-Kamiokande Collaboration (K. Abe et al.), Phys. Rev. D **109**, 092001 (2024), **Cited 8 times.**

[112] “Second Gadolinium Loading to Super-Kamiokande”, Super-Kamiokande Collaboration (K. Abe et al.), Nucl. Instrum. Meth. A **1065**, 169480 (2024), **Cited 2 times.**

[113] “Search for Periodic Time Variations of the Solar ^{8}B Neutrino Flux between 1996 and 2018 in Super-Kamiokande”, Super-Kamiokande Collaboration (K. Abe et al.), Phys. Rev. D **132**, 241803 (2024).

[114] “Supernova Neutrino Light Curves and Spectra for Various Progenitor Stars: From Core Collapse to Proto-neutron Star Cooling”, K. Nakazato, K. Sumiyoshi, H. Suzuki, T. Totani, H. Umeda, and S. Yamada, Astrophys. J. Supp. 205 (2013) 2

[115] https://gcn.nasa.gov/notices

[116] “Real-Time Supernova Neutrino Burst Monitor at Super-Kamiokande”, Super-Kamiokande Collaboration (K. Abe et al.), Astropart. Phys. 81 (2016) 39-48

[117] “Performance of SK-Gd’s Upgraded Real-time Supernova Monitoring System”, Super-Kamiokande Collaboration (Y. Kashiwagi et al.), Accepted by Ap. J. (2024)

[118] “HEALPix: A Framework for High-Resolution Discretization and Fast Analysis of Data Distributed on the Sphere”, K.M. Gorski et al., The Astrophysical Journal, Volume 622, Issue 2, pp. 759-771 (2005).

[119] https://www.lowbg.org/presnalarm/

T2K EXPERIMENT

Summary from 2018 to 2024

We first summarize the results and achievements obtained during the review period. The most significant ones will be described in more detail in the following sections.

- T2K released improved constraints on the CP-violating parameter, δ_{CP}, and atmospheric parameters, θ_{23} and Δm^2_{32}, using a new data set and improved analysis method [29, 35, 41, 42, 45, 48]. The results of θ_{23} and Δm^2_{32} are among the world's most precise measurements to date. The data prefers near maximum CP-violation at $\delta_{CP} \sim -\pi/2$, while CP-conserving values are still within the 2σ interval.

- We also conducted many cross-section measurements using both near and far detectors. These include many ν_μ and $\overline{\nu_\mu}$ charged current interaction measurements at the near detectors [27, 28, 34, 37, 38, 39, 40, 43, 46, 47], neutral current interaction measurements at the near detector [26, 31]. We also conducted cross-section measurements using the data at the far detector, Super-Kamiokande; a measurement of neutral-current interactions [33] and measurement of neutron multiplicity from ν_μ and $\overline{\nu_\mu}$ charged-current interactions.

- We conducted two joint oscillation analyses using data collected by different experimental collaborations for the first time: An analysis using Super-K's atmospheric neutrino data and T2K's beam data [49] and an analysis using data from the NOvA and the T2K experiments[1].

- T2K also performed searches for physics beyond the standard model other than the neutrino oscillation studies. Heavy neutrinos were searched using the near detector data [32]. We also searched for neutrino oscillation into sterile neutrinos using the data at Super-Kamiokande [30].

- Significant upgrades on the J-PARC proton accelerator, neutrino beamline, T2K near detector, and Super-Kamiokande were conducted. The beam repetition cycle was shortened from 2.48 s to 1.36 s, and a stable operation at more than 800 kW beam power was achieved. In the neutrino beamline, the power supply for the magnetic horn was upgraded, and the horn current was increased from 250 kA to 320 kA. This increased neutrino flux by $\sim$10%. Various beam monitors were also upgraded. The near detector complex, ND280, was also significantly enhanced in 2023-2024 with a newly constructed Super Fine-Grained-Detector and new time-projection chambers. They allow us to measure neutrino interaction at a much higher precision and larger phase space. Finally, Gadolinium was introduced to Super-Kamiokande in 2020 and 2022, which significantly enhanced neutron detection capability.

Introduction

The Tokai to Kamioka (T2K) experiment [1] is a long baseline neutrino oscillation experiment: a man-made beam of neutrinos is used to do precise studies of the oscillations of neutrinos. Accelerated protons are used to produce the neutrino beam in the J-PARC center in the Ibaraki prefecture, which then travels 295 km to reach the Super-Kamiokande (Super-K) detector in the Gifu prefecture where neutrinos can be detected after oscillations. A complex of near detectors located 280 meters away from the proton target is used to monitor the neutrino beam and constrain systematic uncertainties on the neutrino fluxes and interactions. T2K was the first long baseline experiment to use the off-axis beam technique [2]: the beam is not aimed directly at Super-K but in a direction making a 2.5° angle with the far detector direction. This gives increased sensitivity to neutrino oscillations while reducing the backgrounds by producing a narrow band neutrino beam centered on the energy corresponding to the first maximum of the $\nu_\mu \to \nu_e$ oscillation probability.

The initial physics goal of the experiment is to observe this $\nu_\mu \to \nu_e$ oscillation by detecting electron neutrinos in a beam of neutrinos produced in the muon flavor. This observation would confirm the paradigm of neutrino oscillations by observing for the first time the appearance of neutrinos of a certain flavor through oscillation and allow to measure the last unknown mixing angle at the time of the start of the experiment, θ_{13}. At the same time, T2K can produce precise measurements of the atmospheric parameters θ_{23} and Δm^2_{32} through the precise study of the pattern of the disappearance of the muon neutrinos.

After the appearance of electron neutrinos $\nu_\mu \to \nu_e$ has been observed, the experiment can use its ability to produce a beam of either neutrinos or anti-neutrinos to compare the oscillations of neutrinos and their antiparticles. This allows us to study the main remaining open questions in neutrino oscillations (CP symmetry and ordering of the neutrino mass states) by looking at the differences between the oscillations $\nu_\mu \to \nu_e$ and $\bar{\nu}_\mu \to \bar{\nu}_e$. The experiment can also perform searches for physics beyond the standard model (sterile neutrinos, CPT violation). Finally, the near detectors allow to do a wide range of neutrino and anti-neutrino cross-section measurements.

Experimental apparatus

In J-PARC, protons are accelerated to 30 GeV by a series of three accelerators and hit a 1.9 interaction-length graphite

*1 E. Atkin (on behalf of the T2K and NOvA collaborations), Results from the T2K+NOvA Joint Analysis, KEK seminar Feb. 16th, 2024

*2 D. Beavis, A. Carroll, I. Chiang, *et al.*, Long Baseline Neutrino Oscillation Experiment at the AGS (Proposal E889),1995. Physics Design Report, BNL 52459.

target. The collisions produce hadrons, in particular charged pions and kaons, which are focused by three electromagnetic horns. The hadrons then go through a 96 m-long decay tunnel where they decay in flight into neutrinos. A beam dump at the end of the decay tunnel stops the remaining hadrons, while high energy muons (5 GeV/c or higher) can pass through this beam dump and are measured to provide a first indirect monitoring of the neutrino beam. The horns can be used either with a positive current (ν-mode), in which case the beam is mainly made of ν_μ, or with a negative current ($\bar{\nu}$-mode) which gives a mainly $\bar{\nu}_\mu$ beam.

The near detectors are separated into two groups. On the axis of the beam, the INGRID detector, made of fourteen identical modules, is used to monitor the beam direction and rate stability. Each module is made of a succession of iron plates to provide a large target mass ($\sim$7.1 tons per module) and scintillator planes for detection. Using the number of events reconstructed in each module, the beam direction can be measured daily with better than 0.4 mrad accuracy. Located in the direction of Super-K, the off-axis detector ND280 is made of several detectors located inside a 0.2 T magnet. The higher precision of those off-axis detectors allows to do more detailed measurements of the unoscillated neutrino beam. In neutrino oscillation analyses, the ND280 is used to provide information on the ν_μ and $\bar{\nu}_\mu$ unoscillated spectra directed at SK, constrain the dominant backgrounds, and constrain the combination of flux and interaction cross sections.

The far detector, Super-K, is a 50 kton water Cherenkov detector, shielded from atmospheric muons by 1000 m of rock, or 2700 meters-water-equivalent (m.w.e.) mean overburden. To select events corresponding to the T2K beam, Super-K is synchronized via GPS to the J-PARC beamline. Hit information within $\pm 500 \mu s$ from the beam arrival timing is used for T2K data analysis. Events with less than three rings were reconstructed (corresponding to one or two charged particles above the Cherenkov threshold) and used in oscillation analysis. Those events are separated into muon-like and electron-like events based on the light pattern of this ring, and additional selection cuts are applied to produce samples enriched in charged-current quasi-elastic interactions for which the energy of the neutrino can be better reconstructed. In 2020, Gadolinium was dissolved into the Super-Kamiokande detector at 0.01%, and the new phase of Super-K, SK-Gd, was started. Additional gadolinium was loaded to Super-K in 2022, and the detector is currently operational with 0.03% gadolinium concentration. Additions of gadolinium significantly increased neutron detection capability, which will benefit T2K's neutrino interaction and oscillation measurements as well.

Experiment status

T2K started collecting physics data in January 2010, and has now completed its 13th run, accumulating a total of 2.70×10^{21} protons on target (POT) in ν-mode and 1.64×10^{21} POT in $\bar{\nu}$-mode. The experiment ran for the first time using an anti-neutrino beam in 2014 and has been alternating since between runs in ν-mode and in $\bar{\nu}$-mode. The details of the data used in the far detector analysis (slightly lower due to data quality cuts) can be found in Tab. 1. Over this period, the event rates and the beam direction were found to be consistent with the expectations and stable by the measurements of the muon monitor and the on-axis near detector. In particular, the beam direction remained stable well within the $\pm$1mrad target.

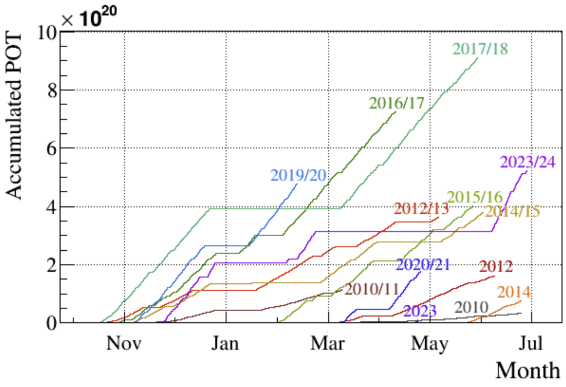

Fig. 1. Protons on target accumulated as a function of time for the thirteen T2K data-taking periods.

Table 1. T2K data taking periods and integrated numbers of protons on target (POT) used in the far detector analysis.

Run Period	Dates	$\times 10^{20}$ POT ν	$\bar{\nu}$
Run 1	Jan.2010 - Jun.2010	0.32	–
Run 2	Nov.2010 - Mar.2011	1.11	–
Run 3	Mar.2012 - Jun.2012	1.60	–
Run 4	Oct.2012 - May.2013	3.60	–
Run 5	May.2014 - Jun.2014	0.24	0.51
Run 6	Oct.2014 - Jun.2015	0.19	3.55
Run 7	Feb.2016 - May.2016	0.48	3.50
Run 8	Oct.2016 - Apr.2017	7.17	–
Run 9	Oct.2017 - May.2018	0.20	8.79
Run 10	Oct.2019 - Feb.2020	4.73	–
Run 11	Mar.2021 - Apr.2021	1.76	–
Run 12	Apr.2023 - Apr.2023	0.09	–
Run 13	Nov.2023 - Jun.2024	5.18	–
Total	**Jan.2010 - Jun.2024**	**26.96**	**16.35**

The intensity of the proton beam has been increasing progressively over time. In particular, a significant upgrade of the J-PARC main ring power supply was conducted in 2021-2022, and the beam repetition cycle was shortened from 2.48 s to 1.36 s. This allowed us to significantly increase the beam power. During run 13, a stable operation at more than 800 kW was achieved. The beam intensity is expected to continue increasing in the future. This increase of the beam intensity, coupled with the improved reliability of the accelerator, has allowed us to progressively collect larger amounts of data over shorter periods of time, as can be seen in Fig. 1.

Status at the beginning of the review period

At the beginning of the review period in 2018, T2K had been collecting data for 8 years (run 1-9), collecting a total of 14.94×10^{20} POT in ν-mode and 16.35×10^{20} POT in $\bar{\nu}$-mode. The maximum beam intensity was around 500 kW.

Using the electron candidate events from the first four years of data taking, T2K observed the appearance of electron neutrinos from the oscillation of muon neutrinos with 7.3σ significance [3]. Constraints on CP-violating phase δ_{CP} and atmospheric parameters θ_{23} and Δm^2_{32} are yielded from simultaneous analysis of many T2K's data sample collected at Super-Kamiokande. Conservation of CP symmetry was excluded with 2σ significance [3]. Atmospheric parameters were measured to be $\sin^2(\theta_{23}) = 0.536^{+0.031}_{-0.046}$ and $|\Delta m^2_{32}| = (2.434 \pm 0.064) \times 10^{-3}\mathrm{eV}^2/\mathrm{c}^4$ [4].

Major scientific results

Neutrino oscillation measurements

In this section, we describe the general method by which neutrino oscillations are studied in T2K, then present the main results obtained during the review period.

Analysis method The data observed at the far detector are compared to the predictions of the three-flavor oscillation model to make statistical inferences. To be able to make those predictions, a model of the experiment is constructed using a simulation of the flux of neutrinos reaching the detectors and a model describing the interactions of neutrinos. The predictions from this model are compared to the data observed in the near detectors to tune the predictions for the far detector by constraining the model parameters.

The fluxes of the different flavors of neutrinos reaching the detectors are predicted by a series of simulations. The flux and properties of the proton beam reaching the target are measured by the proton beam line monitors and used as inputs for the simulations. Interactions of the protons in the graphite target and production of secondary hadrons are then simulated using the FLUKA package [5]. Measurements from hadron production experiments, in particular NA61/SHINE [6], are used to tune this part of the simulation and the out-of-target interactions. The propagation and decay in flight of the hadrons in the decay tunnel are then simulated using the GEANT3 and GCALOR [7] packages. Interactions of ν and $\bar{\nu}$ are modeled using the NEUT Monte Carlo event generator [8].

A binned likelihood fit of the events selected as charged current interactions in the near detectors is used to constrain the flux and neutrino interaction uncertainties. Those events are binned as a function of the momentum and angle of the particle reconstructed as a μ^- or a μ^+ with respect to the axis of the detector and arranged in different samples based on the topology of the event observed in the detector. The result of this fit provides the initial values and uncertainties of the flux and interaction model parameters used in the far detector analysis to measure parameters describing neutrino oscillations.

Oscillation parameter extraction and test of CP symmetry T2K published its result of excluding some parameter space of δ_{CP} at more than 3σ in Ref. [35], followed by improved results with larger data sets in Refs. [42, 48].

In the summer of 2024, T2K released new results on neutrino oscillation parameter measurements with an additional event topology sample and new data set up to Run 11 [9]. Previous oscillation analyses at T2K only used events with a single reconstructed Cherenkov ring at Super-K. Multi-ring events from the ν_μ sample were newly introduced to the oscillation analysis. This new sample adds up statistics of the neutrino mode ν_μ sample by about 30%. Data from run 11, which was the first data taken with Gadolinium-loaded Super-K, was also used in this analysis. Figure 2 shows the reconstructed neutrino energy distributions of the six data samples used for the oscillation analysis; (ν-mode) single electron-like ring, single electron-like ring with decay-electron, single muon-like ring, multiple muon-like ring, ($\bar{\nu}$-mode) single electron-like ring and single μ-like ring samples.

Oscillation parameters were extracted by simultaneously fitting these six data samples. Figure 3 shows the constraints for δ_{CP} obtained from the data fit. The data prefers near-maxim CP violation at $\delta_{CP} \sim -\pi/2$, while the CP conserving values are still within the 2σ interval. The data also prefers normal mass ordering and the upper θ_{23} octant as shown in Figure 4, although none of them are significant yet. The Bayes factor for (Normal Ordering)/(Inverted Ordering) was computed to be 3.3, and the Bayes factor for $(\theta_{23} > 0.5)/(\theta_{23} < 0.5)$ was 2.6.

First joint oscillation analysis of Super-Kamiokande atmospheric and T2K accelerator neutrino data

We conducted a first joint oscillation analysis using both atmospheric neutrino and the T2K beam neutrino data collected at Super-Kamiokande [49]. The beam neutrino data have the advantages of well-defined beam spectra and baseline, while the atmospheric neutrino can have much longer path lengths and hence, more sensitive to the θ_{23} octant and mass-ordering through the matter effect. Further sensitivity enhancement was realized thanks to the correlations of the neutrino interaction models and Super-K's detector response uncertainties.

Constraints on neutrino oscillation parameters were extracted using 3244.4 days of atmospheric data and a beam exposure of $19.7(16.3) \times 10^{20}$ protons on target in (anti)neutrino mode. Constraints from T2K's near-detector data were also implemented in the analysis. Figure 5 shows credible regions obtained from a Bayesian analysis. The atmospheric

*3 M. Hartz (on behalf of the T2K collaboration), T2K Neutrino Oscillation Results with Data up to 2017 Summer, KEK special seminar Aug. 4th, 2017

*4 M. Wascko (on behalf of the T2K collaboration), T2K Status, Results, and Plans, Presentation at the Neutrino 2018 conference

*5 T. Bhlen *et al.*, Nucl. Data Sheets **120**, 211 (2014)

*6 N. Abgrall et al. (NA61/SHINE Collaboration), Eur. Phys. J. C **76**, 84 (2016).

*7 C. Zeitnitz and T. A. Gabriel, Proceedings of International Conference on Calorimetry in High Energy Physics (World Scientific, Corpus Christi, Texas, 1992), ISBN 9789810213039, pp. 394–404.

*8 Y. Hayato, L. Pickering, The NEUT neutrino interaction simulation program library. Eur. Phys. J. Spec. Top. 230, 4469–4481 (2021)

*9 C. Giganti (on behalf of the T2K collaboration), T2K recent results and plans, Presentation at the Neutrino 2024 conference

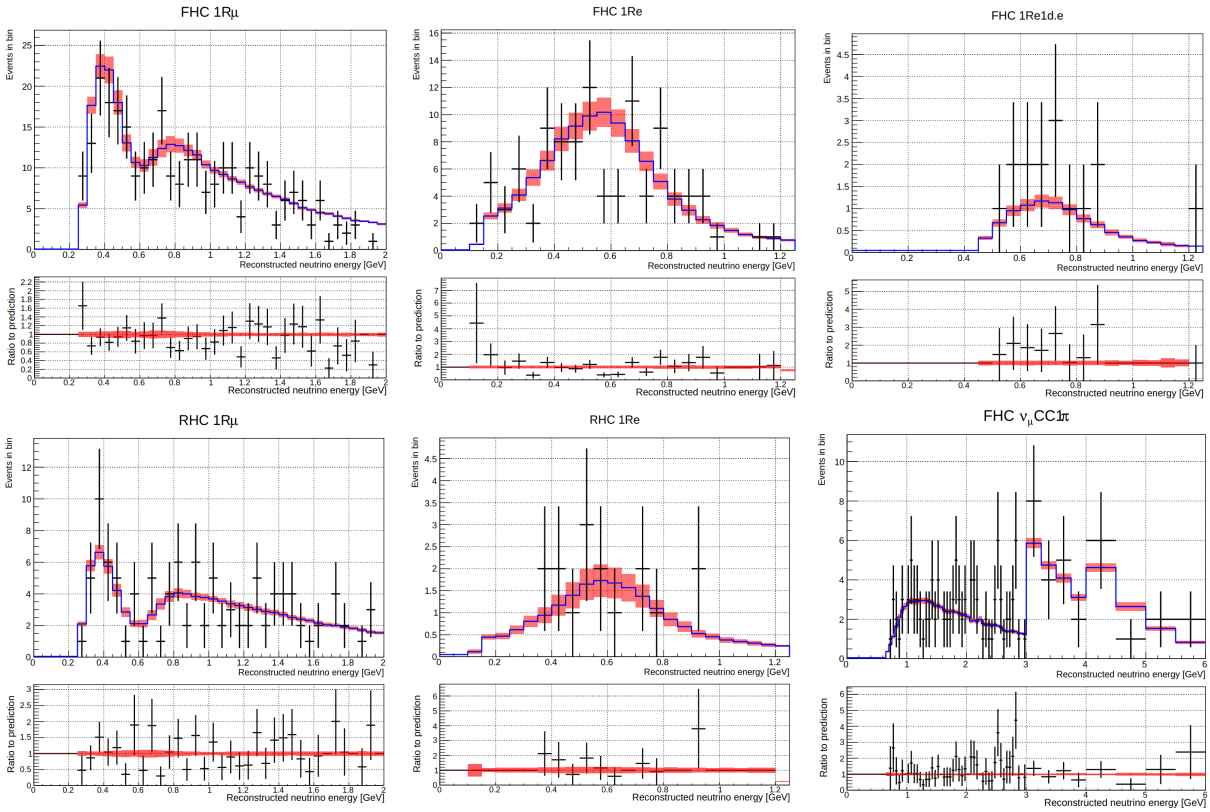

Fig. 2. Reconstructed energy distributions at Super-Kamiokande taken in the T2K run 1-11. Black points represent data with statistical uncertainty. Blue histograms and red-shaded regions show the best-fit spectra and their one-sigma uncertainty bands, respectively. Distributions for ν-mode single muon-like ring (top-left), ν-mode single electron-like ring (top-center), ν-mode single electron-like ring with decay-electron (top-right), $\bar{\nu}$-mode single muon-like ring (bottom-left), $\bar{\nu}$-mode single electron-like ring (bottom-center), ν-mode multiple μ-like ring (bottom-right) samples are separately shown. The bottom panels in each plot show the ratios to the best-fit predictions.

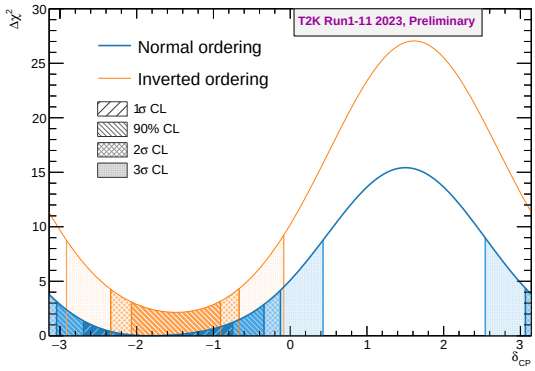

Fig. 3. $\Delta\chi^2$ of the data fit vs. δ_{CP} for both normal (blue) and inverted (orange) orderings. The computed confidence intervals are displayed in different textures.

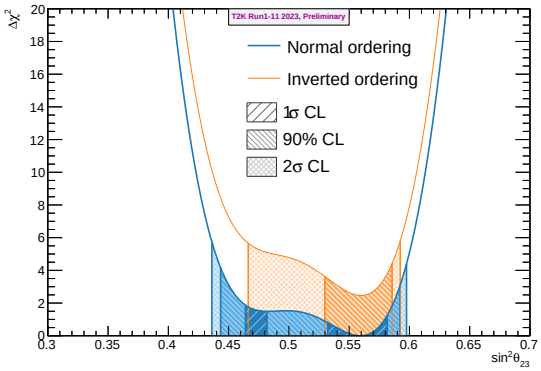

Fig. 4. $\Delta\chi^2$ of the data fit vs. $\sin^2\theta_{23}$ for both normal (blue) and inverted (orange) orderings. The computed confidence intervals are displayed in different textures.

data and the beam data have different θ_{23} octant preferences, which resulted in weaker octant preference in the joint analysis. Both data set prefers a δ_{CP} value around $-\pi/2$. A test of CP violation was performed by using Jarlskog invariant. Figure 6 shows the distributions posterior density distributions for the Jarlskog invariant from a Bayesian analysis. The CP-conserving value ($J_{CP} = 0$) was excluded at a 1.9-2.0σ level. A frequentist-based analysis also found an exclusion of the CP-conserving value at a similar significance. The data also showed a preference for the normal mass-ordering.

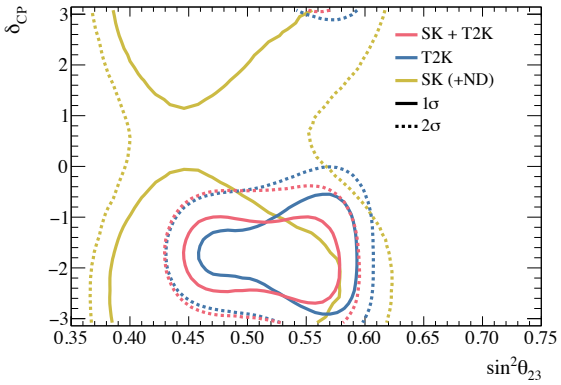

Fig. 5. The credible regions in the δ_{CP} vs. $\sin^2\theta_{23}$ plane obtained with the SK, T2K, and combined datasets. The mass ordering is marginalized over and a prior uniform in δ_{CP} is used.

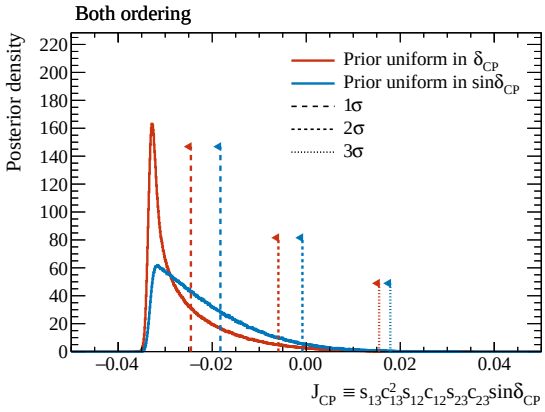

Fig. 6. The posterior density for the Jarlskog invariant with credible intervals. It is marginalized over both mass-orderings and assuming a uniform prior in either δ_{CP} or $\sin\delta_{CP}$.

Search for light sterile neutrinos with the T2K far detector Super-Kamiokande at a baseline of 295 km

Over the last few decades, the theory of neutrino oscillations has been well established through a series of experiments with neutrinos produced by the Sun, nuclear reactors, accelerators and in the atmosphere. Most data from these studies are consistent with the three-flavor paradigm, where the three weakly interacting neutrino flavors are related to three neutrino mass states by the PMNS matrix. However, deviations from the three flavor schemes have been reported, such as LSND and MiniBooNE, there were excesses of ν_e found in short-baseline ν_μ beams; MiniBooNE also reported an excess in ν_e appearance. These results could be explained by a fourth neutrino state with a mass difference $\Delta m^2 \sim 1$ eV^2. A search for light sterile neutrinos using the data from the T2K far detector at a baseline of 295 km was performed [22] in a framework of simple "3+1" model, which involves the three active neutrinos and one sterile neutrino, and study its effect on the oscillation signatures. At the far detector, the muon neutrino survival probability can be approximated (omitting δ_{CP} terms) as

$$P(\nu_\mu \to \nu_\mu) \sim 1 - \sin^2 2\theta_{23}\cos^4\theta_{24}\sin^2\frac{\Delta m^2_{31}L}{4E} - \cos^2\theta_{23}\sin^2 2\theta_{24}\sin^2\frac{\Delta m^2_{41}L}{4E} - \sin^2\theta_{23}\sin^2 2\theta_{24}\sin^2\frac{\Delta m^2_{43}L}{4E},$$

and the electron neutrino probability as

$$P(\nu_\mu \to \nu_e) \sim \sin^2 2\theta_{13}\cos^2\theta_{24}\sin^2\theta_{23}\sin^2\frac{\Delta m^2_{31}L}{4E}.$$

The dataset with an exposure of 14.7 (7.6) $\times 10^{20}$ protons on target in FHC (RHC) mode are used for the analysis. A selection of neutral-current interaction samples is also used to enhance the sensitivity to sterile mixing. No evidence of sterile neutrino mixing in the 3+1 model was found from a simultaneous fit to the charged-current muon, electron, and neutral-current neutrino samples. Fig. 7 shows the T2K 90% exclusion limits together with results from other experiments. We have set the most stringent limit on the sterile oscillation amplitude $\sin^2\theta_{24}$ for the sterile neutrino mass splitting $\Delta m^2_{41} < 3\times10^{-3}$eV^2.

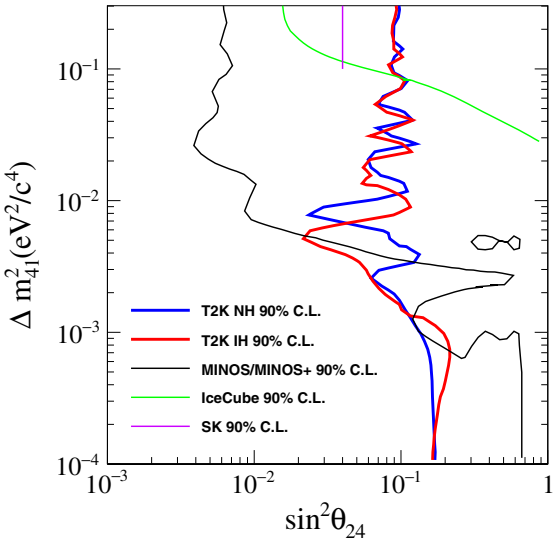

Fig. 7. The T2K 90% exclusion limits on $\sin^2\theta_{24}$ as a function of Δm^2_{41}, with results from other experiments. The areas on the right are excluded.

Measurement of neutrons associated with neutrino and antineutrino interactions on water target at the T2K far detector

Neutrons production associated with neutrino interactions is utilized to improve the physics program of neutrino experiments, such as the search for diffuse supernova background (DSNB) neutrino, neutrino oscillation measurement, search

for proton decay event, etc. employing water Cherenkov detectors, like SK-Gd and Hyper-Kamiokande. These experiments plan to utilize neutrons associated with neutrino interactions in water for their main physics analyses. However, current prediction is highly dependent on simulations due to large uncertainties related to the modeling of neutrino interactions in nuclear medium, hadronic final-state interactions in nuclei, and secondary interactions in detector medium. In addition, no extensive study has been made on water. Therefore, it is quite valuable to study these neutrons and evaluate the validity of the simulations by using a well-understood neutrino source. We have observed neutrons associated with neutrino interactions at the T2K far detector and measured the neutron multiplicities induced by the interactions of muon neutrino and antineutrino in water, respectively. We employed and analyzed the data collected at the far detector until 2018, which corresponds to 1.4938×10^{21} POT for the FHC mode and 1.6346×10^{21} POT for the RHC mode. Charged current ν_μ and $\bar{\nu}_\mu$ enriched samples, which 1Rν_μ selection is applied to the T2K FC neutrino events, were used for the analysis. The observed neutrino events agreed well with the corresponding expectations; however, the tagged neutrons showed fewer tagged neutrons than expected, as shown in Table 2. The measured mean neutron multiplicity is 1.00 ± 0.17 (stat.)$^{+0.07}_{-0.08}$(syst.) and 1.40 ± 0.26 (stat.) $^{+0.10}_{-0.11}$ (syst.) while the equivalent expectation by the reference simulation is 1.50 and 2.14, for FHC and RHC 1Rν_μ samples, respectively. The deviation from the expectation is 2.75σ and 2.69σ based on the total error of the measured value.

Table 2. Summary of the number of neutrino events and tagged neutrons for the Runs 1−9 POT with oscillation effect.

	Number of ν events		Number of tagged n	
	expected	observed	expected	observed
FHC 1Rν_μ	202.12	201	64.08	44
RHC 1Rν_μ	109.61	110	49.42	33

Fig. 8 shows the mean neutron multiplicity as a function of muon transverse momentum. Since neutron production depends on the four-momentum transfer squared (Q^2) to the hadronic system at the primary ν-nucleus interaction, the reconstructed transverse muon momentum P_t, which is a good indicator of Q_2 is used. Despite the large statistical uncertainties for the higher transverse momentum events, the measured multiplicities show a substantial deficit from the expected values in all transfer momentum regions.

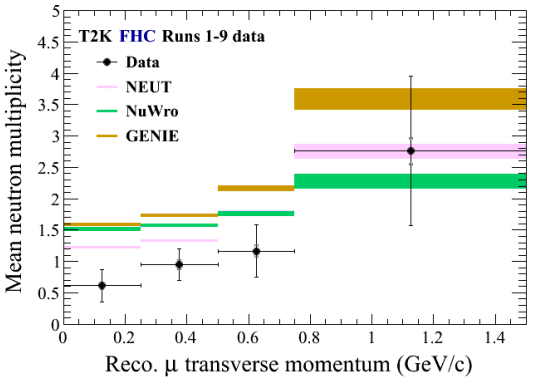

Fig. 8. Mean neutron multiplicity as a function of reconstructed muon transverse momentum in comparison to the equivalent expectations of the NEUT-, NuWro-, and GENIE-based MCs. The figures show the FHC 1Rν_μ samples.

T2K collaboration

Spokesperson: Ken Sakashita (KEK, From May 2023), Atsuko Ichikawa (Tohoku University, From July 2021 to May 2023, Kyoto University From May 2019), Tsuyoshi Nakaya (Kyoto University, till May 2019)

Host institutes of the T2K experiment are the High Energy Accelerator Research Organization (KEK) and ICRR. One of the members of the Executive Committee of the experiment is from ICRR: Yoshinari Hayato.

Institute	Country	(*)
ICRR	Japan	26
KEK	Japan	29
Kavli IPMU (WPI), University of	Japan	7
University of Tokyo	Japan	14
Keio University	Japan	2
Kobe University	Japan	4
Kyoto University	Japan	15
Miyagi University of Education	Japan	1
Okayama University	Japan	4
Osaka Metroplitan University	Japan	7
Tohoku University	Japan	8
Tokyo Institute of Technology	Japan	2
Tokyo Metropolitan University	Japan	5
Tokyo University of Science	Japan	3
University of Tokyo	Japan	8
Yokohama National University	Japan	4
Ghent University	Belgium	4
TRIUMF	Canada	12
University of Tronto	Canada	1
York University	Canada	4

Institute	Country	(*)
CEA/DAPNIA Saclay	France	21
LLR Ecole polytechnique (IN2P3)	France	13
LPNHE-Paris	France	19
Johannes Gutenberg-Universitat Mainz	Germany	6
RWTH Aachen University	Germany	5
ELTE	Hungary	2
INFN Bari	Italy	7
INFN Roma	Italy	4
Napoli University and INFN	Italy	5
Padova University and INFN	Italy	17
IFJ PAN, Cracow	Poland	7
NCBJ, Warsaw	Poland	7
Technical University, Warsaw	Poland	5
University of Silesia, Katowice	Poland	4
Warsaw University	Poland	3
Wroclaw University	Poland	3
INR	Russia	24
JINR	Russia	12
IFAE, Barcelona	Spain	10
UAM, Madrid	Spain	2
University of Seville	Spain	6
Bern	Swiss	1
CERN	Swiss	9
ETHZ	Swiss	14
University of Geneva	Swiss	17
Imperial College London	UK	23
King's College London	UK	9
Lancaster University	UK	13
Oxford University	UK	9
Royal Holloway, Univ. of London	UK	4
STFC/RAL/Daresbury Laboratory	UK	11
University of Glasgow	UK	7
University of Liverpool	UK	12
University of Sheffield	UK	6
University of Warwick	UK	6
Boston University	USA	3
Duke University	USA	2
LBNL	USA	3
Louisiana State University	USA	9
Michigan State University	USA	4
SDSMT	USA	2
SLAC	USA	1
Stony Brook University	USA	24
University of California, Irvine	USA	3
University of Colorado	USA	5
University of Houston	USA	3
University of Minnesota	USA	2
University of Pennsylvania	USA	11
University of Pittsburgh	USA	1
University of Rochester	USA	5
University of Washington	USA	7
Hanoi University of Science	Vietnam	2
IFIRSE, Quy Nhon/IOP, Hanoi	Vietnam	2
Total		566

(*): Number of collaborators

Members

Staff

Kamioka Observatory

Masayuki Nakahata, Professor
Shigetaka Moriyama, Professor
Masato Shiozawa, Professor
Yoshinari Hayato, Assoc. Professor
Yasuhiro Kishimoto, Assoc. Professor (till Mar. 2019)
Hiroyuki Sekiya, Assoc. Professor
Shoei Nakayama, Assoc. Professor
Atsushi Takeda, Assoc. Professor (from Feb. 2020)
Atsushi Takeda, Research Associate (till Jan. 2020)
Yoichi Asaoka, Assoc. Professor (from Jun. 2023)
Katsuki Hiraide, Project Assoc. Professor (from May 2020)
Makoto Miura, Research Associate
Jun Kameda, Research Associate
Ko Abe, Research Associate
Motoyasu Ikeda, Research Associate
Yasuhiro Nakajima, Research Associate (till Mar. 2021)
Hidekazu Tanaka, Research Associate (from Feb. 2019)
Hidekazu Tanaka, Project Research Associate (till Jan. 2019)
Kei Ieki, Research Associate (from Nov. 2021)
Kei Ieki, Project Research Associate (Apr. 2021 - Oct. 2021)
Lluis Magro Marti, Project Research Associate (till Aug. 2020)
Yo Kato, Project Research Associate (till Mar. 2019)
Christophe Bronner, Project Research Associate (till Apr. 2022)
Christophe Bronner, Project Research Associate (from Apr. 2023)
Yosuke Kataoka, Research Associate (from Jun. 2020)
Yosuke Kataoka, Project Research Associate (till May 2020)
Takatomi Yano, Project Research Associate (from Dec. 2017)
Yuki Nakano, Project Research Associate (Sep. 2021 - Mar. 2024)
Keishi Hosokawa, Project Research Associate (from Sep. 2021)
Shunichi Mine, Project Academic Specialist (from Apr. 2022)

Research Center for Cosmic Neutrinos

Takaaki Kajita, Professor (till Mar. 2024)
Kimihiro Okumura, Assoc. Professor
Yasuhiro Nishimura, Research Associate (till Mar. 2019)

Institute for Comic Ray Research

Takaaki Kajita, Professor (from Apr. 2024)

Postdoctorial Fellows

Kamioka Observatory

Yuuki Nakano (till Mar. 2019)
Hiroshi Ito (Apr. 2019 - Mar. 2021)
Kiseki Nakmura (Apr. 2020 - Mar. 2021)
Yohei Noguchi (from Apr. 2022)
Seisho Abe (from Apr. 2023)

Graduate students

Three students was awarded doctor degree during 2018–

2024, supervised by ICRR staff members.

Bibliography

Before Year 2018

[1] K. Abe *et al.* (T2K Collaboration), "The T2K Experiment," Nucl. Instrum. Meth. A **659**, 106 (2011) doi:10.1016/j.nima.2011.06.067 **(1074 citations)**

[2] K. Abe *et al.* (T2K Collaboration), "First Muon-Neutrino Disappearance Study with an Off-Axis Beam," Phys. Rev. D **85**, 031103 (2012) doi:10.1103/PhysRevD.85.031103. **(199 citations)**

[3] K. Abe *et al.* (T2K Collaboration), "Observation of Electron Neutrino Appearance in a Muon Neutrino Beam," Phys. Rev. Lett. **112**, 061802 (2014). doi:10.1103/PhysRevLett.112.061802. **(728 citations)**

[4] K. Abe *et al.* (T2K Collaboration), "Measurements of neutrino oscillation in appearance and disappearance channels by the T2K experiment with $6.6\text{x}10^{20}$ protons on target," Phys. Rev. D **91**, no. 7, 072010 (2015). doi:10.1103/PhysRevD.91.072010. **(434 citations)**

[5] K. Abe *et al.* (T2K Collaboration), "Combined Analysis of Neutrino and Antineutrino Oscillations at T2K," Phys. Rev. Lett. **118**, no. 15, 151801 (2017) doi:10.1103/PhysRevLett.118.151801. **(273 citations)**

[6] K. Abe *et al.* (T2K Collaboration), "Measurement of neutrino and antineutrino oscillations by the T2K experiment including a new additional sample of ν_e interactions at the far detector," Phys. Rev. D **96**, no. 9, 092006 (2017) Erratum: [Phys. Rev. D **98**, no. 1, 019902 (2018)] doi:10.1103/PhysRevD.96.092006, 10.1103/PhysRevD.98.019902. **(244 citations)**

[7] K. Abe *et al.* (T2K Collaboration), "Precise Measurement of the Neutrino Mixing Parameter θ_{23} from Muon Neutrino Disappearance in an Off-Axis Beam," Phys. Rev. Lett. **112**, no. 18, 181801 (2014) doi:10.1103/PhysRevLett.112.181801. **(360 citations)**

[8] K. Abe *et al.* (T2K Collaboration), "Updated T2K measurements of muon neutrino and antineutrino disappearance using 1.5×10^{21} protons on target," Phys. Rev. D **96**, no. 1, 011102 (2017) doi:10.1103/PhysRevD.96.011102. **(58 citations)**

[9] K. Abe *et al.* (T2K Collaboration), "Measurement of the Inclusive Electron Neutrino Charged Current Cross Section on Carbon with the T2K Near Detector," Phys. Rev. Lett. **113**, no. 24, 241803 (2014) doi:10.1103/PhysRevLett.113.241803. **(109 citations)**

[10] K. Abe *et al.* (T2K Collaboration), "Measurement of the inclusive ν_μ charged current cross section on carbon in the near detector of the T2K experiment," Phys. Rev. D **87**, no. 9, 092003 (2013) doi:10.1103/PhysRevD.87.092003 **(178 citations)**

[11] K. Abe *et al.* (T2K Collaboration), "Measurement of the inclusive ν_μ charged current cross section on iron and hydrocarbon in the T2K on-axis neutrino beam," Phys. Rev. D **90**, no. 5, 052010 (2014) doi:10.1103/PhysRevD.90.052010. **(84 citations)**

[12] K. Abe *et al.* (T2K Collaboration), "Measurement of the ν_μ charged current quasielastic cross section on carbon with the T2K on-axis neutrino beam," Phys. Rev. D **91**, no. 11, 112002 (2015) doi:10.1103/PhysRevD.91.112002. **(70 citations)**

[13] K. Abe *et al.* (T2K Collaboration), "Measurement of the electron neutrino charged-current interaction rate on water with the T2K ND280 π^0 detector," Phys. Rev. D **91**, 112010 (2015) doi:10.1103/PhysRevD.91.112010. **(25 citations)**

[14] K. Abe *et al.* (T2K Collaboration), "Measurement of the ν_μ charged-current quasielastic cross section on carbon with the ND280 detector at T2K," Phys. Rev. D **92**, no. 11, 112003 (2015) doi:10.1103/PhysRevD.92.112003. **(81 citations)**

[15] K. Abe *et al.* (T2K Collaboration), "Measurement of the muon neutrino inclusive charged-current cross section in the energy range of 1-3 GeV with the T2K INGRID detector," Phys. Rev. D **93**, no. 7, 072002 (2016) doi:10.1103/PhysRevD.93.072002. **(40 citations)**

[16] K. Abe *et al.* (T2K Collaboration), "Measurement of double-differential muon neutrino charged-current interactions on C_8H_8 without pions in the final state using the T2K off-axis beam," Phys. Rev. D **93**, no. 11, 112012 (2016) doi:10.1103/PhysRevD.93.112012. **(142 citations)**

[17] K. Abe *et al.* (T2K Collaboration), "Measurement of Coherent π^+ roduction in Low Energy Neutrino-Carbon Scattering," Phys. Rev. Lett. **117**, no. 19, 192501 (2016) doi:10.1103/PhysRevLett.117.192501. **(42 citations)**

[18] K. Abe *et al.* (T2K Collaboration), "First measurement of the muon neutrino charged current single pion production cross section on water with the T2K near detector," Phys. Rev. D **95**, no. 1, 012010 (2017) doi:10.1103/PhysRevD.95.012010. **(75 citations)**

[19] K. Abe *et al.* (T2K Collaboration), "First measurement of the ν_μ charged-current cross section on a water target without pions in the final state," Phys. Rev. D **97**, no. 1, 012001 (2018) doi:10.1103/PhysRevD.97.012001. **(52 citations)**

[20] K. Abe *et al.* (T2K Collaboration), "Measurement of $\bar{\nu}_\mu$ and ν_μ charged current inclusive cross sections and their ratio with the T2K off-axis near detector," Phys. Rev. D **96**, no. 5, 052001 (2017) doi:10.1103/PhysRevD.96.052001 **(21 citations)**

[21] K. Abe *et al.* (T2K Collaboration), "Measurement of the neutrino-oxygen neutral-current interaction

cross section by observing nuclear deexcitation γ rays," Phys. Rev. D **90**, no. 7, 072012 (2014) doi:10.1103/PhysRevD.90.072012. **(62 citations)**

[22] K. Abe *et al.* (T2K Collaboration), "Search for short baseline ν_e disappearance with the T2K near detector," Phys. Rev. D **91**, 051102 (2015) doi:10.1103/PhysRevD.91.051102. **(45 citations)**

[23] K. Abe *et al.* (T2K Collaboration), "Search for Lorentz and CPT violation using sidereal time dependence of neutrino flavor transitions over a short baseline," Phys. Rev. D **95**, no. 11, 111101 (2017) doi:10.1103/PhysRevD.95.111101. **(40 citations)**

[24] K. Abe *et al.* (T2K Collaboration), "Upper bound on neutrino mass based on T2K neutrino timing measurements," Phys. Rev. D **93**, no. 1, 012006 (2016) doi:10.1103/PhysRevD.93.012006. **(13 citations)**

[25] K. Abe *et al.* (T2K Collaboration), "Measurement of Neutrino Oscillation Parameters from Muon Neutrino Disappearance with an Off-axis Beam," Phys. Rev. Lett. **111**, no. 21, 211803 (2013) doi:10.1103/PhysRevLett.111.211803. **(189 citations)**

From Year 2018

[26] K. Abe *et al.* (T2K Collaboration), "Measurement of the single π^0 production rate in neutral current neutrino interactions on water," Phys. Rev. D **97**, 032002 (2018) doi:10.1103/PhysRevD.97.032002. **(15 citations)**

[27] K. Abe *et al.* (T2K Collaboration), "Measurement of inclusive double-differential ν_μ charged-current cross section with improved acceptance in the T2K off-axis near detector," Phys. Rev. D **98**, 012004 (2018) doi:10.1103/PhysRevD.98.012004. **(43 citations)**

[28] K. Abe *et al.* (T2K Collaboration), "Characterization of nuclear effects in muon-neutrino scattering on hydrocarbon with a measurement of final-state kinematics and correlations in charged-current pionless interactions at T2K," Phys. Rev. D **98**, 032003 (2018) doi:10.1103/PhysRevD.98.032003. **(129 citations)**

[29] K. Abe *et al.* (T2K Collaboration), "Search for CP Violation in Neutrino and Antineutrino Oscillations by the T2K Experiment with 2.2 x 10^{21} Protons on Target," Phys. Rev. Lett. **121**, 171802 (2018) doi:10.1103/PhysRevLett.121.171802. **(287 citations)**

[30] K. Abe *et al.* (T2K Collaboration), "Search for light sterile neutrinos with the T2K far detector Super-Kamiokande at a baseline of 295 km," Phys. Rev. D **99**, 071103(R) (2019) doi:10.1103/PhysRevD.99.071103. **(52 citations)**

[31] K. Abe *et al.* (T2K Collaboration), "Search for neutral-current induced single photon production at the ND280 near detector in T2K," J. Phys. G: Nucl. Part. Phys. **46**, 08LT01 (2019) doi:10.1088/1361-6471/ab227d. **(21 citations)**

[32] K. Abe *et al.* (T2K Collaboration), "Search for heavy neutrinos with the T2K near detector ND280," Phys. Rev. D **100**, 052006 (2019) doi:10.1103/PhysRevD.100.052006. **(133 citations)**

[33] K. Abe *et al.* (T2K Collaboration), "Measurement of neutrino and antineutrino neutral-current quasielastic-like interactions on oxygen by detecting nuclear deexcitation γ rays," Phys. Rev. D **100**, 112009 (2020) doi:10.1103/PhysRevD.100.112009. **(33 citations)**

[34] K. Abe *et al.* (T2K Collaboration), "Measurement of the muon neutrino charged-current single π^+ production on hydrocarbon using the T2K off-axis near detector ND280," Phys. Rev. D **101**, 012007 (2020) doi:10.1103/PhysRevD.101.012007. **(35 citations)**

[35] K. Abe *et al.* (T2K Collaboration), "Constraint on the matter-antimatter symmetry-violating phase in neutrino oscillations," Nature **580**, 7803 (2020) doi:10.1038/s41586-020-2177-0. **(562 citations)**

[36] K. Abe *et al.* (T2K Collaboration), "Search for Electron Antineutrino Appearance in a Long-Baseline Muon Antineutrino Beam," Phys. Rev. Lett. **124**, 161802 (2020) doi:10.1103/PhysRevLett.124.161802. **(21 citations)**

[37] K. Abe *et al.* (T2K Collaboration), "First combined measurement of the muon neutrino and antineutrino charged-current cross section without pions in the final state at T2K," Phys. Rev. D **101**, 112001 (2020) doi:10.1103/PhysRevD.101.112001. **(38 citations)**

[38] K. Abe *et al.* (T2K Collaboration), "Simultaneous measurement of the muon neutrino charged-current cross section on oxygen and carbon without pions in the final state at T2K," Phys. Rev. D **101**, 112004 (2020) doi:10.1103/PhysRevD.101.112004. **(56 citations)**

[39] K. Abe *et al.* (T2K Collaboration), "First measurement of the charged current $\overline{\nu_\mu}$ double differential cross section on a water target without pions in the final state," Phys. Rev. D **102**, 012007 (2020) doi:10.1103/PhysRevD.102.0120074. **(20 citations)**

[40] K. Abe *et al.* (T2K Collaboration), "Measurement of the charged-current electron (anti-)neutrino inclusive cross-sections at the T2K off-axis near detector ND280," J. High Energ. Phys. **2020**, 114 (2020) doi:10.1007/JHEP10(2020)114. **(38 citations)**

[41] K. Abe *et al.* (T2K Collaboration), "T2K measurements of muon neutrino and antineutrino disappearance using 3.13 x 10^{21} protons on target," Phys. Rev. D **103**, L011101 (2021) doi:10.1103/PhysRevD.103.L011101. **(23 citations)**

[42] K. Abe *et al.* (T2K Collaboration), "Improved constraints on neutrino mixing from the T2K experiment with 3.13 x 10^{21} protons on target," Phys. Rev. D **103**, 112008 (2021) doi:10.1103/PhysRevD.103.112008. **(184 citations)**

[43] K. Abe *et al.* (T2K Collaboration), "First T2K measurement of transverse kinematic imbalance in the muon-neutrino charged-current single-π^+ production channel containing at least one proton," Phys. Rev. D **103**, 112009 (2021) doi:10.1103/PhysRevD.103.112009. **(33 citations)**

[44] K. Abe *et al.* (T2K Collaboration), "Scintillator ageing of the T2K near detectors from 2010 to 2021," JINST **17**, P10028 (2022) doi:10.1088/1748-0221/17/10/P10028. **(7 citations)**

[45] K. Abe *et al.* (T2K Collaboration), "Updated T2K measurements of muon neutrino and antineutrino disappearance using 3.6 x 10^{21} protons on target," Phys. Rev. D **108**, 072011 (2023) doi:10.1103/PhysRevD.108.072011. **(7 citations)**

[46] K. Abe *et al.* (T2K Collaboration), "Measurements of the ν_μ and $\bar{\nu_\mu}$-induced coherent charged pion production cross sections on ^{12}C by the T2K experiment," Phys. Rev. D **108**, 092009 (2023) doi:10.1103/PhysRevD.108.092009. **(4 citations)**

[47] K. Abe *et al.* (T2K Collaboration), "First measurement of muon neutrino charged-current interactions on hydrocarbon without pions in the final state using multiple detectors with correlated energy spectra at T2K," Phys. Rev. D **108**, 112009 (2023) doi:10.1103/PhysRevD.108.112009. **(90 citations)**

[48] K. Abe *et al.* (T2K Collaboration), "Measurements of neutrino oscillation parameters from the T2K experiment using 3.6×10^{21} protons on target," Eur. Phys. J. C **83**, no.9, 782 (2023) doi:10.1140/epjc/s10052-023-11819-x. **(81 citations)**

[49] K. Abe *et al.* (T2K and Super-Kamiokande Collaborations), "First joint oscillation analysis of Super-Kamiokande atmospheric and T2K accelerator neutrino data," Phys. Rev. Lett. - Accepted 29 October, 2024, [arXiv:2405.12488 [hep-ex]]. **(1 citation)**

XMASS/XENON EXPERIMENTS

Introduction

This experimental group intends to find dark matter particles and neutrino-less double beta decay, and measure pp/^{7}Be/^{8}B solar neutrinos. Highly-purified liquid xenon (LXe) scintillator in an ultra-low radioactivity environment is suitable for these studies: its advantages are a large scintillation light yield, scalability of the LXe target mass, proven methods to remove radioactive contamination, and, due to its high atomic number $Z = 54$, the ability to shield itself against external gamma radiation.

The XMASS-I detector [1] construction was completed in September 2010, and commissioning data was taken from December 2010 to May 2012. It contained $\sim$830 kg of LXe of which $\sim$100 kg were in its fiducial volume (FV). FV is a standard volume in which physics studies can be conducted. 642 photomultiplier tubes surrounded the active LXe volume, defining its almost spherical shape. After a year of detector refurbishment, data-taking resumed in November 2013, significantly reducing background. Under these improved conditions, stable data acquisition continued for more than five years until February 2019. The XMASS collaboration concluded its activity by publishing full-data dark matter search results in 2023. Data from the periods above provided many unique physics studies leading the research field based on this unique single-phase LXe detector.

In parallel to the studies above, we aimed at a higher sensitivity for the discovery of dark-matter particles. To achieve this, XMASS-1.5 with five tonnes of LXe, one tonne in its FV, and with a sensitivity of 10^{-47}cm^2 for the scattering cross sections of weakly interactive massive particles (WIMPs) and nucleons was proposed. However, as the second generation (G2) XENONnT, LZ and PandaX-4T experiments (using a two-phase detector with about 10 tonnes of LXe each) were trying to achieve a search sensitivity of about 10^{-48} cm^2, XMASS-1.5 lost its competitiveness. It is assumed that target size will become the decisive factor in the future, creating a situation where a large-scale detector, something that can only be produced singularly in the world, becomes essential, which then leads to the formation of an international collaborative experiments that will have to integrate such initiatives as XMASS. In view of this situation, the group proposed to change the policy of aiming at the realisation of XMASS-1.5 and to form a research group to participate in one of the existing G2 experiments and to promote research and development for the realisation of the future third generation (G3) experiment. This was proposed to the ICRR future planning committee in 2017, and was considered reasonable to execute at the Kamioka Observatory. Following this, some of the XMASS members started to participate in the XENON collaboration and its XNEONnT experiment toward future discovery and detailed studies of dark-matter particles.

XENONnT is the most sensitive direct dark matter search experiment [2] conducted at LNGS in Italy. It is based on a two-phase time projection chamber with a sensitive LXe mass of 5.9 ton. The construction of XENONnT detector was completed in 2020 and data taking started in 2021. One of the major technical contributions from the ICRR group is purification of xenon directly in the liquid phase, which significantly enhances the sensitivity of the experiment. With our expertise developed for XMASS, we could achieve much longer electron lifetime compared to our design goal and decisively minimize losses from the charge signal during its drift towards detection in the gas phase above the liquid xenon target. Our other major technical contribution is the neutron veto counter (nVeto or NV) technology. By introducing the neutron detection technology developed for SK-Gd to the XENONnT experiment, we can tag nuclear recoil events caused by neutrons and reduce this important BG. With these technical and intellectual contribution, ICRR aims at discovering dark matter by maximizing the performance of XENONnT.

Summary from 2018 to 2024

Notable achievements in the last six years were:

XMASS

- Data taking was completed in Feb. 2019. Stable XMASS-I data taking accumulated a total livetime of 1590.9 days between November 20, 2013 and February 1, 2019 with an analysis threshold of 1.0 keVee. In the latter half of data taking a lower analysis threshold of 0.5 keVee was achieved through a new low threshold trigger.

- The final results of the WIMP search using all XMASS data have been published [3]. We summarized the search for nuclear recoil signal in the fiducial volume and the annual modulation signals from both, nuclear recoil and electron recoil. These WIMP searches cover a broad mass range from 0.32 to 10^4 GeV/c^2 and provide cross-section limits from a same single detector, which are the best results from a single-phase LXe detector.

- Many pioneering physics results from the long stable XMASS-I operation and innovative technical achievements were published: (1) A WIMP dark-matter search via inelastic scattering on ^{129}Xe for a range of DM masses still provides the most stringent limit [4], (2) an exotic neutrino-electron interactions search provided flavor-dependent constraints on a hypothetical millicharge of neutrinos [5], (3) a search for neutrinoless quadruple beta decay produced a unique limit [6], (4) the world's lowest background PMT was developed [7].

XENON

- The construction of the XENONnT detector was completed in 2020 and data taking started in 2021, despite severe COVID19 restriction. The ICRR group makes a significant contribution toward the discovery of dark matter particles based on a purification technology for LXe developed in XMASS and the neutron detection technology developed for Super-Kamiokande.
- The results of the first science run (1.16 ton-years) for nuclear recoils from WIMP dark matter were published in 2023 and a new limit on the spin-independent WIMP nuclear cross section of $2.58 \times 10^{-47}\,\mathrm{cm}^2$ for a WIMP mass of $28\,\mathrm{GeV/c^2}$ at the 90% confidence level was established [8].
- Owing to the lowest level of electronic recoil (ER) BG, $(15.8 \pm 1.3)\,\mathrm{events/(t \cdot y \cdot keV)}$ in the 1-30 keV region; new limits were set on solar axions, a potential enhanced neutrino magnetic moment, and bosonic dark matter [9], which exclude these as possible interpretations of the XENON1T excess [10]. The overall BG rate in this analysis was $\sim$5 times lower than that in XENON1T.
- Neutrinos from the Sun can interact with the nuclei of the xenon atoms in the XENONnT target via coherent elastic neutrino-nucleus scattering. An excess of low-energy nuclear recoil events over the expected BG was recently measured, compatible with a signal from solar ^{8}B neutrino interactions, with a statistical significance of 2.73σ.

Some acronyms are summarized here:

- Nulear recoil (NR)
- Electronic recoil (ER)
- Neutron veto counter (NV)
- Muon veto counter (MV)
- Liquid xenon time projection chamber (TPC)

1. XMASS

In the following, major results obtained in XMASS-I from 2018 to 2024 are described in more detail.

Search for WIMP dark matter using full data set of XMASS-I

WIMPs are one of the well-motivated dark matter candidates and are thought to be observable through nuclear recoils or electron recoil produced in their elastic scattering interactions with a target material. It is one of the main targets of XMASS and we reported many WIMP search results.

As the final result of XMASS-I, a unique single-phase LXe detector, we published results of various WIMP dark matter searches with the full-data of XMASS-I [3]. Over the long period of observation of XMASS-I, it accumulated 1590.9 live days of data with an analysis threshold of 1 $\mathrm{keV_{ee}}$. The final 768.8 days subset of these data allows for an even lower analysis threshold of 0.5 $\mathrm{keV_{ee}}$. We searched for a nuclear recoil signal in the detector's fiducial volume and also for annual modulation signatures caused by nuclear recoil (NR) and electron recoil (ER) interactions.

Extending the fiducial volume search with a target mass of 97 kg to the full 1590.9 days allowed us to improve our earlier world-best single phase LXe limit on spin-independent high mass WIMP interactions by a factor of 1.6 down to $1.4 \times 10^{-44}\,\mathrm{cm}^2$ for a $60\,\mathrm{GeV}/c^2$ WIMP at the 90% CL.

Updated searches for the annual modulation signature expected for true galactic DM halo particle interactions in terrestrial detectors, were also extended to the full XMASS-I data set and using XMASS-I's full active target mass of 832 kg, improved on our own old limits for NR by a factor of 1.3 to reach $2.3 \times 10^{-42}\,\mathrm{cm}^2$ for a $8\,\mathrm{GeV}/c^2$ WIMP.

Also updated was our bremsstrahlung result, which for a $0.5\,\mathrm{GeV}/c^2$ WIMP reached a cross section limit of $1.1 \times 10^{-33}\,\mathrm{cm}^2$, an improvement of a factor 1.5.

The newly added analysis exploiting the Migdal effect for low mass WIMP searches closed the WIMP mass gap that previously existed in our analyses between the lower WIMP mass end of the NR modulation analysis and the upper WIMP mass end of our bremsstrahlung based modulation analysis. The analysis exploiting the Migdal effect reached down to $1.4 \times 10^{-35}\,\mathrm{cm}^2$ for $0.5\,\mathrm{GeV}/c^2$ WIMPs.

Altogether, as summarized in Fig. 1, these WIMP searches cover the wide mass range from 0.32 to 10^4 GeV/c^2 with our cross section limits in a single detector, and are the world best results from a single phase LXe detector.

Search for WIMP-^{129}Xe inelastic scattering with particle identification

A WIMP search through inelastic scattering, in which ^{129}Xe nuclei were excited, was conducted with a live time of 800.0 days collected between November 2013 and July 2016 [4]. An observation of WIMP-nucleus inelastic scattering would be direct evidence of a spin dependent (SD) interaction mechanism as well as that WIMPs have spin since nuclear excitation in inelastic scattering can be mediated only by SD interactions. This updates our previous study published in 2014.

The sensitivity for inelastic excitation was improved by a detailed evaluation of background, event classification based on scintillation timing that distinguished γ-rays from β-rays, and simultaneous fitting of the energy spectra of γ-like and β-like samples. No evidence of a nuclear excitation was found. Thus, we set an upper limit for the inelastic cross section at 90% CL. At $200\,\mathrm{GeV}/c^2$, this result improved the limit for SD WIMP-neutron interactions via the inelastic channel by a factor of 7.7, as can be seen in Fig. 2. This is still the most stringent constraint for the WIMP masses less than 100 GeV/c^2 even after XENON1T published a new result in 2021 [11].

Search for exotic neutrino-electron interactions

Its very low energy threshold and low background make the XMASS-I detector also suitable for variety of rare event

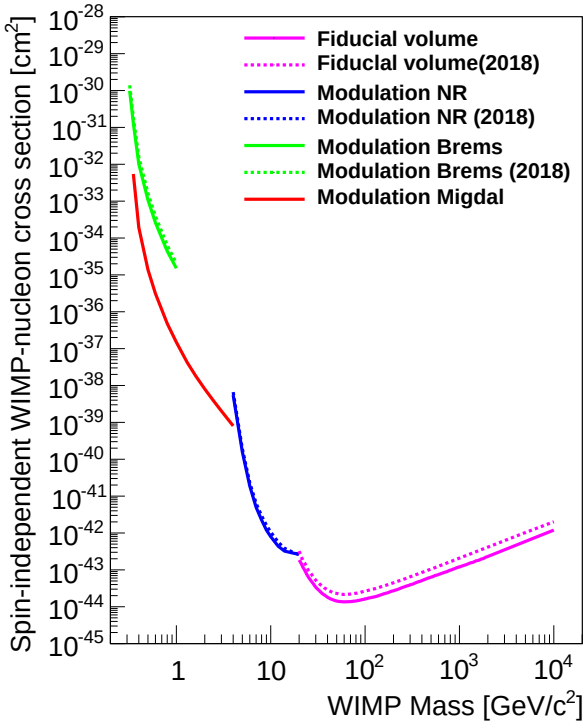

Fig. 1. Limits obtained from various analyses. Solid lines are new results, using the full XMASS-I data sets, in particular the fiducial volume analysis, the muliti-GeV modulation analysis via NR and the sub-GeV modulation analysis via Migdal effect and bremsstrahlung. Dotted lines show our respective earlier results.

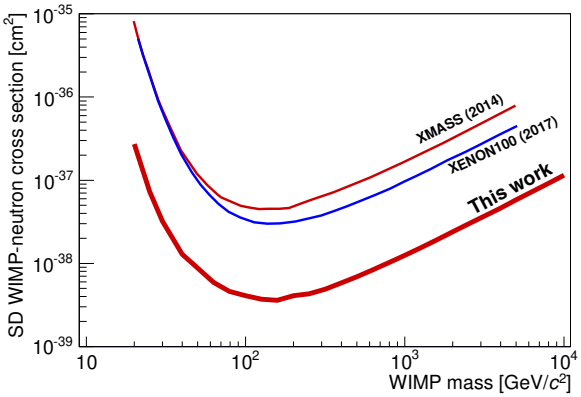

Fig. 2. 90% CL upper-limit for the WIMP-neutron cross section obtained by inelastic scattering searches. The result of this analysis is shown as a solid bold line. The results of other experimental SD inelastic scattering searches are shown with solid lines: XMASS (2014), XENON100 (2017). Our constraint still provides the most stringent limit for a WIMP mass less than 100 GeV/c^2.

searches. Apart from dark matter limits, we also pioneered other searches. One of these was our search for exotic neutrino-electron interactions [5]. Those interactions could be produced by a neutrino millicharge, by a neutrino magnetic moment, or by dark photons, and the existence of these components would provide hints on models beyond the standard model (SM). We searched for a signal associated respective increases in the cross section for electron-recoil from solar neutrino interactions.

A total of 711 days of livetime taken between November 2013 and March 2016 was used in these analyses. For neutrino millicharge case, we found no significant signal excess, which would have been expected around 5 keV, and accordingly we set an upper limit for neutrino millicharge of $5.4 \times 10^{-12} e$ at the 90% confidence level (CL), assuming all three species of neutrino have carry a common millicharge. Although there were previous constraints on the millicharges of $\overline{\nu}_e$ existed, this was the first study to provide constraints for all flavors of neutrinos. Figure 3 compares our result with those of other experiments.

We also searched for a signal excess due to a neutrino magnetic moment, but found none. The 90% CL upper limit for the neutrino magnetic moment was estimated from the χ^2 probability density function to be $\mu_\nu = 1.8 \times 10^{-10} \mu_B$.

We also found no significant excess in a search for a signal due to a dark photon with $M_{A'}$ in the range from 1×10^{-3} MeV/c^2 to 1×10^3 MeV/c^2, leading to a 90% CL upper limit on the coupling constant as a function of the dark photon mass as shown in Figure 4 together with the limits and allowed region from other experimental and astrophysical analyses.

Search for neutrinoless quadruple beta decay of ^{136}Xe in XMASS-I

The neutrinoless double beta decay ($0\nu\beta\beta$) is one of a lepton number(L) violating process ($\Delta L = 2$) beyond the SM. Observing the $0\nu\beta\beta$ would explain the extremely light neutrino mass and baryon number asymmetry in the universe via leptogenesis. Although a number of experiments have been performed, no evidence has been found so far. On the other hand, Heeck and Rodejohann proposed that even if the neutrino is a Dirac particle, a decay that violates the lepton number by four ($\Delta L = 4$) can occur by adding three right-handed neutrinos to the SM. This $\Delta L = 4$ process is naturally linked to the light Dirac mass terms of neutrinos, CP violation and leptogenesis. The neutrinoless quadruple beta decay ($0\nu4\beta$) violates lepton number by four units. Of the three nuclei than can undergo this process, only ^{150}Nd had been probed experimentally already. The Q-value of the ^{136}Xe $0\nu4\beta$ ($Q_{0\nu4\beta}$) is 79 keV. In a neutrinoless quadruple beta decay of ^{136}Xe, four β-rays with a total energy of 79 keV are emitted simultaneously. Since these β-rays are expected to deposit all their energy in the LXe at each decay, a monochromatic peak is expected in the energy spectrum.

A search for $0\nu4\beta$ decay from ^{136}Xe in XMASS-I was carried out with the data accumulated from November 2013 to July 2016 [6]. As a result, no significant signal excess was found over the expected BG. The calculated 90% CL lower limit is 3.7×10^{24} years for the neutrinoless quadruple beta decay of ^{136}Xe. This was the first experimental constraint on the neutrinoless quadruple beta decay of ^{136}Xe, a pioneering experimental result.

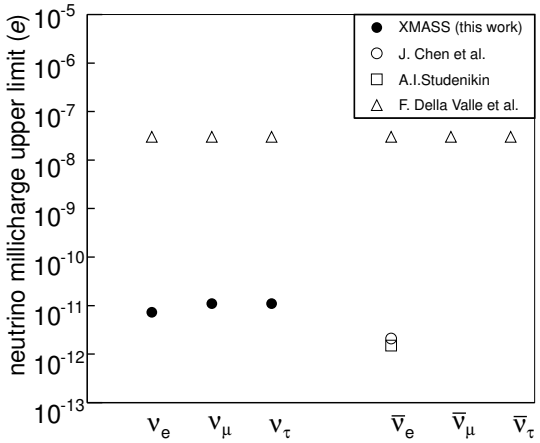

Fig. 3. 90% CL upper limits for neutrino millicharge for each flavor in our and other experiments. Although there were constraints on millicharges for $\overline{\nu}_e$, this was the first study to provide constraints for each flavor of neutrinos.

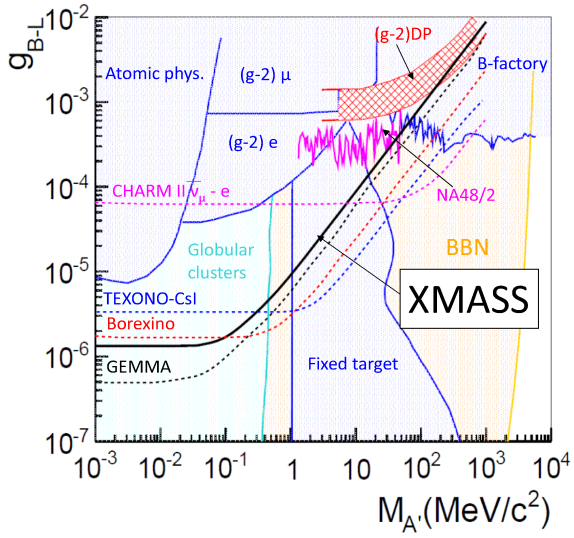

Fig. 4. 90% CL exclusion limits and allowed regions for the coupling constant g_{B-L} as a function of the dark photon mass $M_{A'}$. The black-solid line shows the exclusion limit from our analysis (XMASS). The 2σ-allowed-region band from the muon (g-2) experiment is shown as "(g-2) DP" as the red-meshed region. Colored regions have been constrained by other experiments and theoretical considerations.

Development of low-background photomultiplier tubes for liquid xenon detectors

While the R10789 PMT used in the XMASS-I experiment is a very low BG PMT developed especially for XMASS-I [12], it is still crucial to develop PMTs with lower radioactive impurities (RIs) and better performance. Such improved PMTs will not only be needed to improve dark matter searches, but also be useful in other rare event searches beyond the standard model, such as search for neutrinoless double beta decay.

With Hamamatsu Photonics we successfully developed a new such PMT with a three-inch diameter, convex-shaped photocathode, the R13111 [7]. It excelled in both, performance and ultra-low radioactivity. The convex-shaped photocathode realized a larger angular acceptance and better timing resolution. Low radioactivity was achieved by three improvements: (1) low radioactive synthesized quartz glass was employed for the entrance window, (2) glass beads for the electrode feedthroughs that were synthesized from low radioactivity materials selected with HPGe detectors and ICPMS, and (3) a photocathode produced with ^{39}K enriched potassium.

As a result, each R13111 PMT contains only about 0.4 mBq of ^{226}Ra, less than 2 mBq of ^{238}U, 0.3 mBq of ^{228}Ra, 2 mBq of ^{40}K and 0.2 mBq of ^{60}Co. Among PMTs the R13111 achieved the lowest radioactive contamination in the world. With its low radioactivity, excellent timing resolution, and large angular acceptance the new R13111 PMT will be an excellent candidate for use in future low BG LXe detectors.

Other scientific results and technical achievements

Beyond the core achievements discussed above, XMASS-I data produced results that marked significant improvements all throughout its long and stable data taking. Those were further WIMP dark matter searches using a fiducialized volume [13] and annual modulation [14], and two pioneering analyses: search for hidden photons [15], and a gravitational wave related event search [16]. As technical results, a liquid xenon scintillation decay time measurement [17] and the description of the low BG PMT development for the XMASS-I PMT R10789 [12], were published. XMASS thus left us a sound foundation on which future dark matter experiments can be build.

XMASS Collaboration

Spokesperson : Shigetaka Moriyama (Kamioka Observatory, ICRR, The University of Tokyo)

Institute	Country	(*)
ICRR, Univ. of Tokyo	Japan	5
Kavli IPMU, Univ. of Tokyo	Japan	1
Kobe Univ.	Japan	2
Tokai Univ.	Japan	1
Yokohama National Univ.	Japan	1
Miyagi Kyoiku Univ.	Japan	1
Nagoya Univ.	Japan	1
Tokushima Univ.	Japan	1
Nihon Univ.	Japan	1
Tohoku Univ. (from Apr. 2019)	Japan	2
Waseda Univ. (from Apr. 2020)	Japan	1
Institute for Basic Science	Korea	2
Korea Research Institute of Standards and Science (KRISS)	Korea	2
Seoul National Univ.	Korea	2
Tsuinhua Univ.	China	4
Total		27

(*) Number of collaborators.

Members

Staff

Masayuki Nakahata, Professor
Yasuhiro Kishimoto, Associate Professor (till March 2019)
Hiroyuki Sekiya, Associate Professor
Atsushi Takeda, Associate Professor (from Feb. 2020)
Atsushi Takeda, Research Associate (till Jan. 2020)
Ko Abe, Assistant Professor
Kazuyoshi Kobayashi, Project Assistant Professor (till March 2020).
Katsuki Hiraide, Project Assistant Professor (till April 2020).
Koichi Ichimura, Project Assistant Professor (till January 2019)

Postdoctoral Fellows

Kazufumi Sato, PD Researcher Associate (till March 2019)

Graduate students

One student was awarded doctor degrees during 2018-2024, supervised by UT staff members.

2. XENON

In this section, contributions of the ICRR group and major scientific results are described.

Liquid xenon purification and monitoring

Purifying LXe is crucial for extracting the maximum information available about events in the detector, be they signal or BG. In a LXe time projection chamber (TPC), depicted in Fig. 5, signals are generated as follows: when a recoil occurs, scintillation light produces an S1 signal, and an applied electric field extracts the electrons formed by ionization from the recoil to produce the S2 signal. If the S2/S1 ratio is high, the event is classified as an electron recoil (ER) event; if low, it is classified as a nuclear recoil (NR) event, such as a potential WIMP dark matter candidate. Efficient extraction of ionized electrons is essential for accurate discrimination between these events. Impurities in LXe that trap electrons before they can be extracted reduce the S2 signal and negatively impact this discrimination.

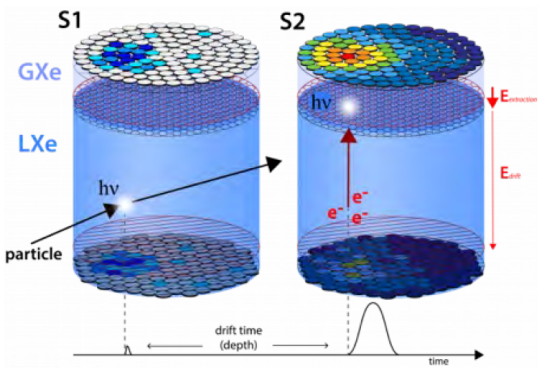

Fig. 5. Principle of operation of LXe time projection chamber (TPC).

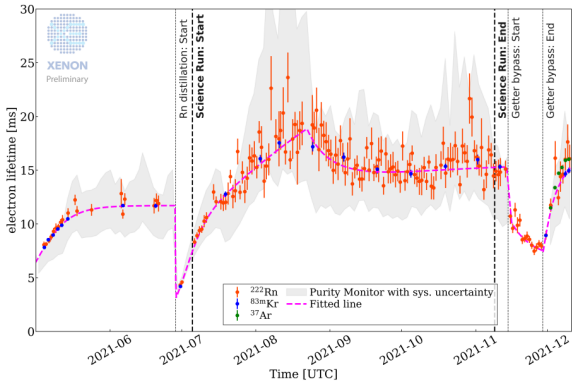

Fig. 6. Electron lifetime during the science run 0. Red, blue, green points show electon lifetime measured using ^{222}Rn, ^{83m}Kr, ^{37}Ar, respectively. A filter material St707 proposed by ICRR was used as it emits negligible radon gas. ICRR also developed and provided a purity monitor, whose measurement results are shown by the gray band.

Our research focused on developing a technique to reduce these electron-capturing impurities, with oxygen being a typical example. Previous experiments, like XENON1T and XMASS-I, purified LXe by evaporating it into the gas phase, passing it through a getter to remove impurities, and reliquefying it. However, the XENONnT experiment used about five times more LXe than XENON1T, and gas-phase purification was going to be insufficient due to its slower purification speed. Therefore, liquid-phase purification was planned and implemented.

This R&D effort was conducted in collaboration with Columbia University. A filter material Q5 used in liquid argon, was considered but known to emit radon gas, which is detrimental to dark matter searches. As it is known to emit only negligible amounts of Rn, the ICRR group proposed using St707, a getter material typically used for gas purification at high temperatures, at LXe temperatures for LXe purification. With assistance from the Columbia group, St707 was tested and confirmed effective for LXe purification. Initially, Q5, with its high impurity removal performance, was used to reduce impurities in the early stages of the experiment. Subsequently, St707 was used to continuously remove impurities slowly emitted from detector components. Radon has a half-life of 3.8 days, so even if Q5 emits radon, it decays within a manageable period without negatively impacting the results after switching over St707. During science run data taking St707 then kept removing newly emerging electronegative contaminants without adding noticeable amount of radon. Figure 6 shows the electron lifetime, as measured by the ICRR built purity monitor, during the actual science run, confirming purity from electronegative contaminants well beyond the original 3 ms electron survival time goal. These methods will be applied to larger detectors in the future. The purity monitor was developed utilizing the existing facilities of XMASS in the underground laboratory. Initial studies on liquid purification were detailed in a doctoral dissertation from the University of Tokyo [18].

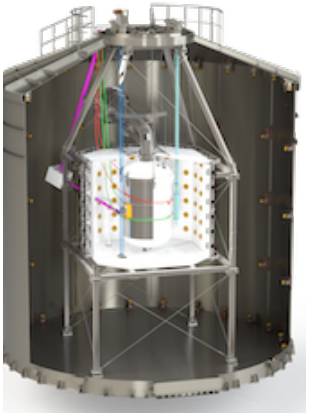

Fig. 7. Overview of the XENONnT detector. The white part is the neutron veto detector. The LXe TPC is at the center, surrounded by the white reflective material, and 120 PMTs are used to detect the Cherenkov lights produced by gamma rays when neutrons are captured by gadolinium or other nuclei and used to identify the neutrons. The water tank is 10 m in diameter and 10 m in height, and 0.2% of gadolinium will be added to the entire system.

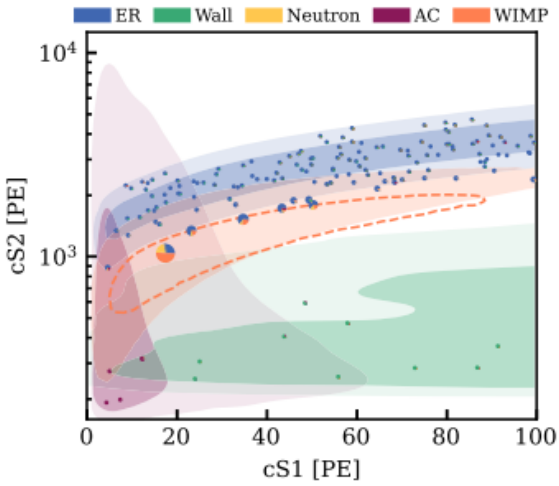

Fig. 8. SR0 dark matter search data in the cS1-cS2 space. Each event is represented with a pie chart showing the fraction of the best-fit model, including the expected number of $200\,\mathrm{GeV/c^2}$ WIMPs (orange) evaluated at the position of the event. The size of the pie chart is proportional to the signal model at that position. Distributions of background probability density are shown as 1σ (dark) and 2σ (light) for ER (blue), AC (purple), and wall (green). The orange dashed contour contains 50% of a $200\mathrm{GeV/c^2}$ WIMP signal. The neutron background has a similar distribution to the WIMPs. Figure from Ref. [8].

Neutron background tagging utilizing SK-Gd technology

Background reduction is critical in rare event searches, and XENONnT focuses on two primary background sources, radon in the LXe and neutrons emitted from other instrument materials. The ICRR group contributed to the design, development, and operation of a neutron veto detector that identifies these neutrons and reduces the background on an event-by-event basis. This is achieved using the gadolinium-doped water Cherenkov detector technology developed at Kamioka for Super-Kamiokande. Figure 7 shows a full view of the XENONnT detector, housed in a water tank with a white reflective material that optically isolates the neutron veto, which surrounds the LXe TPC at its center. The neutron veto is equipped with 120 PMTs, recording flashes of Cherekov light in the highly reflective neutron veto volume. By adding 0.2% gadolinium to the tank water, neutrons emitted from the detector components are expected to be captured by gadolinium with a high probability if they reach the neutron veto after recoiling from xenon nuclei in the TPC. Once the gadolinium captures a neutron, the PMTs in the neutron veto detect the Cherenkov light emitted by gamma rays absorbed in the water after emission from the gadolinium nucleus that captured the neutron. This highly efficient tagging of neutrons helps eliminate background events in the WIMP search, thereby maximizing the sensitivity of the experiment. XENONnT aims to tag approximately 87% of such neutron events, which would otherwise be indistinguishable from dark matter events.

The construction of the neutron veto detector was completed in 2020. With the assistance of the Super-Kamiokande collaboration, ICRR obtained 3 tons of the purest grade gadolinium sulfate in Japan and delivered it to LNGS. In 2021, the installation of a gadolinium-loaded water purification plant, modeled on EGADS' nanofiltration technology, was completed, and in 2022, commissioning tests of the plant were conducted using both pure water and Gd-loaded water. These tests were successful and subsequent calibrations led to an optimized neutron veto analysis.

During the first science run, Science Run 0 (SR0), the neutron veto was operated with pure water, which through capture on hydrogen already provided a neutron tagging efficiency of 53%. By the end of 2023 an initial 350 kg of Gd sulfate had been dissolved in XENONnT' veto counter system, arriving at a Gd loading of 0.02% in the neutron veto's water. Even only 1/10 of the planned final Gd loading, we achieved 77% of the neutron tagging efficiency. This demonstrated the expected performance of the nVeto. We plan to load the full amount of Gd sulfate and achieve a tagging efficiency of 87%, which will reduce the neutron BG in future NR analyses by a factor of eight.

First Dark Matter Search with Nuclear Recoils from the XENONnT Experiment

XENONnT's first, fully blind NR analysis was using the SR0 dataset collected from July 6, 2021 to November 10, 2021 with a total exposure of (1.09 ± 0.03) ton-years [8]. Since the NV was operated as a pure water Cherenkov detector during SR0 as stated above, neutron tagging was conducted through their capture on hydrogen, which upon neutron capture releases a 2.22 MeV γ ray.

Data quality cuts were applied in order to include only well-reconstructed events in the TPC and to suppress backgrounds. All cuts were optimized based on calibration data and simulations. Events tagged by the muon veto (MV) or NV are removed from the data selection, as are multiple-scatter events: WIMPs are not expected to scatter more than once in the detector.

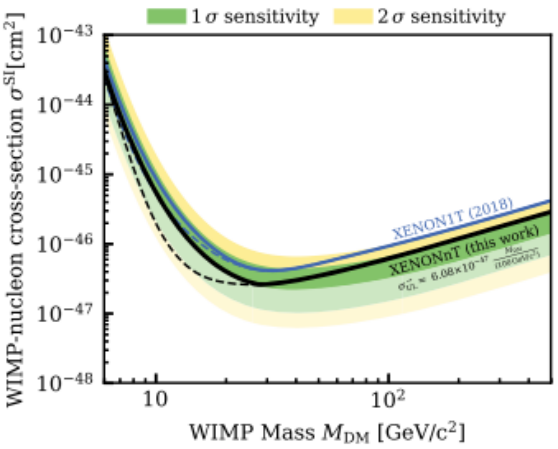

Fig. 9. Upper limit (black line) and sensitivity (color shaded region) on spin-independent WIMP-nucleon cross section at 90% confidence level as a function of the WIMP mass. A power constraint is applied to the limit to restrict it at or above the median unconstrained upper limit. The dashed lines show the upper limit without a power constraint applied. Figure from Ref. [8].

Figure 8 shows the data in XENONnT's cS1-cS2 analysis space [8], containing 152 events in the region of interest, 16 of which emerged after unblinding data. The WIMP discovery p-value indicates no significant excess ($p \geq 0.20$, with the minimum for masses above $100\,\mathrm{GeV/c^2}$), and the resulting limits on spin-independent WIMP-nucleon cross section at 90% confidence level are shown in Fig. 9. The minimum upper limit was $2.58 \times 10^{-47}\,\mathrm{cm^2}$ for a WIMP mass of $28\,\mathrm{GeV/c^2}$.

Currently, XENONnT continues to take data, with a further reduction of ^{222}Rn ER background, using the radon distillation system with combined gaseous and LXe flows. The NV started to operate with 0.02% of Gd concentration, as stated above.

Search for New Physics In Electronic Recoil Data from XENONnT

As we had reported excess electric recoil (ER) events in XENON1T [10], we conducted a search for new physics using ER interactions in the SR0 dataset [9]. The ER signal region in S1-S2 space was blinded below 20 keV. A fiducial mass of (4.37 ± 0.14) tons is used for this analysis, yielding a total exposure of 1.16 ton-years. We considered three categories of potential signals in this search: (a) solar axions, (b) solar neutrinos with an enhanced magnetic moment, and (c) bosonic dark matter, which primarily includes axionlike particles and dark photons.

In the BG model B_0 we considered nine components: ^{214}Pb, ^{85}Kr, gamma rays from detector materials, ^{136}Xe, electron scattering caused by solar neutrinos, ^{124}Xe, ACs, ^{133}Xe and ^{83m}Kr. After all aspects of the blind analysis had been fixed and good agreement between the BG model and data above 20 keV was found (p-value$\sim$0.2), the region between $\pm 2\sigma$ quantiles of ER events in S2 was unblined. The best fit of B_0 is shown in Fig. 10. The SR0 dataset agrees well with B_0, and no excess above the BG is found.

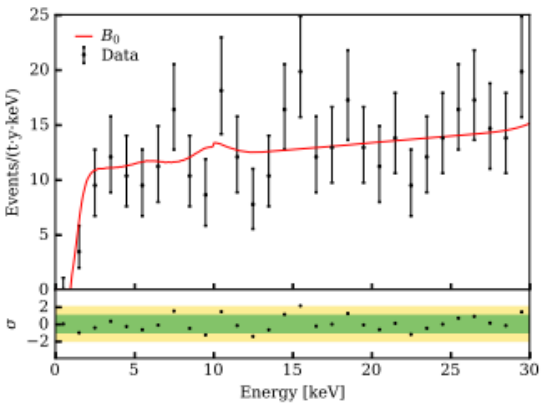

Fig. 10. Data and best-fit B_0 model below 30 keV. No significant excess above the BG was found. Figure from Ref. [9].

The efficiency-corrected average ER BG rate betwee 1 and 30 keV is measured to be $(15.8 \pm 1.3_{\mathrm{stat}})$ events/(t y keV), a factor of 5 lower than the rate measured in XENON1T. This is the lowest BG rate achieved at these energies by any existing dark matter direct detection experiments.

We determined the 90% confidence level upper limits on solar axions, solar neutrinos with an enhanced magnetic moment, axionlike particles, and dark photons together with sensitivity bands estimated from the BG only fit. We also searched for a tritium component on top of the BG model B_0. The best-fit rate of tritium is 0 and the upper limit (90% confidence level) is 15 events/(t y). Since our ER background is the world's lowest, our limits are also the most stringent.

First measurement of a nuclear recoil signal from solar neutrinos

Neutrinos from the Sun can interact with the nuclei of the xenon atoms in the XENONnT target via coherent elastic neutrino-nucleus scattering (CEvNS). Now, XENONnT is the first experiment to measure CEvNS with neutrinos produced in the core of the sun, and to measure CEvNS on xenon nuclei. XENONnT's low-energy detection capabilities and ultra-low BG environment enabled this first measurement. This analysis used data collected over two years, from July 7, 2021 to August 8, 2023, for a total exposure of approximately 3.5 tonne-years. An excess of low-energy nuclear recoil events over the expected BG was measured, compatible with the expected signal from solar ^{8}B neutrino interactions, with a statistical significance of 2.73σ. The result was obtained through a blind analysis. This marks the first measurement of CEvNS from an astrophysical neutrino source. Moreover, such a significant result opens a new chapter in the direct dark matter detection field: XENONnT started exploring the so-called neutrino fog, where neutrino interactions are becoming a BG that mimics dark matter signals.

Other scientific results and technical achievements

We are actively publishing scientific results from XENON1T and XENONnT, describing searches for new

physics and rare events [11, 19, 20, 21, 22, 23], and technical matters [24, 25, 26, 27, 28, 29, 30, 31, 32].

Toward future G3 experiments

There are activities to realize future G3 experiments in the world [33]. One representative group is XLZD. It consists of members of the XENON, LZ, and DARWIN collaborations, who aim to realize a G3 experiment. This activity was endorsed by the Cosmic Ray Research Congress (CRC) and listed in the "Future Academic Initiative" published by the Science Council of Japan in 2023. ICRR senior staff signed an XLZD collaboration agreement. The ICRR members will decide the material extent of their participation to the collaboration when Hyper-K construction and commissioning are mostly completed.

XENON Collaboration

PI of ICRR, UT : Shigetaka Moriyama (Kamioka Observatory, ICRR, The University of Tokyo)

The XENON collaboration consists of about 200 researchers and technicians from 29 institutes in 12 countries.

Institute	Country	(*)
ICRR, Univ. of Tokyo	Japan	6
Kavli IPMU, Univ. of Tokyo	Japan	3
Kobe Univ.	Japan	3
Nagoya Univ.	Japan	5
Total		17

(*) Number of collaborators from Japanese institutes as of July 2024.

Members in ICRR

There are 17 collaborators in XENONnT from Japanese institutions. Here we only list ICRR members, the University of Tokyo.

Staff

Atsushi Takeda, Associate Professor (from Feb. 2020)
Atsushi Takeda, Assistant Professor (till Jan. 2020)
Ko Abe, Assistant Professor
Masaki Yamashita, Project Associate Professor (till March 2020)
Katsuki Hiraide, Project Assistant Professor (till April 2020).

Postdoctorial Fellows

Masatoshi Kobayashi, JSPS research fellowship (till September 2019)
Masashi Yoshida, ICRR Postdoctoral Fellowship

Graduate students

One student was awarded doctor degrees and three students earned master degrees during 2018–2024, supervised by ICRR staff members.

Bibliography

Before Year 2018

[1] K. Abe *et al.* (XMASS Collaboration), "XMASS detector", Nucl. Instrum. Meth. A **716** (2013) 78 arXiv:1301.2815, **Cited 177 times.**

After Year 2018

[2] E. Aprile *et al.* (XENON Collaboration), "Projected WIMP Sensitivity of the XENONnT Dark Matter Experiment", JCAP 11 (2020) 031 arXiv:2007.08796, **Cited 360 times.**

[3] K. Abe *et al.* (XMASS Collaboration), "Direct dark matter searches with the full data set of XMASS-I", Phys. Rev. D **108** (2023) 083022 arXiv:2211.06204, **Cited 7 times.**

[4] T. Suzuki *et al.* (XMASS Collaboration), "Search for WIMP-^{129}Xe inelastic scattering with particle identification in XMASS-I", Astropart. Phys. **110** (2019) 1 arXiv:1809.05358, **Cited 17 times.**

[5] K. Abe *et al.* (XMASS Collaboration), "Search for exotic neutrino-electron interactions using solar neutrinos in XMASS-I", Phys. Lett. B **809** (2020) 135741 arXiv:2005.11891, **Cited 22 times.**

[6] K. Abe *et al.* (XMASS Collaboration), "Search for neutrinoless quadruple beta decay of 136Xe in XMASS-I" Phys. Lett. B **833** (2022) 137355 arXiv:2205.05231, **Cited 0 times.**

[7] K. Abe *et al.* (XMASS Collaboration), "Development of low-background photomultiplier tubes for liquid xenon detectors", JINST **15** (2020) P09027 arXiv:2006.00922, **Cited 6 times.**

[8] E. Aprile *et al.* (XENON Collaboration), "First Dark Matter Search with Nuclear Recoils from the XENONnT Experiment", Phys. Rev. Lett. 131, 041003 (2023) arXiv:2303.14729, **Cited 226 times.**

[9] E. Aprile *et al.* (XENON Collaboration), "Search for New Physics In Electronic Recoil Data from XENONnT", Phys. Rev. Lett. 129, 161805 (2022) arXiv:2207.11330, **Cited 212 times.**

[10] E. Aprile *et al.* (XENON Collaboration), "Excess Electronic Recoil Events in XENON1T", Phys. Rev. D 102, 072004 (2020) arXiv:2006.09721, **Cited 641 times.**

[11] E. Aprile *et al.* (XENON Collaboration), "Search for inelastic scattering of WIMP dark matter in XENON1T", Phys. Rev. D 103, 063028 (2021) arXiv:2011.10431, **Cited 27 times.**

[12] K. Abe *et al.* (XMASS Collaboration), "Development of low radioactivity photomultiplier tubes for the XMASS-I detector", Nucl. Instrum. Meth. A **922** (2019) 171 arXiv:1808.03617, **Cited 14 times.**

[13] K. Abe *et al.* (XMASS Collaboration), "A direct dark matter search in XMASS-I", Phys. Lett. B **789** (2019) 45 arXiv:1804.02180, **Cited 69 times.**

[14] M. Kobayashi *et al.* (XMASS Collaboration), "Search for sub-GeV dark matter by annual modulation using XMASS-I detector", Phys. Lett. B **795** (2019) 308 arXiv:1808.06177, **Cited 30 times.**

[15] K. Abe *et al.* (XMASS Collaboration), "Search for dark matter in the form of hidden photons and axion-like particles in the XMASS detector", Phys. Lett. B **787** (2018) 153 arXiv:1807.08516, **Cited 45 times.**

[16] K. Abe *et al.* (XMASS Collaboration), "Search for event bursts in XMASS-I associated with gravitational-wave events", Astropart. Phys. **129** (2021) 102568 arXiv:2007.16046, **Cited 6 times.**

[17] K. Abe *et al.* (XMASS Collaboration), "A measurement of the scintillation decay time constant of nuclear recoils in liquid xenon with the XMASS-I detector", JINST **13** (2018) P12032 arXiv:1809.05988, **Cited 14 times.**

[18] N. Kato, doctoral dissertation, The University of Tokyo, 2021.

[19] E. Aprile *et al.* (XENON Collaboration), "Search for Coherent Elastic Scattering of Solar ^{8}B Neutrinos in the XENON1T Dark Matter Experiment", Phys. Rev. Lett. 126, 091301 (2021) arXiv:2012.02846, **Cited 112 times.**

[20] E. Aprile *et al.* (XENON Collaboration), "Emission of Single and Few Electrons in XENON1T and Limits on Light Dark Matter", Phys. Rev. D 106, 022001 (2022) arXiv:2112.12116, **Cited 78 times.**

[21] E. Aprile *et al.* (XENON Collaboration), "Searching for Heavy Dark Matter near the Planck Mass with XENON1T", Phys. Rev. Lett. 130, 261002 (2023) arXiv:2304.10931, **Cited 9 times.**

[22] E. Aprile *et al.* (XENON Collaboration), "Search for events in XENON1T associated with Gravitational Waves", Phys. Rev. D 108, 072015 (2023) arXiv:2306.11871, **Cited 1 times.**

[23] E. Aprile *et al.* (XENON Collaboration), "Double-Weak Decays of ^{124}Xe and ^{136}Xe in the XENONnT and XENONnT Experiments", Phys. Rev. C 106, 024328 (2022) arXiv:2205.04158, **Cited 24 times.**

[24] E. Aprile *et al.* (XENON Collaboration), "Energy resolution and linearity of XENON1T in the MeV energy range", Eur. Phys. J. C 80, 785 (2020) arXiv:2003.03825, **Cited 83 times.**

[25] E. Aprile *et al.* (XENON Collaboration), "^{222}Rn emanation measurements for the XENON1T experiment", Eur. Phys. J. C 81, 337 (2021) arXiv:2009.13981, **Cited 36 times.**

[26] E. Aprile *et al.* (XENON Collaboration), "Application and modeling of an online distillation method to reduce krypton and argon in XENON1T", Prog. Theor. Exp. Phys. 2022, 5 (2022) arXiv:2112.12231, **Cited 14 times.**

[27] E. Aprile *et al.* (XENON Collaboration), "Material radiopurity control in the XENONnT experiment", Eur. Phys. J. C 82, 599 (2022) arXiv:2112.05629, **Cited 26 times.**

[28] E. Aprile *et al.* (XENON Collaboration), "An approximate likelihood for nuclear recoil searched with XENON1T data", Eur. Phys. J. C 82, 989 (2022) arXiv:2210.07231, **Cited 3 times.**

[29] E. Aprile *et al.* (XENON Collaboration), "Low-energy Calibration of XENON1T with an Internal ^{37}Ar Source", Eur. Phys. J. C 83, 542 (2023) arXiv:2211.14191, **Cited 6 times.**

[30] E. Aprile *et al.* (XENON Collaboration), "Detector signal characterization with a Bayesian network in XENONnT", Phys. Rev. D 108, 012016 (2023) arXiv:2304.05428, **Cited 3 times.**

[31] E. Aprile *et al.* (XENON Collaboration), "The Triggerless Data Acquisition System of the XENONnT Experiment", JINST 18, P07054 (2023) arXiv:2212.11032, **Cited 6 times.**

[32] E. Aprile *et al.* (XENON Collaboration), "Design and performance of the field cage for the XENONnT experiment", Eur. Phys. J. C 84, 138 (2024) arXiv:2309.11996, **Cited 167 times.**

[33] J. Aalbers *et al.*, "A next-generation liquid xenon observatory for dark matter and neutrino physics", J. Phys G: Nucl. Part. Phys. 50 013001 (2023), **Cited 110 times.**

HYPER-KAMIOKANDE EXPERIMENT

Summary from 2018 to 2024

Key milestones achieved during the period covered by this review are as follows:

- 2020.2 The HyperK project has officially started [8].
- 2020.5 UTokyo and KEK sign MoU [9].
- 2020.6 Collaboration Agreement has been ratified.
- 2021.1 The production of 50 cm ϕ PMTs starts.
- 2021.5 The access tunnel excavation starts [10].
- 2022.11 Excavation of the main cavern has begun [11].
- 2023.10 Completion of the main cavern dome [12].
- 2023.12 J-PARC achieved a record 760kW beam [13].

In February 2020 the Hyper-Kamiokande (HyperK or HK) project has officially started with the approval of the first-year construction budget by the Japanese Diet [8]. Right after that, the University of Tokyo (UTokyo) and the High Energy Accelerator Research Organisation (KEK), and International Collaboration have established an organization and task sharing to promote the large international project. The collaboration has successfully doubled in size since 2018 and consists of 583 members from 104 institutes of 22 countries as of April 2024. Construction budgets are also successfully being obtained not only in Japan but also abroad including Canada, Czech Republic, France, Italy, South Korea, Mexico, Morocco, Poland, Russia, Spain, Switzerland, and UK. Moreover steady progress has been made in the 'construction of the Hyper-Kamiokande detector (hosted by UTokyo)' and the 'Upgrade of J-PARC neutrino beam power and near detector suite (hosted by KEK)'. Despite unforeseen challenges such as the pandemic, the invasion of Ukraine, various cost increases and extended delivery times, the project is expected to achieve its originally planned performance and is expected to start operation in the target year of 2027, after an extension of the construction period by about a half year. The DUNE US-based Next Neutrino Experiment Programme has been revised to start operating the beam in 2031 (originally planned for 2026), and the HyperK needs to be promoted steadily for the world-wide community.

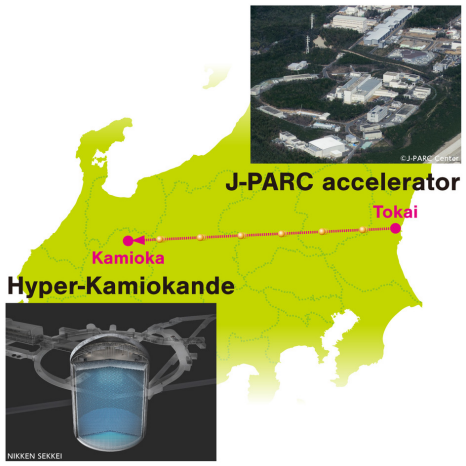

Fig. 1. Overall picture of the project. A neutrino beam produced by the upgraded J-PARC accelerator is observed by the Hyper-Kamiokande, built 295 km away underground in Kamioka town.

Introduction

The construction of the HyperK detector (see Fig. 1), a large, advanced detector containing 260,000 tons of ultrapure water, with an effective mass of 190,000 tons – eight times larger than that of SuperK, and an enhancement of the J-PARC Main Ring beam power to 1.3 MW, which is 2.5 times greater compared to 2020, are being carried out as part of the HyperK project [1, 7]. As shown in Fig. 2, the construction of the HyperK detector officially began in 2020. Starting in 2027, the combination of the HyperK detector and the upgraded J-PARC accelerator will enable measurements of neutrino oscillations with unprecedented precision, helping to uncover the full nature of these oscillations. Additionally, the HyperK detector, which features state-of-the-art photosensors with twice the performance of traditional ones, will play a unique role in searching for nucleon decay and observing supernova neutrinos. The HyperK detector will be a key international instrument for research in particle and astroparticle physics over the next 20 years.

Physics potentials

HyperK will be able to measure the magnitude of the leptonic *CP* violation with high precision, which could explain the baryon asymmetry in the Universe. Fig. 3 shows an expected significance of the *CP* violation (nonzero $\sin\delta_{CP}$) discovery by ten years operation. HyperK covers the 78% of δ_{CP} parameter space with 3σ or more significance, and 63% of the parameter space with 5σ or more. HyperK will go beyond 7σ significance if $\delta_{CP} = -90^\circ$ as suggested by T2K results. In this case, furthermore, HyperK will reach 5σ significance within three years assuming the improved systematic model. Moreover HyperK will have significant sensitivities to mass hierarchy, θ_{23} octant determination, and day-night asymmetry and spectrum upturn detection in solar neutrinos.

In Grand Unified Theories, which unify quarks and leptons and unify three forces other than gravity, the decay of proton is one of the most dramatic predictions. A proton decay $p \to e^+\pi^0$ is dominant decay mode mediated by heavy gauge bosons in various models with a prediction close to the current limit of the proton decay life time. Fig. 4 shows the 3σ discovery potential for the $p \to e^+\pi^0$ mode as a function of year. HyperK is an only realistic proposal which can go beyond the proton lifetime of 10^{35} years. HyperK will also

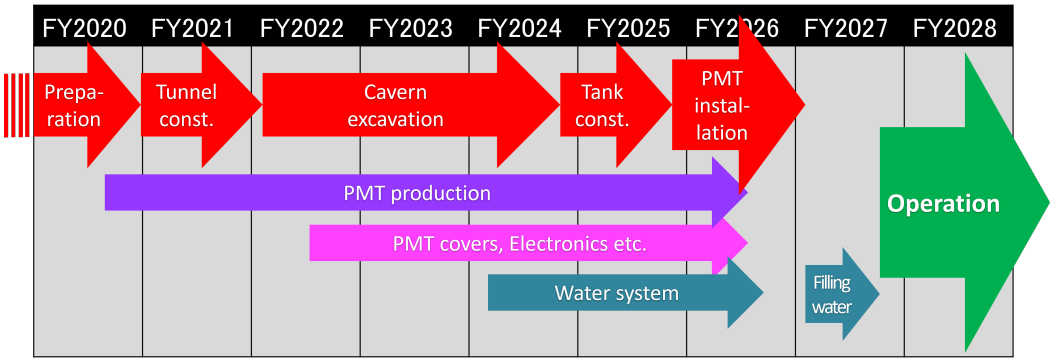

Fig. 2. Construction schedule of the HyperK project.

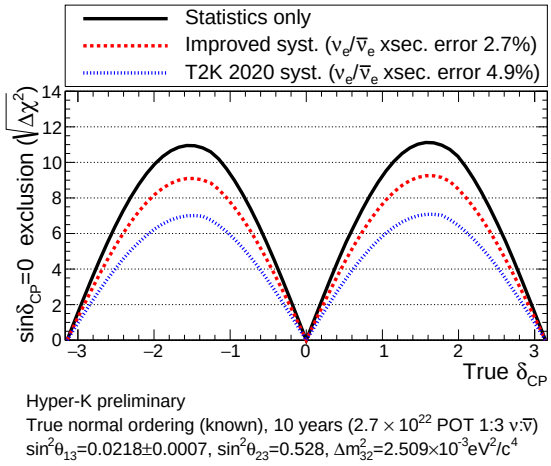

Fig. 3. $\sin\delta_{CP} = 0$ exclusion as a function of true δ_{CP} for 10 HK-years and different systematics models.

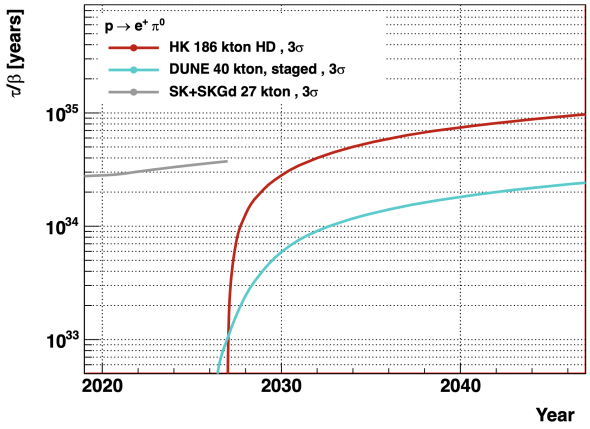

Fig. 4. The $p \to e^+\pi^0$ discovery reach in proton lifetime with 3σ significance as a function of year. It shows HyperK (HK) planing to start in 2027, superimposed with the ongoing SuperK (SK) + SK-Gd and planned DUNE experiments. The DUNE project assumes 10 kton operation from 2026, toward full 40 kton by increasing 10 kton every year.

extend reach to many other decay modes such as SUSY favored $p \to \bar{\nu}K^+$, decays into heavier mesons, and di-nucleon decays.

High statistics observations of neutrinos from a Core-Collapse Supernova (CCSN) along with gravitational waves are the only way to obtain precious inside information on the dynamics of the CCSN central engine and the explosion mechanism. If a CCSN explosion were to take place near the center of our Galaxy, HyperK would observe as many as tens of thousands of neutrinos with their arrival times precisely determined. Moreover the continuous flux of relic supernova neutrinos from all past CCSN explosions in the observable universe will guarantee a steady accumulation of valuable astrophysical data.

Project organization

UTokyo and KEK are the core institutions of the HyperK project, and researchers from domestic and overseas research institutes and universities have been cooperating to promote the project. UTokyo and KEK signed an MoU in 2020 to promote the HyperK project. Here UTokyo is defined to be responsible for construction and operation of the HyperK detector while KEK isfor the upgrade of the J-PARC accelerator and neutrino beamline, improvement of the facilities and equipment of the near detectors, and their operation. Under the host institutions, the Project Advisory Committee (PAC) is held 3 times a year to evaluate the progress of the project from technical and scientific viewpoints, and the Funding Oversight Panel (FOP) is held twice a year to advance securing budget in each country and forming consensus on a cost-sharing plan among countries.

An international research group “Hyper-Kamiokande Collaboration” was officially formed in 2020 (nearly 80% of the members are from overseas), and a set of bylaws outlining the collaboration’s agreement was established to define management structure, various construction working groups, spokespersons and other positions. Thus, we defined the overall scope of the HyperK experiment, clarified the division of responsibilities among the host institution and the collaboration within that context, and established a project promotion system.

Facility construction

The excavation of the underground cavern and subsequent construction of the water tank and photomultiplier tube support structure (hereafter referred to as “PMT support structure”) form the first critical path in the construction of the Hyper-Kamiokande.

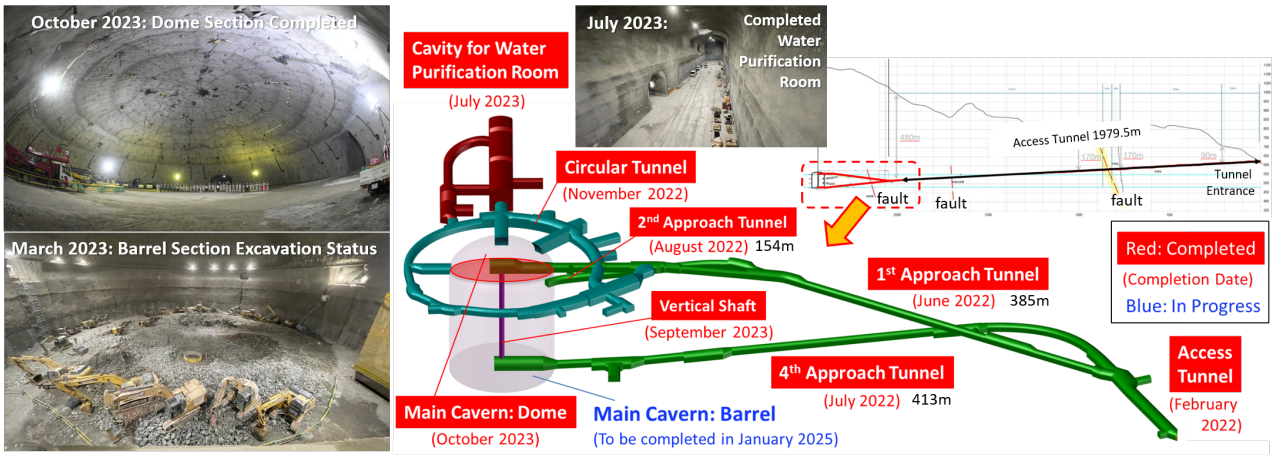

Fig. 5. Overview of the Hyper-K cavern excavation.

Cavern excavation

The main cavern facility where the Hyper-Kamiokande will be installed consists of a 69 m diameter, 73 m high cylindrical section and a 21 m high dome section that supports it, making it one of the largest underground artificial cavern in the world. Due to the high degree of difficulty in design and construction, the Early Contractor Involvement (ECI) scheme was adopted, which allows the technical capabilities of the contractor to be reflected in the design of the project from the design stage.

Figure 5 shows an overview of the cavern excavation. In FY2018-2020, a focused geological survey was conducted to finally pin-down the HK cavern location and to obtain the necessary information for the cavern stability analysis. Preparation work at the access tunnel entrance to the underground site was conducted in FY2020. In May 2021, excavation of the access tunnel (2.0 km) to reach the water tank construction location began, and was completed in February 2022. In June 2022, the tunnel to the top of the main cavern (0.4 km) reached the center of the dome section. Excavation of the surrounding cavities around the main cavern followed, and the circular tunnel was penetrated in November 2022. The circular tunnel runs around the main cavern (445 m) and is used to install the necessary equipment for the experiments. Although the amount of excavation increased significantly from the original plan due to the detailed design, we were able to minimize the impact on the overall construction period by excavating the circular tunnel in parallel with the main cavern. The excavation of the water system cavern (16 m wide, 17 m high, and 100 m length), which houses the water purification system, also proceeded in parallel with the main cavern, and was successfully completed in FY2023.

Excavation of the dome section began in November 2022. Based on the results of geological survey in FY2020, the dome height was changed from 14.5 m to 21 m in order to significantly improve excavation safety and cavern stability. Since it is impossible to grasp the entire bedrock condition around the cavern, information-oriented design and construction was essential to reflect the behavior of the bedrock due to excavation in the design and construction process. In October 2023, the 69 m diameter, 21 m high dome section was completed. 600 m worth of ground pressure was supported by the excavated dome section, which is the key to ensuring the cavern stability, and an important milestone in the construction of the HyperK was achieved without any major accidents.

Toward the end of 2023, the circumferential crane used for water tank lining was installed. The dust-proof painting of the dome section is also being carried out at the same time. To optimize the overall construction period and cost, the plan has been changed to be implemented during cavern excavation. Excavation of the barrel section of the main cavern began in January 2024. As of March 2024, excavation of 17 m out of the total height of 73 m has been completed. Excavation is underway with completion scheduled for January 2025, while keeping a close eye on bedrock behavior during excavation. Despite the increased excavation volume due to the change in dome height, activity restrictions due to COVID-19, and the installation of the circumferential crane during the excavation, the excavation period was only extended by two months compared to a total of 48 months.

Water tank construction

The “basic design” for the water tank lining, PMT support structure, and peripheral equipment planned for construction after the completion of cavern excavation was completed at the end of 2021, and the “detailed design” and “construction plan” at the end of 2023. As shown in Fig. 6, the tank has an inner diameter of 68 m and a height of 72 m (water level 71 m). The PMT support structure is arranged so that the thickness of the outer detector layer is 1 m at the sides, 2 m at the bottom, and 2 m from the water surface at the roof, thus ensuring a total water capacity of 260,000 tons and an effective mass of 190,000 tons. The tolerance for the position of the PMT is $\pm$25 mm, and the tolerance for the inner radius of the tank lining surface is between -0 mm and +100 mm from the reference value (= 34 m). In addition, the structure is designed to be safe so that the structure will not be plastically deformed even if an earthquake of the maximum intensity expected in the area (L2 earthquake, assuming both horizontal and vertical shaking) occurs under the most severe conditions with no water in the tank at all. The Noto earthquake that occurred in January 2024, which included the area in question,

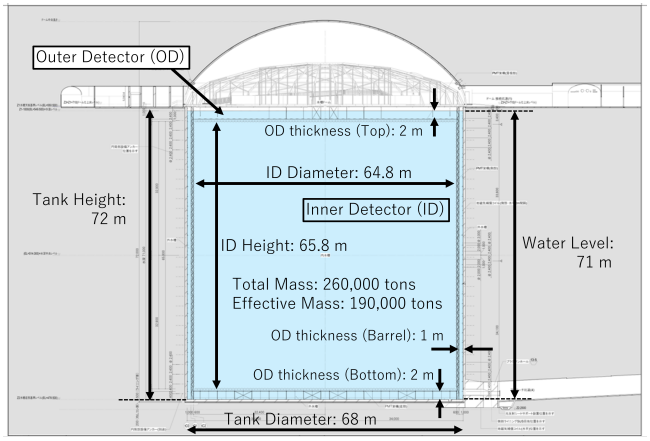

Fig. 6. Cross-sectional view of the water tank.

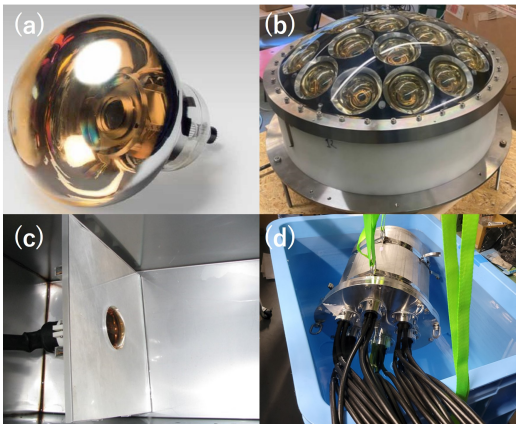

Fig. 7. (a) a 50cm PMT developed for HyperK, (b) a prototype of a multi-PMT module, (c) a prototype of an OD photo detection module, and (d) a prototype of electronics in the water-tight vessel.

is said to be a once-in-a-century earthquake in the area, but it was within the scope of this design assumption.

The design work started by the design company at the end of FY2020, and technical cooperation work by the construction company was added in April 2021, using the ECI scheme, which is the same scheme used for cavern excavation. The basic design was carried out to minimize the overall cost and construction period while meeting the required detector performance, and to ensure safety. In the construction of the PMT support structure, where the PMT installation work by the researchers and the support structure construction work by the contractor had to be separated, the construction height per cycle of the side of the structure was devised so that the work by the researchers would not be performed at a high place. Another important feature is the steel dome. By modifying the top section of the PMT support structure to a structurally rational dome shape (the outside of the tank is made of ordinary steel), we succeeded in reducing the quantity of stainless steel materials, which are susceptible to price hikes, while increasing the load capacity and improving safety. This design change is the dominant reason for the extension of the construction period by about a half year.

The design work for the ultrapure water system, which will supply water to the HyperK tank in 2027 and continue in operation thereafter, has been completed. The contract for constructing the system was awarded as scheduled in April 2024.

Detector construction

The HyperK detector will be equipped with 50cm photomultiplier tubes (PMTs) and multi-PMTs for the Inner Detector (ID). The ID is surrounded by the Outer Detector (OD). The integrated electronics system will be instrumented both for ID and OD PMTs. The design and development of these components have been promoted by international coorperation from many countries including Japan.

50cm PMTs

The development and performance evaluation of 50cm PMTs for HyperK (see Fig. 7 (a)) had been completed by the summer of 2020. The charge resolution and timing resolution of the HyperK PMTs are 27±4% and 1.5±0.1 ns, respectively. These values are approximately half of those of the SuperK PMTs (HAMAMATSU R3600). Additionally, the single-photon detection efficiency of the HyperK PMTs is improved by a factor of 2 compared to that of the SuperK PMTs.

Mass production had started in 2020, and 9,257 units were delivered by April 2024. The PMT production progressed as scheduled despite the activity restrictions due to COVID-19. In the early stage of the mass production, we found a part of the PMTs showed unstable noise count rate during inspection at the delivery. Mass production was temporarily suspended to investigate the causes and by the improvements of the design the defective product rate was greatly reduced to meet the required specifications. The production of the glass bulbs, which is a rate-limiting part of PMTs, were continued to be manufactured during this period, and the delivery of the product is scheduled to be completed without any change in the originally planned cost and schedule.

The Spanish group is responsible for the design, manufacture, and assembling of the anti-chain-implosion covers to be attached to PMTs to prevent chain implosions of PMTs underwater and to ensure the safety of the HyperK. As the development is taking longer than originally planned, we formed a steering group to monitor the progress and make timely strategic decisions. We expect to complete the mass production without changing the originally planned cost and delivery date, since the improved design and manufacturing processes have enabled us to lower the cost and significantly increase the speed of mass production.

Multi-PMTs

A new type of photosensor called a “multi-PMT” that resembles a compound eye, consisting of 19 3-inch PMTs in a vessel, has been proposed by a group from Italy, Canada, Poland, the Czech Republic, and Mexico. The ID will be equipped with approximately 800 multi-PMTs in addition to the 50cm PMTs, which is expected to improve detector calibration with help of segmented angular coverage and better timing resolution of the multi-PMT. The design of the multi-PMT module has been completed and prototype modules have

been constructed as shown in Fig. 7 (b). To avoid the schedule delays, we have already begun procurement of the 3-inch PMTs which have a long delivery time.

Outer Detector (OD)

The OD surrounds the ID and acts mainly as a veto for entering particles such as cosmic-ray muons. It will consist of 3,600 outward-facing 3-inch PMTs embedded in 30 cm$\times$30 cm wavelength-shifting plates. The inner walls of the OD will be covered with highly reflective sheets. The design and construction of the OD system are being promoted by the UK, Korea, and Australia, with individual contributions from Japanese researchers. Initially, the UK was responsible for most of the OD, but they faced rising material costs and budget cuts. Therefore, we had set up a task force and made a new strategy. In addition to calling for participation from new countries, costs were reduced by changing the design to halve the number of PMTs while ensuring the required performance as originally planned. As shown in Fig. 7 (c), the design and performance evaluations have been completed.

Electronics

The frontend electronics will be placed under water nearby PMTs to avoid degradation of PMT signals. One set of frontend electronics consists of two digitizer boards, a communication board and HV/LV boards, which are assembled into a 1 MPa tolerant water-tight vessel. About 1,000 vessels process the signals from all ID and OD PMTs. The prototypes of the boards and water-tight equipments have been developed under international cooperation. The comprehensive tests under water was conducted in 2024 as shown in Fig. 7 (d), and the performance was confirmed to meet HyperK requirements. Many countries including Japan share the mass production of the components that began in 2024 on schedule.

Hyper-Kamiokande Collaboration

Co-spokespersons : Masato Shiozawa (Kamioka Observatory, ICRR, The University of Tokyo), Francesca Di Lodovico (King's College London)

Hyper-Kamiokande collaboration consists of 577 researches form 105 institutes in 22 countries: Armenia, Australia, Brazil, Canada, Czech, France, Germany, Greece, India, Italy, Japan, Korea, Mexico, Morocco, Poland, Russia, Spain, Sweden, Swiss, UK, Ukraine and USA.

[Host Institutes]

University of Tokyo, High Energy Accelerator Research Organization (Japan)

[Collaboration Institutes]

Keio Univ., Kobe Univ., Kyoto Univ., Miyagi Kyoiku Univ., Nagoya Univ., Okayama Univ., Osaka Metropolitan Univ., Tohoku Univ., Tokyo Institute of Technology, Tokyo Metropolitan Univ., Tokyo Univ. of Science, Yokohama National Univ.(Japan)
INFN and Dipartimento Interateneo di Fisica di Bari (Italy), Institute for Nuclear Research (Russia), King's College London (UK), Laboratoire Leprince-Ringuet, Ecole Polytechnique (France), National Centre for Nuclear Research (Poland), Oxford University (UK), Sungkyunkwan University (Korea), TRIUMF (Canada), University Autonoma Madrid (Spain), University of Geneva (Switzerland) and others.

Members

Staff

Kamioka Observatory
Masayuki Nakahata, Professor
Shigetaka Moriyama, Professor
Yoshinari Hayato, Assoc. Professor
Yasuhiro Kishimoto, Assoc. Professor (till Mar. 2019)
Hiroyuki Sekiya, Assoc. Professor
Shoei Nakayama, Assoc. Professor
Atsushi Takeda, Assoc. Professor (from Feb. 2020)
Atsushi Takeda, Research Associate (till Jan. 2020)
Yoichi Asaoka, Assoc. Professor (from Sep. 2023)
Yoichi Asaoka, Project Assoc. Prof. (May 2020 - Aug. 2023)
Katsuki Hiraide, Project Assoc. Professor (from May 2020)
Makoto Miura, Research Associate
Jun Kameda, Research Associate
Ko Abe, Research Associate
Motoyasu Ikeda, Research Associate
Yasuhiro Nakajima, Research Associate (till Mar. 2021)
Hidekazu Tanaka, Research Associate (from Feb. 2019)
Hidekazu Tanaka, Project Research Associate (till Jan. 2019)
Kei Ieki, Research Associate (from Nov. 2021)
Kei Ieki, Project Research Associate (Apr. 2021 - Oct. 2021)
Lluis Magro Marti, Project Res. Assoc. (till Aug. 2020)
Yo Kato, Project Research Associate (till Mar. 2019)
Christophe Bronner, Project Res. Assoc. (till Apr. 2022, from Apr. 2023)
Yosuke Kataoka, Research Associate (from Jun. 2020)
Yosuke Kataoka, Project Research Associate (till May 2020)
Takatomi Yano, Project Research Associate (from Dec. 2017)
Yasuhiro Takemomo, Project Res. Assoc. (from Apr. 2019)
Guillaume Pronost, Project Res. Assoc. (Jul. 2019 - Mar. 2022, from Apr. 2024)
Yuki Nakano, Project Res. Assoc. (Sep. 2021 - Mar. 2024)
Kazufumi Sato, Project Research Associate (from Sep. 2021)
Keishi Hosokawa, Project Res. Assoc. (from Sep. 2021)
Shunichi Mine, Project Academic Specialist (from Apr. 2022)

Research Center for Cosmic Neutrinos
Takaaki Kajita, Professor (till Mar. 2024)
Kimihiro Okumura, Assoc. Professor
Yasuhiro Nishimura, Research Associate (till Mar. 2019)
Takuya Tashiro, Project Research Associate (from Oct. 2019)

Institute for Comic Ray Research
Takaaki Kajita, Professor (from Apr. 2024)

Postdoctorial Fellows

Kamioka Observatory
Yuuki Nakano (till Mar. 2019)
Kazufumi Sato (till Mar. 2019)

Guillaume Pronost (till Jun. 2019)
Hiroshi Ito (Apr. 2019 - Mar. 2021)
Kiseki Nakmura (Apr. 2020 - Mar. 2021)
Yohei Noguchi (from Apr. 2022)
Masayuki Harada (from Apr. 2024)

Graduate students

Five students earned master degrees during 2018–2024, supervised by ICRR staff members.

Bibliography

Before Year 2018

[1] K. Abe *et al.*, "Letter of Intent: The Hyper-Kamiokande Experiment — Detector Design and Physics Potential —," arXiv:1109.3262 [hep-ex], **Cited 487 times.**

[2] E. Kearns *et al.* [Hyper-Kamiokande Working Group], "Hyper-Kamiokande Physics Opportunities," arXiv:1309.0184 [hep-ex], **Cited 84 times.**

[3] K. Abe *et al.* [Hyper-Kamiokande Working Group], "A Long Baseline Neutrino Oscillation Experiment Using J-PARC Neutrino Beam and Hyper-Kamiokande," arXiv:1412.4673 [physics.ins-det], **Cited 181 times.**

[4] K. Abe *et al.* [Hyper-Kamiokande Proto-Collaboration], "Physics potential of a long-baseline neutrino oscillation experiment using a J-PARC neutrino beam and Hyper-Kamiokande," PTEP **2015**, 053C02 (2015) doi:10.1093/ptep/ptv061 [arXiv:1502.05199 [hep-ex]], **Cited 418 times.**

[5] [Hyper-Kamiokande Proto-Collaboration], "Hyper-Kamiokande Design Report," KEK Preprint 2016-21 / ICRR-Report-701-2016-1, **Cited 77 times.**

After Year 2018

[6] K. Abe *et al.* [Hyper-Kamiokande Collaboration], "Physics potentials with the second Hyper-Kamiokande detector in Korea," PTEP **2018**, no. 6, 063C01 (2018) doi:10.1093/ptep/pty044 [arXiv:1611.06118 [hep-ex]], **Cited 265 times.**

[7] [Hyper-Kamiokande Proto-Collaboration], "Hyper-Kamiokande Design Report," arXiv: 1805.04163, **Cited 889 times.**

[8] https://www-sk.icrr.u-tokyo.ac.jp/en/news/detail/300

[9] https://www-sk.icrr.u-tokyo.ac.jp/en/news/detail/307

[10] https://www-sk.icrr.u-tokyo.ac.jp/en/news/detail/158

[11] https://www-sk.icrr.u-tokyo.ac.jp/en/news/detail/684

[12] https://www-sk.icrr.u-tokyo.ac.jp/en/news/detail/738

[13] https://j-parc.jp/c/en/press-release/2024/01/17001276.html

[14] "Supernova Model Discrimination with Hyper-Kamiokande," Hyper-Kamiokande Collaboration, Astrophys. J. **916**, 15 (2021), **Cited 64 times.**

[15] "Hyper-Kamiokande construction status and prospects," Ko Abe, Hide-Kazu Tanaka on behalf of the Hyper-Kamiokande Collaboration, Front.in Phys. **12**, 1378254 (2024), **Cited 1 times.**

HIGH ENERGY COSMIC RAY DIVISION

CTAO: CHERENKOV TELESCOPE ARRAY OBSERVATORY

Summary from 2018 to 2024

- The first Large Size Telescope (LST-1) of CTAO was completed in 2018, and the inauguration was held inviting distinguished guests.
- The commissioning of LST-1 has been performed. All configurations were optimized, and the obtained performance was characterized. A critical design review by an external committee was successfully passed.
- Science runs of LST-1 have been initiated by the LST working group of CTAO since 2020, and the total observation time has exceeded 2000 hours. The observed data were also analyzed by young researchers from Japan, with preliminary results presented at international conferences and other events.
- The PMT modules for LST-2–4 were produced in Tenerife mainly by people from ICRR. The quality control measurements were also performed there.
- LST-2-4 has been constructed since 2022 and will be completed in 2026.
- The CTAO project was selected in 2023 as a project shown on the "Roadmap 2023" formulated by the Working Group of MEXT on Large Scientific Projects.

Introduction

Over the past several decades, Very High Energy (VHE) gamma-ray astronomy has made remarkable progress, establishing itself as a crucial branch of astrophysics. The field began with the discovery of VHE gamma rays from the Crab Nebula by the Whipple Observatory in 1989. The current generation of Imaging Atmospheric Cherenkov Telescopes (IACTs), such as H.E.S.S., MAGIC, and VERITAS, have since identified over 200 Galactic and extragalactic sources of various types. This includes GRB 190114C, where TeV photons were detected, definitively proving that half of the radiation energy is deposited in the inverse Compton regime [9]. Additionally, the detection of a flare from the blazar TXS 0506+056, coinciding with a neutrino detection by IceCube, marked the beginning of a new era in multi-messenger astronomy [8].

Cherenkov Telescope Array Observatory (CTAO), a next-generation VHE gamma-ray observatory, in the framework of worldwide and international collaboration has been proposed to advance this field, as well as the emerging field of multi-messenger astronomy, alongside the recently flourishing neutrino and gravitational wave observations.

CTAO Project

CTAO is designed to achieve superior sensitivity and performance, utilizing established technologies and experience gained from the current IACT. It will be constructed in both hemispheres of the earth, the northern site on La Palma island in Spain and the southern site in Paranal in Chile. The CTAO will consist of several tens of IACTs of three different sizes (Large Size Telescopes, Middle Size Telescopes, and Small Size Telescopes) (Fig. 1). With a factor of 10 increase in sensitivity (1 mCrab, 10^{-14} erg s^{-1} cm^{-2}), together with much broader energy coverage from 20 GeV up to 300 TeV, CTAO is anticipated to discover more than 1000 Galactic and extragalactic sources.

CTAO will allow us to explore numerous, diverse topics in physics and astrophysics [10]. The century-old question of the origin of cosmic rays is expected to be finally settled through detailed observations of supernova remnants and other Galactic objects along with the diffuse Galactic gamma ray emission, which will also shed light on the physics of the interstellar medium. Observing pulsars and associated pulsar wind nebulae will clarify physical processes in the vicinity of neutron stars and extreme magnetic fields. The physics of accretion onto supermassive black holes, the long-standing puzzle of the origin of ultrarelativistic jets emanating from them, as well as their cosmological evolution will be addressed by extensive studies of active galactic nuclei (AGN). Through dedicated observing strategies, CTAO will also elucidate many aspects of the mysterious nature of gamma ray bursts (GRBs), the most energetic explosions in the Universe. Detailed studies of both AGNs and GRBs can also reveal the origin of the highest energy cosmic rays in the Universe, probe the cosmic history of star formation including the very first stars, as well as provide high precision tests of theories of quantum gravity. Finally, CTAO will search for signatures from elementary particles constituting dark matter with the highest sensitivity so far. The realization of the rich scientific potential of CTAO is very much feasible, thanks to the positive experience gained from the current IACTs.

The project has completed the prototype construction phase. It is now progressing towards developing and operating interim array configurations, with international efforts from Japan, the EU countries, USA, and other countries.

The CTAO project was selected in 2023 as one of 12 projects shown on the "Roadmap 2023" as the Fundamental Concepts for Promoting Large Scientific Research Projects that the Working Group of the Ministry of Education, Culture, Sports, Science and Technology (MEXT) formulated on Large Scientific Projects.

Fig. 1. Computer graphics of the CTAO North observatory in La Palma island, Spain. CTAO consists of three types of telescopes: Large Size Telescopes (23m diameter), Middle Size Telescopes (12m), and Small Size Telescopes (4m, only in the CTAO south), and covers the broad energy band from 20 GeV to 300 TeV.

Construction and Inauguration of LST-1

The structure, drive, mirror, and camera support structure of the first LST (LST-1) were completed by the summer of 2018. The installation of the mirror facets, along with the interface plates connecting the mirrors to the structure, was carried out by a team from Japan, the producers of these components. Shortly after the camera was installed in October, the inauguration ceremony for the first telescope of CTAO-North was successfully held, with notable attendees including the President of La Palma Island, Spain's Minister of Science, the Vice President of the University of Tokyo, and other distinguished guests (Fig. 2).

The First Light from cosmic ray air shower was detected already in December 2018 as shown in Fig. 3. As the photosensor modules including the readout board was developed and produced in Japan, the contribution of Japan team was essential to take these very first data.

Fig. 2. Inauguration of the first LST in the CTAO-north.

Commissioning of LST-1

After the first light detection, we began to calibrate the telescope. First, the trigger and clock delays were tuned using electrical test pulses. Next, we calibrated the gain of photomultipliers (PMTs) using the calibration laser flashes, achieving a gain flatness of all PMTs within 2% precision. We also fine-tuned the threshold levels of the discriminators in each

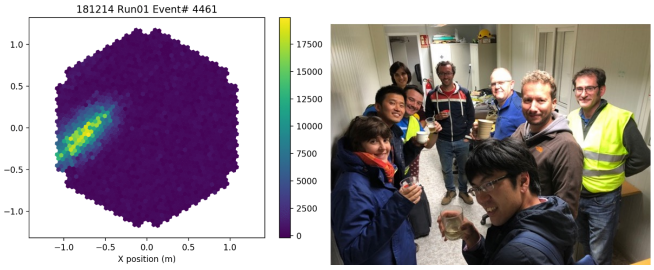

Fig. 3. Left: the one of the first air showers images detected by LST1 in December, 2018. Right: The photo of Camera/DAQ team celebrating the detection of first air shower images.

PMT module (see Fig. 7) to ensure uniform sensitivity across the camera.

Once all these configuration parameters were well calibrated, we evaluated the performance of the camera. The readout noise, including the photons from the night sky, was found to be about 1.3 photoelectron (p.e.) under dark sky conditions and remained stable within 1%. The noise level scaled with a square root of anode current, as expected. Charge and timing resolutions were also studied as shown in Fig. 4 and Fig. 5. Both were proven to be within requirements.

The actuators of mirror facets were also calibrated. Depending on the pointing zenith angle, the telescope structure slightly deforms under its own weight. To compensate for this, each mirror facet can adjust its orientation using the equipped actuators. We created a look-up-table that stores the values of all actuators for different zenith angles. As shown in Fig. 6, the point spread function (PSF) is about 35 mm and remain stable over the wide range of zenith angles. It is worth noting that the diameter of one camera pixel is 50 mm.

After the commissioning, the critical design review was conducted by an external committee and it was successfully passed.

PMT module production and Quality Control for LST-2–4

While commissioning LST-1, we built the PMT modules for the 2nd to 4th LSTs (LST-2–4). The production and quality control (QC) of these modules were carried out in Insti-

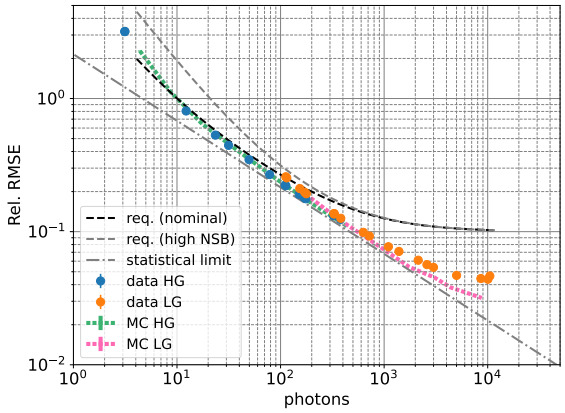

Fig. 4. The charge resolution evaluated from data and MC simulation. The requirements for two different night sky background levels are shown by dashed lines. The dashed-dotted line is the statistical limit of the charge resolution. Photodetection efficiency is assumed to be 0.264.

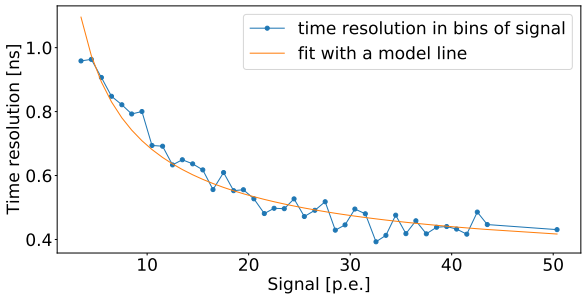

Fig. 5. The time resolution dependence on the signal strength in p.e. for an exemplary pixel.

tute of Astrophysics of the Canary Islands (IAC) in Tenerife in Canary islands. All elements were sent from Japan, and several scientists and students from Japan worked on-site. It took several months to build 800 PMT modules. The QC measurements were conducted using a setup known as the mini-camera, as shown in Fig. 7, allowing 19 modules to be tested simultaneously. The QC process assessed noise level, gain, pulse width, afterpulse rates, linearity, crosstalk amplitude, and trigger efficiency. The results of pulse width and linearity are shown in Fig. 8.

Status of LST-2–4 constructions

Permission for the telescope construction was granted by the local government in October, 2022. Construction began shortly thereafter, and the current status is shown in Fig. 9. We still need to install the camera support structure, mirror facets, and the camera. All four telescopes are expected to be completed in 2026.

Status of LST-5–6 development

For the CTAO southern site, the budget for two LSTs has been secured in Italy as part of the National Recovery and Resilience Plan (PNRR). While the structure, drive system, and mirrors of the southern LSTs will be newly designed to suit the environmental conditions in Paranal, Chile, the camera

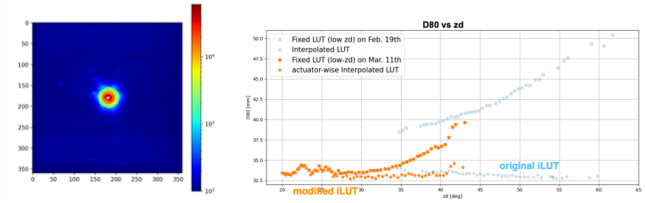

Fig. 6. Left: The point spread function (PSF) of LST-1 optics. The unit in vertical and horizontal axes is mm. Right: PSF as a function of zenith angle. PSF is defined as a diameter within which 80% of reflected lights are contained.

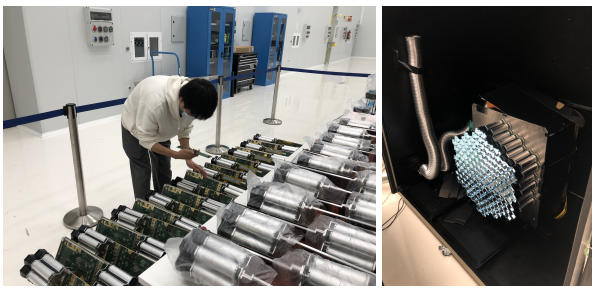

Fig. 7. Left: A photo of PMT modules produced in IAC in Tenerife. Right: A photo of the mini-camera used for QC measurements of the PMT modules.

design remains the same as that used for the northern LSTs. As the PMT modules are originally designed, produced, and qualified in Japan for the northern LSTs, we are actively supporting the Italian team through close collaboration. This includes providing comprehensive technical assistance, such as detailed schematics, firmware, software, and expertise in the assembly and quality control of the PMT modules.

Activities in the Analysis and Simulation working group (ASWG) : effect of the uncertainty of the hadronic interaction models

The most important factor in determining the sensitivity of an IACT array to gamma rays is its efficiency in rejecting background events. Sensitivity refers to the minimum detectable flux at which the excess of gamma-like events is statistically and systematically significant relative to the estimated background levels. The primary sources of background noise for IACTs are cosmic ray protons and electrons, which produce air shower patterns similar to those of gamma rays. For this reason, the accuracy of the estimation of the residual background level is crucial for a precise and realistic assessment of gamma-ray sensitivity. As for IACT arrays under construction, such as CTAO, Monte Carlo (MC) simulation plays an important role in estimating the residual background level.

From previous studies (Maier 2007, Sitarek 2018 etc.), it is known that protons mimic gamma rays when a large fraction of energy of the primary proton is transferred to a single neutral pion in the early stage of air shower development. One concern regarding this is that there exists a certain level of uncertainty among the hadronic interaction models used to describe secondary particles in proton shower MC simulations. This uncertainty is naturally expected to propagate to the residual background level and eventually gamma-ray sen-

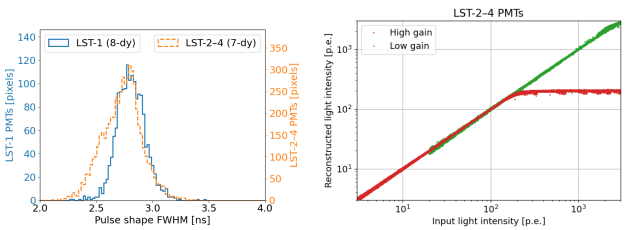

Fig. 8. Left: Histogram of the PMT pulse widths defined as the full width at the half maximum. Distributions of LST-1 PMTs and LST-2–4 PMTs are shown. Right: Linearity of LST-2–4 PMTs. Red and green dots indicate high gain and low gain readouts, respectively.

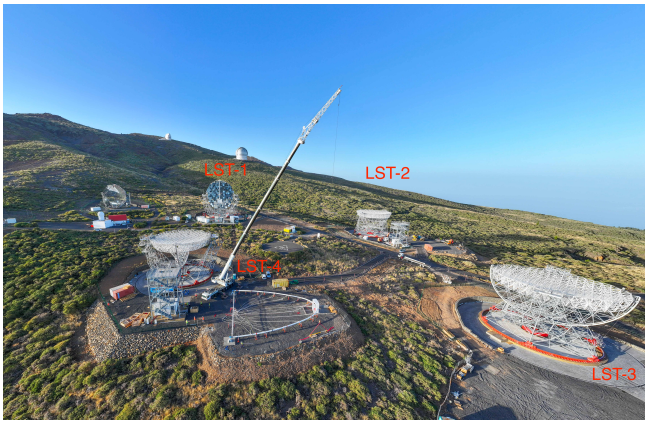

Fig. 9. Status of LST-1 to LST-4 as of summer 2024. LST-1 is already operational and three others are being constructed.

sitivity.

To investigate the effects of uncertainty in hadronic interaction models on the estimation of gamma-ray sensitivity for the CTAO prod3b-v1 (Omega configuration) southern array, we conducted MC simulations using four hadronic interaction models (QGSJET-II-03, QGSJET-II-04, EPOS-LHC, and SIBYLL2.3c) available in CORSIKA 6.99 and 7.69, with and without the CTAO detector response. The simulations without the detector response were performed to analyze the characteristics of the produced secondary particles, particularly the spectral shape of neutral pions at high energies. EPOS-LHC and SIBYLL2.3c were found to generate more high-energy neutral pions compared to the two QGSJET-II models, which is expected to result in higher background levels.

The MC data with the CTAO response were processed using the standard analysis pipeline to evaluate the background levels and the sensitivity curves. The results show the variations in background rates of up to a factor of 2 compared to QGSJET-II-03 were observed between the models (Fig. 10). These variations resulted in approximately 30% differences in the estimated gamma-ray sensitivity in the 1–30 TeV range, assuming a 50-hour observation of a point-like gamma-ray source. The results also demonstrate that CTAO and possibly other IACTs have significant potential for verifying hadronic interaction models. This work was led by an ICRR member and published as a CTAO non-consortium science paper [11] in collaboration with researchers from Brazil, Germany, Spain, and France.

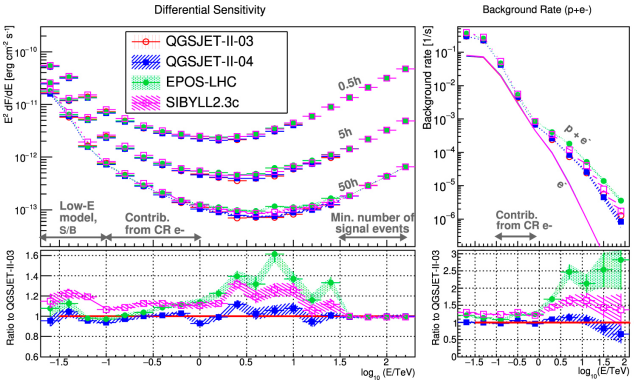

Fig. 10. Differential sensitivities and background rates for the CTAO prod3b-v1 southern array with four hadronic interaction models [11]. A point-like source and observation time of 0.5, 5, 50 hours were assumed.

AGN observations with LST-1

Among three different types of CTAO telescopes, LST is the most essential for AGN observations because of its low-energy threshold (∼20 GeV) since VHE gamma-ray photons (> 100 GeV) are absorbed by extragalactic background light (EBL). Since 2022, more than 1000 hours of observations have been dedicated to AGN studies. AGN observations with LST-1 are summarized in Table 1. In addition to the monitoring observations, we also performed Target of Opportunity observation following reports of flares at other wavelengths and detected several VHE gamma-ray flares from AGN, BL Lacertae and radio galaxy NGC 1275 for example.

Table 1. Summary of main AGN observations with LST-1 until May 2022.
Effective time is computed after data quality selection cuts.

Target	Redshift	Time	Significance
Mrk 421	0.031	31.9 h	53σ
Mrk 501	0.034	39.7 h	21σ
1ES 1959+650	0.048	11.8 h	13σ
1ES 0647+250	0.45	8.2 h	7σ
PG 1553+113	0.433	9.9 h	16σ

High-frequency-peaked BL Lac Mrk 421

Mrk 421 was observed over 34 nights between December 12, 2020 and May 23, 2022. LST-1 detected a VHE gamma-ray flare with an intra-night variability reaching ∼3 times of Crab Nebula flux on May 18, 2022. Figure 11 shows the spectral energy distribution of Mrk 421 on that night [25]. The spectrum was measured down to around the expected energy threshold of LST (∼30 GeV) and fitted by an exponential cutoff power-law function folded by the EBL model. The spectral energy distributions (SEDs) up to several TeV are comparable between two different reconstruction methods (source-independent and source-dependent methods). We obtained the spectral index of 1.86 ± 0.05 and the amplitude of $(9.06 \pm 0.36) \times 10^{-10}$cm^{-2} s^{-1} TeV^{-1} at the reference energy of 0.40 TeV.

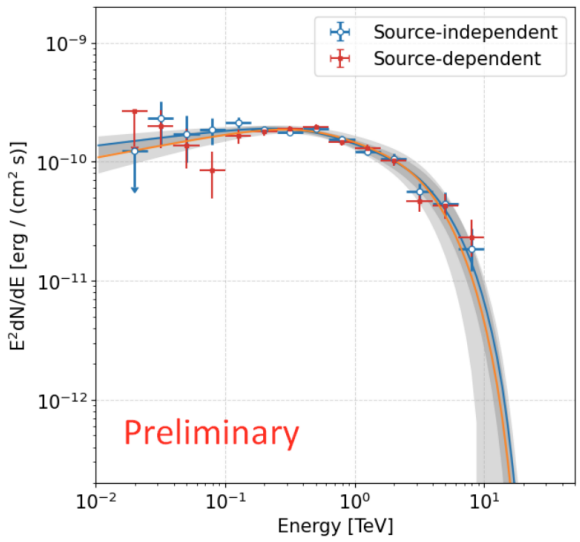

Fig. 11. Mrk 421 spectrum on May 18, 2022. Blue and red correspond to source-independent and source-dependent analyses, respectively.

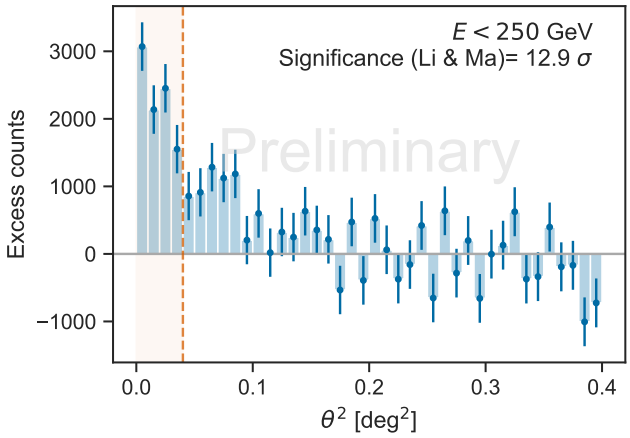

Fig. 12. Theta-squared plot of OP 313 in December 2023 measured with LST-1.

Discovery of VHE emission from the quasar OP 313

OP 313 is a distant Flat Spectrum Radio Quasar (FSRQ) located at redshift z=0.997. This source had multiple flare episodes, although IACT did not manage to detect this source. LST-1 observed this source since Dec 2023 following the gamma-ray flare detection by *Fermi*-LAT. After we collected 6-hours of observation data for 6 nights, we succeeded in detecting the VHE gamma-ray signal from OP 313. LST-1 continued to observe this source before the full moon and obtained 14.6 hours of observation data, reaching an excess significance of about 13σ. The average flux above 100 GeV during December 2023 was 28% of the integral flux of the Crab Nebula. Figure 12 shows a theta-squared plot of OP 313 in December 2023 measured with LST-1. This detection makes this source the 10th FSRQ, the furthest AGN in the VHE gamma-ray sky, and the second furthest VHE source after GRB 201216C. The gamma-ray signal is only detected below $E < 250$ GeV. This dataset is useful for constraining the EBL model and we are working on it now.

RS Ophiuchi: the first transient detected with the LST-1

Classical novae are explosive events occurring in binary star systems where material from a companion star is drawn onto a white dwarf. As hydrogen accumulates on the white dwarf's surface, a critical point is reached, triggering a thermonuclear explosion. This sudden burst of energy brightens the white dwarf to around 100,000 times the luminosity of the Sun, causing the ejection of accumulated matter. Novae do not result in the destruction of the white dwarf, allowing the process to occur repeatedly, leading to what are known as recurrent novae. The intense environment of these explosions creates the perfect conditions for accelerating particles, such as electrons and protons, to high energies, a process detectable through gamma-ray emissions.

Especially after the first detection of the nova V407 Cyg in 2010 in the GeV energy range by the *Fermi*-LAT, Cherenkov telescopes had searched for a VHE component in novae for more than a decade without any detection. In August 2021 then, the well-known binary system RS Ophiuchi displaying major outbursts every $\sim$15 years as a recurrent symbiotic nova, had its latest outburst and was detected in the VHE range by H.E.S.S., MAGIC, and LST-1 [26].

RS Ophiuchi became the first nova to be observed in VHE gamma rays and also the first transient source detected by LST-1. In the initial days following the outburst (approximately 1, 2, and 4 days after), RS Ophiuchi was detected with a statistical significance of 6.6σ by LST-1, showing soft power-law emission at energies ranging from 0.03 to 1 TeV. The spectral data from LST-1 align well with the findings from simultaneous observations conducted by MAGIC and H.E.S.S. However, after 21 days from the onset of the outburst, RS Ophiuchi was no longer detectable by LST-1.

During the LST-1 observations shortly after the RS Ophiuchi outburst, the particle energy spectrum by combining the most comprehensive gamma-ray data available, incorporating spectral information from Fermi-LAT, LST-1, H.E.S.S., and MAGIC was determined. The hadronic model, with its simpler spectral shape and stability during the fitting process, provides stronger support for a hadronic origin of the RS Ophiuchi gamma-ray emission, although both the hadronic and leptonic models have similar relative likelihoods. Over time, the proton energy spectrum shifts, with the maximum energy of accelerated protons rising from hundreds of GeV to TeV energies between the first and fourth days after the outburst (see Fig. 13, [16]).

In the coming years, it is anticipated that additional novae will be detectable by IACTs. The next outburst of T CrB is predicted to occur and could potentially become a bright source of gamma-ray emissions. This event would provide valuable insights into the evolution of gamma-ray emission throughout the outburst and help determine the maximum energy reached by accelerated particles in embedded novae. Looking ahead, the improved sensitivity of the LST array at low energies, compared to current instruments, will allow for the detection of fainter gamma-ray fluxes. This enhanced sen-

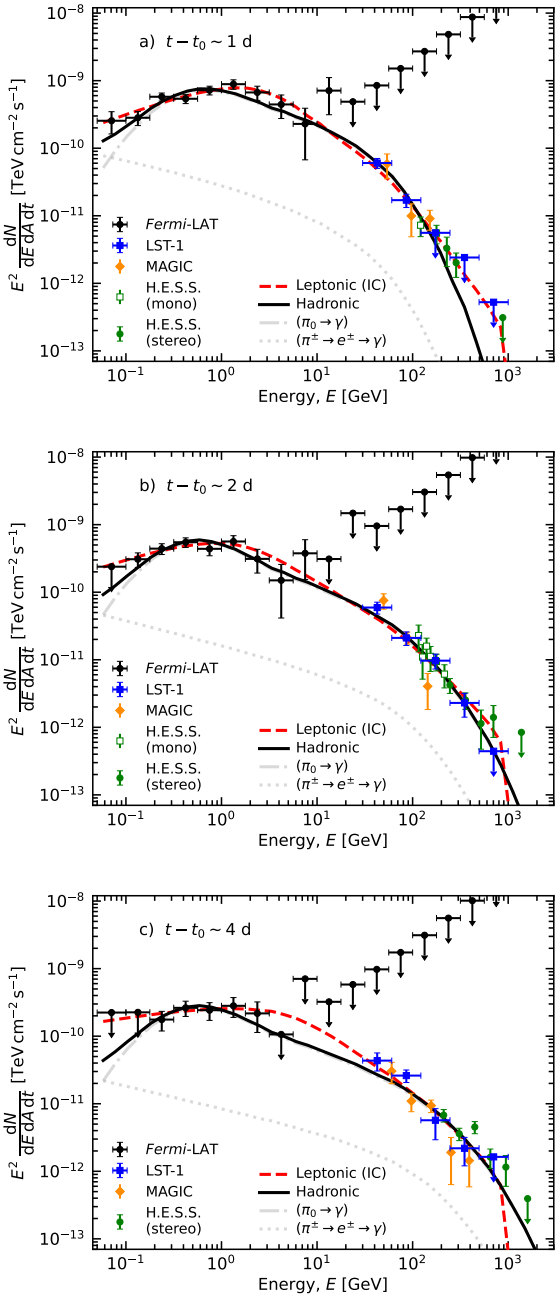

Fig. 13. Daily SEDs of RS Ophiuchi. *Fermi*-LAT (black circles), LST-1 (blue squares), MAGIC (orange diamonds), H.E.S.S. (green empty squares and filled circles for mono and stereo analysis, respectively). Panels a, b, and c correspond to observation intervals of approximately 1, 2, and 4 days after the outburst, respectively. The best-fit models are represented by red dashed lines for the leptonic model and black solid lines for the hadronic model, with the latter also displaying contributions from neutral and charged–pion decays in grey.

sitivity could make it possible to detect classical novae, a type of nova that has not yet been observed at VHE gamma rays (see Fig. 14).

Crab and Geminga Pulsars observed by LST1

Observations of pulsars above 10 GeV are particularly important for understanding their gamma-ray emission mecha-

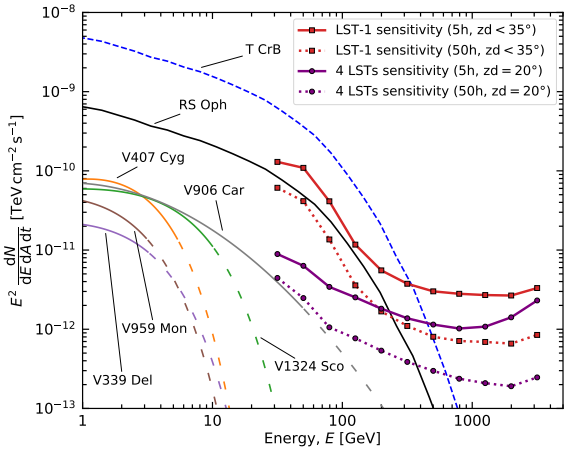

Fig. 14. Best-fit SED models of several detected novae and the expected SED from T CrB (blue). The solid line region of the nova SEDs corresponds approximately to the energy range where the model was fitted to the data, while the spaced-dashed region corresponds to the extrapolation region of the model. In addition, the sensitivity curves for LST-1 are shown. Please see the inlet for details.

nisms. The good sensitivity of CTAO allows us to investigate various aspects of their gamma-ray properties, including energy-dependent pulse shapes and phase-dependent spectral shapes.

Combined studies with CTAO LST1 and Fermi-LAT data have revealed that the gamma-ray pulse widths of the Crab pulsar are generally shrinking with the photon energy, and its ratio of two peaks is changing with the photon energy [14]. Equivalently, the gamma-ray spectral shape of the Crab pulsar differs from phase to phase [14].

The same chain of data analyses has been being performed for the Geminga pulsar, whose second pulse peak (P2) has been detected by LST1 with a $\sim 12\sigma$ significance in 60 hr (Fig. 15).

Galactic Center

The Galactic Center region inhabits an array of particle accelerators: namely the supermassive black hole, supernova remnants, and pulsar wind nebulae. The region likely supplies the Galaxy with a significant amount of accelerated particles, even potentially reaching up to PeV energies. Hence very-high-energy gamma-ray observations of this region allow for a morphological study of cosmic-ray propagation around the supermassive black hole Sgr A*. The uniqueness of LST-1 for the Galactic Center observation is built upon two perspectives: the large-zenith-angle observation and the wide field of view (FoV). The location requires LST-1 to observe the Galactic Center at the zenith distance (Zd) above about 58° in the horizontal coordinate system, which in general enhances the sensitivity at the high energy (typically above 1TeV) at a cost of increased energy threshold. Additionally, in contrast with other northern Cherenkov telescopes in particular, the relatively wide FoV of LST-1, which is wider than the other Cherenkov telescopes in the northern hemisphere (i.e. MAGIC and VERITAS), allows to maintain the sensi-

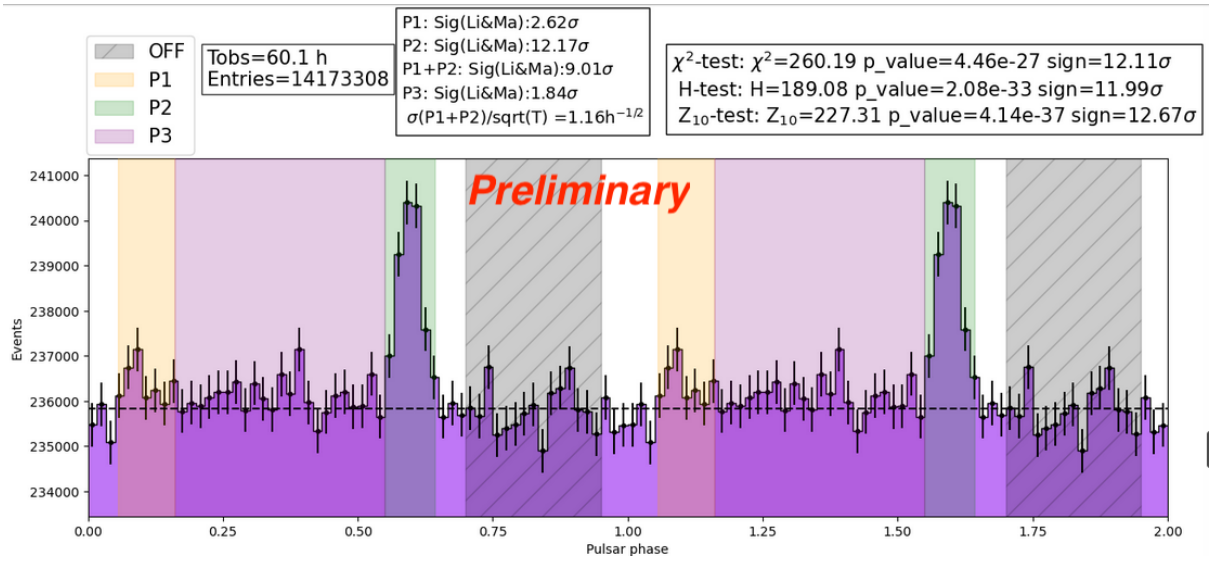

Fig. 15. Phase diagram of the Geminga pulsar observed by LST1 [15].

tivity across the region where the reported longitudinal diffuse gamma-ray emissions are distributed. As such, even despite the mono-scopic observations, LST-1 can already provide a comparable, or rather better, view towards the Galactic Center region. LST-1 collected Galactic Center data of about 40 hours in 2021 and 2022. We analyzed data through our newly developed software. The sky map visualization in Fig.16 highlights prominent signals of Sgr A* and SNR G0.9+0.1, and the diffuse emission along the Galactic plane. Our analysis reconfirmed the previous findings on the diffuse component with a higher detection significance; The spectral and morphological characteristics of the diffuse component can reasonably be associated with ultra-relativistic hadronic cosmic rays colliding with the dense gas. We have reported these results in major international conferences [27, 28].

Collaboration list

The CTAO project involves more than 1,500 scientists from over 150 institutes across 25 countries. The lists of CTAO-Japan consortium and the CTAO-LST collaboration are shown after the bibliography list.

Members

Staff

Hidetoshi Kubo, Professor, Mar. 2022 to the present
Masahiro Teshima, Professor, Oct. 2010 to Mar. 2023
Daniel Mazin, Project Professor, Sep. 2014 to the present
Takanori Yoshikoshi, Assoc. Professor, May. 2004 to the present
Takayuki Saito, Assoc. Professor, Apr. 2024 to the present; Assis. Professor, Apr. 2017 to Mar. 2024
Koji Noda, Assoc. Professor, Feb. 2018 to Dec. 2022
Michiko Ohishi, Assis. Professor, Oct. 2005 to the present
Daniela Hadasch, Assis. Professor, Sep. 2014 to the present
Ievgen Vovk, Assis. Professor, Nov. 2019 to the present
Seiya Nozaki, Assis. Professor, Jan. 2025 to the present
Strzys Marcel Constantin, Project Assis. Professor, Oct. 2019 to the present

Postdoctral Fellows

Chai Yating, Apr. 2024 to the present
Ryuji Takeishi, May 2020 to the present
Yeung Kin Hang, Apr. 2023 to the present
Yukiho Kobayashi, Apr. 2023 to Oct. 2023
Huetten Caspar Moritz, Jul. 2021 to Jan. 2023
Ceribella Giovanni, Oct. 2021 to Oct. 2022
Mitsunari Takahashi, Sep. 2018 to Nov. 2021
Tomohiro Inada, Oct. 2020 to Aug. 2021
Satoshi Fukami, May 2020 to Jul. 2021
Michiyuki Chikawa, Apr. 2020 to May 2021

Graduate Students

Shotato Abe, Apr. 2020 to the present
Joshua Ryo Baxter, Apr. 2020 to the present
Kazuaki Hashiyama, Apr.2020 to the present
Takumi Itokawa, Apr. 2023 to the present
Yoshiki Ohtani, Apr. 2018 to Mar. 2024
Kazuki Usui, Apr. 2022 to Mar. 2024
Shunsuke Sakurai, Apr. 2016 to Mar. 2023
Yukiho Kobayashi, Apr. 2018 to Mar. 2023
Shotaro Kanamori, Apr. 2021 to Mar. 2023
Hyuga Abe, Apr. 2019 to Mar. 2023
Masataka Miwa, Apr. 2021 Mar. 2023
Mari Takahashi, Apr. 2019 to Mar. 2021
Ryosuke Nomura, Apr. 2019 to Mar. 2021
Satoshi Fukami, Apr. 2014 to Mar. 2020
Tomohiro Inada, Apr. 2015 to Mar. 2020
Yuki Iwamura, Apr. 2015 to Mar. 2020
Taku Kumon, Apr. 2017 to Mar. 2019
Mitsunari Takahashi, Apr. 2013 to Sep. 2018
Hayato Kuroda, Apr. 2016 to Mar. 2018
Sho Kato, Apr. 2015 to Mar. 2017
Momoko Ogino, Apr. 2013 to Mar. 2015
Takumi Kojima, Apr. 2013 to Mar. 2015

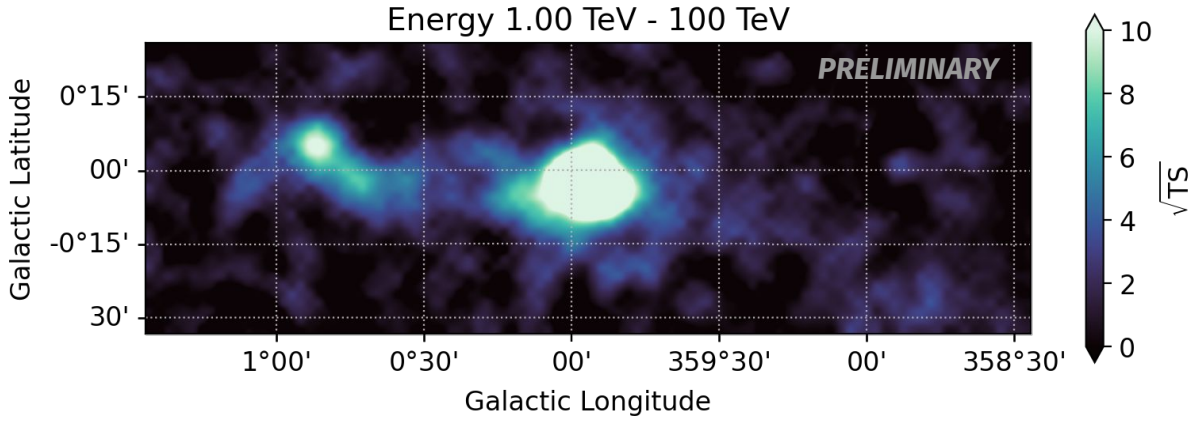

Fig. 16. Sky map of the Galactic Center region obtained with the LST-1 observations of about 40 hours.

Kazuma Ishio, Apr. 2013 to Mar.2015

Bibliography

Papers in Refereed Journals before 2018

[1] **Design concepts for the Cherenkov Telescope Array CTA: An advanced facility for ground-based high-energy gamma-ray astronomy,** CTA Consortium (M. Actis, K. Ioka, H.Kubo, R. Orito, H. Tajima, M. Teshima, T. Totani, T. Yoshida, T. Yoshikoshi, 60 other CTA-Japan members *et al.*). Exper.Astron. **32**, 193 (2011).

[2] **Introducing the CTA concept**, B.S. Acharya *et al.*, Astropart. Phys. 43 (2013) 3-18 **(357 cited)**.

[3] **Black hole lightning due to particle acceleration at subhorizon scales**, J. Aleksic, D. Hadasch, M. Hayashida, H. Kubo, D.Mazin, K. Noda, K. Saito, T. Saito, M. Teshima et al., Science **346** (2014) 1080-1084 **(119 cited)**.

[4] **Limits to dark matter annihilation cross-section from a combined analysis of MAGIC and Fermi-LAT observations of dwarf satellite galaxies**, MAGIC Collaboration, M.L. Ahnen *et al.*, JCAP **1602** (2016) no.02, 039.

[5] **Prospects for Cherenkov Telescope Array Observations of the Young Supernova Remnant RX J1713.7-3946,** CTA Consortium, Astrophys.J. **840** (2017) no.2, 74.

[6] **Evaluation of novel PMTs of worldwide best parameters for the CTA project** R. Mirzoyan, D. Nakajima, M. Takahashi, M. Teshima, T. Yamamoto it et al., Nucl.Instrum.Meth. A845 (2017) 603-606.

[7] **A technique for estimating the absolute gain of a photomultiplier tube,** M. Takahashi, *et al.*, Nucl.Instrum.Meth. **A894** (2018) 1-7.

Papers in Refereed Journals after 2018

[8] **Multimessenger observations of a flaring blazar coincident with high-energy neutrino IceCube-170922A,** IceCube, Fermi and MAGIC Collaborations, M. M. Aartsen, H.Kubo, D. Mazin, D. Hadasch, M. Hayashida, K. Noda, T. Saito, M.Takahashi, M. Teshima, *et al.*, Science **361** (2018) no.6398, eaat1378 **(692 Cited)**.

[9] **Teraelectronvolt emission from the γ-ray burst GRB 190114C,** MAGIC Collaborations, V. A. Acciari, H.Kubo, D. Mazin, D. Hadasch, M. Hayashida, K. Noda, T. Saito, M.Takahashi, M. Teshima, *et al.*, Nature **575** (2019) 455-458 **(207 Cited)**.

[10] **Science with the Cherenkov Telescope Array,** arXiv:1709.07997; https://doi.org/10.1142/10986 (2019) (non-refereed) **(318 Cited)**.

[11] **Effect of the uncertainty in the hadronic interaction models on the estimation of the sensitivity of the Cherenkov telescope array**, M. Ohishi, L. Arbeletche, V. de Souza, G. Mair, K. Bernlöhr, A. Moralejo, J. Bregeon, L. Arrabito, T. Yoshikoshi, *J. Phys. G: Nucl. Part. Phys.* **48** 075201 (2021).

[12] **Observations of the Crab Nebula and Pulsar with the Large-sized Telescope Prototype of the Cherenkov Telescope Array** LST Collaboration, ApJ, 956, id.80 (2023).

[13] **Performance of the joint LST-1 and MAGIC observations evaluated with Crab Nebula data**, LST Collaboration and MAGIC Collaboration, A&A, 680, A66 (2023).

[14] **A detailed study of the very-high-energy Crab pulsar emission with the LST-1**, LST Collaboration, A&A, 690, A167 (2024).

[15] **Observations of the Geminga pulsar with the LST-1**, LST Collaboration, in preparation.

[16] **RS Ophiuchi: the first transient detected with the LST-1**, LST Collaboration, in preparation.

Conference proceeding papers before 2018

[17] **Design Study of a CTA Large Size Telescope,** M. Teshima *et al.*, *Proc. of ICRC2012 at Beijing China,* arXiv:1111.2183.

[18] **Development of PMT Clusters for CTA-LST Camera,** R. Orito *et al.*, *Proc. of ICRC2012 at Beijing China,* arXiv:1111.2183.

[19] **Development of the Readout System for CTA Using the DRS4 Waveform Digitizing Chip,** H. Kubo *et al.*, *Proc. of ICRC2012 at Beijing China,* arXiv:1111.2183.

[20] **Development of the photomultiplier tube readout system for the first Large-Sized Telescope of the Cherenkov Telescope Array**, S. Masuda *et al.*, PoS ICRC2015 (2016) 1003.

[21] **Development of Slow Control Boards for the Large Size Telescopes of the Cherenkov Telescope Array**, D. Hadasch et al., PoS ICRC2015 (2016) 1024.

[22] **Status of the Cherenkov Telescope Array's Large Size Telescopes,** J. Cortina and M. Teshima, Proc. of ICRC2015 at Hague, Netherlands. arXiv:1508.06438, (2015).

[23] **The Optical System for the Large Size Telescope of the Cherenkov Telescope Array,** M. Hayashida et al., PoS ICRC2015 (2016) 927.

[24] **Large size telescope report**, D. Mazin, J. Cortina and M. Teshima, AIP Conf.Proc. **1792** (2017) no.1, 080001.

Conference proceeding papers after 2018

[25] **Observation of Active Galactic Nuclei with the Large-Sized Telescope prototype of the Cherenkov Telescope Array** R. Takeishi et al. PoS ICRC2023 (2023) 711.

[26] **Detection of the 2021 Outburst of RS Ophiuchi with the LST-1** Y. Kobayashi et al., PoS ICRC2023 (2023) 677.

[27] **Galactic Center Studies with CTA-LST-1**, S. Abe et al., Pos ICRC2023 (2023) 574.

[28] **Galactic Center observations with CTA-LST-1**, S. Abe et al., Proceedings in Moriond VHEPU 2024.

CTAO-Japan Consortium

Institute	Country	(*)
ICRR, Univ. of Tokyo	Japan	21
Academia Sinica Inst.	China	1
Aoyama Gakuin Univ.	Japan	5
Chiba Univ.	Japan	3
Chinese Academy of Sciences	China	2
Chungnam National Univ.	Korea	1
ETH Zurich	Switzerland	1
Gifu Univ.	Japan	1
Hiroshima Univ.	Japan	10
Huazhong Univ. of Sci. and Tech.	China	1
Ibaraki Univ.	Japan	3
Institute for Advanced Study	USA	1
IPNS, KEK	Japan	1
ISAS/JAXA	Japan	2
Kanagawa Univ.	Japan	1
Kitasato Univ.	Japan	1
Konan Univ.	Japan	5
Kumamoto Univ.	Japan	1
Kyoto Univ.	Japan	5
Lomonosov Moscow State Univ.	Russia	1
Max Planck Institute for Physics	Germany	1
Nagoya Univ.	Japan	11
National Tsing Hua Univ.	Taiwan	1
NAOJ	Japan	1
Osaka Metropolitan Univ.	Japan	1
Osaka Univ.	Japan	4
RIKEN	Japan	5
Rikkyo Univ.	Japan	3
Ritsumeikan Univ.	Japan	1
Saha Institute of Nuclear Physics	India	1
Saitama Univ.	Japan	3
Sendai College	Japan	2
Sun Yat-Sen Univ.	China	2
Grad. Sch. Sci., Univ. of Tokyo	Japan	4
Tohoku Univ.	Japan	1
Tokai Univ.	Japan	6
Tokyo Metropolitan Univ.	Japan	2
Tsinghua Univ.	China	1
Univ. of Hong Kong	China	1
Univ. of Miyazaki	Japan	1
Univ. of Tokushima	Japan	1
Waseda Univ.	Japan	1
Yamagata Univ.	Japan	3
Yamanashi Gakuin Univ.	Japan	2
Yokohama National Univ.	Japan	1
Total		127

(*) Number of participants as of August 2024.

CTAO-LST Collaboration

Institute	Country	(*)
Japanese Institutes (**)	Japan	89
CBPF	Brazil	3
INRNE, BAS	Bulgaria	2
FESB	Croatia	2
Univ. Osijek	Croatia	2
Univ. Rijeka	Croatia	5
ASU	Czechia	1
FZU	Czechia	12
Univ. Olomouc	Czechia	4
Univ. Prague	Czechia	2
IRFU	France	2
LAPP	France	29
CPPM	France	8
Univ. de Paris, APC	France	2
Sorbonne Univ.	France	1
RUB	Germany	3
TU Dortmund	Germany	12
Univ. Hamburg	Germany	3
MPP	Germany	25
U Wurzburg	Germany	8
IAPS Roma	Italy	2
INAF	Italy	6
OA Brera	Italy	4
OA Capodimonte	Italy	3
OA Padova	Italy	1
OA Roma	Italy	18
OAS Bologna	Italy	8
INFN	Italy	33
Politecnico and INFN Bari	Italy	5
Univ. Bari and INFN	Italy	5
Univ. Padova and INFN	Italy	19
Univ. Palermo	Italy	2
Univ. Siena and INFN	Italy	11
Univ. Trieste INFN Trieste	Italy	2
Univ. Udine and INFN Trieste	Italy	4
IAPS Roma	Italy	1
INAF HQ	Italy	3
Univ. Lodz	Poland	6
CIEMAT	Spain	14
IAA, Granada	Spain	13
IAC	Spain	12
ICE-CSIC	Spain	5
IFAE-BIST	Spain	21
LST	Spain	1
Universidad de Alcala	Spain	4
ICC-UB	Spain	6
UCM	Spain	14
Univ. Jaen	Spain	3
Universidad de Alcala	Spain	1
EPFL	Switzerland	4
University of Geneva	Switzerland	17
Total		463

(*) Number of participants as of August 2024.
(**) CTAO-Japan Consortium

TA: TELESCOPE ARRAY EXPERIMENT

Introduction of TA, TALE and TAx4

The Telescope Array (TA) is the largest ultra-high energy cosmic ray (UHECR) observatory in the Northern Hemisphere; the main purpose of the TA is to probe the origin and nature of UHECRs by measuring energy spectrum, direction of arrival distribution and mass composition.

The TA detector consists of a surface array of 507 plastic scintillator detectors (SDs) and three stations of fluorescence detectors (FDs). The TA detector is located in Utah, U.S.A. The SDs were deployed on a square grid with 1.2-km spacing, and the SD array covers an area of approximately 700 km^2. Each SD has two layers of 1.2-cm-thick scintillator with an area of 3 m^2. The full operation of SDs started in March 2008. The duty cycle is approximately 95% on average. One northern FD station at the Middle Drum (MD) site uses 14 refurbished HiRes telescopes. Two southern FD stations at the Black Rock Mesa (BRM) and Long Ridge (LR) sites were built newly each with 12 telescopes. All three FD stations started the observation in November 2007, and have duty cycles of approximately 10%.

We found evidence for intermediate-scale anisotropy of arrival directions of cosmic rays above 5.7×10^{19} eV. With enhanced statistics, it is expected to observe the structure of the hotspot along with other possible excesses and point sources along with the correlations with extreme phenomena in the nearby universe. We proposed the TAx4 project to quadruple the effective area of the TA SD aperture including the existing TA SD array by installing additional 500 newly designed SDs on a square grid with wider, 2.08-km spacing between each. Detector installation for TAx4 began in 2019, and 257 SDs were deployed in February and March 2019. By this installation, the total coverage area with SDs including the original TA SD array has been increased by a factor of 2.5. The new SD array started the data acquisition in April 2019. Since the new SD array is divided into two lobes, two FD stations are required to overlook each lobe in order to increase the number of hybrid events for the measurement of Xmax and to confirm the energy scale. These FD stations consist of refurbished HiRes telescopes: four telescopes at the MD site and eight telescopes at the BRM site. The TAx4 FD stations at the northern site and the southern site started the stable observation in 2018 and 2019, respectively. The recent status of TAx4 was reported in [140].

The TA Low energy Extension (TALE) enables detailed studies of the energy spectrum and composition from $\sim10^{16.5}$ eV. The main target of TALE is to clarify the expected transition from galactic to extra-galactic cosmic ray origins and the comparison of the data with Monte Carlo (MC) simulation that takes into account the results of the latest LHC experiments. The TALE detector is located north of the TA site (at around the MD FD station). The TALE FD station consists of 10 refurbished HiRes telescopes [149]. The TALE FD operation was commenced in the spring of 2013.

The TALE SD array consists of 80 SDs (40 SDs with 400-meter spacing and 40 SDs with 600-meter spacing). The TALE SD array was completed in February 2018 and is in stable operation [151]. The mode energy of TALE hybrid events is $10^{16.8}$ eV.

Fig. 1 shows the layout of TA, TALE, and TAx4.

The TALE infill SD array consists of 50 SDs with 100-meter spacing near the TALE FD station to observe even lower-energy cosmic rays, for which the mode energy is $10^{15.5}$ eV [136]. The array was installed in October 2022, and started the operation in October 2023.

The Non-Imaging CHErenkov (NICHE) prototype array consists of 14 counters each with a 3-inch PMT that collects non-imaging air-Cherenkov light, which started stable observation in May 2018 [95]. The array is situated 600-1000 m from the TALE FD. NICHE and TALE work together as a hybrid detector for cosmic rays with energies in the range between 10^{15} eV and $10^{18.5}$ eV.

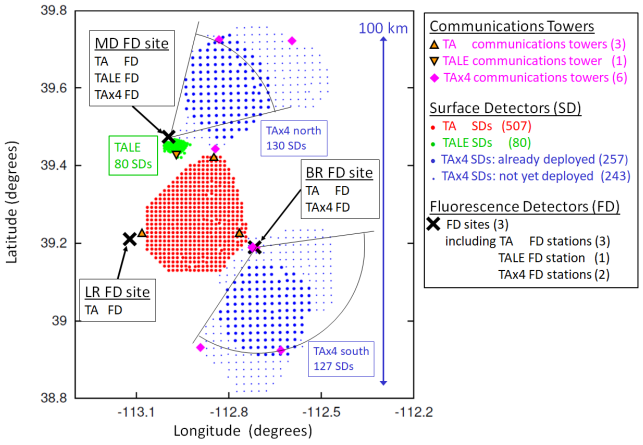

Fig. 1. The layout of TA, TALE and TAx4. The symbols for the layout are explained on the right side of the plot. Numbers in parentheses indicate the number of SDs, FD stations, and communications towers.

TA, TAx4 and TALE SD arrays continued regular operations during recent three years even if various activities ceased due to the spread of COVID-19. On the other hand, FD observations that require on-site operations had been suspended. However, in June 2020, TA FDs and TAx4 FDs at the MD site resumed operations. In addition, the operation of TAx4 FDs at the BRM site, TALE FDs, and TA FDs at the BRM site resumed in July 2020, January 2021 and June 2022, respectively.

The north and south sites of the TAx4 experiment are each divided into three sub-arrays, which are operated as independent arrays. In 2022, a system for triggering air showers that fall on the boundaries of the independent sub-arrays, which we call “boundary trigger” was installed. This has roughly

doubled the trigger frequency and increased detection efficiency by 60% for $10^{19.5}$ eV.

All three FD sites have been operated with on-site power generators. The generators need to be started up and shut down for daily FD observation, and occasional breakdowns interfered with the observations. Therefore, a power line was installed at the BRM FD site where the commercial power line station is the closest among three FD sites and that power supply started in summer 2022, allowing for more stable operation of the BRM site.

Summary from 2018 to 2024

Here we summarize the TA achievements from 2018 through 2024.

- The TALE SD array and TALE infill SD array were completed. The TAx4 array has partially constructed (2.5×TA SD array and two full FDs). They are taking data and preliminary results are obtained.
- Excess of the TA flux to Auger above $10^{19.5}$ eV in energy spectrum
- The cosmic ray energy spectrum and composition were measured with the TALE FD between 2 $\times 10^{15}$ eV and 2 $\times 10^{18}$ eV, and also with TALE hybrid between $10^{16.5}$ eV and $10^{18.5}$ eV.
- Several evidences for anisotropy of UHECR arrival directions such as TA hotspot and an excess in the region of the Perseus-Pisces supercluster were found.
- An extremely energetic cosmic ray observed by a surface detectr array was observed at 2.44 $\times$ 10^{20} eV.
- Isotropy of cosmic rays beyond 10^{20} eV favors their heavy mass compostion.

Results

Instep feature of UHECR spectrum with the TA SD

The TA SD array has been steadily collecting data since May 11, 2008. We measured the energy spectrum using 14 years of TA SD data. The energy spectrum showed not only the previously known spectral features of ankle and cutoff, but also ”instep” or ”shoulder” (softening) at $10^{19.22}$ eV between ankle and cut off as shown in Fig. 2 [119].

Comparison of energy spectra between Auger and TA

The differences in the energy spectra of the highest energy cosmic rays reported from the TA and Auger experiments were carefully examined by a working group made by members of the TA and Auger collaborations. It was found that the two measurements agree well below $10^{19.5}$ eV, but at higher energies the TA flux was found to be in excess of Auger (see Fig.3).

The energy spectra was calculated using different energy reconstructions by changing the fluorescence yield, the invisible energy, the attenuation correction and by using the individual shower energies rather than by shifting the energy spectrum data points. The size of the energy shifts found in this study was fully consistent with the expectation from the previous studies [150, 153].

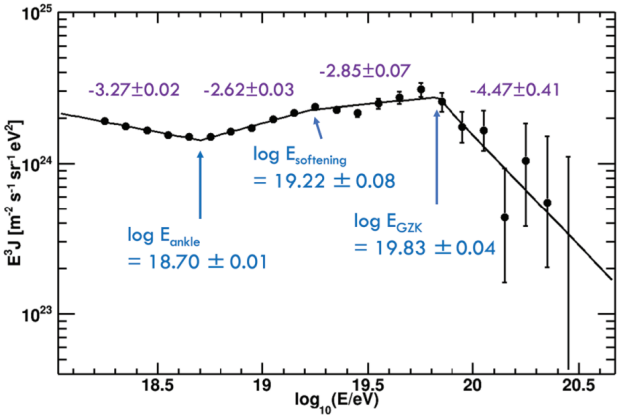

Fig. 2. Energy spectrum using 14 years of TA SD data. The data are represented by black points with error bars, and a fit to the broken power law having three break points is represented by the black solid line.

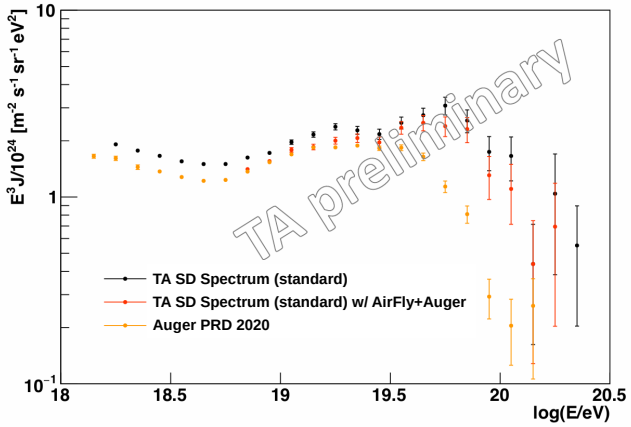

Fig. 3. TA and Auger spectra. The spectrum in black is data from 14 years of TA SD data analyzed in the standard way, using the conventional energy scale factor of 1/1.27. The spectrum in red uses the same data as the black one, but analyzed with the AirFly fluorescence yield model and the missing energy same as the Auger experiment and with the energy scale factor of 1/1.35 after recalculation. Orange is the result of the measurement by Auger.

UHECR spectrum measured by the TAx4 SD

The TAx4 SD array began operation in 2019 as an air shower array of 257 SDs and has been collecting data steadily since then [140]. In 2023, we reported an UHECR enenrgy spectrum based on TAx4 SD data obtained from October 2019 to September 2022 (See Fig.4, [144]). The TAx4 SD spectrum is consistent with the TA SD spectrum.

The TAx4 FD and TAx4 hybrid spectra were also consistent with the TA SD spectrum.

Energy spectrum measured with the TALE FD

The updated energy spectrum between 2 $\times 10^{15}$ eV and 2 $\times 10^{18}$ eV using the TALE FD data in the eight years is shown in Fig.5 [149]. We see two clear breaks at $10^{16.27}$ eV and $10^{17.04}$ eV.

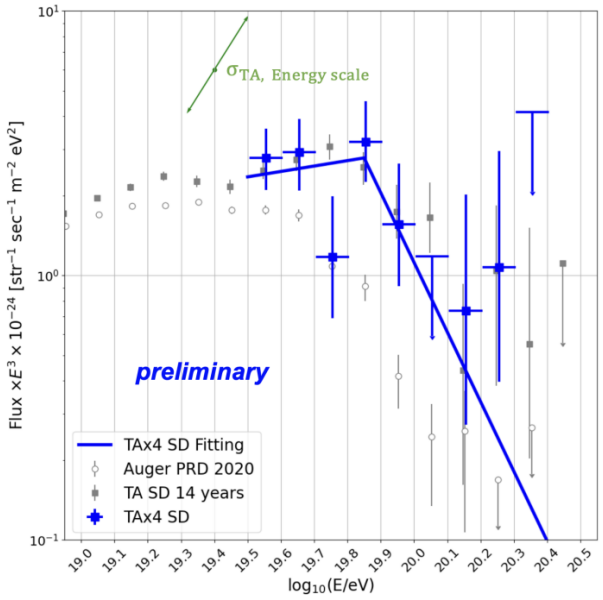

Fig. 4. The TAx4 SD energy spectrum (blue squares) with a broken line fit. The TA SD energy spectrum (gray squares) and the Auger energy spectrum (open circles) are also shown. The green arrow indicates the systematic uncertainty due to the energy scale uncertainty of ∼21%.

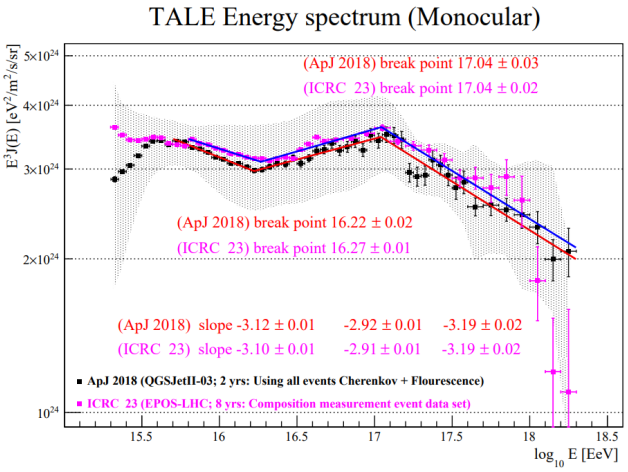

Fig. 5. The TALE FD updated energy spectrum [149] along with 2018 TALE FD spectrum using the data in the four years [5].

Highest energy cosmic rays with the TA SD

A cosmic ray air shower of 2.44× 10^{20} eV ("Amaterasu" particle) was detected at dawn on 27 May 2021 as shown in Fig.6 [24]. This was the largest energy event in the 15 years of the TA operation and was comparable to the highest energy cosmic ray detected in 1991 ("Oh My God" particle, 3.20 × 10^{20} eV) in the history of observations. If cosmic rays of such extreme high energy are of astronomical origin, the candidates are expected to be limited to intense astronomical phenomena such as supermassive black holes of Active Galactic Nuclei and/or StarBurst Galaxies, and to the vicinity of the Earth (within about 150 million light years). However, the Amaterasu particle arrived from a direction where there are no nearby candidate objects, called Local Void in the large-scale structure of the Universe, and from a different direction from the cosmic ray excess above 5.7 × ^{19} eV ("TA hotspot") and from the elliptical galaxy (M87) in the Virgo cluster as shown in Fig.7.

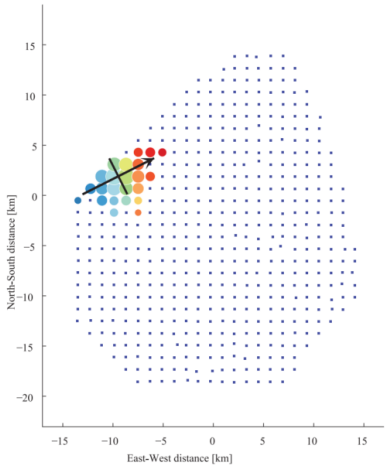

Fig. 6. The highest energy particle event observed by TA SD array. Each dot indicates the location of an SD station. The area of the colored circles is proportional to the common logarithm of the number of particles detected by each station and the color denotes the relative time from the earliest detector.

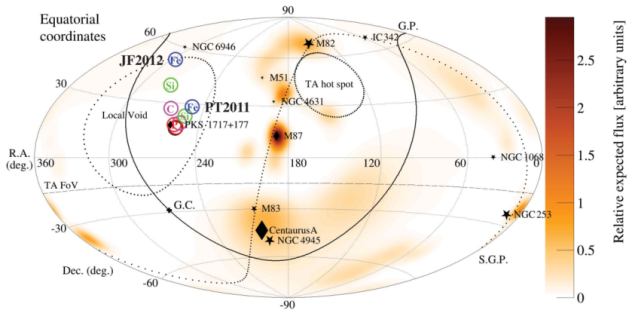

Fig. 7. The arrival direction of the highest energy event at 2.44 × 10^{20} eV (○) and the direction of the source when deflection by the Galactic magnetic field is taken into account for several elements. The orange shading is the cosmic ray relative abundance expected from candidate nearby sources.

Xmax measured using the TA hybrid data

Fig.8 shows the average Xmax from 10 years of hybrid events using the surface detectors and the BRM and LR FD telescopes as a function of energy together with MC expectations [59]. The result is consistent with light composition. The dependence of another parameter σ(Xmax), the width of Xmax, on energy is shown in Fig.9. The result is consistent with QGSJet II-04 proton model.

Xmax measured using the TALE hybrid data

We presented the preliminary result of the cosmic rays mass composition measured with the TALE FD data from 2 ×10^{15} eV to 2 ×10^{18} eV [149]. Here we present the preliminary result of the mass composition from $10^{16.5}$ eV to $10^{18.5}$ eV measured with the TALE hybrid data [151]. The result for the mean of the shower maximum, ⟨Xmax⟩ as a function

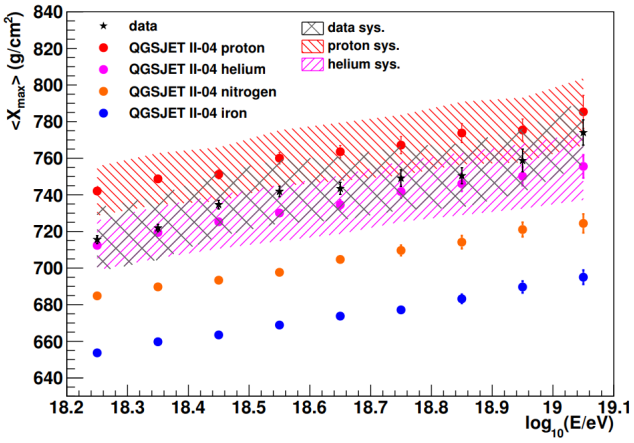

Fig. 8. The preliminary result of the average reconstructed Xmax as a function of energy. The black, red, magenta, orange and blue colors denote the data, pure proton, helium, nitrogen and iron QGSJet II-04 predictions, respectively.

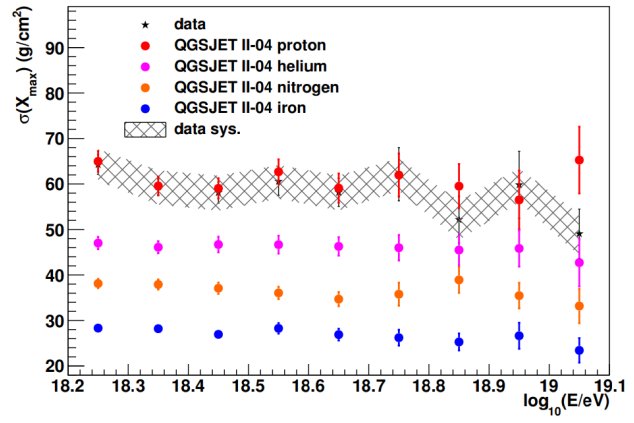

Fig. 9. The preliminary result of the average reconstructed σ(Xmax) as a function of energy.

of the shower energy is presented in Fig.10. The observed elongation rate shows clearly a break, where the energy is just above 10^{17} eV. We also estimate the primary fraction of cosmic rays assuming three elements (proton, nitrogen, and iron). The nitrogen fraction becomes dominant at $10^{16.75}$ eV, then iron fraction shows the peak at $10^{17.25}$ eV. It is interesting as expected by the Peters cycle while the low contribution of proton primary at around 10^{17} eV.

Mass composition of UHECRs from their arrival direction distribution

Conventionally, the particle species (nuclear species) of cosmic rays have been estimated by the FD Xmax. Here, we developed a new method to determine nuclear composition using the SD data, which has 10 times more data than the FD data. The method assumes that the UHECRs originate from galaxies that form the material structure of the universe, and compares the distribution of arrival directions predicted by the UHECR flux model with that of the actual data, and evaluates which composition fits the data due to deflections by the cosmic magnetic field. The 19 events above 10^{20} eV for 14 years were observed and the distribution of their arrival

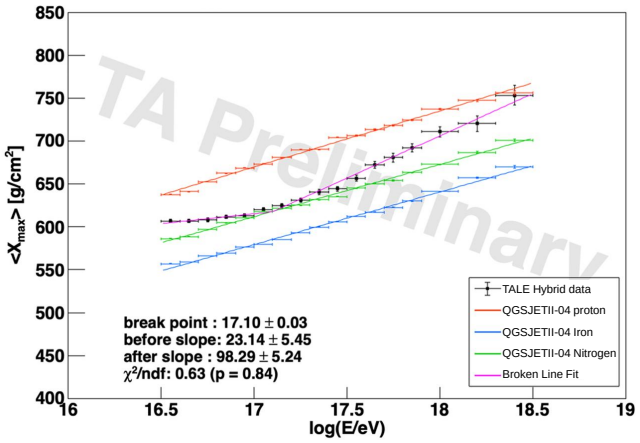

Fig. 10. ⟨Xmax⟩ as a function of shower energy, measured by using 5 years of the TALE hybrid data (black points). The pink line indicates a broken line fit of the TALE hybrid <Xmax> data. The red, blue, and green lines represent reconstructed MC rails for proton, nitrogen, and iron, respectively.

directions were isotropic. The application of the new model indicates that the deflection from the source due to the cosmic magnetic field may be very large, which is consistent with the result that UHECR above 10^{20} eV are heavy nuclei with large electric charges as shown in Fig.11 [26, 27].

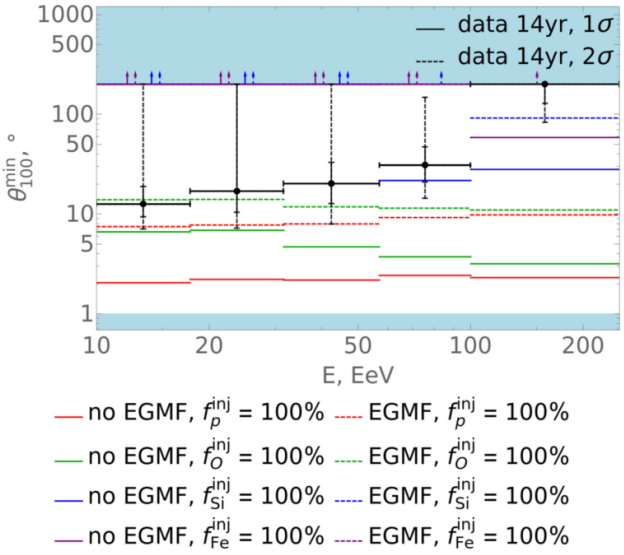

Fig. 11. Cosmic ray deflection angle θ_{100} estimated from observations in 14 years of TA data (dots) and from simulations (coloured horizontal lines). The colours and line shapes represent the nuclear composition (red for proton, green for oxygen, blue for silicon and purple for iron) and the strength of the intergalactic magnetic field assumed in the calculations (solid line = zero, dotted line = very strong (1.7 nG)). The observations fit well with lighter nuclei below 5.0×10^{19} eV and with heavier nuclei such as iron above 1.0×10^{20} eV.

TA hotspot and PPSC excess

In 2014, we reported an indication of arrival directions of cosmic rays above 5.7×10^{19} eV concentrated near the direction of Ursa Major, which we called a hotspot. For the updated hotspot analysis using the 15-year data set, we have 216 events with $E > 5.7 \times 10^{19}$ eV [141]. The maximum Li-Ma

pri-trial significance was obtained using a 25°-radius circle oversampling, and 44 events were located within the circle, whereas 18.0 events were expected from an isotropic distribution. Fig.12 shows the sky map of the TA hotspot in equatorial coordinates. The chance probability of finding such an excess was estimated to be 2.7×10^{-3}, $\sim 2.8\sigma$.

For a bit lower energy thresholds ($E > 10^{19.4}$, $10^{19.5}$, and $10^{19.6}$ eV), we obtained a new excess. For $E > 10^{19.4}$ eV, we have 1125 events. Using 20°-radius circle, the maximum Li-Ma significance of 4.0σ was obtained at the position of (17.9°, 35.2°), which is coincident with the overall distribution of the elements of the Perseus-Pisces Supercluster (PPSC). The angular distance between the center of the PPSC and position of the maximum of Li-Ma significance was 7.7°. The chance probabilities of having equal or higher excess within 7.7° from the center of the PPSC was estimated to be 3.3σ.

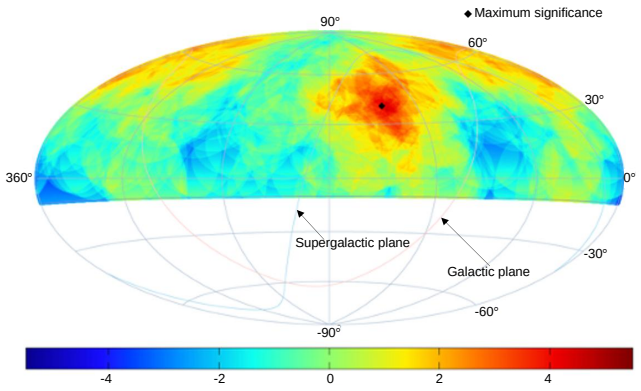

Fig. 12. The sky map of the TA hotspot in equatorial coordinates. Color represents the Li-Ma significance using a 25°-radius circle angular window. The black diamond indicates the maximum Li-Ma significance position at (144.0°, 40.5°).

Monitoring/calibration for FD

TA has a central laser facility (CLF), located equaldistant to three FD stations. It monitors atmospheric transparaency and we measure the vertical aerosol optical depth (VAOD) [138].

To monitor the presence of clouds, the TA has installed a CCD camera for visible light with a fish-eye lens at each of the BRM and LR FD stations and the CLF site [79].

To measure the PMT pointing directions precisely, the "Opt-copter", an Unmanned Aerial Vehicle (UAV) mounted with a light source and RTK-GPS, was developed and was flown within the telescope's field of view. [139].

Other activities for analyses

- Energy spectrum with TALE in hybrid mode [120]
- Energy spectrum with TALE SD array [152]
- Constraints on the starburst galaxy source model [6]
- Supergalactic Structure of Magnetic Deflection Multiplets of UHECRs [11]
- Proton-air cross section [12]
- Search for UHE photons [8, 9]
- Search for UHE neutrinos [13]
- Study on lightning/thunderstorms [3, 14, 18, 23]
- Mass composition with the TA SD data [7]
- Dipole anisotropy analysis [10]
- Joint analysis of the energy spectrum measured at Auger and TA [153]
- Joint study of the Xmax and the mass composition measured at Auger and TA [121]
- The TA SD muon analysis [2] and the joint study of muons by nine air shower experiments [107]
- Correlations of neutrinos with UHECRs by ANTARES, IceCube, Auger, and TA [19]
- Joint study on the arrival directions of UHECRs observed by Auger and TA [154, 155]

R&D of next-generation detectors and prototype detectors

The TA experimental site is used for the development of next-generation detectors and prototype detectors from other Universities/groups. These include:

- TALMA – Lightning and correlation with gamma rays and other particles [3, 14, 18, 23]
- EUSO-TA Extreme Universe Space Observatory Prototype at the TA BRM FD site [156, 157]
- EUSO-SPB - EUSO Super-Pressure Balloon with Fluorescence Telescope: SPB1 [158] and SPB2 [159] tested at the TA site
- FAST - The Fluorescence detector Array of Single-pixel Telescopes [160]
- CRAFFT - Cosmic Ray Air Fluorescence Fresnel lens Telescope at the TA BRM FD site [161]
- Auger at TA – Cross calibration of Auger North water tanks and an Auger South water tank along with TA scintillator detectors [162]
- IceCube SD and Antenna test and cross-calibration at the TALE infill SD array [163]
- DIMS – Search for macroscopic Dark Matters and Interstellar Meteoroids with fast/sensitive cameras [164]

The discussions are underway for next-generation observatories such as TA2 and GCOS (The Global Cosmic Ray Observatory). The GCOS was also included in the Snowmass process as a future plan for this field [20].

Spokespersons

After December 2017 and before December 2022
Charles Jui, Dept. of Physics, Univ. of Utah
After December 2017 and before December 2023
Shoichi Ogio, Osaka City Univ. (−2022.03), Osaka Metropolitan Univ. (2022.04−2022.12), ICRR, Univ. of Tokyo (2023.03−)

After December 2022
John Matthews, Dept. of Physics, Univ. of Utah
After December 2023
Yoshiki Tsunesada, Dept. of Physics, Osaka Metropolitan Univ.

Collaboration Name

Institute	Region	(*)
Loyola Univ.	USA	2
Univ. of Utah	USA	27
Hanyang Univ.	Korea	2
Osaka Metropolitan Univ.	Japan	13
ICRR, Univ. of Tokyo	Japan	24
Inst. of Phys., Academia Sinica	Taiwan	2
RIKEN	Japan	6
Kanagawa Univ.	Japan	5
Univ. of Yamanashi	Japan	1
Sungkyunkwan Univ.	Korea	5
Tokyo City Univ.	Japan	1
Inst. for Nucl. Res. of the Russian Acad. of Sci.	Russia	12
Shibaura Inst. of Tech.	Japan	1
Shinshu Univ.	Japan	7
Osaka Electro-Comm. Univ.	Japan	9
Univ. Libre de Bruxelles	Belgium	2
Yonsei Univ.	Korea	1
Univ. of Nova Gorica	Slovenia	1
Kochi Univ.	Japan	1
Chubu Univ.	Japan	1
NICT	Japan	1
Univ. of Lodz	Poland	1
Moscow M.V. Lomonosov State Univ.	Russia	1
UNIST	Korea	2
Natl. Centre for Nucl. Res.	Poland	2
Earthquake Res. Inst., Univ. of Tokyo	Japan	1
UNIST	Korea	2
Hiroshima City Univ.	Japan	1
KEK	Japan	1
Inst. of Phys., Czech Acad. of Sci.	Czech	1
Total		137(**)

(*) Number of participants as of June 2024.
(**) Twelve members belong to two universities.

Members

Staff

Shoichi Ogio, Professor from Mar. 2023 to the present
Takashi Sako, Associate Professor from Oct. 2022 to the present
Kazuhiro Kawata, Assistant Professor from Mar. 2018 to Aug. 2024, Associate Professor from Sep. 2024 to the present
Masahiro Takeda, Assistant Professor from Feb. 2004 to the present
Toshiyuki Nonaka, Assistant Professor from Apr. 2009 to the present
Hiroyuki Sagawa, Professor to Mar. 2023, Project Researcher from Apr. 2023 to the present
Nao Okazaki, Technical Staff from Oct. 2022 to the present

Postdoctoral Fellows

Eiji Kido, Project Assistant Professor from Nov. 2015 to Oct. 2019, from Sep. 2024 to the present
Keitaro Fujita, Project Researcher from Apr. 2022 to Mar. 2024, Project Researcher from Jun. 2024 to the present
Hitoshi Oshima, Project Researcher from Apr. 2022 to Mar. 2023, Project Researcher (ICRR Fellow) from Apr. 2023 to the present
Toshihiro Fujii, JSPS Research Fellowship for Young Scientists from Apr. 2016 to Nov. 2018

Graduate Students

Three students were awarded doctor degrees and four students earned master degrees during 2018−2024, supervised by ICRR staff members.

List of Publications
After Year 2018
Papers in Refereed Journals

Bibliography

[1] R.U. Abbasi *et al.*, "Depth of Ultra High Energy Cosmic Ray Induced Air Shower Maxima Measured by the Telescope Array Black Rock and Long Ridge FADC Fluorescence Detectors and Surface Array in Hybrid Mode", Astrophys. J. **858**,76 (2018).

[2] R.U. Abbasi *et al.*, "Study of muons from ultra-high energy cosmic ray air showers measured with the Telescope Array experiment", Phys. Rev. D **98**, 022002 (2018).

[3] R.U. Abbasi *et al.*, "Gamma Ray Showers Observed at Ground Level in Coincidence With Downward Lightning Leaders", J. Geophys. Res.: Atmospheres **123**, 6864-6879 (2018).

[4] R.U. Abbasi *et al.*, "Evidence of Intermediate-scale Energy Spectrum Anisotropy of Cosmic Rays $E \geq 10^{19.2}$ eV with the Telescope Array Surface Detector", Astrophys J. **862**, 91 (2018).

[5] R.U. Abbasi *et al.*, "The Cosmic Ray Energy Spectrum between 2 PeV and 2 EeV Observed with the TALE Detector in Monocular Mode", Astrophys. J. **865**, 74 (2018).

[6] R.U. Abbasi *et al.*, "Testing a Reported Correlation between Arrival Directions of Ultra-high-energy Cosmic Rays and a Flux Pattern from nearby Starburst Galaxies using Telescope Array Data", Astrophys. J. **867**, L27 (2018).

[7] R.U. Abbasi *et al.*, "Mass composition of ultra-high-energy cosmic rays with the Telescope Array Surface Detector Data", Phys. Rev. D **99**, 022002 (2019).

[8] R.U. Abbasi *et al.*, "Constraint on the diffuse photon flux with energies above 10^{18} eV using the surface detector of the Telescope Array experiment", Astropart. Phys. **110**, 8-14 (2019).

[9] R.U. Abbasi *et al.*, "Search for point sources of ultra-high-energy photons with the Telescope Array surface detector", MNRAS **492**, 3984-3993 (2020).

[10] R.U. Abbasi *et al.*, "Search for Large-scale Anisotropy on Arrival Directions of Ultra-high-energy Cosmic Rays Observed with the Telescope Array Experiment", Astrophys. J. **898**, L28 (2020).

[11] R.U. Abbasi *et al.*, "Evidence for a Supergalactic Structure of Magnetic Deflection Multiplets of Ultra-high-energy Cosmic Rays", Astrophys. J. **899**, 86 (2020).

[12] R.U. Abbasi *et al.*, "Measurement of the proton-air cross section with Telescope Array's Black Rock Mesa and Long Ridge fluorescence detectors, and surface array in hybrid mode", Phys. Rev. D **102**, 062004 (2020).

[13] R.U. Abbasi *et al.*, "Search for Ultra-High-Energy Neutrinos with the Telescope Array Surface Detector", JETP **131**, 255-264 (2020).

[14] J.W. Belz *et al.*, "Observations of the Origin of Downward Terrestrial Gamma-Ray Flashes", JGR Atmosphere **125**, 1-26 (2020).

[15] D. Ivanov, O.E. Kalashev, M.Y. Kuznetsov, G.I. Rubtsov, T. Sako, Y. Tsunesada, Y.V. Zhezher, "Using Deep Learning to Enhance Event Geometry Reconstruction for the Telescope Array Surface Detector", Machine Learning Science and Technology **2**, 015006 (2021).

[16] R.U. Abbasi *et al.*, "The Cosmic-Ray Composition between 2 PeV and 2 EeV Observed with the TALE Detector in Monocular Mode", Astrophys. J **909**, 178 (2021).

[17] R.U. Abbasi *et al.*, "Surface detectors of the TAx4 experiment", NIM A **1019**, 165726 (2021).

[18] R.U. Abbasi *et al.*, "Observation of variations in cosmic ray single count rates during thunderstorms and implications for large-scale field changes", Phys. Rev. D **105**, 062002 (2022).

[19] A. Albert *et al.*, "Search for Spatial Correlations of Neutrinos with Ultra-high-energy Cosmic Rays", Astrophys. J. **934**, 164 (2022).

[20] A. Coleman *et al.*, "Ultra high energy cosmic rays The intersection of the Cosmic and Energy Frontiers", Astropart. Phys. **149**, 102819 (2023).

[21] R.U. Abbasi *et al.*, "The energy spectrum of cosmic rays measured by the Telescope Array using 10 years of fluorescence detector data", Astropart. Phys. **151**, 102864 (2023).

[22] R. Higuchi *et al.*, "Effects of the Galactic Magnetic Field on the UHECR Correlation Studies with Starburst Galaxies", Astrophys. J, **949**, 107 (2023).

[23] R.U. Abbasi *et al.*, "First High-Speed Video Camera Observations of a Lightning Flash Associated With a Downward Terestrial Gamma-Ray Flash", Geophys. Res. Lett. **50** (2023) e2023GL102958.

[24] R.U. Abbasi *et al.* "An extremely energetic cosmic ray observed by a surface detector array", Science **382**, 903-907 (2023).

[25] R.U. Abbasi *et al.* "The energy spectrum of cosmic rays measured by the Telescope Array using 10 years of fluorescence detector data", Astropart. Phys. **151** 102864 (2023).

[26] R.U. Abbasi *et al.*, "Isotropy of Cosmic Rays beyond 10^{20} eV Favors Their Heavy Mass Composition", Phys. Rev. Lett. **133**, 041001 (2024).

[27] R.U. Abbasi *et al.*, "Mass composition of ultrahigh energy cosmic rays from distribution of their arrival directions with the Telescope Array", Phys. Rev. D **110**, 022006 (2024).

Papers in Conference Proceedings

[28] D. Ivanov, "TA Spectrum", Proceedings of Ultra High Energy Cosmic Rays 2018 (UHECR2018), EPJ WEB Conf. **210** (2019) 01001.

[29] T. AbuZayyad, D. Ikeda, D. Ivanov, T. Nonaka *et al.*, "Auger-TA energy spectrum working group report", Proceedings of Ultra High Energy Cosmic Rays 2018 (UHECR2018), EPJ WEB Conf. **210** (2019) 01002.

[30] K. Kawata, T. Fujii, S. Ogio, H. Sagawa *et al.*, "TA Anisotropy Summary", Proceedings of Ultra High Energy Cosmic Rays 2018 (UHECR2018), EPJ WEB Conf. **210** (2019) 01004.

[31] J. Biteau, T. Fujii, K. Kawata *et al.*, "Covering the celestial sphere at ultra-high energies: Full-sky cosmic-ray maps beyond the ankle and the flux suppression", Proceedings of Ultra High Energy Cosmic Rays 2018 (UHECR2018), EPJ WEB Conf. **210** (2019) 01005.

[32] J.P. Lundquist and P.V. Sokolsky, "Supergalactic Structure of Multiplets with the Telescope Array Surface Detector", Proceedings of Ultra High Energy Cosmic Rays 2018 (UHECR2018), EPJ WEB Conf. **210** (2019) 01006.

[33] A.d. Matteo, T. Fujii and K. Kawata, "Investigating an angular correlation between nearby starburst galaxies and UHECRs with the Telescope Array experiment", Proceedings of Ultra High Energy Cosmic Rays 2018 (UHECR2018), EPJ WEB Conf. **210** (2019) 01007.

[34] W. Hanlon, "Measurements of UHECR Mass Composition by Telescope Array", Proceedings of Ultra High Energy Cosmic Rays 2018 (UHECR2018), EPJ WEB Conf. **210** (2019) 01008.

[35] A. Yushkov, W. Hanlon, D. Ikeda, Y. Tsunesada *et al.*, "Depth of maximum of air-shower profiles: testing the compatibility of measurements performed at the Pierre Auger Observatory and the Telescope Array experiment", Proceedings of Ultra High Energy Cosmic Rays 2018 (UHECR2018), EPJ WEB Conf. **210** (2019) 01009.

[36] T. Sako, "Hadronic Interaction studied by TA", Proceedings of Ultra High Energy Cosmic Rays 2018 (UHECR2018), EPJ WEB Conf. **210** (2019) 02003.

[37] R. Takeishi, "Study of muons from ultrahigh energy cosmic ray air showers measured with the Telescope Array experiment", Proceedings of Ultra High Energy Cosmic Rays 2018 (UHECR2018), EPJ WEB Conf. **210** (2019) 02012.

[38] J. Aublin *et al.*, "Search for a correlation between the UHECRs measured by the Pierre Auger Observatory and the Telescope Array and the neutrino candidate events from IceCube and ANTARES", Proceedings of Ultra High Energy Cosmic Rays 2018 (UHECR2018), EPJ WEB Conf. **210** (2019) 03003.

[39] D.R. Bergman, Y. Tsunesada, J.F. Krizmanic and Y. Omura, "NICHE: Air-Cherenkov observation at the TA site", Proceedings of Ultra High Energy Cosmic Rays 2018 (UHECR2018), EPJ WEB Conf. **210** (2019) 05001.

[40] F. Sarazin, T. Fujii, T. Nonaka, H. Sagawa, T. Sako *et al.*, "Overview of the Auger@TA project and preliminary results from Phase I", Proceedings of Ultra High Energy Cosmic Rays 2018 (UHECR2018), EPJ WEB Conf. **210** (2019) 05002.

[41] C. Covault, T. Fujii, T. Nonaka, H. Sagawa, T. Sako, F. Sarazin *et al.*, "The Auger@TA Project: Phase II Progress and Plans", Proceedings of Ultra High Energy Cosmic Rays 2018 (UHECR2018), EPJ WEB Conf. **210** (2019) 05004.

[42] F. Bisconti, J.W. Belz, M.E. Bertaina, M. Casolino, T. Ebisuzaki, J. Eser, J.N. Matthews, L.W. Piotrowski, Z. Plebaniak, H. Sagawa, "The Auger@TA Project: Phase II Progress and Plans", Proceedings of Ultra High Energy Cosmic Rays 2018 (UHECR2018), EPJ WEB Conf. **210** (2019) 05004.

[43] T. Tomida, T. Inadomi, T. Seki, Y. Tameda, Y. Oku and K. Sano, "Development of the calibration device using UAV mounted UV-LED light source for the fluorescence detector", Proceedings of Ultra High Energy Cosmic Rays 2018 (UHECR2018), EPJ WEB Conf. **210** (2019) 05015.

[44] R. Nakamura, T. Tomida, Y. Saito and K. Yamazaki, "Cloud monitoring system at Telescope Array site by Visible Fisheye CCD", Proceedings of Ultra High Energy Cosmic Rays 2018 (UHECR2018), EPJ WEB Conf. **210** (2019) 05016.

[45] E. Kido, "Status and prospects of the TAx4 experiment", Proceedings of Ultra High Energy Cosmic Rays 2018 (UHECR2018), EPJ WEB Conf. **210** (2019) 06001.

[46] T. Fujii *et al.*, "A next-generation ground array for the detection of ultrahigh-energy cosmic rays: the Fluorescence detector Array of Single-pixel Telescopes (FAST)", Proceedings of Ultra High Energy Cosmic Rays 2018 (UHECR2018), EPJ WEB Conf. **210** (2019) 06003.

[47] Y. Tameda *et al.*, "Detection of ultra-high energy cosmic ray air showers by Cosmic Ray Air Fluorescence Fresnel lens Telescope for next generation", Proceedings of Ultra High Energy Cosmic Rays 2018 (UHECR2018), EPJ WEB Conf. **210** (2019) 06004.

[48] S. Ogio for the Telescope Array Collaboration, "Highlights from the Telescope Array experiment", Proceedings of International Cosmic Ray Conference 2019 (ICRC2019), Pos(ICRC2019)013, 2021.

[49] J. Belz for the Telescope Array Collaboration, "Observations of Terrestrial Gamma-ray Flashes at the Telescope Array Cosmic Ray Detector", Pos(ICRC2019)168, 2021.

[50] T. AbuZayyad for the Telescope Array Collaboration, "TALE FD Cosmic Rays Composition Measurement", Pos(ICRC2019)169, 2021.

[51] D.R. Bergman for the Telescope Array Collaboration, "First Results from NICHE and the NICHE-TALE Hybrid Detector", Pos(ICRC2019)189, 2021.

[52] D.R. Bergman for the Telescope Array Collaboration, "Combined Fit of the Spectrum and Composition from Telescope Array", Pos(ICRC2019)190, 2021.

[53] D.R. Bergman for the Telescope Array Collaboration, "TA 10-Year Stereo Composition Measurement", Pos(ICRC2019)191, 2021.

[54] F. Bisconti, H. Sagawa *et al.*, "EUSO-TA ground based fluorescence detector: analysis of the detected events", Pos(ICRC2019)197, 2021.

[55] O. Deligny for the Pierre Auger and Telescope Array Collaborations, "The energy spectrum of ultra-high energy cosmic rays measured at the Pierre Auger Observatory and at the Telescope Array", Pos(ICRC2019)234, 2021.

[56] T. Fujii *et al.*, "Observing ultra-high energy cosmic rays with prototypes of Fluorescence detector Array of Single-pixel Telescopes (FAST) in both hemispheres", Pos(ICRC2019)259, 2021.

[57] G. Furlich for the Telescope Array Collaboration, "Towards a Telescope Array 10 Year FD Monocular Energy Spectrum", Pos(ICRC2019)260, 2021.

[58] G. Furlich for the Telescope Array Collaboration, "Telescope Array FD Weather Classification using Machine Learning", Pos(ICRC2019)261, 2021.

[59] W. Hanlon for the Telescope Array Collaboration, "Telescope Array 10 Year Composition", Pos(ICRC2019)280, 2021.

[60] D. Ivanov for the Telescope Array Collaboration, "Energy Spectrum Measured by the Telescope Array Experiment", Pos(ICRC2019)298, 2021.

[61] K. Kawata, E. Kido, T. Nonaka, S. Ogio, H. Sagawa, T. Sako, M. Takeda, R. Takeishi for the Telescope Array Collaboration, "Updated Results on the UHECR Hotspot Observed by the Telescope Array Experiment", Pos(ICRC2019)310, 2021.

[62] E. Kido for the Telescope Array Collaboration, "Status and prospects of the TAx4 experiment", Pos(ICRC2019)312, 2021.

[63] E. Kido for the Telescope Array Collaboration, "Implications of the cosmic ray spectrum from the second knee to the ankle region for the cosmic ray proton sources", Pos(ICRC2019)313, 2021.

[64] JiHee Kim for the Telescope Array Collaboration, "The Cosmic Ray Energy Spectrum above 2 PeV measured by the TALE Fluorescence Telescopes", Pos(ICRC2019)314, 2021.

[65] M. Kuznetsov for the Telescope Array Collaboration, "Telescope Array Search for EeV Photons", Pos(ICRC2019)326, 2021.

[66] J.P. Lundquist and P. Sokolsky for the Telescope Array Collaboration, "Supergalactic Structure of Energy-Angle Correlations", Pos(ICRC2019)343, 2021.

[67] R. Mayta, Y. Tsunesada, S. Ogio for the Telescope Array Collaboration, "Time structure analysis of extensive air showers using the Telescope Array Data", Pos(ICRC2019)347, 2021.

[68] T. Nonaka, E. Kido, S. Ogio, H. Sagawa for the Telescope Array Collaboration, "Long distance network link for TA×4 expansion", Pos(ICRC2019)372, 2021.

[69] S. Ogio for the Telescope Array Collaboration, "Telescope Array Low-energy Extension (TALE) hybrid", Pos(ICRC2019)375, 2021.

[70] Y. Omura for the Telescope Array Collaboration, "NICHE detector and operations", Pos(ICRC2019)379, 2021.

[71] J. Remington for the Telescope Array Collaboration, "Detection and Resolution of Terrestrial Gamma Flashes at Telescope Array", Pos(ICRC2019)400, 2021.

[72] Y. Tameda *et al.*, "The status and performance of Cosmic Ray Air Fluorescence Fresnel lens Telescope (CRAFFT) for the next generation UHECR observatory", Pos(ICRC2019)435, 2021.

[73] A. di Matteo, K. Kawata, T. Nonaka, H. Sagawa for the Pierre Auger Collaboration and the Telescope Array Collaboration, "Full-sky searches for anisotropies in UHECR arrival directions with the Pierre Auger Observatory and the Telescope Array", Pos(ICRC2019)439, 2021.

[74] T. Tomida for the Telescope Array Collaboration, "Geometry calibration of Fluorescence Detector using standard light source mounted on UAV", Pos(ICRC2019)441, 2021.

[75] T. Uehama for the Telescope Array Collaboration, "Measurement of atmospheric transparency in Telescope Array using Central Laser Facility", Pos(ICRC2019)442, 2021.

[76] K. Yamazaki for the Telescope Array Collaboration, "Cloud monitoring system by Visible-light Fisheye CCD for the Telescope Array", Pos(ICRC2019)474, 2021.

[77] G. Rubtsov, Y. Zhezher for the Telescope Array Collaboration, "Anisotropy in the mass composition from the Telescope Array Surface Detector data", Pos(ICRC2019)494, 2021.

[78] The IceCube Collaboration, The Pierre Auger Collaboration, The Telescope Array Collaboration, The ANTARES Collaboration, "Search for correlations of high-energy neutrinos and ultra-high energy cosmic rays", Pos(ICRC2019)842, 2021.

[79] K. Yamazaki, T. Tomida, R. Nakamura, Y. Saito for the Telescope Array Collaboration, "Cloud monitoring system by Visible-light Fisheye CCD for the Telescope Array", Pos(ICRC2019)1177, 2021.

[80] G.I. Rubtsov for the Telescope Array Collaboration, "Highlights from the Telescope Array experiment", Proceedings of International Cosmic Ray Conference 2021 (ICRC2021), Pos(ICRC2021)012, 2022.

[81] T. Okuda for the Telescope Array Collaboration, "Telescope Array Cloud Ranging Test", Pos(ICRC2021)192, 2022.

[82] A. Nakazawa, T. Tomida, Y. Tameda, D. Daisuke for the Telescope Array Collaboration, "FOV direction and image size calibration of Fluorescence Detector using light source on UAV", Pos(ICRC2021)196, 2022.

[83] E. Kido for the Telescope Array Collaboration, "Current status and prospects of surface detector of the TAx4 experiment", Pos(ICRC2021)203, 2022.

[84] T. Tomida, T. Nakamura for the Telescope Array Collaboration, "The atmospheric transparency of Telescope Array observation site by the CLF", Pos(ICRC2021)217, 2022.

[85] I. Buckland for the Telescope Array Collaboration, "CHASM (CHerenkov Air Shower Model): Simulating the Cherenkov Profiles of Cosmic Ray Air Showers", Pos(ICRC2021)234, 2022.

[86] F. Yoshida, Y. Tameda for the Telescope Array Collaboration, "A study of analysis method for the identification of UHECR source type", Pos(ICRC2021)242, 2022.

[87] A. Iwasaki, S. Ogio for the Telescope Array Collaboration, "The status of the TALE surface detector array and a TALE infill project", Pos(ICRC2021)255, 2022.

[88] T. Fujii for the Telescope Array Collaboration, "Update on the large-scale cosmic-ray anisotropy search at the highest energies by the Telescope Array Experiment", Pos(ICRC2021)291, 2022.

[89] M. Kuznetsov for the Telescope Array Collaboration, "UHECR mass composition from anisotropy of their arrival directions with the Telescope Array SD", Pos(ICRC2021)294, 2022.

[90] R. Abbasi for the Telescope Array Collaboration, "Observation of Variations in Cosmic Ray Shower Rates During Thunderstorms and Implications for Large-Scale Electric Field Changes", Pos(ICRC2021)297, 2022.

[91] Y. Zhezher for the Telescope Array Collaboration, "Mass composition anisotropy with the Telescope Array Surface Detector data", Pos(ICRC2021)299, 2022.

[92] Y. Zhezher for the Telescope Array Collaboration, "Cosmic-ray mass composition with the TA SD 12-year data", Pos(ICRC2021)300, 2022.

[93] H. Shin for the Telescope Array Collaboration, "The measurements of the cosmic ray energy spectrum and the depth of maximum shower development of Telescope Array Hybrid trigger events", Pos(ICRC2021)305, 2022.

[94] J. Kim, K. Kawata, H. Sagawa for the Telescope Array Collaboration, "Hotspot Update, and a new Excess of Events on the Sky Seen by the Telescope Array Experiment", Pos(ICRC2021)328, 2022.

[95] Y. Omura for the Telescope Array Collaboration, "Energy spectrum and the shower maxima of cosmic rays above the knee region measured with the NICHE detectors at the TA site", Pos(ICRC2021)329, 2022.

[96] H. Jeong for the Telescope Array Collaboration, "Reconstruction of Air Shower Events Measured by the Surface Detectors of the TAx4 Experiment", Pos(ICRC2021)331, 2022.

[97] S.W Kim for the Telescope Array Collaboration, "Analysis of TAx4 hybrid trigger and events", Pos(ICRC2021)332, 2022.

[98] Y. Tsunesada on behalf of the Pierre Auger and the Telescope Array Collaboration, "Joint analysis of the energy spectrum of ultra-high-energy cosmic rays measured at the Pierre Auger Observatory and the Telescope Array", Pos(ICRC2021)337, 2022.

[99] D.R. Bergman for the Telescope Array Collaboration, "Telescope Array Combined Fit to Cosmic Ray Spectrum and Composition", Pos(ICRC2021)338, 2022.

[100] D.R. Bergman for the Telescope Array Collaboration, "Telescope Array 10-Year Monocular Spectrum Measurement", Pos(ICRC2021)339, 2022.

[101] D. Ivanov, Y. Tsunesada for the Telescope Array Collaboration, "Recent measurement of the Telescope Array energy spectrum and observation of the shoulder feature in the Northern Hemisphere", Pos(ICRC2021)341 2022.

[102] M. Potts for the Telescope Array Collaboration, "Monocular Energy Spectrum using the TAx4 Fluorescence Detector", Pos(ICRC2021)343 2022.

[103] T. Nonaka for the Telescope Array Collaboration, "Anisotropy search in the Ultra High Energy Cosmic Ray Spectrum in the Northern Hemisphere using latest data obtained with Telescope Array surface detector", Pos(ICRC2021)344 2022.

[104] J. Remington for the Telescope Array Collaboration, "Insight Into Lightning Initiation via Downward Terrestrial Gamma-ray Flash Observations at Telescope Array", Pos(ICRC2021)345 2022.

[105] T. AbuZayyad for the Telescope Array Collaboration, "Cosmic Ray Composition between 2 PeV and 2 EeV measured by the TALE Fluorescence Detector", Pos(ICRC2021)346 2022.

[106] T. AbuZayyad for the Telescope Array Collaboration, "Cosmic Ray Energy Spectrum measured by the TALE Fluorescence Detector", Pos(ICRC2021)347 2022.

[107] D. Soldin for the EAS-MSU, IceCube, KASCADE-Grande, NEVOD-DECOR, Pierre Auger, SUGAR, Telescope Array, and Yakutsk EAS Array Collaborations, "Update on the Combined Analysis of Muon Measurements from Nine Air Shower Experiments", Pos(ICRC2021)349 2022.

[108] K. Fujita for the Telescope Array Collaboration, "Cosmic Ray Composition in the Second Knee Region as Measured by the TALE Hybrid Detector", Pos(ICRC2021)353, 2022.

[109] K. Fujisue for the Telescope Array Collaboration, "Performance and simulation of the surface detector array of the TAx4 experiment", Pos(ICRC2021)355, 2022.

[110] R. Higuchi, T. Sako, K. Kawata, T. Fujii, E. Kido for the Telescope Array Collaboration, "Effects of Galactic magnetic field on the UHECR anisotropy studies", Pos(ICRC2021)358, 2022.

[111] K. Sato for the Telescope Array Collaboration, "Cosmic ray energy spectrum in the 2nd knee region measured by the TALE-SD array", Pos(ICRC2021)362, 2022.

[112] P. Tinyakov on behalf of the Pierre Auger and the Telescope Array Collaboration, "The UHECR dipole and quadrupole in the latest data from the original Auger and TA surface detectors", Pos(ICRC2021)375, 2022.

[113] I. Kharuk for the Telescope Array Collaboration, "Mass composition of Telescope Array's surface detectors events using deep learning", Pos(ICRC2021)384, 2022.

[114] T. Fujii, K. Kawata, T. Nonaka, S. Ogio, H. Sagawa, I. Tkachev for the Telescope Array Collaboration, "Telescope Array anisotropy summary", Pos(ICRC2021)392, 2022.

[115] T. Fujii *et al.*, "Latest results of ultra-high-energy cosmic ray measurements with prototypes of the Fluorescence detector Array of Single-pixel Telescopes (FAST)", Pos(ICRC2021)402, 2022.

[116] O. Kalashev for the Telescope Array Collaboration, "Telescope Array search for EeV photons", Pos(ICRC2021)864, 2022.

[117] T. Nonaka for the Telescope Array Collaboration, "Study on the cosmic ray intensity variation using scintillation counters for air shower observation", Pos(ICRC2021)1255, 2022.

[118] D.R. Bergman, T. Fujii, K. Fujita *et al.*, "The energy spectrum of ultra-high energy cosmic rays measured at the Pierre Auger Observatory and the Telescope Array", Proceedings of Ultra High Energy Cosmic Rays 2022 (UHECR2022), EPJ WEB Conf. **283** (2023) 02003.

[119] J. Kim *et al.*, "Energy Spectrum Measured by the Telescope Array Surface Detectors", EPJ WEB Conf. **283** (2023) 02005.

[120] H. Oshima, K. Fujita, S. Ogio and T. Sako, "Measurement of Cosmic-ray Energy Spectrum with the TALE Detector in Hybrid Mode", EPJ WEB Conf. **283** (2023) 02006.

[121] D.R. Bergman *et al.*, "Testing the Compatibility of the Depth of the Shower Maximum Measurements performed at Telescope Array and the Pierre Auger Observatory - Auger-TA Mass Composition Working Group Report", EPJ WEB Conf. **283** (2023) 02008.

[122] K. Fujita, "Cosmic ray mass composition measurement with the TALE hybrid detector", EPJ WEB Conf. **283** (2023) 02009.

[123] R. Arimura, "A machine learning approach for mass composition analysis with TALE-SD data", EPJ WEB Conf. **283** (2023) 02011.

[124] A. di Matteo, R. Higuchi *et al.*, "2022 report from the Auger-TA working group on UHECR arrival directions", EPJ WEB Conf. **283** (2023) 03002.

[125] M. Kuznetsov and P. Tinyakov, "UHECR anisotropy and extragalactic magnetic fields with the Telescope Array", EPJ WEB Conf. **283** (2023) 03004.

[126] J. Kim, K. Kawata, H. Sagawa *et al.*, "Updates on the Hotspot and the Perseus-Pisces supercluster Excess Observed by the Telescope Array Experiment", EPJ WEB Conf. **283** (2023) 03005.

[127] Y. Kimura, T. Fujii, S. Ogio and Y. Tsunesada, "Search for the large-scale cosmic-ray anisotropies using the TA and TALE surface detector arrays", EPJ WEB Conf. **283** (2023) 03007.

[128] K. Watanabe, A. Fedynitch, F. Capel and H.Sagawa, "A Bayesian source association analysis of UHECRs: Impact of the Galactic magnetic field and composition", EPJ WEB Conf. **283** (2023) 03009.

[129] R. Higuchi, T. Sako, T. Fujii, K. Kawata and E. Kido, "Estimation and reduction of the biases by the galactic magnetic field on the UHECR correlation studies", EPJ WEB Conf. **283** (2023) 03011.

[130] R. Saito, T. Tomida and D. Ikeda, "Examination of Xmax anisotropy for the next generation Ultra-high energy cosmic rays observations", EPJ WEB Conf. **283** (2023) 03012.

[131] E. Kido, "Current status of the TAx4 surface detectors", EPJ WEB Conf. **283** (2023) 06003.

[132] K. Fujisue, "TAx4 surface detectors data analysis", EPJ WEB Conf. **283** (2023) 06004.

[133] S. Mayotte, T. Fujii, H. Sagawa, T. Sako *et al.*, "Auger@TA: Deploying an independent Pierre Auger Observatory SD micro-array at the Telescope Array Project - Auger@TA Working Group Report", EPJ WEB Conf. **283** (2023) 06005.

[134] T. Fujii *et al.*, "Recent results from prototypes of the Fluorescence detector Array of Single-pixel Telescopes (FAST) in both hemispheres", EPJ WEB Conf. **283** (2023) 06010.

[135] Y. Tameda, T. Tomida, D. Ikeda, K. Yamazaki *et al.*, "Progress and future prospect of the CRAFFT project for the next generation UHECR observatory", EPJ WEB Conf. **283** (2023) 06011.

[136] A. Iwasaki, K. Fujita, S. Ogio, T. Fujii and Y. Tsunesada, "Performance of the TALE infill experiment as a TA-TALE extension down to the PeV region", EPJ WEB Conf. **283** (2023) 06015.

[137] J. Kim, "Highlights from the Telescope Array Experiment", Proceedings of International Cosmic Ray Conference 2023 (ICRC2023), PoS(ICRC2023)008, 2023.

[138] K. Mizuno, T. Tomida and K. Yamazaki for the Telescope Array collaboration, "Effects of atmospheric transparency on Telescope Array air shower analysis", Proceedings of International Cosmic Ray Conference 2023 (ICRC2023), PoS(ICRC2023)226, 2023.

[139] D. Sato, T. Tomida R. Hibi, A. Matuzawa, Y. Tameda, D. Ikeda, "Effect of optical properties of FDs on reconstrction analysis", PoS(ICRC2023)227, 2023.

[140] E. Kido, "Updates of the surface detector array of the TAx4 experiment", PoS(ICRC2023)239, 2023.

[141] J. Kim *et al.*, "Anisotropies in the arrival direction distribution of ultra-high energy cosmic rays measured by the Telescope Array surface detector", PoS(ICRC2023)244, 2023.

[142] R. Abbasi *et al.*, "High-speed Video Camera Observations Associated with a Terrestrial Gamma-ray Flash at the Telescope Array Detector", PoS(ICRC2023)250, 2023.

[143] H. Oshima *et al.*, "Measurement of cosmic-ray energy spectrum with the TALE detector in hybrid mode", PoS(ICRC2023)271, 2023.

[144] K. Takahashi *et al.*, "TA SD analysis for inclined air showers", PoS(ICRC2023)306, 2023.

[145] K. Fujisue *et al.*, "Measurement of the cosmic ray energy spectrum with the TAx4 SD array", PoS(ICRC2023)308, 2023.

[146] I. Kharuk *et al.*, "Search for EeV photon-induced events at the Telescope Array", PoS(ICRC2023)324, 2023.

[147] K. Komori *et al.*, "Systematic uncertainty in the analysis of the TA fluorescence detector from fluorescence yield models", PoS(ICRC2023)330, 2023.

[148] Y. Kusumori *et al.*, "Monocular and Hybrid Analysis for TA×4 Fluorescence Detectors", PoS(ICRC2023)331, 2023.

[149] T. AbuZayyad *et al.*, "Cosmic Ray Energy Spectrum and Mass Composition measured by the TALE Fluorescence Detector", PoS(ICRC2023)379, 2023.

[150] K. Fujita and S. Ogio *et al.*, "A study of the systematic effects on the energy scale for the measurement of UHECR spectrum by the TA SD array", PoS(ICRC2023)400, 2023.

[151] K. Fujita, "Cosmic ray mass composition measurement with the TALE hybrid detector", PoS(ICRC2023)401, 2023.

[152] I. Komae, "Measurement of the cosmic ray energy spectrum in the 2nd knee region with the TALE-SD array", PoS(ICRC2023)405, 2023.

[153] Y. Tsunesada *et al.*, "Measurement of UHECR energy spectrum with the Pierre Auger Observatory and the Telescope Array", PoS(ICRC2023)406, 2023.

[154] L. Caccianiga *et al.*, "Update on the searches for anisotropies in UHECR arrival directions with the Pierre Auger Observatory and the Telescope Array", PoS(ICRC2023)521, 2023.

[155] M. Kuznetsov *et al.*, "Possible interpretations of the joint observations of UHECR arrival directions using data recorded at the Telescope Array and the Pierre Auger Observatory", PoS(ICRC2023)528, 2023.

Papers for R/D detectors

[156] G. Abdellaoui *et al.*, "EUSO-TA - First results from a ground-based EUSO telescope", Astropart. Phys. **102**, 98, 2018.

[157] J.H. Adams Jr. *et al.*, "Detection limits and trigger rates for ultra-high energy cosmic ray detection with the EUSO-TA ground-based EUSO telescope", Astropart. Phys. **163**, 103007, 2024.

[158] M. Battisti *et al.*, "Performance results of the trigger logic implemented in EUSO-SPB", Nucl. Inst. and Meth. A **936**, 349, 2019.

[159] M. Battisti *et al.*, "EUSO-SPB2 Fluorescence Telescope trigger test within the EUSO@TurLab Project", Nucl. Inst. and Meth. A **1045**, 167611, 2023.

[160] T. Fujii, "Recent results from prototypes of the Fluorescence detector Array of Single-pixel Telescopes (FAST) in both hemispheres", EPJ Web of Conferences, **283**, 06010, 2023.

[161] Y. Tameda *et al.*, "Progress and future prospect of the CRAFFT project for the next generation UHECR observatory", EPJ Web of Conferences, **283**, 06011, 2023.

[162] S. Mayotte *et al.*, "Auger@TA: An Auger-like surface detector micro-array embedded within the Telescope Array Project", PoS(ICRC2023)368, 2023.

[163] S. Shefali *et al.*, "Status and plans for the instrumentation of the IceCube Surface Array Enhancement", PoS(ICRC2023)342, 2023.

[164] F. Kajino *et al.*, "DIMS Experiment for Macroscopic Dark Matter and Interstellar Meteoroid Study", PoS(ICRC2023)1376, 2023.

Telescope Array Collaboration

R.U. Abbasi[1], T. Abu-Zayyad[1,2], M. Allen[2], J.W. Belz[2], D.R. Bergman[2], I. Buckland[2], W. Campbell[2], B.G. Cheon[3], K. Endo[4], A. Fedynitch[5,6], T. Fujii[4,7], K. Fujisue[5,6], K. Fujita[5], M. Fukushima[5], G. Furlich[2], Z. Gerber[2], N. Globus[8*], W. Hanlon[2], N. Hayashida[9], H. He[8†], K. Hibino[9], R. Higuchi[8], D. Ikeda[9], T. Ishii[10], D. Ivanov[2], S. Jeong[11], C.C.H. Jui[2], K. Kadota[12], F. Kakimoto[9], O. Kalashev[13], K. Kasahara[14], Y. Kawachi[4], K. Kawata[5], I. Kharuk[13], E. Kido[8], H.B. Kim[3], J.H. Kim[2], J.H. Kim[2‡], S.W. Kim[11§], R. Kobo[4], I. Komae[4], K. Komatsu[15], K. Komori[16], C. Koyama[5], M. Kudenko[13], M. Kuroiwa[15], Y. Kusumori[16], M. Kuznetsov[13,17], Y.J. Kwon[18], K.H. Lee[3], M.J. Lee[11], B. Lubsandorzhiev[13], J.P. Lundquist[2,19], A. Matsuzawa[15], J.A. Matthews[2], J.N. Matthews[2], K. Mizuno[15], M. Mori[16], M. Murakami[16], S. Nagataki[8], M. Nakahara[4], T. Nakamura[20], T. Nakayama[15], Y. Nakayama[16], T. Nonaka[5], S. Ogio[5], H. Ohoka[5], N. Okazaki[5], M. Onishi[5], A. Oshima[21], H. Oshima[5], S. Ozawa[22], I.H. Park[11], K.Y. Park[3], M. Potts[2], M. Przybylak[23], M.S. Pshirkov[13,24], J. Remington[2¶], C. Rott[2,11], G.I. Rubtsov[13], D. Ryu[25], H. Sagawa[5], N. Sakaki[5], R. Sakamoto[16], T. Sako[5], N. Sakurai[5], S. Sakurai[4], D. Sato[15], S. Sato[16], K. Sekino[5], T. Shibata[5], J. Shikita[4], H. Shimodaira[5], B.K. Shin[25], H.S. Shin[4,7], K. Shinozaki[26], J.D. Smith[2], P. Sokolsky[2], B.T. Stokes[2], T.A. Stroman[2], Y. Takagi[16], K. Takahashi[5], M. Takeda[5], R. Takeishi[5], A. Taketa[27], M. Takita[5], Y. Tameda[16], K. Tanaka[28], M. Tanaka[29], S.B. Thomas[2], G.B. Thomson[2], P. Tinyakov[13,17], I. Tkachev[13], T. Tomida[15], S. Troitsky[13], Y. Tsunesada[4,7], S. Udo[9], F. Urban[30], I.A. Vaiman[13‖], M. Vrábel[26], D. Warren[8], K. Yamazaki[21], Y. Zhezher[5,13], Z. Zundel[2], and J. Zvirzdin[2]

[1] *Department of Physics, Loyola University Chicago, Chicago, Illinois 60660, USA*
[2] *High Energy Astrophysics Institute and Department of Physics and Astronomy, University of Utah, Salt Lake City, Utah 84112-0830, USA*
[3] *Department of Physics and The Research Institute of Natural Science, Hanyang University, Seongdong-gu, Seoul 426-791, Korea*
[4] *Graduate School of Science, Osaka Metropolitan University, Sugimoto, Sumiyoshi, Osaka 558-8585, Japan*
[5] *Institute for Cosmic Ray Research, University of Tokyo, Kashiwa, Chiba 277-8582, Japan*
[6] *Institute of Physics, Academia Sinica, Taipei City 115201, Taiwan*
[7] *Nambu Yoichiro Institute of Theoretical and Experimental Physics, Osaka Metropolitan University, Sugimoto, Sumiyoshi, Osaka 558-8585, Japan*
[8] *Astrophysical Big Bang Laboratory, RIKEN, Wako, Saitama 351-0198, Japan*
[9] *Faculty of Engineering, Kanagawa University, Yokohama, Kanagawa 221-8686, Japan*
[10] *Interdisciplinary Graduate School of Medicine and Engineering, University of Yamanashi, Kofu, Yamanashi 400-8511, Japan*
[11] *Department of Physics, Sungkyunkwan University, Jang-an-gu, Suwon 16419, Korea*
[12] *Department of Physics, Tokyo City University, Setagaya-ku, Tokyo 158-8557, Japan*
[13] *Institute for Nuclear Research of the Russian Academy of Sciences, Moscow 117312, Russia*
[14] *Faculty of Systems Engineering and Science, Shibaura Institute of Technology, Minato-ku, Tokyo 337-8570, Japan*
[15] *Academic Assembly School of Science and Technology Institute of Engineering, Shinshu University, Nagano, Nagano 380-8554, Japan*
[16] *Graduate School of Engineering, Osaka Electro-Communication University, Neyagawa-shi, Osaka 572-8530, Japan*
[17] *Service de Physique Théorique, Université Libre de Bruxelles, Brussels 1050, Belgium*
[18] *Department of Physics, Yonsei University, Seodaemun-gu, Seoul 120-749, Korea*
[19] *Center for Astrophysics and Cosmology, University of Nova Gorica, Nova Gorica 5297, Slovenia*
[20] *Faculty of Science, Kochi University, Kochi, Kochi 780-8520, Japan*
[21] *College of Science and Engineering, Chubu University, Kasugai, Aichi 487-8501, Japan*
[22] *Quantum ICT Advanced Development Center, National Institute for Information and Communications Technology, Koganei, Tokyo 184-8795, Japan*
[23] *Doctoral School of Exact and Natural Sciences, University of Lódź, Lódź, Lódź 90-237, Poland*
[24] *Sternberg Astronomical Institute, Moscow M.V. Lomonosov State University, Moscow 119991, Russia*
[25] *Department of Physics, School of Natural Sciences, Ulsan National Institute of Science and Technology, UNIST-gil, Ulsan 689-798, Korea*
[26] *Astrophysics Division, National Centre for Nuclear Research, Warsaw 02-093, Poland*
[27] *Earthquake Research Institute, University of Tokyo, Bunkyo-ku, Tokyo 277-8582, Japan*
[28] *Graduate School of Information Sciences, Hiroshima City University, Hiroshima, Hiroshima 731-3194, Japan*
[29] *Institute of Particle and Nuclear Studies, KEK, Tsukuba, Ibaraki 305-0801, Japan*
[30] *CEICO, Institute of Physics, Czech Academy of Sciences, Prague 182 21, Czech Republic*

* [*] Presently at: KIPAC, Stanford University, Stanford, CA 94305, USA
* [†] Presently at: Purple Mountain Observatory, Nanjing 210023, China
* [‡] Presently at: Physics Department, Brookhaven National Laboratory, Upton, NY 11973, USA
* [§] Presently at: Korea Institute of Geoscience and Mineral Resources, Daejeon, 34132, Korea
* [¶] Presently at: NASA Marshall Space Flight Center, Huntsville, Alabama 35812, USA
* [‖] Presently at: Gran Sasso Science Institute, 67100 L'Aquila, L'Aquila, Italy

Tibet AS$_\gamma$ PROJECT

Introduction

The Tibet air shower experiment has been successfully operated at Yangbajing (90°31' E, 30°06' N; 4300 m above sea level) in Tibet, China since 1990. It has continuously made a wide field-of-view (approximately 2 steradian) observation of cosmic rays and gamma rays in the northern sky. The operation of the underground muon detectors has started in 2014 and it opened a new window of astronomy in the sub-PeV energy region.

Summary from 2018 to 2024

- Sub-PeV gamma-ray astronomy was established by the first detection of the Crab nebula above 100 TeV using the powerful particle identification using the underground muon detectors implemented in the Tibet air shower array.
- Various types of sub-PeV sources are detected, among which SNR G106.3+2/7, HESS J1843-033 and HESS J1849-000 are suggested as good candidates of PeV cosmic-ray accelerators.
- Galactic diffuse gamma-ray emission above 398 TeV was detected for the first time. Its distribution along the galactic disk is a strong evidence that the parent PeV cosmic-ray particles also have galactic origin.
- Using the power of the muon detectors a new study to identify proton initiated showers is on going. Another study using neural network to identify gamma-ray-initiated showers only by the surface array data is ongoing. This allows to analyse big data before the implementation of the muon detectors. A validation of the neural network analysis becomes possible by using the muon detector data.
- Analyses on the cosmic-ray anisotropy and the burst events related with the thundercloud electric field are also in progress.

Experiment

The Tibet I array was constructed in 1990 and it was gradually upgraded to the Tibet II by 1994 which consisted of 185 fast-timing (FT) scintillation counters placed on a 15 m square grid covering 36,900 m^2, and 36 density (D) counters around the FT-counter array. Each counter has a plastic scintillator plate of 0.5 m^2 in area and 3 cm in thickness. All the FT counters are equipped with a fast-timing 2-inch-in-diameter photomultiplier tube (FT-PMT), and 52 out of 185 FT counters are also equipped with a wide dynamic range 1.5-inch-in-diameter PMT (D-PMT) by which we measure up to 500 particles which saturates FT-PMT output, and all the D-counters have a D-PMT. A 0.5 cm thick lead plate is put on the top of each counter in order to increase the counter sensitivity by converting gamma rays into electron-positron pairs in an electromagnetic shower. The mode energy of the triggered events in Tibet II is 10 TeV.

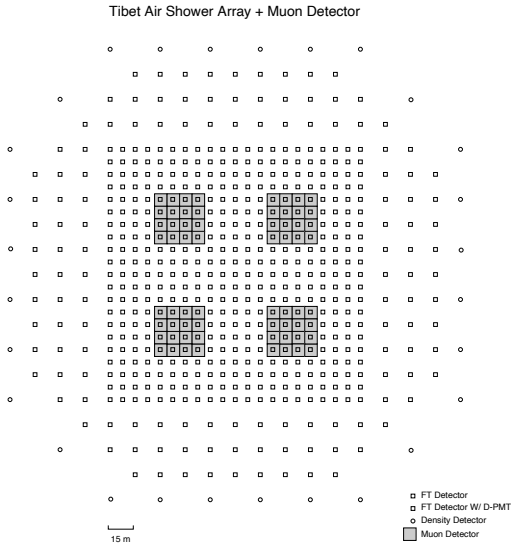

Fig. 1. Schematic view of the Tibet air shower array and the muon detector array.

In 1996, we added 77 FT counters with a 7.5 m lattice interval to a 5,200 m^2 area inside the northern part of the Tibet II array. We called this high-density array Tibet HD. The mode energy of the triggered events in Tibet HD is a few TeV.

In the late fall of 1999, the array was further upgraded by adding 235 FT-counters so as to enlarge the high-density area from 5,200 m^2 to 22,050 m^2, and we call this array and further upgraded one Tibet III. In 2002, all of the 36,900 m^2 area was covered by the high-density array by adding 200 FT-counters more. Finally we set up 56 FT-counters around the 36,900 m^2 high density array and equipped 8 D-counters with FT-PMT in 2003.

The performance of the Tibet air shower array has been well examined by observing the Moon's shadow (approximately 0.5 degrees in diameter) in cosmic rays. The deficit map of cosmic rays around the Moon demonstrates the angular resolution to be around 0.9° at a few TeV for the Tibet III array. The pointing error is estimated to be better than $\sim$0.01° by the displacement of the shadow's center from the apparent center in the north-south direction, as the east-west component of the geomagnetic field is very small at the experimental site. On the other hand, the shadow center displacement in the east-west direction due to the geomagnetic field enables us to spectroscopically estimate the energy scale uncertainty at $\pm$12% level.

The idea of the underground water Cherenkov muon detectors (MDs) was proposed in [1] and validated by an operation of a prototype detector [2]. The full scale MD array cov-

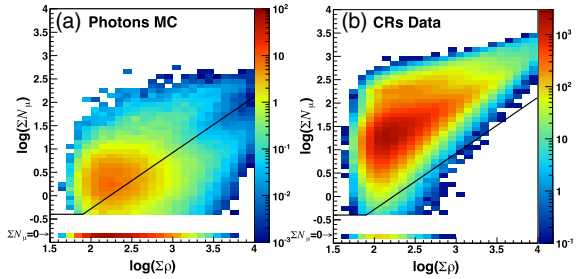

Fig. 2. $\Sigma\rho$ versus ΣN_μ for the MC simulated gamma-ray events (left) and observed CR events (right). Events with $\Sigma N_\mu = 0$ are accumulated in the bins of $\log(\Sigma N_\mu) = -0.8$ [18].

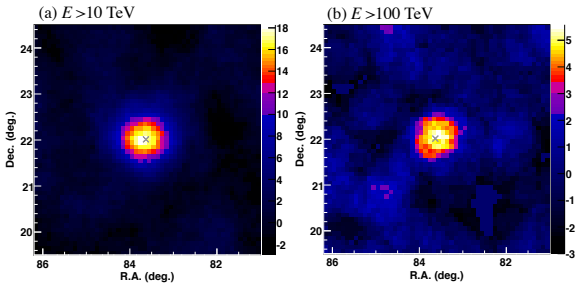

Fig. 3. Significance maps around the Crab nebula [18].

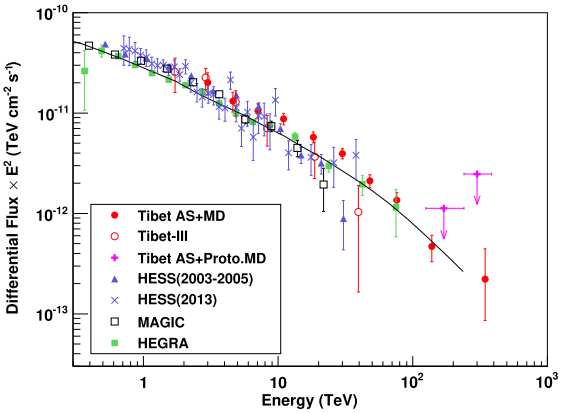

Fig. 4. Energy spectra of the Crab nebula. The red points extending beyond 100 TeV are the results of Tibet experiment [18].

ers a total area of $\sim$3400 m^2 and is divided in the 4 units as shown in Fig.1. Each unit contains 16 cells of 7.35 m$\times$7.35 m area and is filled by clean water of 1.5 m depth. A 20-inch PMT facing downward into water is installed in each cell. With 2.5 m soil overburden corresponding to 17 radiation lengths, most of the electromagnetic particles are absorbed but muons of energy above 1 GeV can arrive at the MD. In average 24 photo-electrons are detected when a muon passes through water. MD array was constructed and the operation started at the beginning of 2014.

At present, the Tibet air shower array consists of 569 FT-counters (249 of which have a D-PMT), 28 D-counters and 4 units of underground muon detectors as shown in Fig.1.

Physics Results

First Detection of Sub-PeV Gamma Rays from the Crab Nebula

Using the excellent background rejection power of the MDs, an emission of sub-PeV ($>$100 TeV) gamma rays from the Crab nebula was detected for the first time [18]. Fig.2 shows the distribution of events in $\Sigma\rho$ (total number of particles detected by the scintillating counters) and ΣN_μ (total number of muons detected by the MDs) for the gamma-ray showers (Monte Carlo) and CR (hadronic) showers (experimental data). The solid straight line indicates the event selection criterion. Events below this line are categorized as gamma-ray like events. Above 100 TeV, 99.92% of background events are rejected while 90% of gamma-ray events remains. After the background rejection, as shown in Fig.3 excesses of gamma-ray like events around the direction of the Crab at significances of 18.3σ and 5.6σ above 10 TeV and 100 TeV, respectively were detected. Fig.4 shows the energy spectra reported by various experiments. The red points given by the Tibet experiment in this study determined the flux above 100 TeV for the first time.

SNR G106.3+2.7 : First Candidate of the Former PeV CR Accelerators

The direction of SNR G106.3+2.7 is a complex gamma-ray emission region extensively studied by many experiments. The Tibet experiment detected the gamma-ray emission from the G106 region above 100 TeV for the first time [15]. As shown in Fig.5, the gamma-ray emission above 10 TeV detected by the Tibet experiment coincides with the SNR shown by the black contours and a molecular cloud detected in the ^{12}CO (J=1-0) line emission shown by the cyan contours. These observations support a scenario in which the gamma-rays detected by the Tibet experiment originate from the decay of π^0's produced through the hadronic interaction between cosmic rays in the SNR and molecular nuclei. On the other hand, the emission is 0.44° away from the position of a pulsar PSR J2229+6114 located at the northeast edge of the SNR radio emission (marked as a diamond in Fig.5). High-energy electrons provided by the pulsar or its surrounding nebula are not plausible origin of the gamma-ray emission. From a spectral fitting with a hadronic model shown in Fig.6, the cut off energy, E_{cut}, of the parent particles defined as $dN/dE \propto E^\alpha exp(-E/E_{cut})$ is 0.5 PeV. This indicates G106+2.7 was a PeV cosmic-ray accelerator in its early phase at $\tau \sim$1,000 years old.

Gamma-ray Detection from the Cygnus OB Associations

Cygnus is another interesting complex region to study the high-energy gamma-ray emissions. The Tibet experiment reported detection of two gamma-ray sources above 10 TeV at the pretrial (post-trial) statistical significances of 5.3 (4.7)σ and 6.7 (6.2)σ from the directions of the Cygnus OB2 and OB1 associations, respectively [16]. Fig.7 (a) and (b) show the significance maps of the Cygnus OB2 and OB1 regions, respectively. Position of the emission from the OB2 region is consistent with the position of the pulsar PSR J2032+4127. On the other hand the pulsar PSR J2021+3651 is located at 0.23° east of the center of the Tibet source at the OB1 re-

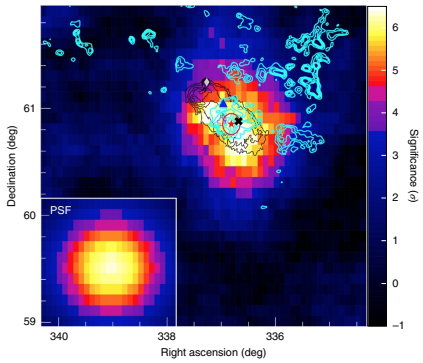

Fig. 5. Color map shows the excess significance around SNR G106.3+2.7 observed by the Tibet experiment. The red star with a 1σ statistical position error circle is the centroid of gamma-ray emission. The magenta open cross, the black X mark and the blue triangle are the centroids determined by VERITAS, Fermi and HAWC, respectively. The black and cyan contours indicate 1,420 MHz and ^{12}CO radio emissions, respectively. The grey diamond at the northeast corner of the radio emission marks the pulsar PSR J2229+6114. [15]

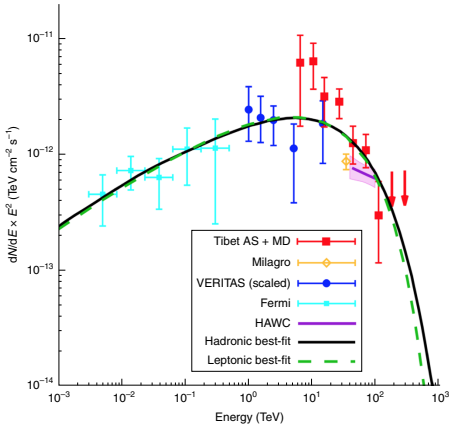

Fig. 6. Energy spectra of SNR G106.3+2.7. Red points are the fluxes determined by the Tibet experiment[15].

gion. Assuming a pulsar velocity of 420 km/s, the 10 TeV emission detected by the Tibet experiment can be interpreted as an emission at the birthplace of the pulsar 17 kyr ago.

First Detection of Galactic Diffuse Gamma Rays in Sub-PeV Energy

Analysis of the galactic diffuse gamma-rays in the sub-PeV region was performed by introducing a tighter event selection than the analysis of individual source and by masking the region around the known TeV sources [17]. Fig.8 shows the distributions of gamma-ray like events after the tight event selection in the energy bands (a) 100<E (TeV)<158, (b) 158<E (TeV)<398, and (c) 398<E (TeV)<1000 in the equatorial coordinates. The black solid lines indicate the galactic plane. Concentration of events along the galactic plane is visibly identified and according to the statistical significances, 6.6σ, 5.1σ and 5.9σ in the three energy bands, respectively, the first detection of galactic diffuse gamma-ray emissions at sub-PeV energy range is established. This is confirmed in Fig.9 showing the distributions of events as a function of the

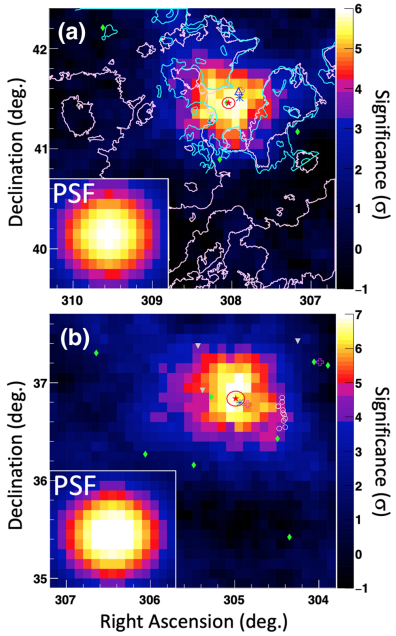

Fig. 7. Significance maps of (a) Cygnus OB2 and (B) Cygnus OB1 regions [16]. The red star with a circle indicates the center of the Tibet detection with its error. The green diamond in the error circle of (a) is PSR J2032+4127. The green diamond 0.23° east of the Tibet source is PSR J2021+3651.

galactic latitude together with the model prediction of diffuse gamma-ray emission shown by the grey histograms. Fig.10 shows the energy spectra in two different ranges of galactic longitude. The results of the Tibet experiment indicated by the red points are consistent with the model prediction by Lipari and Vernetto (PRD 98, 043003 (2018)) shown by the solid and dashed lines. This observation supports that the parent cosmic-ray particles with PeV energy have their origins in our galaxy.

A naive question to the discovery of the diffuse gamma rays is "how much fraction can be explained by the uncovered dark individual sources?" As the LHAASO collaboration published their first source catalog in 2024 (Cao et al., ApJS, 271, 25(2024)) with a higher sensitivity than the Tibet experiment, we tried to answer this question [9]. As shown in Fig.11, no Tibet diffuse event was located in the extension of the LHAASO sources. This supports the Tibet diffuse events are dominated by the real diffuse events. Zero association is not surprising when we consider either a chance probability (0.86 events expected) or the extrapolation of the flux of the LHAASO sources (1.2 events expected).

First Spectrum Measurement of HESS J1843-033 beyond 100 TeV

A detection of gamma-ray emission from the direction of HESS J1843-033 was reported with a statistical significance of 6.2σ above 25 TeV [13]. As shown in Fig.12, the Tibet experiment measured the flux above 100 TeV for the first time and determined the cut off energy of gamma-rays to be 49.5±9.0 TeV. A morphological study gives an extension of the source, which is larger than the PSF of the experiment, to be 0.34°±0.12°. The energy spectrum and the morphology

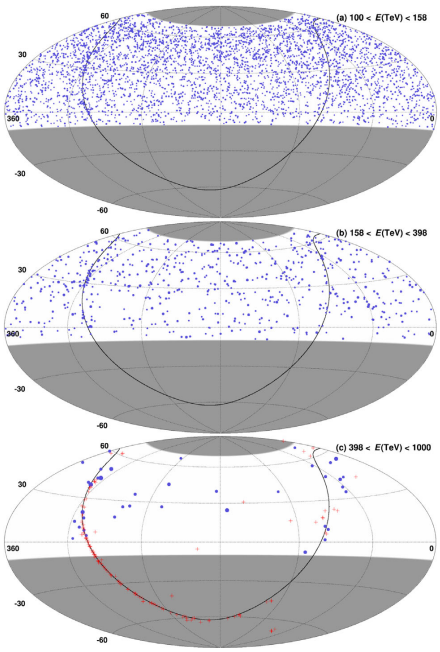

Fig. 8. Distributions of gamma-ray like events in the three energy bands in the equatorial coordinates [17].

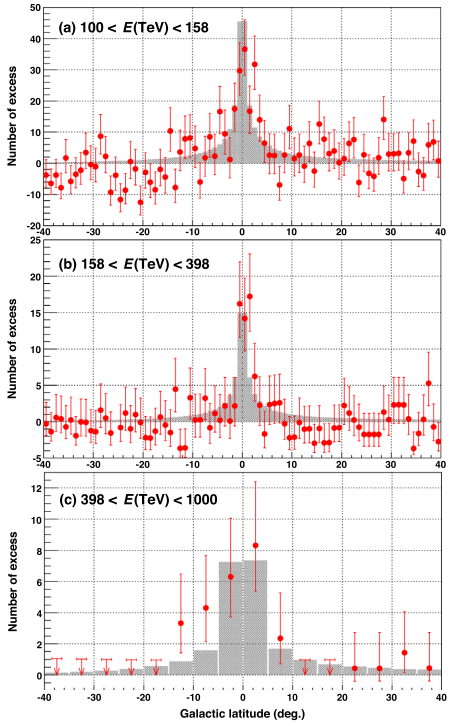

Fig. 9. Gamma-ray like event distributions as a function of the galactic latitude in the three energy bands. The grey histograms indicate the model predictions of the diffuse gamma ray emission [17].

can be explained by both hadronic and leptonic scenarios. In case of the hadronic scenario, a possible source is a nearby supernova remnant G28.6-0.1. The system resembles to the case of SNR G106.3+2.7. In case of the leptonic scenario, a possible source is a pulsar wind nebula associated with the pulsar PSR J1844-0346.

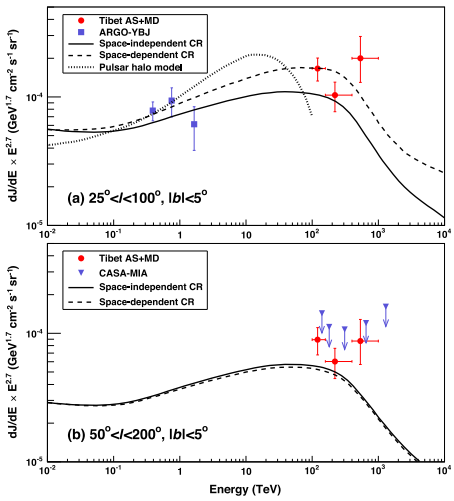

Fig. 10. Energy spectra of diffuse gamma rays in the two regions of galactic longitude [17].

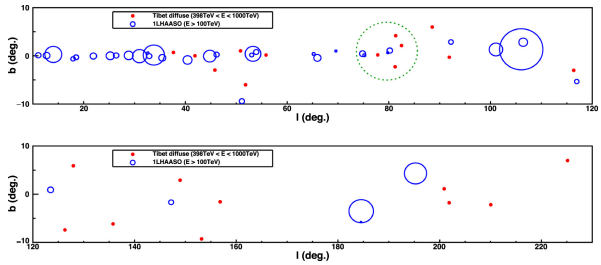

Fig. 11. Distribution of the Tibet diffuse events in the red plots and the LHAASO source extension in the blue circles [9].

A New Candidate of PeV Accelerator HESS J1849-000

Gamma-ray emissions from the direction of HESS J1849-000 were detected with statistical significances of 4.0σ and 4.4σ above 25 TeV and 100 TeV, respectively [12]. The significance map in Fig.13 shows excellent positional agreements with HESS J1849 and PSR J1849-0001, indicating the leptonic origin of the gamma-ray emission. At the same time another good overlap with a molecular cloud found in the ^{12}CO (J=1-0) line emission (green contours) suggests a hadronic origin. Energy spectrum is well fitted by both hadronic and leptonic models. The cut off energy of the parent protons in the hadronic model, $log_{10}(E_{cut,p}/TeV)$=3.73$^{+0.09}_{-0.66}$, suggests this source as a candidate of PeV CR accelerating object.

Ongoing Activities

Analysis of Energy Spectrum of Protons

A sensitivity to analyze the proton spectrum using the muon detectors was studied based on the Monte Carlo simulations [14]. Fig.14 shows the distributions of ΣN_μ in proton-induced showers (red) and iron-induced showers (blue) in a certain range of the shower size ($\Sigma\rho$). The idea is to extract high purity proton samples using the events in the small ΣN_μ side. For various combinations of primary composition model and hadronic interaction model in air shower simulations to determine the response function, the reconstructed proton spectra are shown in Fig.15 The test shower dataset was produced using the SIBYLL/FLUKA models in COR-

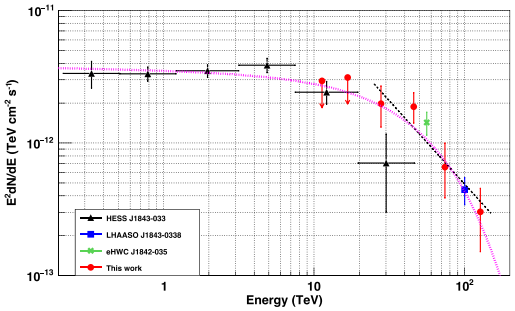

Fig. 12. Energy spectra of the source near HESS J1843-033. The red points are the results obtained by the Tibet experiment [13].

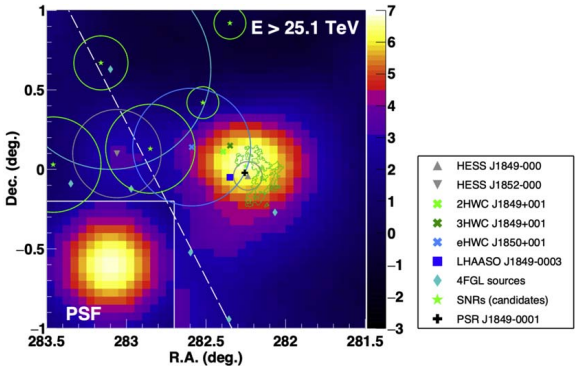

Fig. 13. Significance map around HESS J1849-000 (grey circle) above 25 TeV. The green contours indicate the position of a molecular cloud. [12].

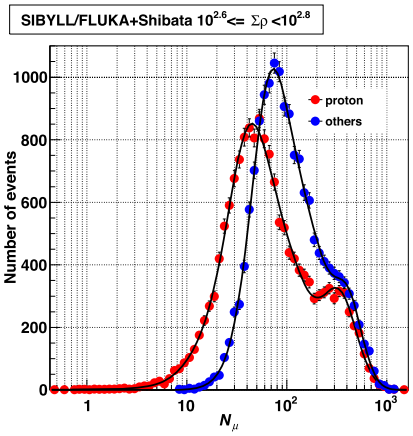

Fig. 14. Distributions of ΣN_μ for proton-induced showers (red) and iron-induced showers (blue) in the shower size range of $10^{2.6} <= \Sigma\rho < 10^{2.8}$ [14].

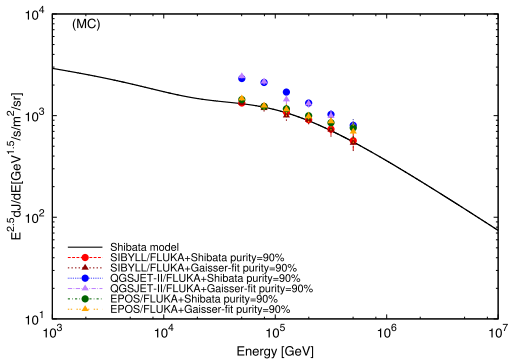

Fig. 15. Reconstructed proton energy spectra using response functions based on the various combinations of models. The black solid line is the injection spectrum [14].

SIKA following the primary spectrum of the Shibata model (Shibata et al., ApJ, 716, 1076 (2010)) shown in the black solid line. The spectrum given by the response function using the same models (red points) reproduces the injection spectrum perfectly. The variation of the results amounts to $\pm 37\%$, which is mostly dominated by the contribution from the choice of the hadronic interaction model, and it is thought to be the systematic uncertainty of this method. Analysis using the experimental data is on going [22].

Gamma-ray Shower Identification by using Neural Network

To search for gamma-ray signals in the large archival data of the Tibet experiment obtained before the operation of the MDs, new analysis technique of the surface array data by using neural network was studied [10]. Before introducing neural network, some variables characterizing the lateral distribution and uniformity were defined and their power to separate proton showers and gamma-ray showers was studied. It is found that a simple parameter $R = (\Sigma_i \rho_i \times r_i)/\Sigma_i \rho_i$ gives the best separation power among the parameters tested and it is considered to be a benchmark of the conventional analysis. Analyses using the multilayer perceptron (MLP) neural network and the convolutional neural network (CNN) were tested and compared. In MLP and CNN analyses, the parameters defined above and the matrix of the surface detector array filled with the number of detected particles, respectively, were used for the input. Fig.16 shows the distributions of the gamma-ray likeness parameter, P_γ, given by CNN. Primary energies of gamma rays (100 TeV) and protons (165 TeV) are chosen to give a similar shower size $\Sigma\rho$ at the Tibet altitude. Fig.17 shows the receiver operating characteristic (ROC) curves defined as a relation between true positive rate and false positive rate after the event identification. The fact that the ROC curve of CNN (red curve) is closer to the left top corner than the other curves (blue for MLP and black for the R parameter) means CNN gives the best gamma-ray selection power. By applying the CNN technique to the data of the Tibet air shower array (without MDs), the statistical significance of the gamma-ray detection from the Crab nebula will increase by a factor of 1.3 at 11.4 TeV and 1.8 at 115 TeV. A verification using the experimental data with MDs and application to the archival data are on going.

Anisotropy of TeV Cosmic Rays Outside of the Heliosphere

Anisotropy of TeV cosmic rays with an amplitude of $\sim 0.1\%$ is known but its origin is yet to be understood. A study to resolve the deflection of CR trajectories by the magnetic field inside the heliosphere and to reconstruct the anisotropy in the inter-stellar space is on going [19][27]. The CR intensities at the earth are mapped to the outside of the heliosphere through back-trajectory calculations in an MHD model helio-

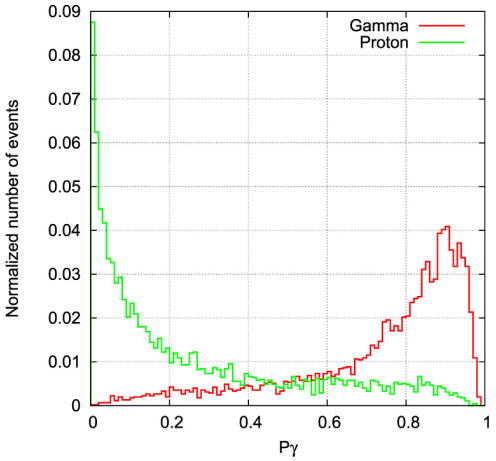

Fig. 16. Distributions of gamma-ray likeness parameter P_γ given by CNN for 100 TeV gamma-ray showers (red) and 165 TeV proton showers (green). [10].

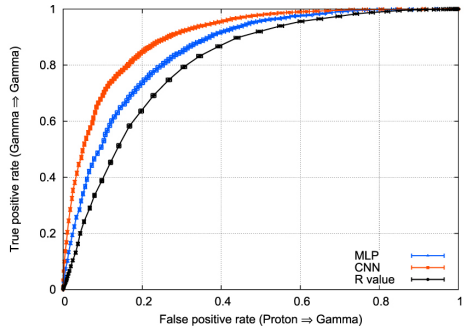

Fig. 17. ROC curves of the conventional parameter analysis (black), MLP (blue) and CNN (red) for gamma/proton separation [10].

sphere. The mass dependent spectra of CRs are taken into account, which means that the trajectories are correctly calculated according to the rigidity of each particle. The direction of the obtained anisotropy in the interstellar space is discussed with respect to the directions of the local interstellar magnetic field and nearby possible CR accelerators such as Vela and Geminga.

Long-Duration Monitoring of Thundercloud-Induced Bursts

A neutron monitor NM64 has been operating as a part of the Tibet air shower array. Bursts in the counting rate with time scales of 10-40 minutes, associated with the passages of thunderclouds identified by the electric field strength measured on site, were searched in the data from 1998 to 2017 [11]. Because it is known that the NM has a sensitivity to gamma rays above 7 MeV through a reaction of $\gamma + {}^{A}\mathrm{Pb} \rightarrow n + {}^{A-1}\mathrm{Pb}$, the events are assumed to be produced as a result of electron acceleration in the electric field and their radiations. Through a systematic search of the burst events, the distribution of the event duration, dependencies on the local time and the season are clearly detected. Finally a long-term variation of the event occurrence rate is compared with the solar activity (sunspot number) and the cosmic-ray flux as shown in Fig.18. We found a periodicity of 16.4 ± 1.7 yrs, but it does not coincide with the cycles and phases of the solar and

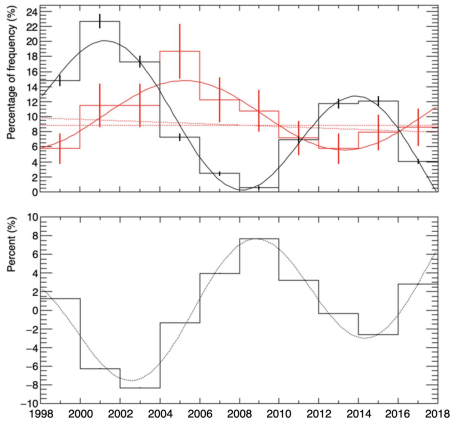

Fig. 18. (Top) Relative occurrence rate of the NM bursts (red), the sunspot number (black) and (Bottom) the cosmic-ray flux as a function of year. [11].

CR variations. The nature of this long-term variation is still an open question.

THE TIBET ASγ COLLABORATION

Institute	Country	(*)
ICRR, Univ. of Tokyo	Japan	11
China Meteorological Administration	China	1
China Univ. of Petroleum	China	1
Hebei Nornal Univ.	China	2
Hirosaki Univ.	Japan	2
Institute of High Energy Physics	China	31
Japan Atomic Energy Agency	Japan	1
Kanagawa Univ.	Japan	4
Konan Univ.	Japan	1
Nagano Prefectural Institute of Technology	Japan	1
Nanjing University	China	3
National Astronomical Observatories	China	11
National Institute of Informatics	Japan	1
National Institute of Information and Communications Technology	Japan	1
Nihon Univ.	Japan	2
Purple Mountain Observatory	China	1
Research Organization of Information and Systems	Japan	1
Shandon Arigiculture Univ.	China	1
Shandong Univ.	China	3
Shandong Management Univ.	China	1
Shibaura Institute of Technology	Japan	1
Shinshu Univ.	Japan	5
Shonan Institute of Technology	Japan	1
SouthWest Jiaotong Univ.	China	5
Tibet Univ.	China	16
Tokyo Metropolitan College of Industrial Technology	Japan	1
University of Science and Technology of China	China	1
Utsunomiya Univ.	Japan	1
Waseda Univ.	Japan	1
Yokohama National Univ.	Japan	8
Total		120

(*) Number of participants as of August 2024.

Members

Staff

Masato Takita, Associate Professor (February 2001 to November 2016), Professor (November 2016 to the present)
Takashi Sako, Associate Professer (TA/Tibet, October 2017 to the present)
Munehiro Ohnishi, Assistant Professor (April 1993 to the present)
Kazumasa Kawata, Specially Appointed Assistant Professor (April 2013 to March 2018), Assistant Professor (Tibet/TA, April 2018 to August 2024), Associate Professer (Tibet/TA, September 2024 to the present)

Postdoctoral Fellows

Takashi Sako (April 2010 to March 2017 and from June 2018 to March 2024)
Sei Kato (April 2023 to the present)

Graduate Students

One graduate student obtained PhD degree [4] during 2018–2024, supervised by ICRR staff members.

Bibliography

Before Year 2018

Papers in Refereed Journals

[1] "Exploration of a 100 TeV gamma-ray northern sky using the Tibet air-shower array combined with an underground water-Cherenkov muon-detector array", T.K. Sako, K. Kawata, M. Ohnishi, A. Shiomi, M. Takita, H. Tsuchiya, Astropart. Phys., **32** , 177-184 (2009).

[2] "Search for Gamma Rays above 100 TeV from the Crab Nebula with the Tibet Air Shower Array and the 100 m^2 Muon Detector", M. Amenomori *et al.* (The Tibet ASγ Collaboration), Astrophys. J., **813** , 98 (2015).

[3] "Energy Determination of Gamma-Ray Induced Air Showers Observed by An Extensive Air Shower Array", K. Kawata *et al.*, Experimental Astronomy, **44** , 1-9 (2017).

After Year 2018

Invited Articles

[4] "Gamma Rays in the 100 TeV Region from Potential Galactic PeVatron Candidates", Sei Kato, Series: Springer Theses, ISBN: 9789819716425 (2024).

[5] "Galaxy's Gamma Glow Illuminates Cosmic-Ray Origins", Kazumasa Kawata, Physics, **16**, 169 (2023).

[6] "Detection of the Highest Energy Cosmic Gamma Ray — Approaching the Acceleration Limit of Galactic Cosmic Rays", K. Kawata, M. Ohnishi, T. K. Sako, and M. Takita, Journal of the Physical Society of Japan, **77**, 155 (2022).

[7] "Approaching the elucidation of the origin of galactic cosmic rays", Masato Takita, Kagaku, **9**, (2022).

[8] "Observation of Very-High-Energy Cosmic Rays with the Tibet Air Shower Experiment - Quest for the Galactic Cosmic Ray Origin", Kazumasa Kawata, RADIOISOTOPES, **68**, 829 (2019)

Papers in Refereed Journals

[9] "On the Source Contribution to the Galactic Diffuse Gamma Rays above 398 TeV Detected by the Tibet ASγ Experiment", S. Kato *et al.*, Astrophys. J. Lett., **961** , 1, L13 (2024).

[10] "Neural networks for separation of cosmic gamma rays and hadronic cosmic rays in air shower observation with a large area surface detector array", S. Okukawa *et al.*, Machine Learning : Science and Technology, **5** , 2, 025016 (2024).

[11] "Characteristics of temporal variability of long-duration bursts of high-energy radiation associated with thunderclouds on the Tibetan plateau", H. Tsuchiya *et al.*, Progress in Earth and Planetary Science, **11**, 26 (2024).

[12] "Observation of Gamma Rays up to 320 TeV from the Middle-aged TeV Pulsar Wind Nebula HESS J1849–000", M. Amenomori *et al.* (The Tibet ASγ Collaboration), Astrophys. J., **954** , 2, 200 (2023).

[13] "Measurement of the Gamma-Ray Energy Spectrum beyond 100 TeV from the HESS J1843–033 Region", M. Amenomori *et al.* (The Tibet ASγ Collaboration), Astrophys. J., **932** , 2, 120 (2022).

[14] "Sensitivity of the large muon detector with the Tibet air-shower array to measure the primary proton spectrum between 40 and 630 TeV", D. Kurashige *et al.*, Prog. Theor. Exp. Phys., **2022** , 9, 093F01 (2022).

[15] "Potential PeVatron supernova remnant G106.3+2.7 seen in the highest-energy gamma rays", M. Amenomori *et al.* (The Tibet ASγ Collaboration), Nature Astronomy, **5** , 460-465 (2021).

[16] "Gamma-Ray Observation of the Cygnus Region in the 100-TeV Energy Region", M. Amenomori *et al.* (The Tibet ASγ Collaboration), Phys. Rev. Lett., **127** , 3, 031102 (2021).

[17] "First Detection of sub-PeV Diffuse Gamma Rays from the Galactic Disk: Evidence for Ubiquitous Galactic Cosmic Rays beyond PeV Energies", M. Amenomori *et al.* (The Tibet ASγ Collaboration), Phys. Rev. Lett., **126** , 14, 141101 (2021).

[18] "First Detection of Photons with Energy beyond 100 TeV from an Astrophysical Source", M. Amenomori *et al.* (The Tibet ASγ Collaboration), Phys. Rev. Lett., **125** , 5, 051101 (2019).

Papers in International Conference Proceedings

[19] "Modeling of TeV Galactic Cosmic-ray Anisotropy based on Intensity Mapping in an MHD Model Heliosphere", M. Amenomori et al., J. Phys.: Conf. Ser. 2742, 012014 (2024).

[20] "Highlights from the Tibet ASγ experiment", M. Takita for the Tibet ASγ Collaboration, PoS(ICRC2023)213.

[21] "Observation of gamma rays from the northern celestial sky up to the sub-PeV range with the Tibet air shower array and its underground muon detector array", S. Kato for the Tibet ASγ Collaboration, PoS(ICRC2023)627.

[22] "Measurement of the primary cosmic-ray proton spectrum between 40 TeV and a few hundred TeV with the Tibet hybrid experiment (Tibet-III + MD)", Y. Katayose for the Tibet ASγ Collaboration, PoS(ICRC2023)301.

[23] "Study of muons from high energy cosmic ray air showers measured with the Tibet hybrid experiment (YAC-II + Tibet-III + MD)", J. Huang for the Tibet ASγ Collaboration, PoS(ICRC2023)508.

[24] "Versatile Trigger Time Recording System for Air Shower Array", M. Ohnishi, T. Ohura and Y. Katayose, PoS(ICRC2023)477.

[25] "Study of water Cherenkov detector designs to determine air shower arrival directions with accuracy", A. Shiomi et al., PoS(ICRC2023)475.

[26] "Unveiling the molecular environment of the enigmatic PeVatron candidate LHAASO J2108+5157", I. Toledano–Juárez et al., PoS(ICRC2023)809.

[27] "Modeling of the galactic cosmic-ray anisotropy at TeV energies using an intensity-mapping method in an MHD model heliosphere", T.K. Sako for the Tibet ASγ Collaboration, and N.V. Pogorelov, PoS(ICRC2023)1238.

[28] "Neural Networks for Gamma Ray/Cosmic Ray Separation in Air Shower Observation with a Large Area Surface Scintillation Detector Array", S. Okukawa et al., PoS(ICRC2023)786.

[29] "Highlights from Gamma-ray Observation by the Tibet ASγ Experiment", M. Takita for the Tibet ASγ Collaboration, PoS(ICRC2021)015.

[30] "Sensitivity of the Tibet hybrid experiment (Tibet-III + MD) for primary proton spectrum between 30 TeV and a few hundreds of TeV's", D. Kurashige et al., PoS(ICRC2021)205.

[31] "Observation of Ultra-High-Energy Diffuse Gamma Rays from the Galactic Plane with the Tibet Air Shower Array", K. Kawata for the Tibet ASγ Collaboration, PoS(ICRC2021)795.

[32] "Gamma-ray Observation of the Cygnus Region with the Tibet Air Shower Array", Y. Katayose and T.K. Sako for the Tibet ASγ Collaboration, PoS(ICRC2021)799.

[33] "A northern sky survey for ultra-high-energy gamma-ray source using the Tibet air-shower array and muon-detector array", Xu Chen for the Tibet ASγ Collaboration, PoS(ICRC2021)880.

[34] "Gamma-ray Observation of SNR G106.3+2.7 with the Tibet Air Shower Array", M. Ohnishi for the Tibet ASγ Collaboration, PoS(ICRC2021)882.

[35] "Modeling of the TeV cosmic-ray anisotropy based on intensity mapping in an MHD-simulated heliosphere", T.K. Sako for the Tibet ASγ Collaboration and N.V. Pogorelov, PoS(ICRC2021)1286.

[36] "Primary cosmic-ray spectra and composition in the energy range from 50 TeV to 10^{16} eV observed with the new Tibet hybrid experiment", M. Amenomori et al. (The Tibet ASγ Collaboration), PoS(ICRC2019)288.

[37] "The anisotropy of cosmic rays observed by the Tibet air shower array and muon detector array", M. Amenomonori et al. (The Tibet ASγ Collaboration), PoS(ICRC2019)365.

[38] "Hadronic interactions and EAS muon multiplicity investigated with the new Tibet hybrid experimental muon data", M. Amenomori et al. (The Tibet ASγ Collaboration), PoS(ICRC2019)487.

[39] "Large-scale Cosmic Ray Anisotropy with Tibet air shower array", M. Amenomori et al. (The Tibet ASγ Collaboration), PoS(ICRC2019)488.

[40] "Test of hadronic interaction models in the forward region from 10 TeV to 1 PeV with the new Tibet EAS core data", M. Amenomori et al. (The Tibet ASγ Collaboration), PoS(ICRC2019)491.

[41] "A Northern Sky Survey for 100 TeV γ-ray Source Using the Tibet Air Shower Array and Muon Detector Array", M. Amenomori et al. (The Tibet ASγ Collaboration), PoS(ICRC2019)647.

[42] "On the spectrum of gamma-rays ranging from multi TeV to sub PeV emitted from the MGRO J1908+06 observed by the Tibet-AS+MD array", M. Amenomori et al. (The Tibet ASγ Collaboration), PoS(ICRC2019)648.

[43] "Search for pulsed gamma-ray emission in the 100 TeV region from several pulsars with the Tibet AS+MD array", M. Amenomori et al. (The Tibet ASγ Collaboration), PoS(ICRC2019)695.

[44] "Extended Gamma-Ray Emission beyond 10 TeV from Geminga with the Tibet AS+MD array", M. Amenomori et al. (The Tibet ASγ Collaboration), PoS(ICRC2019)710.

[45] "100 TeV Gamma-Ray Observation of the Crab Nebula with the Tibet Air Shower Array", M. Amenomori et al. (The Tibet ASγ Collaboration), PoS(ICRC2019)712.

[46] "Observation of Gamma-ray Emission Above 10 TeV from the Super Nova Remnant G106.3+2.7 with the Tibet Air Shower Array and the Muon Detector Array", M. Amenomori et al. (The Tibet ASγ Collaboration), PoS(ICRC2019)778.

[47] "Can we estimate the variation of the z-component of the interplanetary magnetic field from the sun shadow?", M. Amenomori et al. (The Tibet ASγ Collaboration), PoS(ICRC2019)1132.

[48] "Modeling of the Anisotropy of Galactic Cosmic Rays in an MHD-simulated Heliosphere", M. Amenomori et al. (The Tibet ASγ Collaboration), PoS(ICRC2019)1146.

ALPACA

Introduction

We have started up the Andes Large area PArticle detector for Cosmic ray physics and Astronomy (ALPACA) project to observe sub-PeV gamma rays and TeV to PeV cosmic rays for the first time in the southern hemisphere. The ALPACA experiment is composed of an 82,800 m^2 air shower array and a 3,600 m^2 underground muon detector array to make wide field-of-view high-sensitivity observation of high-energy cosmic rays/cosmic gamma rays at the plateau of 4,740 m altitude above sea level near the Mount Chacaltaya, Bolivia.

Summary from 2018 to 2024

- Construction of a quarter size array, ALPAQUITA, started. The surface array is running continuously since April 2023. The design of the underground muon detector unit was completed and the construction of the first unit will start in 2024 (as of August 2024).
- The analyses of the even-odd method and the shadow of the moon confirmed that the ALPAQUITA surface array is running with expected performance. A detection of a Forbush Decrease event occurred in May 2024 demonstrated a unique potential of ALPAQUITA for solar and heliospheric science.
- The sensitivity of ALPAQUITA with a muon detector unit was studied. It is found that the extrapolated fluxes of some known TeV sources in the southern hemisphere are above the 5σ sensitivity of an ALPAQUITA 1 yr observation. Uncertainty in the gamma-ray detection efficiency, hence the flux determination, due to the choice of hadronic interaction model was studied and concluded to be $\pm 3.6\%$ at maximum.
- A new version of PMT voltage divider was developed to maintain a wide dynamic range with a single PMT instead of using two PMTs. A general purpose GPS timing module was developed and implemented in the ALPAQUITA data taking system. New front-end and back-end electronics are under development for future further extension of the ALPACA array.
- Case studies to correlate sub-PeV gamma-ray observations and molecular cloud detected by CO line emissions were performed using the objects in the northern hemisphere. The knowledge will be applied in the data analysis of ALPACA and southern radio telescopes such as NANTEN and ASTE.
- As a new project of the community, the scientific goals and feasibility of ALPACA have been discussed in the Cosmic Ray Researchers Congress (CRC) of Japan. In 2018, CRC expressed a recognition of the value of ALPACA and an endorsement of a prompt realization of the project.

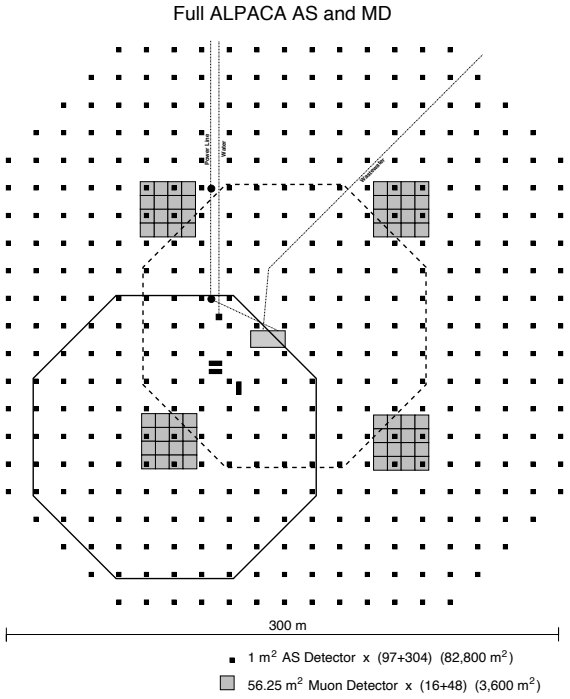

Fig. 1. Schematic view of the ALPACA experiment. The small black squares indicate 401 1 m^2 plastic scintillation detectors, forming an air shower array with 82,800 m^2 in area. The grey rectangles indicate four underground muon detector units, each of which contains sixteen 56 m^2 muon detector cells. The total area of the underground muon detector array is 3,600 m^2.

Experiment

Design of ALPACA

ALPACA is under construction near the Chacaltaya mountain at an altitude of 4,740 m above sea level in Bolivia (68°08' W, 16°23' S). As shown in Fig.1, total 401 plastic scintillating counters of 1 m^2 (5 cm thickness) aligned with a 15 m interval cover the 82,800 m^2 ground area compose a surface detector air shower array (black small squares in Fig.1). Using the signal size and timing measured by the surface array, energy of the primary particle and arrival direction, respectively, are determined. The angular and energy resolutions are 0.2° and 20%, respectively, for 100 TeV gamma-ray showers. In addition to this conventional surface array, four underground water Cherenkov muon detector (MD) units are constructed below 2 m soil overburden (grey hatched area in Fig.1). Each MD unit is composed of 16 cells, where a single cell has a 7.5 m×7.5 m area filled with clean water of 1.5 m depth and monitored by a 20" PMT. Because of the soil layer, most of the electromagnetic particles are absorbed and only muons above 1 GeV can be detected. Using this high-purity muon signal, mu-poor electromagnetic showers produced by gamma-ray primaries are selected from the sea of mu-rich isotropic hadronic showers to achieve a necessary sensitivity to detect gamma-ray sources. This technique was first pro-

Fig. 2. Photo of the ALPAQUITA array. The mountain behind the array is Chacartaya.

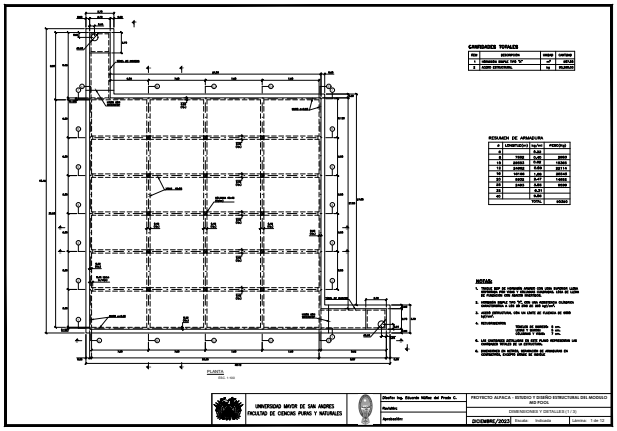

Fig. 3. A part of the final MD design.

posed and established by the TibetASγ collaboration (Tibet ASγ Collaboration, ApJ, 813:98 (2015), Sako, T. K et al., Astropart.Phys., 32, 177-184 (2009), Tibet ASγ Collaboration, PRL, 123, 051101 (2009)).

ALPAQUITA Prototype

For the first step a small array covering a quarter of the full ALPACA array, named ALPAQUITA, is in operation. The construction of 97 surface detectors enclosed by the dashed octagon line at the center of Fig.1 was completed in September 2022. After a half year of test operation and an initial maintenance in March 2023, the array has been continuously observing air shower events since April 2023. The performance of the array obtained from the experimental data analyses is summarized later. A photograph of the ALPAQUITA array is shown in Fig.2. The central hut with the red roof housing the data acquisition room, engineering workshop, kitchen, dining, bathroom and bedroom is found at the center of the array. Electrical power line is also identified in the photo.

A muon detector unit is a concrete structure of 30 m$\times$30 m$\times$4.7 m dimensions buried underground. The design has been discussed with the Bolivian construction companies and finalized in May 2024. A part of the design drawing is shown in Fig.3. In 2024 the construction of the first MD unit at the left bottom side in Fig.1 will start. After the construction of the first MD unit, seventy more surface detectors will be installed to surround the MD as shown by the solid octagon line at the left bottom side of Fig.1. The new array with an MD unit at the center is called ALPAQUITA+MD and will start first gamma-ray sensitive observation.

ALPAQUITA Status and Performance Studies

ALPAQUITA Sensitivity

When the design of ALPAQUITA was defined as the first step of the ALPACA construction, the sensitivity of ALPAQUITA (with an MD unit, hereafter) for gamma-ray source detection was studied with Monte Carlo simulation [6]. Fig.4 shows the 5σ detection sensitivity with a 1-year observation. The black (purple) solid curve is the result obtained for ALPAQUITA (ALPACA). The thin lines indicate the energy spectra known in the field of view of ALPACA mostly reported by H.E.S.S. Cherenkov telescope in the TeV range. The spectra in the measured energy range are drawn with the solid lines while the extrapolations to higher energy are drawn with the dashed lines. It is seen that the existing measurements terminate at a few 10's TeV at maximum while the ALPAQUITA and ALPACA can cover the energy range above. ALPAQUITA is expected to detect about 5 known gamma-ray sources within one year of operation. As the extrapolated flux of a mysterious source HESS J1702-420, for which H.E.S.S. reported a hard energy spectrum (H.E.S.S. Collaboration, A&A 653, A152(2021)), is located above the sensitivity of ALPAQUITA, it becomes one of the interesting initial targets.

To calculate the fluxes of the gamma rays the detection efficiency must be estimated by means of Monte Carlo simulation. Because an incident gamma-ray produces an electromagnetic cascade shower in the atmosphere, uncertainty of the simulation is usually ignored. However, ALPAQUITA and ALPACA rely on the number of muons for gamma/hadron separation, hence the uncertainty in the muon production through the photo-nuclear interaction is an issue to be discussed. A simulation study to estimate the dependence of the hadronic interaction models in the calculation of the gamma-ray detection efficiency was performed [1]. Fig.5 shows the gamma-ray survival efficiencies through all processes including air shower development, trigger and analysis of ALPAQUITA for various combinations of hadronic interaction models as a function of the reconstructed shower size, $\Sigma\rho$. The deviation from a benchmark model combination (QGSJET-II + FLUKA) in the bottom panel amounting to $\pm$3.6% is considered as the uncertainty of the flux determination due to the hadronic interaction.

ALPAQUITA Observations

The ALPAQUITA surface array has been in stable operation since April 2023. Here some analysis results from the initial data are presented [7][12][13][14][16]. A graphical display of an air shower event detected by ALPAQUITA is shown in Fig.6. Small dots indicate the positions of the scintillating counters and colored circles show the counters with particle signal. The circle size and color correspond to the signal

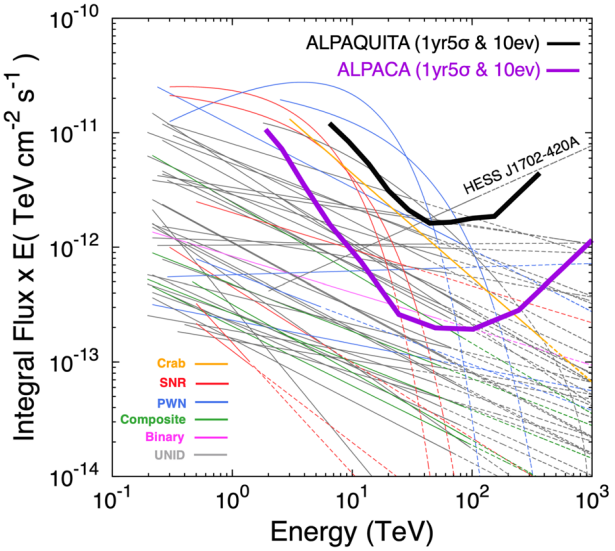

Fig. 4. Sensitivity of ALPAQUITA (thick black line) and ALPACA (thick purple line) for high-energy gamma-ray source detection. Thin curves are energy spectra of known gamma-ray sources in the field of view of ALPACA. Solid lines cover the energy range measured by the former experiments while the dotted lines are extrapolation. The different colors indicate the different categories of astrophysical objects as indicated in the figure. Crab is an object in the northern hemisphere, but shown here as a reference. UNID (unidentified) means the gamma-ray sources which have no or unclear associated objects in the other wavelengths. [6].

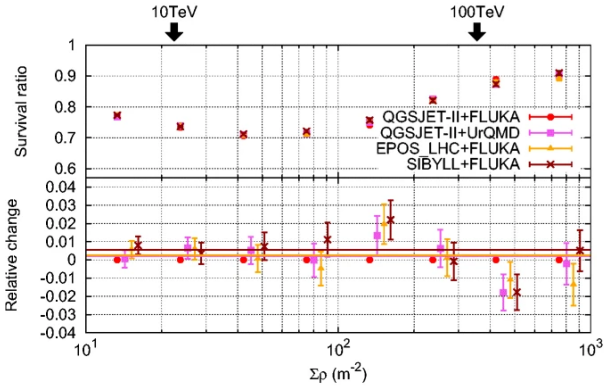

Fig. 5. Interaction model dependence in the gamma-ray survival efficiency through the chain of detection and analysis. Top panel shows the efficiency as a function of shower size ($\Sigma\rho$) and the bottom panel shows the ratio to a benchmark model [1].

size and the relative timing of the particle arrival, respectively. This event corresponds to a CR shower of $\sim$100 TeV.

Data-Driven Angular Resolution Estimate: To estimate the angular resolution of the array in a data-driven way, a traditional 'even-odd method' was applied. The counters were alternately divided into two groups, namely in the even array and the odd array, to compose two identical and independent air shower arrays. The arrival directions were independently reconstructed by two arrays and their angular difference was evaluated in each event. Fig.7 shows the distributions of the opening angles for the experimental data (blue crosses) and the Monte Carlo simulation (green crosses). A good agreement between the experimental data and Monte Carlo is seen. The median values, $1.95^\circ \pm 0.01^\circ$ and $1.76^\circ \pm 0.03^\circ$ for experiment and Monte Carlo, respectively, are related to the angular resolution of the array, but are degraded because of a division of the array into half (a factor $\sqrt{2}$) and a calculation of the difference between two measurements (another factor $\sqrt{2}$). Consequently, a good measure of the angular resolution of the ALPAQUITA array is half of the median value, $\sim 1^\circ$. Note that this result corresponds to the angular resolution of cosmic-ray showers at the mode energy of several TeV.

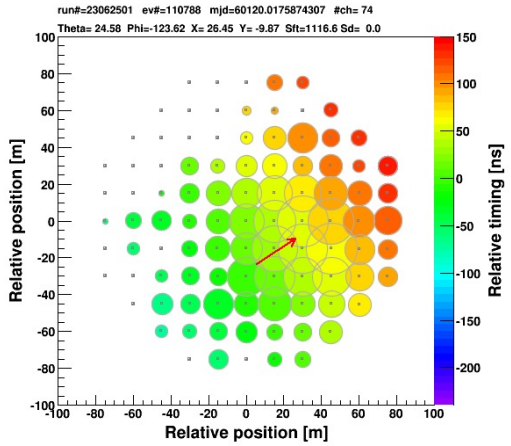

Fig. 6. Graphical display of an event observed by the ALPAQUITA surface array. The size of the circle and the color indicate the number of detected particles and relative signal timing, respectively, in each scintillating detector. The position and direction of the arrow show the reconstructed core position and direction, respectively, of the shower.

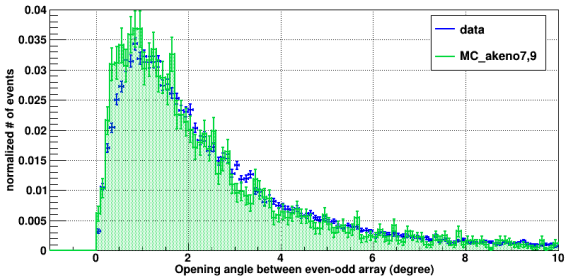

Fig. 7. Distributions of the angular difference between the reconstructed directions by two divided arrays. Blue (green) points are results of the experimental (Monte Carlo) data.

Shadow of the Moon: Another test of performance using the observed data is to study the intensity around the direction of the moon. As the trajectory of the primary cosmic rays is blocked by the moon with an angular diameter of 0.5°, the intensity of cosmic rays is expected to drop around the moon. This is know as 'Shadow of the Moon.' Fig.8 shows the CR intensity around the moon obderved by the ALPAQUITA surface array. A clear deficit of the intensity expressed in blue color centered at the direction of the moon shown by the yellow circle is observed. The evolution of the deficit depth as a function of the cumulative number of background events is shown in Fig.9. Here the horizontal axis can be proportional to the effective observation time. We can find a constant evolution of the deficit, which amounts to the 8σ statistical significance as of June 2024. The black dotted line indicates the expectation in case of the angular resolution of 1°. A good agreement between the measurement and the expectation sup-

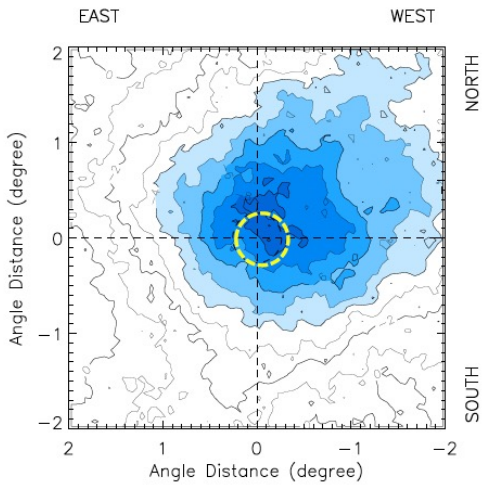

Fig. 8. Cosmic-ray intensity around the direction of the moon indicated by the yellow circle observed by the ALPAQUITA surface array. Blue contours indicate deficit of the intensity known as 'Shadow of the Moon'.

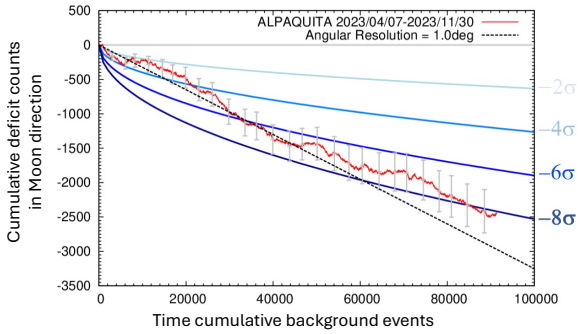

Fig. 9. Depth of the shadow of the moon as a function of the cumulative number of background (red). The black dotted line indicates an expectation assuming the angular resolution of ∼1°.

ports the angular resolution obtained in the 'even-odd' analysis.

Forbush Decrease in Single Counting: In addition to the shower observations, ALPAQUITA also records the counting rates of lower energy cosmic rays. Fig.10 shows the time profile of the single counting rate in May 2024. The large deficit from the end of 10 May is a Forbush Decrease event related to the arrival of a strong shock of an Interplanetary Coronal Mass Ejection at the earth. Among the cosmic-ray detectors recording this event over the world, the Bolivian site provides a unique information because of its high magnetic cut off rigidity. The large area of ALPAQUITA scintillating counters (97 m^2) allows analysis of faster time variation using high statistics. A continuous periodic variation with a smaller amplitude visible in Fig.10 corresponds to the effect of the atmospheric pressure variation.

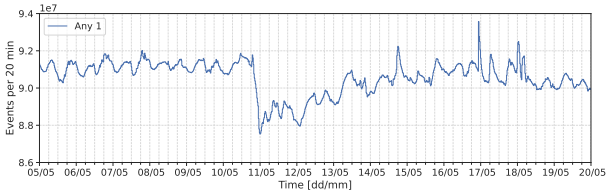

Fig. 10. Time profile of the single counting rate observed by ALPAQUITA surface array. A dip at the middle corresponds to a Forbush Decrease event.

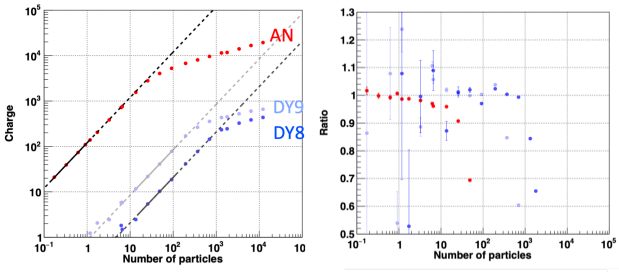

Fig. 11. Linearity of PMT using a new voltage divider. Left panel shows relations between the input light intensity in the unit of equivalent number of particles and output charges from the anode, 8^{th} dynode and 9^{th} dynode. Right panel shows the ratio to the linear line [9].

Preparatory Activities

Development of a Wide Dynamic Range PMT

The base plan of ALPACA to maintain a sufficient dynamic range of the charge measurement is to install two PMTs in each scintillating counter. As an alternative idea to reduce the cost, a new voltage divider circuit was developed [9]. By a modification of the resistances and capacitors and by an introduction to a readout from intermediate dynode signals, a linear dynamic range up to nearly 1,000 particle equivalent charge is achieved as shown in Fig.11. This modified circuit was officially approved as a product of HAMAMATSU and listed as H11284-50-02.

Development of a General Purpose Timing Module

To obtain a precise arrival timing of events, a general purpose NIM-based module was developed [5]. The module named *global navigation satellite system clock generation module* (GNSSDCM) consists of a GNSS disciplined oscillator GF-8803, a signal multiplication circuit, a signal-level conversion circuit and a serial communication port as shown in Fig.12. While the timing of the DAQ host computer is adjusted by the serial signal through an NTP server, measurement of the 40 MHz clock signals, which are reset by the 1PPS signals, through a TDC or a scaler allows fine timing record with a resolution of 25 ns. It was confirmed that the time accuracy compared to UTC was approximately 1 μs, and the time deviation was approximately 11.4 ns with one standard deviation. The development was already completed and a module is used in the ALPAQUITA observation.

Development of New Data Acquisition System

ALPACA uses the LeCroy MQT300A charge-to-timing conversion chips to measure charge of the PMT signal. Because of a shortage of the chips in the market, for a possi-

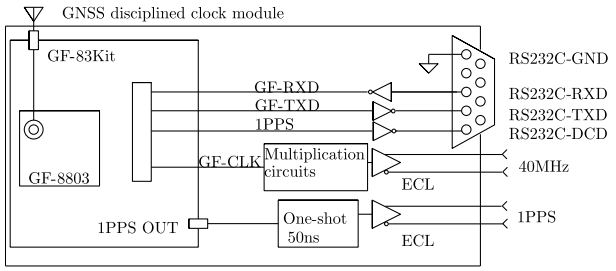

Fig. 12. Block diagram of the GNSS disciplined clock module(GNSSDCM) [5].

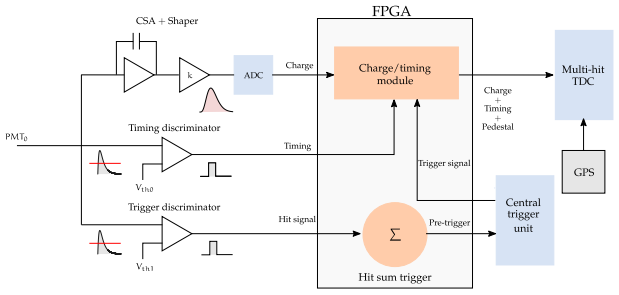

Fig. 13. A block diagram of the new DAQ system [10].

ble future extension of the ALPACA array more flexible and easy-to-maintain data acquisition system is under development [10]. The new system is divided in a front-end analog circuit and a back-end trigger and digital handling circuit as shown in Fig.13. Fig.14 (left) shows a result of linearity measurement of the new front-end ADC. The chain of the front- to back-end system was tested by injecting test pulses emulating air shower-like timing fluctuation. The distribution of the recorded event rate together with the expected one shown in Fig.14 (right) validates a good performance of the new system.

Analysis of Gamma-ray and Molecular Cloud Association

To identify the hadronic cosmic-ray accelerators among the gamma-ray sources to be detected by ALPACA, correlation study with the distribution of molecular cloud observed by the radio telescopes is crucial. Lead by the Mexican ALPACA members, new collaborative studies with radio astronomers including many Japanese experts are ongoing. Studies of molecular clouds around a sub-PeV gamma-ray source LHAASO J2108+5157, which the LHAASO experiment proposes as a PeV cosmic-ray accelerator (Cao et al., Nature, 594, 33 (2021)), were performed [2][3].

Archival data obtained by the telescope of the Osaka Prefecture University (OPU) and newly obtained data by the Nobeyama 45 m telescope were analyzed. Using the Nobeyama data we find that the morphology of the spatial distribution of the CO emission is strikingly similar to that of the Fermi-LAT excess gamma rays, coinciding with the LHAASO J2108+5157, as shown in Fig.15.

From the ^{12}CO (J=2→1) line emission of the OPU telescope data an optically thin cloud associated with LHAASO J2108+5117 was newly discovered. Considering a distance of 1.7 kpc, we estimated a nucleon (HI + H_2) density

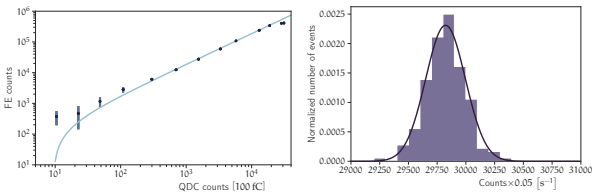

Fig. 14. (Left) Charge linearity of the new front-end circuit. (Right) Distribution of the measured trigger rates through the new DAQ chain. Solid curve indicates the expected distribution according to the input signal [10].

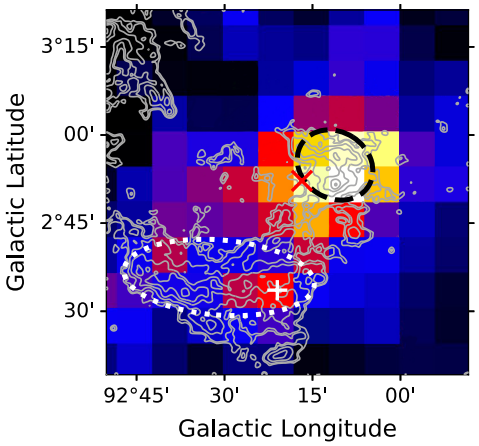

Fig. 15. Fermi-LAT map (in colours) with Nobeyama ^{13}CO map overlaid as grey contours. The ^{13}CO map was integrated between -20 and -8 km s^{-1}. The cross (×) and the plus (+) signs indicate the central positions of LHAASO J2108 and a hard source reported in a Fermi-LAT analysis (Abe et al, A&A, 673, A75 (2023)) , respectively [2].

of 37±14 cm^{-3} and proposed this cloud as a target of hadronic gamma-ray emission.

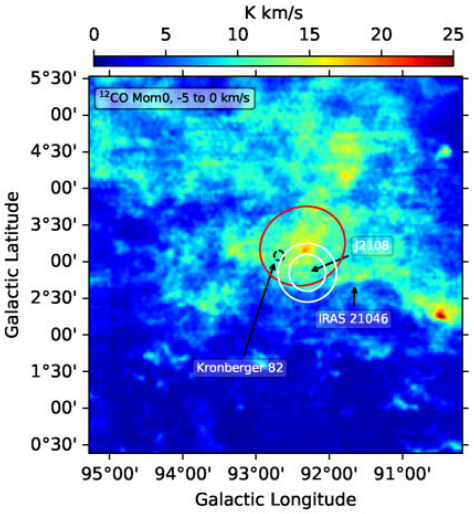

Fig. 16. Distribution of the ^{12}CO (J=2→1) line emission observed by the OPU telescope around the direction of LHAASO J2108+5117. A red ellipse corresponds to the size of the molecular cloud discovered in this study [3].

THE ALPACA COLLABORATION

Institute	Country	(*)
ICRR, Univ. of Tokyo	Japan	15
Chubu Univ.	Japan	6
Hiroshima City Univ.	Japan	1
Japan Atomic Energy Agency	Japan	1
Kanagawa Univ.	Japan	3
Nagano Prefectural Institute of Technology	Japan	1
National Institute of Informatics	Japan	1
Nihon Univ.	Japan	2
Osaka Electro-Communicatoin Univ.	Japan	1
Osaka Metropolitan Univ.	Japan	1
RIKEN	Japan	1
Shinshu Univ.	Japan	5
Tokyo Metropolitan College of Industrial Technology	Japan	1
Universidad Mayor de San Andres	Bolivia	10
Universidad de Guadalajara	Mexico	3
Utsunomiya Univ.	Japan	1
Yokohama National Univ.	Japan	7
Total		60

(*) Number of participants as of August 2024.

Members

Staff

Masato Takita, Associate Professor (February 2001 to November 2016), Professor (November 2016 to the present)
De la Fuente Acosta Eduardo, Visiting Professor (June 2021 to January 2022)
Takashi Sako, Associate Professer (TA/Tibet, October 2017 to the present)
Munehiro Ohnishi, Assistant Professor (April 1993 to the present)
Kazumasa Kawata, Specially Appointed Assistant Professor (April 2013 to March 2018), Assistant Professor (Tibet/TA, April 2018 to August 2024), Associate Professor (Tibet/TA, September 2024 to present)

Postdoctoral Fellows

Takashi Sako (April 2010 to March 2017 and June 2018 to March 2024)
Marcos Anzorena (September 2021 to present)
Sei Kato (April 2022 to present)
Keitaro Fujita (June 2024 to present)

Graduate Students

Three graduate students obtained the master degrees during 2018–2024, supervised by ICRR staff members.

Bibliography

Basically after Year 2018

Papers in Refereed Journals

[1] "Hadronic interaction model dependence in cosmic Gamma-ray flux estimation using an extensive air shower array with a muon detector", S Okukawa et al. (ALPACA Collaboration), Experimental Astronomy, **55**, 325-342 (2023).

[2] "Evidence for a gamma-ray molecular target in the enigmatic PeVatron candidate LHAASO J2108+5157", E. de la Fuente et al., Astronomy and Astrophysics, **675**, L5 (2023).

[3] "Detection of a new molecular cloud in the LHAASO J2108+5157 region supporting a hadronic PeVatron scenario", E. de la Fuente et al., Publ. Astron. Soc. Japan, **75**, 3, 546-566 (2023).

[4] "Study of water Cherenkov detector to improve the angular resolution of an air-shower array for ultra-high-energy gamma-ray observation", H. Nakada, A. Shiomi, M. Ohnishi, T.K. Sako, K. Hibino and Y. Katayose, Experimental Astronomy, **53**, 991-1016 (2022).

[5] "Trigger time acquisition system for ground based air shower experiments", T. Ohura, M. Ohnishi and Y. Katayose, Nulc. Instrum. Methods A **1028**, 166363 (2022).

[6] "Detectability of southern gamma-ray sources beyond 100 TeV with ALPAQUITA, the prototype experiment of ALPACA", S Kato et al. (ALPACA Collaboration), Experimental Astronomy, **52**, 85-107 (2021).

Papers in International Conference Proceedings

[7] "Sub-PeV to PeV Photon Observations Using the New Air Shower Array in Bolivia", T. Sako et al. (The ALPACA Collaboration), Andromeda Proceedings, BSM2023.23.

[8] "Mega ALPACA to explore multi-PeV gamma-ray sky in the southern hemisphere", T. Sako for the ALPACA Collaboration, PoS(ICRC2023)632.

[9] "Extending the dynamic range of the 2-inch-diameter PMT for the ALPACA experiment", T. Kawashima for the ALPACA Collaboration, PoS(ICRC2023)637.

[10] "New Front end and trigger electronics for the ALPACA experiment", M. Anaorena for the ALPACA Collaboration, PoS(ICRC2023)641.

[11] "Performance studies of the ALPACA experiment", Y. Yokoe for the ALPACA Collaboration, PoS(ICRC2023)766.

[12] "Overview status of the ALPACA experiment", M.A. Subieta Vasquez for the ALPACA Collaboration, PoS(ICRC2023)767.

[13] "First Observational Results of the ALPAQUITA Air Shower Array in Bolivia", K. Kawata for the ALPACA Collaboration, PoS(ICRC2023)257.

[14] "The ALPACA experiment: The project of the first sub-PeV gamma-ray observation in the southern sky", T. Kawashima et al. (The ALPACA Collaboration), SciPost Phys. Proc. 13, 008 (2023).

[15] "Study of water Cherenkov detector designs to determine air shower arrival directions with accuracy", A. Shiomi et al., PoS(ICRC2023)475.

[16] "ALPACA experiment: A new air shower array to explore the sub-PeV gamma-ray sky in the southern hemisphere", M Anzorena et al. (The ALPACA Collaboration), Pos(ICHEP2022)091.

[17] "Current status of ALPACA for exploring sub-PeV gamma-ray sky in Bolivia", T. Sako for the ALPACA Collaboration, PoS(ICRC2021)733.

[18] "Half ALPACA and its sensitivity to sub-PeV gamma rays from the Galactic Center", Y. Yokoe for the ALPACA Collaboration, PoS(ICRC2021)899.

[19] "A simulation study on the performance of the ALPAQUITA experiment", S. Kato for the ALPACA Collaboration, PoS(ICRC2021)737.

[20] "Study of water Cherenkov detector to determine air shower arrival directions with accuracy", A Shiomi et al., PoS(ICRC2021)732.

[21] "Expected performance of the prototype experiment for the ALPACA experiment", C. Calle et al. (The ALPACA Collaboration), PoS(ICRC2019)711.

[22] "ALPACA air shower array to explore 100TeV gamma-ray sky in Bolivia", C. Calle et al. (The ALPACA Collaboration), PoS(ICRC2019)779.

[23] "Performance of Air Shower Array with Surface Water Cherenkov Detectors", A. Shiomi et al., PoS(ICRC2019)793.

HIGH ENERGY ASTROPHYSICS GROUP

Introduction

The high energy astrophysics group aims at making theoretical studies of violent astrophysical phenomena, in which cosmic rays (CRs, non-thermal particles) are being accelerated. The targets of the group's study include high-energy astrophysical objects such as supernova (SN) explosions/shocks, neutron stars (NSs), mergers of binary stars, and relativistic jets launched from active galactic nuclei (AGNs) and gamma-ray bursts (GRBs). NSs are usually observed as pulsars, whose wind produces pulsar wind nebulae (PWNe). Strongly magnetized NSs are called magnetars. Fast radio bursts (FRBs), $\sim$ ms transient phenomena in the GHz band, are considered to be emitted from magnetars.

CRs are accelerated in those high-energy objects. The standard theory of the cosmic ray acceleration process invokes effective diffusive-shock-acceleration (DSA) mechanism working around collisionless astrophysical shocks and their turbulent environment. The magnetic reconnection mechanism is another candidate for effective particle acceleration processes. Understanding the transport processes involved in the DSA and magnetic reconnection mechanisms requires deep consideration based on microscopic plasma physics.

The open problems in high-energy astrophysics are not only the acceleration mechanism of cosmic rays. How are relativistic jets from AGNs accelerated? How are very bright gamma-ray emissions emitted in GRBs? How is the magnetic energy of the pulsar winds converted into the kinetic energy to form ultra-relativistic outflows? How are magnetic fields amplified in shocks in supernova remnants (SNRs) or afterglows of GRBs? How do relativistic particles propagate in interstellar space and escape from the galactic plane? Those problems remain unsolved and are our research themes. Our studies concerning high-energy astrophysics will promote multi-messenger astronomy – astronomy via collaborating observations of electromagnetic (EM) waves, CRs, neutrinos, and gravitational waves (GWs).

Our group has joined CALET, CALorimetric Electron Telescope, which is a mission for the Japanese Experiment Module-Exposed Facility (JEMEF) on the International Space Station. The CALET mission carries out accurate measurements of high-energy spectra of electrons, gamma rays, and nuclei. A member of our group has joined EHT, the Event Horizon Telescope collaboration. EHT discovered the black hole (BH) shadow in M87 and Galactic Center. The theoretical interpretation of those observational projects is also our important role.

Summary from 2018 to 2024

Our activity is theoretical and not restricted by a specific theme and schedule. We have published papers in wide fields as listed below.

- Plasma Physics: Turbulence and particle acceleration
- Relativistic Jets: Acceleration and dissipation
- Blazars and Radio Galaxies: Jets and emission mechanism
- BH Shadows: MHD simulations and radiative transfer
- GRBs: Prompt emission, afterglow, and cosmology
- NSs: Giant radio pulses (GRPs), magnetar bursts, and FRBs
- PWNe: CR transfer and emission
- Kilonovae: Optical counterpart of GW sources, lightcurves
- GW Astronomy: BH binary formation history
- SNe: Explosion mechanism, neutrino background, Nucleosynthesis
- Galaxy Clusters (GCs): Multi-messenger signals
- CR Propagation: Electron–positron CRs, Fermi bubble
- Collaborations: CALET, MAGIC, EHT

Non-Thermal Phenomena and Multi-Messenger Astronomy

We discussed the photon and/or neutrino emission mechanisms in GRBs [2, 90, 136], GRB afterglows [9, 15, 16, 22, 43, 131, 132, 139, 141, 144, 150], blazars [5, 20, 21, 99], radio galaxies [23, 24, 87, 110, 120, 142], super massive BHs [67, 73], SNs [44, 46, 49], GRPs [56], PWNe [10], magnetar [38, 145], kilonova afterglow [1], GCs [69, 95, 121, 127, 128, 130, 151], and Fermi bubbles [146].

In the standard blazar models, the nonthermal electrons are assumed to be accelerated via shocks with the Fermi process. However, some blazar spectra imply that the electron power-law index is smaller than 2, the value for the simplest shock acceleration model. We adopted an alternative acceleration mechanism, the stochastic acceleration by turbulence [5, 20]. Our model spectra have reproduced the curved photon spectra of representative blazars from the radio to the high-energy gamma-ray bands well.

Fermi-LAT detected prominent gamma-ray flares from 3C 279 in June 2015. The standard model for the gamma-ray emission is the inverse Compton (IC) scattering. However, we tested the synchrotron emission scenario for this bright gamma-ray flare using time-dependent numerical simulations. The stochastic acceleration model with secondary electron-positron pairs reproduces both the gamma-ray and X-ray data very well.

GRB afterglows are emitted from relativistic shocks propagating in the circumstellar medium. The shock is produced via the interaction between relativistic ejecta from the central engine and circumstellar medium. The standard model with a power-law electron injection in the shocked region predicts a power-law decaying lightcurves from the radio to gamma-ray bands. However, early afterglows show a variety of lightcurves: shallow decay phase in the first ~ 3000 s, X-ray flare, and chromatic behaviors in the X-ray and optical bands. Our simulation can follow the temporal evolution of electron energy distribution in the shocked regions. We successfully reproduced the gamma-ray lightcurve of GRB 190114C detected with MAGIC [43], and the shallow decay phase [144]. In GRB 190114C, we constrained the number fraction of non-thermal electrons. It is natural that only a fraction of electrons are accelerated by the shock and the rest of the electrons remain as the thermal component. However, our results indicate that almost all electrons are accelerated. This gives important clues to probing plasma physics with relativistic shocks.

Collaborated with the Fermi-LAT team, we discussed possible gamma-rays from the reverse shock in GRB180720B [132]. We also carried out 1D-MHD simulations for the external shocks. Based on the simulation results, we model the early afterglow lightcurves taking into account the ejecta magnetization and thickness [150]. Our model succeeded in reproducing the shallow decay phase with an intermediate thickness of the ejecta.

Giant radio halos (RHs) are detected in a fraction of GCs. Considering the short cooling timescale of radio-emitting electrons, continuous acceleration by turbulence is required. With the turbulent acceleration model, we reproduced the radio spectrum, surface brightness, and statistical properties of RHs taking into account the evolution of GCs [69, 95, 121, 130, 151]. Simultaneously we predicted hadronic gamma-ray and neutrino emissions from GCs, which give us useful constraints for the proton CR injection rate. This method was also adopted for the jets in GCs [120]. The surface brightness of long-tail radio jets is reproduced by continuous acceleration.

The Fermi and eROSITA bubbles, large diffuse structures in our Galaxy, can be the by-products of the steady star formation activity. To simultaneously explain the star formation history of the Milky Way and the metallicity of $\sim Z_\odot$ at the Galactic disk, a steady Galactic wind driven by cosmic rays is required. A part of the wind falls back onto the disk like a galactic fountain flow. We model the wind dynamics according to the Galactic evolution scenario and find that the scale height and the surface brightness of the X-ray and the hadronic gamma-ray emissions from such fountain flow region can be consistent with the observed properties of the Fermi and eROSITA bubbles. This implies that the bubbles are persistent structures of the Milky Way existing over (at least) the last ~ 1 Gyr, rather than evanescent structures formed by non-trivial, ~ 10 Myr past Galactic Center transient activities.

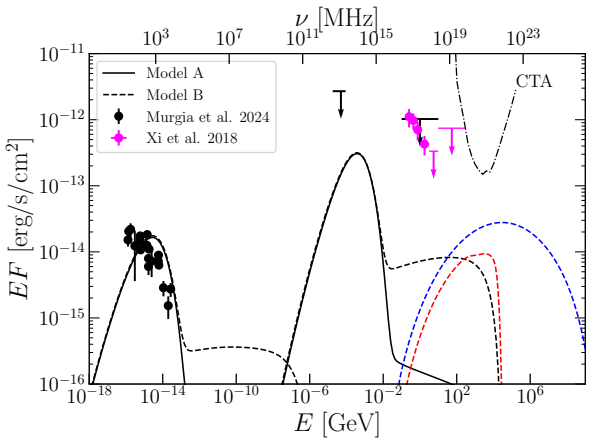

Fig. 1. Multi-messenger signals from Coma cluster [151]. The synchrotron and the inverse-Compton emissions of CR electrons (black), hadronic gamma-ray (red), and neutrino (blue) emissions of CR protons are shown.

Relativistic Jets

To demonstrate the magnetic energy dissipation via relativistic shocks, we carried out spherically symmetrical one-dimensional special relativistic MHD simulations of highly magnetized outflows with an adaptive mesh refinement method. We demonstrated the internal shock dissipation in multiple interactions between magnetically dominated relativistic ejecta and kinetically dominated non-relativistic winds. Our numerical results show that $\sim 10\%$ of the magnetic energy in the ejecta can be converted into the thermal energy of the relativistic and low-magnetized outflows via shocks in the rarefaction waves or the winds. Such hot and less magnetized outflows are relevant for observed non-thermal emissions in blazars or GRBs.

We also studied the kinetic plasma dynamics in collisionless relativistic jets with velocity shear, by carrying out particle-in-cell (PIC) simulations in the transverse plane of a jet [74]. It was discovered that intermittent magnetic reconnections (MRs) are driven by mushroom instability (MI), which is an important kinetic-scale plasma instability in the plasma shear flows with relativistic bulk speed. The MI-driven MRs intermittently occur by moving the location of the reconnection points from the vicinity of the initial velocity-shear surface toward the center of the jet. The MI-driven MR might be related to the formation of the spine structure in relativistic jets.

Kilonovae

Kilonovae are important counterparts of GW sources: the emission is associated with an NS–NS or BH-NS merger as the consequence of the mass ejection from the system. The first GW event from a binary NS merger (GW170817) was associated with a kilonova. The EM counterparts follow-up search for the second binary NS merger event, GW190425, provides the upper limits to the possible kilonova emissions in the localized sky area.

Our radiative transfer simulations for kilonovae taking the

interplay of multiple ejecta components of non-spherical morphology are strong tools to probe the ejecta properties and r-process elements produced in the ejecta [8, 18, 62, 91]. We studied the possible diversity of kilonova emissions in various situations including the cases of prompt collapse to a BH from NS mergers, high-velocity ejecta possibly accelerated by magnetars and a BH-NS merger. We showed that the differences in the peak brightness and time of peak may be useful to distinguish different types of the central engine for kilonovae.

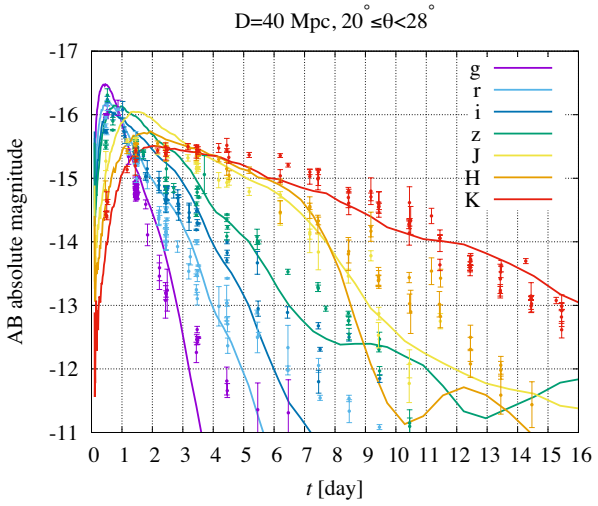

Fig. 2. Optical and infrared lightcurves of EM counterparts in GW170817 compared with the kilonova model [8].

We applied our multi-component kilonova models to explain the excess in optical/near-infrared wavelengths found in the observation of the afterglow of GRB160821B [14]. Ejecta masses estimated from the lightcurve comparison are consistent with the prediction of the numerical simulations, while they are relatively small compared to those estimated in GW170817. This indicates the diversity of kilonovae and could offer some clues to understand short GRBs as well as merger dynamics.

On 2019 August 14 advanced LIGO and advanced Virgo reported the detection of GWs from a BH–NS merger, which is referred to as S190814bv. Although no significant EM counterpart was found, upper limits in the nearly whole sky localization region of the event are obtained by their efforts. Based on the observational upper limits, we derived the upper limit to the ejecta mass of S190814bv with the realistic ejecta density profile as well as the detailed opacity and heating rate models [28].

We studied the long-term evolution of ejecta formed in a binary NS (BNS) merger that results in a long-lived remnant NS by performing a hydrodynamics simulation with the outflow data of a numerical relativity simulation as the initial condition [62]. We find that contrary to a naive expectation from the large ejecta mass and low lanthanide fraction, the optical emission is not as bright as that in GW170817/AT2017gfo, while the infrared emission can be brighter. These results suggest that the remnant in GW170817/AT2017gfo is unlikely to be a long-lived NS, but might have collapsed to a BH [91].

GW Astronomy

The star formation rate (SFR) peaks at a redshift $z \sim 2$, but the SFR in the universe above $z = 2$ is still uncertain. In the very early universe, gasses were not yet polluted by metals, which act as coolants. In such an environment, very massive stars so-called Pop III stars tend to be produced. A direct observation of Pop III stars at very high redshift is almost impossible. GW observations of BH binaries, which are remnants of massive stars, provide clues to revealing the SFR in the early universe. Estimates of the contribution of Pop III remnants to the detected GW events are our main research targets [40, 45, 48, 52, 63, 66, 97].

We showed that the total mass of binary BHs (BBHs) from binary Pop III star evolution can be as large as $\sim 150 M_\odot$ [45], which agrees with the mass of the binary black hole GW190521. The event rate of such massive stellar binary black hole mergers is estimated consistently with the observed value.

The probability number distribution function of BBH mergers observed by LIGO/Virgo O3a has double peaks as a function of chirp mass. We found that the larger chirp mass peak at $\sim 30 M_\odot$ is consistent with the Pop.III origin BHs [63]. We calculated a binary population synthesis calculation incorporating very massive Pop III stars up to 1500 $M_\odot$ and investigated the nature of BBH mergers [65]. Theoretical modeling of massive stars predicts a gap in the BH mass function above $\sim 40 M_\odot$ for BHs formed through single star evolution, arising from (pulsational) pair-instability SNe. Above the pair-instability mass gap, we find that the typical primary BH mass is 135–340 $M_\odot$. No conclusive BBH merger beyond the mass gap has been detected, and the upper limit on the merger rate density has been obtained.

We also considered the merger of a binary white dwarf (WD) for future GW detectors [100]. It is generally believed that Type Ia supernovae are thermonuclear explosions of carbon-oxygen WDs. However, there is currently no consensus regarding the events leading to the explosion. A binary WD (WD-WD) merger is a possible progenitor of Type Ia supernovae. Space-based GW detectors with considerable sensitivity in the deci-Hz range such as the DECi-hertz Interferometer Gravitational wave Observatory (DECIGO) can observe WD-WD mergers directly. Therefore, access to the deci-Hz band of GWs would enable multi-messenger observations of Type Ia supernovae to determine their progenitor and explosion mechanism. We estimated the event rate of WD-WD mergers and the minimum detection range to observe one WD-WD merger per year. We calculated DECIGO's ability to localize WD-WD mergers and to determine the masses of binary mergers.

BH Shadows and GRMHD

The EHT observed M87 in the 2017 observation campaign and detected the BH shadow surrounded by a bright ring-like emission. However, throughout their theoretical interpretation, no emission from the strongly magnetized jet is assumed and, thus, its contribution to the observed ring image has not been thoroughly studied yet. We, therefore, calculated the image of the bases of the relativistic jet using our general rela-

tivistic, radiative transfer code RAIKOU [50]. For the model with the BH spin $a_* = 0.99$, the direct image of the counter-jet and strong gravitational lens image (i.e., photon ring) reproduces a ring with a diameter ~ 40 mas observed by EHT 2017 observation. This indicates that the ring image in M87 may contain important features of the jet bases in addition to the photon ring.

With a baseline of 17 years of observations of M87, there was a shift in the jet's transverse position, possibly arising from an 8-to-10-year quasi-periodicity. Our analysis of radio observations over 22 years suggests a period of about 11 years for the variation in the position angle of the jet. We infer that we are seeing a spinning black hole that induces the Lense–Thirring precession of a misaligned accretion disk [122].

EAVN (East Asia VLBI Network) and EHT detected the intrinsic images of Sgr A*. The morphology of the intrinsic images was almost circular rather than elliptic. To interpret the results, we have calculated the images and spectra of the Sgr A* accretion flow [73]. We found that the circular morphology of the images can be reproduced when the viewing angle is on nearly face-on view. The observed large image sizes, importantly, require accelerated electrons. This may give us important information for the origin of the cosmic rays in the region near the Sgr A*.

SN Explosion

The neutrino heating mechanism is the leading hypothesis for the shock revival in core-collapse SN (CCSN) explosions. After the core bounce, a proto-NS (PNS) is formed at the center. This PNS emits energetic neutrinos, and these neutrinos are absorbed by matter behind the shock. Thanks to the energy supply by this process, the shock revives. This mechanism, however, does not work under spherical symmetry. We developed the multi-dimensional Boltzmann-radiation hydrodynamics (BRH) code for CCSN simulations.

We performed two simulations of the stellar core collapse with different nuclear equations of state (EOSs) to investigate the effect of the nuclear matter modeling on the SN dynamics [39]. The energy loss by the photodissociation of the accreting nuclei is affected by the difference in the EOS, and it results in the different strengths of the later turbulence. The proper treatment of the nuclear composition of the EOS is important to assess the influence of EOSs on the CCSNe.

We ran a 3D simulation [41], which covers until 20 ms after the core bounce. It revealed the fully multidimensional behavior of neutrinos with no symmetry and paved the way for 3D shock revival simulations. Besides, the general relativistic extension of the code was developed [51]. The Boltzmann neutrino transport solver correctly solves transport in curved spacetimes. This is a key to the first-principle code for CCSN.

Observational signals for CCSN neutrinos were investigated in a practical way. We developed an analytic model for CCSN neutrinos based on the Lane–Emden solution and neutrino diffusion [44]. This model gives a very quick estimate of the PNS radius, mass, and surface structure. We further developed a coherent framework for neutrino detection [49]. This includes the neutrino-radiation-hydrodynamics code for CCSN explosion and neutrino detection at the ground detector, i.e., Super-Kamiokande. The model and framework help us to get physical information of CCSN from future observations of CCSN neutrinos.

Magnetar Bursts

High brightness temperature in FRBs implies that the radio wave is emitted by a coherent radiation process although the concrete emission mechanism and the origin are still unclear. Most FRBs have extragalactic origin except one FRB, FRB 20200428A. FRB 20200428A is emitted from a Galactic magnetar, SGR1935+2154, and is associated with hard bursts in the X-ray band. This event implies that other FRBs are also produced in magnetars and they may be associated with hard X-ray short bursts. One of the models that explains the hard X-ray short bust and the FRB from the magnetar is an expanding fireball model.

We analytically studied this expanding fireball model and applied it to the hard X-ray short burst and FRB 20200428A [111]. A fireball of radiation plasma created near the surface of a neutron star (NS) expands under its own pressure along magnetic field lines and produces photon emission and relativistic matter outflow. The photon emission produces the observed hard X-ray short burst and the relativistic matter outflow may trigger the observed FRB. We comprehensively classified the expanding fireball evolution into five cases and obtained the photospheric luminosity and the kinetic energy of the outflow.

If a fireball is formed around a magnetic pole, it expands along the magnetic fields, later producing photon emission and plasma outflow, which can be responsible for radio bursts. We numerically studied the radiative acceleration of this outflowing fireball, which consists of electron-positron pairs and radiation, and obtained the spectrum of the escaped X-ray photons [148]. We consistently take into account cyclotron resonant scattering, which enhances the scattering cross-section resulting in a strong radiative force and high optical depth. Our results indicate that the X-ray spectrum from outflowing fireballs is similar to the observed X-ray spectrum in the Galactic fast radio burst. Additionally, the plasma outflow is concurrently accelerated to a high Lorentz factor due to cyclotron resonant scattering.

Collaboration with other Projects

We have joined CALET, CALorimetric Electron Telescope, which is a mission for the Japanese Experiment Module-Exposed Facility (JEM-EF) on the International Space Station. The CALET mission aims to reveal unsolved problems in high-energy phenomena of the Universe by carrying out accurate measurements of high-energy spectra of electrons, gamma-rays, and nuclei [3, 4, 5, 7, 11, 42, 64, 76, 92, 96, 104, 115, 116, 125]. Motivated by the CALET observation of electron–positron CRs, we calculated the flux contributions of CRs that have escaped from randomly appearing SNRs [71]. We found that without a complicated energy dependence of the diffusion coefficient, simple power-law diffusion coefficients can produce spectra similar to the CALET spectrum. One to three nearby SNe can contribute up to a few tens of percent of the CALET flux at 2–4 TeV, while ten or

more unknown and distant ($>$ 500 pc) SNe account for the remaining several tens of percent of the flux.

Our research fields closely relate to research targets in the other groups in the ICRR, TA, Tibet (CR physics), MAGIC/CTA (gamma-ray emission mechanism), Super Kamiokande (extragalactic neutrinos), Observational Cosmology (GRB and SFR), and KAGRA (binary mergers). Collaborating with the MAGIC team in ICRR, we have contributed to the modeling of the gamma-ray spectra of extremely hard blazars [21] and M87 obtained with MAGIC telescopes [23].

We also collaborated with Observational Cosmology Group in ICRR [13]. Future missions for long GRB observations at high redshift, such as Hi-z GUNDAM, will provide clues to the SFR history in our universe. Focusing on high-redshift ($z > 8$) GRBs, we calculated the detection rate of long GRBs by future observations, considering both Population I and II stars and Population III stars as GRB progenitors.

We also frequently discuss with students in the other groups, especially the CTA and TA/Tibet group, for promoting their studies and writing papers or theses. Thus, we contribute to education for students even in other groups.

Workshops

As a group in one of Joint Usage/Research Centers, we have held workshops on high-energy astrophysics every year. We have assured each lecturer one or two hours. So the audience could hear details on the latest topics. Our workshops have provided valuable opportunities for the astronomical community to learn about studies in unfamiliar fields. The workshop in 2023 is co-hosted by Next-generation Neutrino Science and Multi-messenger Astronomy Organization, which is a university organization to promote multi-messenger astronomy. We also organized two international workshops concerning VLBI. In 2021, we served as LOCs for the Rironkon Symposium, an annual symposium in the theoretical astrophysics community. The list of the workshops is as follows:

- "Diversity of High-Energy Astronomical Phenomena", Nov. 2018
- "Multi-Messenger Observations and Theory of High-Energy Astrophysical Transients", Nov. 2019
- "High-Energy Astrophysics 2020", Dec. 2020
- "Black Hole Astrophysics with VLBI: Multi-Wavelength and Multi-Messenger Era", Jan. 2021
- "Exploring the Diversity of the Universe through High-Energy Phenomena I", Oct. 2021
- "The 34th Rironkon Symposium", Dec. 2021
- "Black Hole Astrophysics with VLBI 2022", Feb. 2022
- "Exploring the Diversity of the Universe through High-Energy Phenomena II", Nov. 2022
- "Exploring the Diversity of the Universe through High-Energy Phenomena III", Nov. 2023
- "Exploring the Diversity of the Universe through High-Energy Phenomena IV", Nov. 2024

Members

Staff

Katsuaki Asano, Professor, Apr. 2013–present
Kyohei Kawaguchi, Assis. Professor, Mar. 2018–Mar. 2023
Tomoya Kinugawa, Assis. Professor, Jan. 2020–Mar. 2023
Jiro Shimoda, Project Assis. Professor, Jun. 2023–present

Postdoctoral Fellows

Akira Harada, ICRR researcher, Apr. 2019–Mar. 2021
Tomohisa Kawashima, ICRR researcher, Apr. 2020–present
Takumi Ohmura, ICRR researcher, Apr. 2021–Mar. 2023
Tomoki Wada, ICRR researcher, Apr. 2022–Mar. 2024
Kosuke Nishiwaki, JSPS Fellow, Apr. 2024–Sep. 2024
Ryo Sawada, ICRR researcher, Apr. 2024–present

Collaboration Researcher

Shotaro Yamasaki, Apr. 2020–Jul. 2020
Takumi Ohmura, Apr. 2023–present
Kosuke Nishiwaki, Oct. 2024–present

Graduate Students

Sho To, Apr. 2013–Mar. 2020
Wataru Ishizaki, Apr. 2014—Mar. 2019
Kosuke Nishiwaki, Apr. 2019–Mar. 2024
Ryota Goto, Apr. 2020–present
Yo Kusafuka, Apr. 2021–present
Théo Abounnasr, Oct. 2021–Sep. 2023
Yuto Ichinose, Apr. 2023–present
Ryohei Inamoto, Apr. 2024–present
Yusaku Fukumoto, Apr. 2024–present

Bibliography

Papers in Refereed Journals

[1] Katsuaki Asano, & Sho To, "Subsequent Nonthermal Emission due to the Kilonova Ejecta in GW170817", Astrophys. J. **852**, 105(5pp) (2018)

[2] Kai Wang, Ruo-Yu Liu, Zi-Gao Dai, & Katsuaki Asano, "Hadronic Origin of Prompt High-Energy Emission of Gamma-Ray Bursts Revisited: In the Case of a Limited Maximum Proton Energy", Astrophys. J. **852**, 24(12pp) (2018)

[3] O. Adriani, Y. Akaike, K. Asano, et al., "Extended Measurement of the Cosmic-Ray Electron and Positron Spectrum from 11 GeV to 4.8 TeV with the Calorimetric Electron Telescope on the International Space Station", Phys. Rev. Lett. **120**, 261102(7pp) (2018)

[4] Y. Asaoka, S. Ozawa, S. Torii, et al., "On-Orbit Operations and Offline Data Processing of CALET onboard the ISS", Astro. Part. Phys. **100**, 29-37 (2018)

[5] Katsuaki Asano, & Masaaki Hayashida, "Blazar Spectra with Hard-Sphere-like Acceleration of Electrons", Astrophys. J. **861**, 31(7pp) (2018)

[6] O. Adriani, Y. Akaike, K. Asano, et al., "Search for GeV Gamma-Ray Counterparts of Gravitational Wave Events by CALET", Astrophys. J. **863**, 160(9pp) (2018)

[7] N. Cannady, Y. Asaoka, F. Satoh, et al., "Characteristics and Performance of the CALorimetric Electron Telescope (CALET) Calorimeter for Gamma-Ray Observations" Astrophys. J. Supp. **238**, 5(16pp) (2018)

[8] Kyohei Kawaguchi, Masaru Shibata, & Masaomi Tanaka, "Radiative Transfer Simulation for the Optical and Near-Infrared Electromagnetic Counterparts to GW170817", Astrophys. J. Lett. **865**, L21(6pp) (2018)

[9] Y. Tachibana, M. Arimoto, K. Asano, et al., "Late Engine Activity of GRB 161017A Revealed by Early Optical Observations", Pub. Astron. Soc. Japan **70**, 92(9pp) (2018)

[10] Wataru Ishizaki, Katsuaki Asano, & Kyohei Kawaguchi, "Outflow and Emission Model of Pulsar Wind Nebulae with the Back Reaction of Particle Diffusion", Astrophys. J. **867**, 141(12pp) (2018)

[11] O. Adriani, Y. Akaike, K. Asano, et al., "Direct Measurement of the Cosmic-Ray Proton Spectrum from 50 GeV to 10 TeV with the Calorimetric Electron Telescope on the International Space Station", Phys. Rev. Lett. **122**, 181102(8pp) (2019)

[12] Yuto Teraki, & Katsuaki Asano, "Particle Energy Diffusion in Linear Magnetohydrodynamic Waves", Astrophys. J. **877**, 71(12pp) (2019)

[13] Tomoya Kinugawa, Yuichi Harikane, & Katsuaki Asano, "Long Gamma-Ray Burst Rate at Very High Redshift", Astrophys. J. **878**, 128(9pp) (2019)

[14] G. P. Lamb, N. R. Tanvir, A. J. Levan et al., "Short GRB 160821B: A Reverse Shock, a Refreshed Shock, and a Well-Sampled Kilonova", Astrophys. J. **883**, 48(12pp) (2019)

[15] Donggeun Tak, Nicola Omodei, Z. Lucas Uhm, Judith Racusin, Katsuaki Asano, & Julie McEnery, "Closure Relations of Gamma-Ray Bursts in High Energy Emission", Astrophys. J. **883**, 134(10pp) (2019)

[16] M. Ajello, M. Arimoto, K. Asano, et al., "Bright Gamma-Ray Flares Observed in GRB 131108A", Astrophys. J. Lett. **886**, L33(7pp) (2019)

[17] Milad Delfan Azari, Shoichi Yamada, Taiki Morinaga, Hiroki Nagakura, Shun Furusawa, Akira Harada, Hirotada Okawa, Wakana Iwakami, & Kohsuke Sumiyoshi, "Fast Collective Neutrino Oscillations inside the Neutrino Sphere in Core-Collapse Supernovae", Phys. Rev. D **101**, 023018(12pp) (2020)

[18] Kyohei Kawaguchi, Masaru Shibata, & Masaomi Tanaka, "Diversity of Kilonova Light Curves", Astrophys. J. **889**, 171(25pp) (2020)

[19] Koutarou Kyutoku, Sho Fujibayashi, Kota Hayashi, Kyohei Kawaguchi, Kenta Kiuchi, Masaru Shibata, & Masaomi Tanaka, "On the Possibility of GW190425 Being a Black Hole–Neutron Star Binary Merger", Astrophys. J. Lett. **890**, L4(6pp) (2020)

[20] Katsuaki Asano, & Masaaki Hayashida, "Synchrotron Gamma-Ray Emission Model of the Giant Outburst of Quasar 3C 279 in 2015 June: Fast Reconnection or Stochastic Acceleration with Electromagnetic Cascade?", Astrophys. J. **890**, 56(7pp) (2020)

[21] V. A. Acciari, S. Ansoldi, L. A. Antonelli, A. Arbet Engels, K. Asano, et al., "New Hard-TeV Extreme Blazars Detected with the MAGIC Telescopes", Astrophys. J. Supp. **247**, 16(24pp) (2020)

[22] Makoto Arimoto, Katsuaki Asano, Yutaro Tachibana, & Magnus Axelsson, "Physical Origin of GeV Emission in the Early Phase of GRB 170405A: Clues from Emission Onsets with Multiwavelength Observations", Astrophys. J. **891**, 106(11pp) (2020)

[23] V. A. Acciari, S. Ansoldi, L. A. Antonelli, et al., "Monitoring of the Radio Galaxy M87 during a Low-Emission State from 2012 to 2015 with MAGIC", Mon. Not. R. Astron. Soc. **492**, 5354-5365 (2020)

[24] Yuh Tsunetoe, Shin Mineshige, Ken Ohsuga, Tomohisa Kawashima, & Kazunori Akiyama, "Polarization Imaging of M 87 Jets by General Relativistic Radiative Transfer Calculation Based on GRMHD Simulations", Pub. Astron. Soc. Japan **72**, 32(17pp) (2020)

[25] Akihiro Inoue, Ken Ohsuga, & Tomohisa Kawashima, "Pulsed Fraction of Super-Critical Column Accretion Flows on to Neutron Stars: Modeling of Ultraluminous X-ray Pulsars", Pub. Astron. Soc. Japan **72**, 34(9pp) (2020)

[26] F. Roelofs, M. Janssen, I. Natarajan, et al., "SYMBA: An End-to-End VLBI Synthetic Data Generation Pipeline Simulating Event Horizon Telescope observations of M 87", Astron. & Astrophys. **636**, A5(19pp) (2020)

[27] Kenta Kiuchi, Kyohei Kawaguchi, Koutarou Kyutoku, Yuichiro Sekiguchi, & Masaru Shibata, "Sub-Radian-Accuracy Gravitational Waves from Coalescing Binary Neutron Stars in Numerical Relativity. II. Systematic Study on the Equation of State, Binary Mass, and Mass Ratio", Phys. Rev. D **101**, 084006(25pp) (2020)

[28] Kyohei Kawaguchi, Masaru Shibata, & Masaomi Tanaka, "Constraint on the Ejecta Mass for a Black Hole–Neutron Star Merger Event Candidate S190814bv", Astrophys. J. **893**, 153(17pp) (2020)

[29] Ataru Tanikawa, Tomoya Kinugawa, Jun Kumamoto, & Michiko S. Fujii, "Formation Rate of LB-1-like Systems through Dynamical Interactions", Pub. Astron. Soc. Japan **72**, 39(10pp) (2020)

[30] A. E. Broderick, R. Gold, M. Karami et al., "THEMIS: A Parameter Estimation Framework for the Event Horizon Telescope", Astrophys. J. **897**, 139(38pp) (2020)

[31] R. Gold, A. E. Broderick, Z. Younsi et al., "Verification of Radiative Transfer Schemes for the EHT", Astrophys. J. **897**, 148(21pp) (2020)

[32] Ataru Tanikawa, Takashi Yoshida, Tomoya Kinugawa, Koh Takahashi, & Hideyuki Umeda, "Fitting Formulae for Evolution Tracks of Massive Stars under Extreme Metal-Poor Environments for Population Synthesis Calculations and Star Cluster Simulations", Mon. Not. R. Astron. Soc. **495**, 4170-4191 (2020)

[33] J.-Y. Kim, T. P. Krichbaum, A. E. Broderick, et al., "Event Horizon Telescope Imaging of the Archetypal Blazar 3C 279 at an Extreme 20 Microarcsecond Resolution", Astron. & Astrophys. **640**, A69(21pp) (2020)

[34] Masaomi Tanaka, Daiji Kato, Gediminas Gaigalas, & Kyohei Kawaguchi, "Systematic Opacity Calculations for Kilonovae", Mon. Not. R. Astron. Soc. **496**, 1369-1392 (2020)

[35] Smaranika Banerjee, Masaomi Tanaka, Kyohei Kawaguchi, Daiji Kato, & Gediminas Gaigalas, "Simulations of Early Kilonova Emission from Neutron Star Mergers", Astrophys. J. **901**, 29(12pp) (2020)

[36] W. Maciek, K. Akiyama, L. Blackburn, et al., "Monitoring the Morphology of M87 in 2009-2017 with the Event Horizon Telescope", Astrophys. J. **901**, 67(28pp) (2020)

[37] D. Psaltis, L. Medeiros, P. Christian, et al., "Gravitational Test beyond the First Post-Newtonian Order with the Shadow of the M87 Black Hole", Phys. Rev. Lett. **125**, 141104(9pp) (2020)

[38] Shotaro Yamasaki, Yuri Lyubarsky, Jonathan Granot, & Ersin Göğüş, "Spectral Modification of Magnetar Flares by Resonant Cyclotron Scattering", Mon. Not. R. Astron. Soc. **498**, 484-494 (2020)

[39] Akira Harada, Hiroki Nagakura, Wakana Iwakami, Hirotada Okawa, Shun Furusawa, Kohsuke Sumiyoshi, Hideo Matsufuru, Shoichi Yamada, "The Boltzmann-Radiation-Hydrodynamics Simulations of Core-Collapse Supernovae with Different Equations of State: The Role of Nuclear Composition and the Behavior of Neutrinos", Astrophys. J. **902**, 150(25pp) (2020)

[40] Tomoya Kinugawa, Takashi Nakamura, & Hiroyuki Nakano, "Chirp Mass and Spin of Binary Black Holes from First Star Remnants", Mon. Not. R. Astron. Soc. **498**, 3946-3963 (2020)

[41] Wakana Iwakami, Hirotada Okawa, Hiroki Nagakura, Akira Harada, Shun Furusawa, Kosuke Sumiyoshi, Hideo Matsufuru, & Shoichi Yamada, "Simulations of the Early Postbounce Phase of Core-Collapse Supernovae in Three-Dimensional Space with Full Boltzmann Neutrino Transport", Astrophys. J. **903**, 82(24pp) (2020)

[42] O. Adriani, Y. Akaike, K. Asano, et al., "Direct Measurement of the Cosmic-Ray Carbon and Oxygen Spectra from 10 GeV/n to 2.2 TeV/n with the Calorimetric Electron Telescope on the International Space Station", Phys. Rev. Lett. **125**, 251102(7pp) (2020)

[43] Katsuaki Asano, Kohta Murase, & Kenji Toma, "Probing Particle Acceleration through Broadband Early Afterglow Emission of MAGIC Gamma-Ray Burst GRB 190114C", Astrophys. J. **905**, 105(9pp) (2020)

[44] Yudai Suwa, Akira Harada, Ken'ichiro Nakazato, & Kohsuke Sumiyoshi, "Analytic Solutions for Neutrino-Light Curves of Core-Collapse Supernovae", Prog. Theor. Exp. Phys. **2021**, 013E01(12pp) (2021)

[45] Tomoya Kinugawa, Takashi Nakamura, Hiroyuki Nakano, "Formation of Binary Black Holes Similar to GW190521 with a Total Mass of $\sim 150 M_{\odot}$ from Population III Binary Star Evolution", Mon. Not. R. Astron. Soc. **501**, L49-L53 (2021)

[46] Shunsaku Horiuchi, Tomoya Kinugawa, Tomoya Takiwaki, Koh Takahashi, & Kei Kotake, "Impact of Binary Interactions on the Diffuse Supernova Neutrino Background", Phys. Rev. D **103**, 043003(13pp) (2021)

[47] Kota Hayashi, Kyohei Kawaguchi, Kenta Kiuchi, Koutarou Kyutoku, & Masaru Shibata, "Properties of the Remnant Disk and the Dynamical Ejecta Produced in Low-Mass Black Hole-Neutron Star Mergers", Phys. Rev. D **103**, 043007(16pp) (2021)

[48] Tomoya Kinugawa, Takashi Nakamura, Hiroyuki Nakano, "Formation of Mass Gap Compact Object and Black Hole Binary from Population III Stars", Prog. Theor. Exp. Phys. **2021**, 021E01(11pp) (2021)

[49] Masamitsu Mori, Yudai Suwa, Ken'ichiro Nakazato, Kohsuke Sumiyoshi, Masayuki Harada, Akira Harada, Yusuke Koshio, & Roger A. Wendell, "Developing an End-to-End Simulation Framework of Supernova Neutrino Detection", Prog. Theor. Exp. Phys. **2021**, 023E01(21pp) (2021)

[50] Tomohisa Kawashima, Kenji Toma, Motoki Kino, Kazunori Akiyama, Masanori Nakamura, & Kotaro Moriyama, "A Jet-Bases Emission Model of the EHT2017 Image of M87*", Astrophys. J. **909**, 168(6pp) (2021)

[51] Ryuichiro Akaho, Akira Harada, Hiroki Nagakura, Kohsuke Sumiyoshi, Wakana Iwakami, Hirotada Okawa, Shun Furusawa, Hideo Matsufuru, & Shoichi

Yamada, "Multidimensional Boltzmann Neutrino Transport Code in Full General Relativity for Core-Collapse Simulations", Astrophys. J. **909**, 210(17pp) (2021)

[52] Ataru Tanikawa, Hajime Susa, Takashi Yoshida, Alessandro A. Trani, & Tomoya Kinugawa, "Merger Rate Density of Population III Binary Black Holes below, above, and in the Pair-Instability Mass Gap", Astrophys. J. **910**, 30(31pp) (2021)

[53] K. Akiyama, J. C. Algaba, A. Alberdi, et al., "First M87 Event Horizon Telescope Results. VII. Polarization of the Ring", Astrophys. J. Lett. **910**, L12(48pp) (2021)

[54] K. Akiyama, J. C. Algaba, A. Alberdi, et al., "First M87 Event Horizon Telescope Results. VIII. Magnetic Field Structure near The Event Horizon", Astrophys. J. Lett. **910**, L13(43pp) (2021)

[55] C. Goddi, I. Martí-Vidal, H. Messias, et al., "Polarimetric Properties of Event Horizon Telescope Targets from ALMA", Astrophys. J. Lett. **910**, L14(54pp) (2021)

[56] T. Enoto, T. Terasawa, S. Kisaka, et al., "Enhanced X-Ray Emission Coinciding with Giant Radio Pulses from the Crab Pulsar", Science **372**, 187-190 (2021)

[57] J. C. Algaba, J. Anczarski, K. Asada, et al., "Broadband Multi-Wavelength Properties of M87 during the 2017 Event Horizon Telescope Campaign", Astrophys. J. Lett. **911**, L11(43pp) (2021)

[58] Takaaki Kitaki, Shin Mineshige, Ken Ohsuga, & Tomohisa Kawashima, "The Origins and Impact of Outflow from Super-Eddington Flow", Pub. Astron. Soc. Japan **73**, 450-466 (2021)

[59] R. Narayan, D. C. M. Palumbo, M. D. Johnson, et al., "The Polarized Image of a Synchrotron-Emitting Ring of Gas Orbiting a Black Hole", Astrophys. J. **912**, 35(26pp) (2021)

[60] James O. Chibueze, Haruka Sakemi, Takumi Ohmura, Mami Machida, Hiroki Akamatsu, Takuya Akahori, Hiroyuki Nakanishi, Viral Parekh, Ruby van Rooyen, & Tsutomu T. Takeuchi, "Jets from MRC 0600-399 Bent by Magnetic Fields in the Cluster Abell 3376", Nature **593**, 47-50 (2021)

[61] Nanae Domoto, Masaomi Tanaka, Shinya Wanajo, & Kyohei Kawaguchi, "Signatures of r-Process Elements in Kilonova Spectra", Astrophys. J. **913**, 26(12pp) (2021)

[62] Kyohei Kawaguchi, Sho Fujibayashi, Masaru Shibata, Masaomi Tanaka, & Shinya Wanajo, "A Low-Mass Binary Neutron Star: Long-Term Ejecta Evolution and Kilonovae with Weak Blue Emission", Astrophys. J. **913**, 100(24pp) (2021)

[63] Tomoya Kinugawa, Takashi Nakamura, & Hiroyuki Nakano, "Gravitational Waves from Population III Binary Black Holes are Consistent with LIGO/Virgo O3a Data for the Chirp Mass Larger than $\sim 20 M_{\odot}$", Mon. Not. R. Astron. Soc. **504**, L28-L33 (2021)

[64] O. Adriani, Y. Akaike, K. Asano, et al., "Measurement of the Iron Spectrum in Cosmic Rays from 10 GeV/n to 2.0 TeV/n with the Calorimetric Electron Telescope on the International Space Station", Phys. Rev. Lett. **126**, 241101(7pp) (2021)

[65] Kotaro Hijikawa, Ataru Tanikawa, Tomoya Kinugawa, Takashi Yoshida, & Hideyuki Umeda, "On the Population III Binary Black Hole Mergers beyond the Pair-Instability Mass Gap", Mon. Not. R. Astron. Soc. **505**, L69-L73 (2021)

[66] Ataru Tanikawa, Tomoya Kinugawa, Takashi Yoshida, Kotaro Hijikawa, & Hideyuki Umeda, "Population III Binary Black Holes: Effects of Convective Overshooting on Formation of GW190521", Mon. Not. R. Astron. Soc. **505**, 2170-2176 (2021)

[67] Yuh Tsunetoe, Shin Mineshige, Ken Ohsuga, Tomohisa Kawashima, & Kazunori Akiyama, "Polarization Images of Accretion Flow around Supermassive Black Holes: Imprints of Toroidal Field Structure", Pub. Astron. Soc. Japan **73**, 912-928 (2021)

[68] M. Janssen, H. Falcke, M. Kadler, et al., "Event Horizon Telescope Observations of the Jet Launching and Collimation in Centaurus A", Nature Astron. **5**, 1017-1028 (2021)

[69] Kosuke Nishiwaki, Katsuaki Asano, & Kohta Murase, "Particle Reacceleration by Turbulence and Radio Constraints on Multimessenger High-Energy Emission from the Coma Cluster", Astrophys. J. **922**, 190(23pp) (2021)

[70] K. Satapathy, D. Psaltis, F. Ozel, et al., "The Variability of the Black-Hole Image in M87 at the Dynamical Time Scale", Astrophys. J. **925**, 13(19pp) (2022)

[71] Katsuaki Asano, Yoichi Asaoka, Yosui Akaike, Norita Kawanaka, Kazunori Kohri, Holger M. Motz, & Toshio Terasawa, "Monte Carlo Study of Electron and Positron Cosmic-Ray Propagation with the CALET Spectrum", Astrophys. J. **926**, 5(10pp) (2022)

[72] Ataru Tanikawa, Takashi Yoshida, Tomoya Kinugawa, Alessandro A. Trani, Takashi Hosokawa, Hajime Susa, & Kazuyuki Omukai, "Merger Rate Density of Binary Black Holes through Isolated Population I, II, III and Extremely Metal-Poor Binary Star Evolution", Astrophys. J. **926**, 83(21pp) (2022)

[73] I. Cho, G.-Y. Zhao, T. Kawashima, et al., "The Intrinsic Structure of Sagittarius A* at 1.3 cm and 7 mm", Astrophys. J. **926**, 108(17pp) (2022)

[74] Tomohisa Kawashima, Seiji Ishiguro, Toseo Moritaka, Ritoku Horiuchi, & Kohji Tomisaka, "Mushroom-Instability-Driven Magnetic Reconnections in Collisionless Relativistic Jets", Astrophys. J. **928**, 62(10pp) (2022)

[75] Ignacio Botella, Shin Mineshige, Takaaki Kitaki, Ken Ohsuga, & Tomohisa Kawashima, "Structure of the Super-Eddington Outflow and its Impact on the Cosmological Scale", Pub. Astron. Soc. Japan **74**, 384-397 (2022)

[76] O. Adriani, Y. Akaike, K. Asano, et al., "Direct Measurement of the Nickel Spectrum in Cosmic Rays in the Energy Range from 8.8 GeV/n to 240 GeV/n with CALET on the International Space Station", Phys. Rev. Lett. **128**, 131103(8pp) (2022)

[77] K. Akiyama, A. Alberdi, W. Alef, et al., "First Sagittarius A* Event Horizon Telescope Results. I. The Shadow of the Supermassive Black Hole in the Center of the Milky Way", Astrophys. J. Lett. **930**, L12(21pp) (2022)

[78] K. Akiyama, A. Alberdi, W. Alef, et al., "First Sagittarius A* Event Horizon Telescope Results. II. EHT and Multiwavelength Observations, Data Processing, and Calibration", Astrophys. J. Lett. **930**, L13(31pp) (2022)

[79] K. Akiyama, A. Alberdi, W. Alef, et al., "First Sagittarius A* Event Horizon Telescope Results. III. Imaging of the Galactic Center Supermassive Black Hole", Astrophys. J. Lett. **930**, L14(64pp) (2022)

[80] K. Akiyama, A. Alberdi, W. Alef, et al., "First Sagittarius A* Event Horizon Telescope Results. IV. Variability, Morphology, and Black Hole Mass", Astrophys. J. Lett. **930**, L15(52pp) (2022)

[81] K. Akiyama, A. Alberdi, W. Alef, et al., "First Sagittarius A* Event Horizon Telescope Results. V. Testing Astrophysical Models of the Galactic Center Black Hole", Astrophys. J. Lett. **930**, L16(49pp) (2022)

[82] K. Akiyama, A. Alberdi, W. Alef, et al., "First Sagittarius A* Event Horizon Telescope Results. VI. Testing the Black Hole Metric", Astrophys. J. Lett. **930**, L17(44pp) (2022)

[83] J. Farah, P. Galison, K. Akiyama, et al., "Selective Dynamical Imaging of Interferometric Data", Astrophys. J. Lett. **930**, L18(21pp) (2022)

[84] M. Wielgus, N. Marchili, I. Marti-Vidal, et al., "Millimeter Light Curves of Sagittarius A Observed during the 2017 Event Horizon Telescope Campaign", Astrophys. J. Lett. **930**, L19(32pp) (2022)

[85] B. Georgiev, D. W. Pesce, A. E. Broderick, et al., "A Universal Power-Law Prescription for Variability from Synthetic Images of Black Hole Accretion Flows", Astrophys. J. Lett. **930**, L20(32pp) (2022)

[86] A. E. Broderick, R. Gold, B. Georgiev, et al., "Characterizing and Mitigating Intraday Variability: Reconstructing Source Structure in Accreting Black Holes with mm-VLBI", Astrophys. J. Lett. **930**, L21(30pp) (2022)

[87] Yuh Tsunetoe, Shin Mineshige, Tomohisa Kawashima, Ken Ohsuga, Kazunori Akiyama, & Hiroyuki R. Takahashi, "Investigating the Disk–Jet Structure in M87 through Flux Separation in the Linear and Circular Polarization Images", Astrophys. J. **931**, 25(26pp) (2022)

[88] R. Hayakawa, S. Yamada, H. Suda, et al., "X-Ray Hot Spots in the Eastern Ear of the Supernova Remnant W 50 and the Microquasar SS 433 System", Pub. Astron. Soc. Japan **74**, 510-520 (2022)

[89] Ataru Tanikawa, Gen Chiaki, Tomoya Kinugawa, Yudai Suwa, & Nozomu Tominaga, "Can Population III Stars be Major Origins of both Merging Binary Black Holes and Extremely Metal Poor Stars?", Pub. Astron. Soc. Japan **74**, 521-532 (2022)

[90] Ryota Goto, & Katsuaki Asano, "GRB Prompt Emission with Anisotropic Electron Distribution", Astrophys. J. **933**, 18(9pp) (2022)

[91] Kyohei Kawaguchi, Sho Fujibayashi, Kenta Hotokezaka, Masaru Shibata, & Shinya Wanajo, "Electromagnetic Counterparts of Binary-Neutron-Star Mergers Leading to a Strongly Magnetized Long-Lived Remnant Neutron Star", Astrophys. J. **933**, 22(18pp) (2022)

[92] O. Adriani, Y. Akaike, K. Asano, et al., "CALET Search for Electromagnetic Counterparts of Gravitational Waves during the LIGO/Virgo O3 Run", Astrophys. J. **933**, 85(16pp) (2022)

[93] Smaranika Banerjee, Masaomi Tanaka, Daiji Kato, Gediminas Gaigalas, Kyohei Kawaguchi, & Nanae Domoto, "Opacity of the Highly Ionized Lanthanides and the Effect on the Early Kilonova", Astrophys. J. **934**, 117(13pp) (2022)

[94] S. Issaoun, M. Wielgus, S. Jorstad, et al., "Resolving the Inner Parsec of the Blazar J1924–2914 with the Event Horizon Telescope", Astrophys. J. **934**, 145(21pp) (2022)

[95] Kosuke Nishiwaki, & Katsuaki Asano, "Statistical Properties of Radio Halos in Galaxy Clusters and the Origin of Seed Electrons for Reacceleration", Astrophys. J. **934**, 182(23pp) (2022)

[96] O. Adriani, Y. Akaike, K. Asano, et al., "Observation of Spectral Structures in the Flux of Cosmic-Ray Protons from 50 GeV to 60 TeV with the Calorimetric Electron Telescope on the International Space Station", Phys. Rev. Lett. **129**, 101102(8pp) (2022)

[97] Tomoya Kinugawa, Takashi Nakamura, & Hiroyuki Nakano, "Constraints on Population I/II Neutron Star-Black Hole Binary Formation by Gravitational Wave and Radio Observations", Mon. Not. R. Astron. Soc. **515**, L78-L83 (2022)

[98] Reetika Dudi, Ananya Adhikari, Bernd Brügmann, Tim Dietrich, Kota Hayashi, Kyohei Kawaguchi, Kenta Kiuchi, Koutarou Kyutoku, Masaru Shibata,

& Wolfgang Tichy, "Investigating GW190425 with Numerical-Relativity Simulations", Phys. Rev. D **106**, 084039(11pp) (2022)

[99] Yuh Tsunetoe, Shin Mineshige, Tomohisa Kawashima, Ken Ohsuga, Kazunori Akiyama, & Hiroyuki R. Takahashi, "Diverse Polarimetric Features of AGN Jets from Various Viewing Angles: Towards a Unified View", Galaxies **10**, 103(11pp) (2022)

[100] Tomoya Kinugawa, Hiroki Takeda, Ataru Tanikawa, & Hiroya Yamaguchi, "Probe for Type Ia Supernova Progenitor in Decihertz Gravitational Wave Astronomy", Astrophys. J. **938**, 52(9pp) (2022)

[101] Nanae Domoto, Masaomi Tanaka, Daiji Kato, Kyohei Kawaguchi, Kenta Hotokezaka, & Shinya Wanajo, "Lanthanide Features in Near-Infrared Spectra of Kilonovae", Astrophys. J. **939**, 8(18pp) (2022)

[102] Motoki Kino, Masaaki Takahashi, Tomohisa Kawashima, Jongho Park, Kazuhiro Hada, Hyunwook Ro, & Yuzhu Cui, "Implications from the Velocity Profile of the M87 Jet: A Possibility of a Slowly Rotating Black Hole Magnetosphere", Astrophys. J. **939**, 83(16pp) (2022)

[103] Shogo Yoshioka, Shin Mineshige, Ken Ohsuga, Tomohisa Kawashima, & Takaaki Kitaki, "Large-Scale Outflow Structure and Radiation Properties of Super-Eddington Flow: Dependence on the Accretion Rates", Pub. Astron. Soc. Japan **74**, 1378-1395 (2022)

[104] O. Adriani, Y. Akaike, K. Asano, et al., "Cosmic-Ray Boron Flux Measured from 8.4 GeV/n to 3.8 TeV/n with the Calorimetric Electron Telescope on the International Space Station", Phys. Rev. Lett. **129**, 251103(7pp) (2022)

[105] G. Giacinti, T. Abounnasr, A. Neronov, D. Semikoz, "Signatures of Anisotropic Diffusion around PeVatrons in 100 TeV Gamma-Ray Data", Phys. Rev. D **106**, 123029(7pp) (2022)

[106] Kyohei Kawaguchi, Sho Fujibayashi, & Masaru Shibata, "Monte Carlo-Based Relativistic Radiation Hydrodynamics Code with a Higher-Order Scheme", Phys. Rev. D **107**, 023026(25pp) (2023)

[107] S. Jorstad, M. Wielgus, R.Lico, et al., "The Event Horizon Telescope Image of the Quasar NRAO 530", Astrophys. J. **943**, 170(19pp) (2023)

[108] J. O. Chibueze, H. Akamatsu, V. Parekh, et al., "MeerKAT's View of Double Radio Relic Galaxy Cluster Abell 3376", Pub. Astron. Soc. Japan **75**, S97-S107 (2023)

[109] Yuta Tashima, Takumi Ohmura, & Mami Machida, "Pseudo-Observation of Spiral Galaxies in the Radio Band to Verify Depolarization Models", Pub. Astron. Soc. Japan **75**, S123-S137 (2023)

[110] Hyunwook Ro, Kunwoo Yi, Yuzhu Cui, Motoki Kino, Kazuhiro Hada, Tomohisa Kawashima, Yosuke Mizuno, Bong Won Sohn, & Fumie Tazaki, "Transverse Oscillations of the M87 Jet Revealed by KaVA Observations", Galaxies **11**, 33(13pp) (2023)

[111] Tomoki Wada, & Kunihito Ioka, "Expanding Fireball in Magnetar Bursts and Fast Radio Bursts", Mon. Not. R. Astron. Soc. **519**, 4094-4109 (2023)

[112] Ataru Tanikawa, Kohei Hattori, Norita Kawanaka, Tomoya Kinugawa, Minori Shikauchi, & Daichi Tsuna, "Search for a Black Hole Binary in Gaia DR3 Astrometric Binary Stars with Spectroscopic Data", Astrophys. J. **946**, 79(11pp) (2023)

[113] X. Cheng, I. Cho, T. Kawashima, et al., "Monitoring the Size and Flux Density of Sgr A during the Active State in 2019 with East Asian VLBI Network", Galaxies **11**, 46(15pp) (2023)

[114] R.-S. Lu, K. Asada, T. P. Krichbaum, et al., "A Ring-like Accretion Structure in M87 Connecting its Black Hole and Jet", Nature **616**, 686-690 (2023)

[115] O. Adriani, Y. Akaike, K. Asano, et al., "Direct Measurement of the Cosmic-Ray Helium Spectrum from 40 GeV to 250 TeV with the Calorimetric Electron Telescope on the International Space Station", Phys. Rev. Lett. **130**, 171002(8pp) (2023)

[116] O. Adriani, Y. Akaike, K. Asano, et al., "Charge-Sign Dependent Cosmic-Ray Modulation Observed with the Calorimetric Electron Telescope on the International Space Station", Phys. Rev. Lett. **130**, 211001(6pp) (2023) Erratum: **131**, 109902(E)(2pp) (2023)

[117] H. Ro, M. Kino, B.-W. Sohn, et al., "Spectral Analysis of a Parsec-Scale Jet in M87: Observational Constraint on the Magnetic Field Strengths in the Jet", Astron. & Astrophys. **673**, A159(16pp) (2023)

[118] Tomohisa Kawashima, Ken Ohsuga, & Hiroyuki R. Takahashi, "RAIKOU: A General Relativistic, Multi-wavelength Radiative Transfer Code", Astrophys. J. **949**, 101(30pp) (2023)

[119] B. S. Prather, J. Dexter, M. Moscibrodzka, et al., "Comparison of Polarized Radiative Transfer Codes Used by the EHT Collaboration", Astrophys. J. **950**, 35(23pp) (2023)

[120] Takumi Ohmura, Katsuaki Asano, Kosuke Nishiwaki, Mami Machida, & Haruka Sakemi, "Nonthermal Emissions from a Head-Tail Radio Galaxy in 3D Magnetohydrodynamic Simulations", Astrophys. J. **951**, 76(12pp) (2023)

[121] Kosuke Nishiwaki, Katsuaki Asano, & Kohta Murase, "High-Energy Neutrino Constraints on Cosmic-Ray Reacceleration in Radio Halos of Massive Galaxy Clusters", Astrophys. J. **954**, 188(9pp) (2023)

[122] Y. Cui, K. Hada, T. Kawashima, et al., "Precessing Jet Nozzle Connecting to a Spinning Black Hole in M87", Nature **621**, 711-715 (2023)

[123] Shogo B. Kobayashi, Hirofumi Noda, Teruaki Enoto, Tomohisa Kawashima, Akihiro Inoue, & Ken Ohsuga, "Decomposing the Spectrum of Ultraluminous X-Ray Pulsar NGC 300 ULX-1", Astrophys. J. **955**, 124(21pp) (2023)

[124] K. Akiyama, A. Alberdi, W. Alef, et al., "First M87 Event Horizon Telescope Results. IX. Detection of Near-horizon Circular Polarization", Astrophys. J. Lett. **957**, L20(42pp) (2023)

[125] O. Adriani, Y. Akaike, K. Asano, et al., "Direct Measurement of the Spectral Structure of Cosmic-Ray Electrons + Positrons in the TeV Region with CALET on the International Space Station", Phys. Rev. Lett. **131**, 191001(7pp) (2023)

[126] Yo Kusafuka, Katsuaki Asano, Takumi Ohmura, & Tomohisa Kawashima, "Dynamical Energy Dissipation of Relativistic Magnetic Bullets", Mon. Not. R. Astron. Soc. **526**, 512-522 (2023)

[127] Takumi Ohmura, & Mami Machida, "Simulations of Two-Temperature Jets in Galaxy Clusters — I. Effect of Jet Magnetization on Dynamics and Electron Heating", Astron. & Astrophys. **679**, A160(19pp) (2023)

[128] Takumi Ohmura, Mami Machida, & Hiroki Akamatsu, "Simulations of two-temperature jets in galaxy clusters — II. X-Ray Properties of the Forward Shock", Astron. & Astrophys. **679**, A161(15pp) (2023)

[129] P. Torne, K. Liu, R. P. Eatough, et al., "A Search for Pulsars around Sgr A* in the First Event Horizon Telescope Data Set", Astrophys. J. **959**, 14(27pp) (2023)

[130] Kosuke Nishiwaki, Gianfranco Brunetti, Franco Vazza, & Claudio Gheller, "Efficiency of Turbulent Reacceleration by Solenoidal Turbulence and its Application to the Origin of Radio Megahalos in Cluster Outskirts", Astrophys. J. **961**, 15(12pp) (2024)

[131] H. Abe, S. Abe, V. A. Acciari, et al., "MAGIC detection of GRB 201216C at $z = 1.1$", Mon. Not. R. Astron. Soc. **527**, 5856-5867 (2024)

[132] M. Arimoto, K. Asano, K. S. Kawabata, et al., "Gamma Rays from a Reverse Shock with Turbulent Magnetic Fields in GRB 180720B", Nature Astron. **8**, 134-144 (2024)

[133] K. Akiyama, A. Alberdi, W. Alef, et al., "The Persistent Shadow of the Supermassive Black Hole of M 87 I. Observations, Calibration, Imaging, and Analysis", Astron. & Astrophys. **681**, A79(63pp) (2024)

[134] Jiro Shimoda, Shu-ichiro Inutsuka, & Masahiro Nagashima, "The History of the Milky Way: The Evolution of Star Formation, Cosmic Rays, Metallicity, and Stellar Dynamics over Cosmic Time", Pub. Astron. Soc. Japan **76**, 81-97 (2024)

[135] G. F. Paraschos, J.-Y. Kim, M. Wielgus, et al., "Ordered Magnetic Fields around the 3C 84 Central Black Hole", Astron. & Astrophys. **682**, L3(15pp) (2024)

[136] Ryota Goto, & Katsuaki Asano, "Radiation Process in Relativistic MHD Waves: The Case of Circularly Polarized Alfvén Waves", Astrophys. J. **965**, 178(9pp) (2024)

[137] Kensuke Kakiuchi, Takeru K. Suzuki, Shu-ichiro Inutsuka, Tsuyoshi Inoue, & Jiro Shimoda, "MHD Simulation in Galactic Center Region with Radiative Cooling and Heating", Astrophys. J. **966**, 230(19pp) (2024)

[138] Taichi Igarashi, Hiroyuki R. Takahashi, Tomohisa Kawashima, Ken Ohsuga, Yosuke Matsumoto, & Ryoji Matsumoto, "Radiation MHD Simulations of Soft X-ray Emitting Regions in Changing Look AGN", Astrophys. J. **968**, 121(15pp) (2024)

[139] Naoki Ogino, Makoto Arimoto, Hamid Hamidani, Takanori Sakamoto, Daisuke Yonetoku, Tatsuya Sawano, Motoko Serino, Katsuaki Asano, & Nobuyuki Kawai, "Possible X-Ray Cocoon Emission from GRB 050709", Pub. Astron. Soc. Japan **76**, 550-559 (2024)

[140] Hiroki Kawashimo, Ryo Sawada, Yudai Suwa, Takashi J. Moriya, Ataru Tanikawa, & Nozomu Tominaga, "Impacts of the ^{12}C(α,γ)^{16}O Reaction Rate on ^{56}Ni Nucleosynthesis in Pair-Instability Supernovae", Mon. Not. R. Astron. Soc. **531**, 2786-2801 (2024)

[141] Kanji Morikawa, Yutaka Ohira, & Takumi Ohmura, "Particle Acceleration and Magnetic Field Amplification by Relativistic Shocks in Inhomogeneous Media", Astrophys. J. Lett. **969**, L1(6pp) (2024)

[142] Taiki Ogihara, Tomohisa Kawashima, & Ken Ohsuga, "Radio Images inside Highly Magnetized Jet Funnels Based on Semianalytic GRMHD Models", Astrophys. J. **969**, 22(11pp) (2024)

[143] Kai Matsunaga, Hiroyuki Uchida, Rei Enokiya, Toshiki Sato, Ryo Sawada, Hideyuki Umeda, Takuto Narita, & Takeshi Go Tsuru, "Progenitor Constraint-Incorporating Shell Merger: The Case of Supernova Remnant G359.0—0.9", Astrophys. J. **970**, 4(8pp) (2024)

[144] Katsuaki Asano, "Multiwavelength Modeling for the Shallow Decay Phase of Gamma-Ray Burst Afterglows", Astrophys. J. **970**, 141(8pp) (2024)

[145] Tomoki Wada, & Jiro Shimoda, "The Dzhanibekov Effect as a Possible Source of Magnetar Activity", Astrophys. J. **972**, 58(6pp) (2024)

[146] Jiro Shimoda, & Katsuaki Asano, "Fermi and eROSITA Bubbles as Persistent Structures of the Milky Way Galaxy", arxiv:2403.18474, accepted for Astrophys. J.

[147] Shogo Yoshioka, Shin Mineshige, Ken Ohsuga, Tomohisa Kawashima, & Takaaki Kitaki, “Radiation and Outflow Properties of Super-Eddington Accretion Flows around Various Mass Classes of Black Holes: Dependence on the Accretion Rates”, arxiv:2407.15927, accepted for Pub. Astron. Soc. Japan

[148] Tomoki Wada, & Katsuaki Asano, “Radiative Acceleration and X-ray Spectrum of Outflowing Pure Electron-Positron Pair Fireball in Magnetar Bursts”, arxiv:2403.17668, submitted to Astrophys. J.

[149] J. C. Algaba, M. Balković, S. Chandra, et al., “Broadband Multi-Wavelength Properties of M87 during the 2018 EHT Campaign including a Very High Energy Flaring Episode”, arxiv:2404.17623, submitted to Astron. & Astrophys.

[150] Yo Kusafuka, & Katsuaki Asano, “Ejecta Width and Magnetization Reflected in Gamma-Ray Burst Early Afterglows: Implication for Reverse Shock Component and Shallow Decay Phase”, arxiv:2408.10750, submitted to Mon. Not. R. Astron. Soc.

[151] Kosuke Nishiwaki, & Katsuaki Asano, “Low Injection Rate of Cosmic-Ray Protons in the Turbulent Reacceleration Model of Radio Halos in Galaxy Clusters”, arxiv:2408.13846, submitted to Astrophys. J.

ASTROPHYSICS AND GRAVITY DIVISION

KAGRA GROUP

Introduction

KAGRA[16, 17, 22, 88] is one of km-scale gravitational wave(GW) telescopes that form an international GWs detection network with two Advanced LIGO and one Advanced Virgo GW telescope. In addition to many sensitivity enhancement technologies that are generally utilized in these detectors, KAGRA introduces cryogenic mirror technology and low seismic noise underground environment[42] that are both regarded as the possible technologies to realize the third generation GW telescopes' sensitivities that are designed to be about 10 times better than the present GW telescopes. The KAGRA project started in 2010, and the designed configuration of KAGRA was mostly finished in 2019 spring after several operations as an interferometer with simpler configurations from 2016 to 2018. Finally, KAGRA started its GW observation in 2020 and realized international GW observation with GEO600 (O3GK) in April 2020, and also started the fourth LIGO-Virgo-KAGRA(LVK) international observing run (O4) in 2023.

Summary from 2018 to 2024

• Finalization of installation, except for the output mode cleaner(OMC) and some optical baffles, from April 2018 to May 2019.

• Commissioning for the third LVK International observing run (O3) including OMC installation. 1 Mpc binary neutron star (BNS) merger range sensitivity realization, from May 2019 to March 2020. MoU signed with LIGO and Virgo on data sharing and network detection of GWs in October 2019.

• International GW observation with GEO600 as O3GK in April 2020.

• Many upgrades and repairs for KAGRA, including mid-size baffles installation, from May 2020 to around June 2022.

• Commissioning for the fourth LVK international observing run (O4), targeting $1 \sim 3$ Mpc BNS range sensitivity, from July 2022 to May 2024.

• O4 for KAGRA with ~ 1.3 Mpc BNS range sensitivity, from May 24th to June 21st, 2023. LV performed the first half of the fourth LVK international observing run (O4a) until the middle of January 2024. (Later, the end of O4 was reset on June 9th, 2025.)

• Commissioning for the better BNS range sensitivity to join the second half of the fourth LVK international observing run (O4b), from July 2023 to December 2023.

• Damages on mainly 10 seismic noise isolators by Noto-Peninsula earthquakes. Recovery from January 2024.

Commissioning for O3 and O3GK Observation

Commissioning

KAGRA was operated as a simple Michelson Interferometer whose one of the end test masses was at the cryogenic temperature in April and May 2018[8]. Almost all designed components were installed in April 2019. Fig. 1 shows the KAGRA optical configuration and mirror suspension and seismic noise isolators. After that, commissioning started to realize Dual-Recycled Fabry-Perot Michelson Interferometer (DRFPMI) operation as a GW telescope with the targeted binary neutron star (BNS) merger range sensitivity of $8\sim25$ Mpc, which is defined as the distance where GWs signal from binary neutron star merger events can be detected with a signal-to-noise ratio of 8. In July, the Y-arm FP cavity resonance control was done, while the X-arm FP cavity was already done in January 2019. Finally, the FPMI operation was done in August 2019, and the first displacement noise was obtained as shown in Fig. 2. Although cooling for all mirrors was done until August 2019, we gave up cooling mirrors because frosting phenomena on mirror surfaces and some optical windows on radiation shields happened several times, and also because the time for commissioning was wasted at the weekly level to remove the frosted material[5]. To avoid frosting on mirrors and to keep a better vacuum level of 10^{-6} Pa around cryostats, we decided to keep cooling only the 5-meter radiation duct shields at $\sim$100 K. Because of radiation cooling with these cooled radiation duct shields, the temperature of sapphire mirrors became $\sim$250 K[21].

Although DRFPMI was the designed configuration as a GW telescope for KAGRA, the Power-Recycled Fabry-Perot Michelson Interferometer(PRFPMI) step was inserted to reach DRFPMI from FPMI according to advice from the KAGRA program advisory board recommendation from August 2019. For this purpose, the Signal Recycling Mirror(SRM) was misaligned so as not to disturb PRFPMI performance even if it resulted in less available laser power. We not only developed the interferometer control scheme[13] and automation but also optimized the digital control filters to mitigate mirror motions at many pendulum resonance modes in seismic noise isolators[24]. We also tuned the pitch/yaw decoupling for precise actuation of mirrors along the optical axis. For the reliable GW signal selections, many physical environmental sensors (accelerometers, seismometers, microphones, thermometers, humidity meters, barometers, magnetic field sensors, lightning monitor system[38], etc.) were prepared. In parallel, we prepared some readiness items, such as offline computing coordination, calibration, state vector information, low/high-latency data transfer of KAGRA data to Caltech/Virgo, a DQ segment database, the webpage to see the interferometer information, and a rapid response team for joining O3.

Finally, PRFPMI operation was successfully realized at the end of January 2020, and more optimization of the control

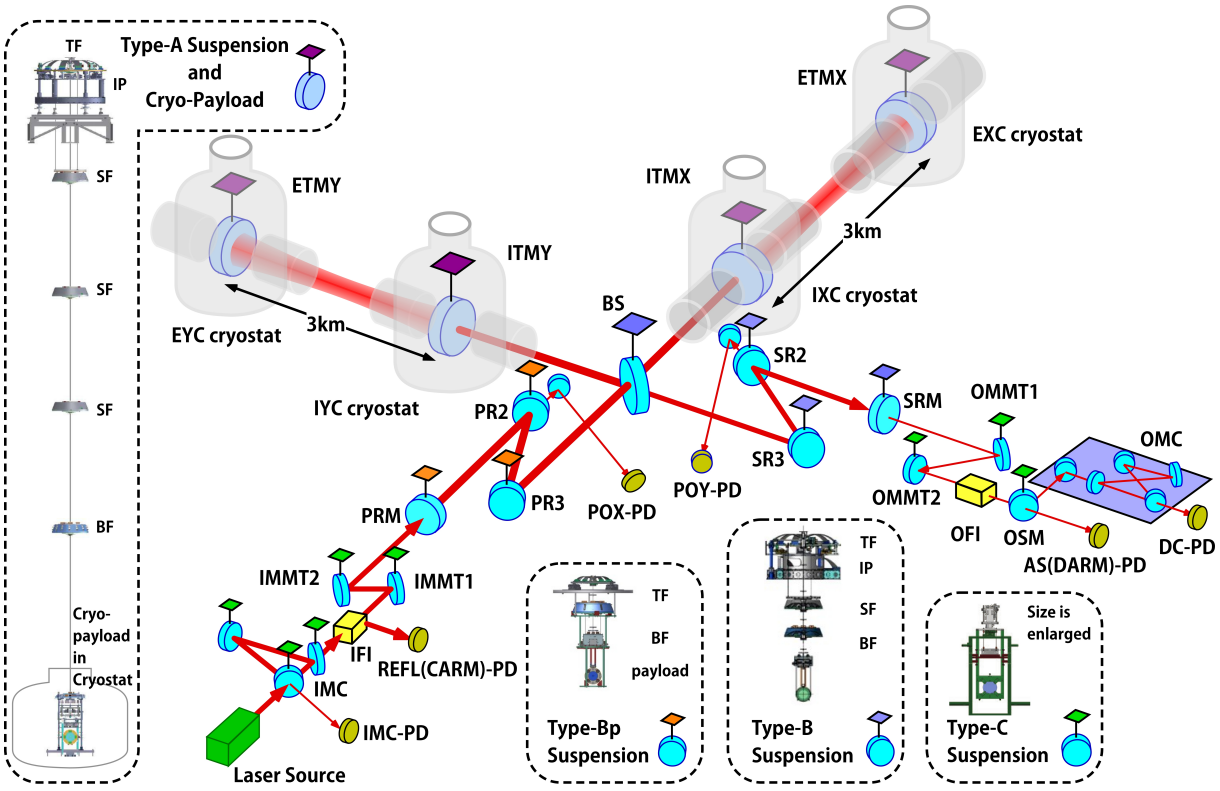

Fig. 1. Optical configuration of KAGRA and seismic noise isolators for optical components. IMC: Input mode cleaner; IFI: Input Faraday isolator; IMMT(1/2): Input mode matching telescope 1,2; PR(M/2/3): Power recycling mirror, 2,3; BS: Beam splitter; SR(M/2/3): Signal recycling mirror, 2, 3; (I/E)TM(X/Y): Input/End test mass in X/Y arm; OMMT(1/2): Output mode matching telescope 1, 2; OSM: Output steering mirror; OFI: Output Faraday isolator; OMC: Output mode cleaner; IMC/REFL/PO(X/Y)/AS/DC-PD: Input mode cleaner/Reflection port/Pick off for X/Y arm/Anti-symmetric port/DC readout Photodetector. Four types of seismic noise isolators in KAGRA are also shown in a dotted square area as Type-A including a cryo-payload, Type-B, Type-Bp, and Type-C, denoted by violet, blue, orange, and green rhombus. TF: Top Filter; IP: Inverted pendulum; SF: Standard filter: BF: Bottom filter. KAGRA utilizes a power-recycled Fabry-Perot Michelson interferometer with resonant sideband extraction and DC readout techniques as GW telescopes. This style is common among Advanced LIGO and Advanced Virgo. The frequency-dependent squeezed light with a filter cavity will be introduced to reduce radiation pressure noise and shot noise in the future. (I/E)TM(X/Y) are housed in (I/E)(X/Y)C cryostat, respectively.

filters, a shift to the DC readout technique, and noise identification that collaborated with physical environmental monitor tools resulted in ∼100 times better sensitivity (∼220 kpc) than the best in the FPMI configuration. The recycling gain was estimated at around 11, which was near the designed value of 10. A mirror alignment control using the dither system was also introduced for the longer continuous operation, and the sensor correction technique was also introduced to mitigate the micro-seismic noise due to the violent ocean condition. Some "noise hunting" activities resulted in sensitivity enhancement up to 590 kpc mainly due to displacement noise reduction around 200 Hz by the introduction of the feedforward of Michelson Interferometer part control signals. The longest continuous lock was ∼9 hours, however, the violent ocean condition sometimes stopped KAGRA operation due to the failure of lock acquisition of the FP cavity arms. From March 11th to April 6th, 2020, more optimization of optical axes and/or beam spots on mirrors, noise contribution checks from the frequency and intensity noise, and more noise hunting were done. Finally, 1 Mpc BNS range sensitivity was realized in March 2020. The sensitivity improvement history according to date and the interferometer configurations was summarized in Fig. 2.

Overview of O3GK Observing run

In October 2019, KAGRA signed a Memorandum of Agreement (MoA) between LIGO and Virgo. The MoA defines the policy of the joint observing run, data analysis, and data sharing. KAGRA intended to perform a joint observing run with LIGO and Virgo detectors during O3. However, while KAGRA was preparing the observing run, the LIGO and Virgo detectors were forced to terminate operations on March 27th, 2020 due to the COVID-19 pandemic. On the other hand, GEO600 in Germany was operated and continuously taking data. Thus, GEO600 and KAGRA decided to perform an observing run jointly. In the LVK collaboration, this observation was officially approved as a joint observing run under the LVK framework and was named O3GK[94].

The O3GK joint observing run was performed between April 7th, 2020 08:00 (UTC) and April 21st, 2020 00:00 (UTC). The total observation time with the science mode of the detector was 10.9 days for GEO600 and 7.29 days for KAGRA. The duty cycle was 79.8% and 53.3% for GEO600 and KAGRA respectively. The median of the average observable distance of the binary neutron star coalescence was 1.06 Mpc and 0.66 Mpc for GEO600 and KAGRA respectively. The relatively low duty cycle of KAGRA was due to bad weather

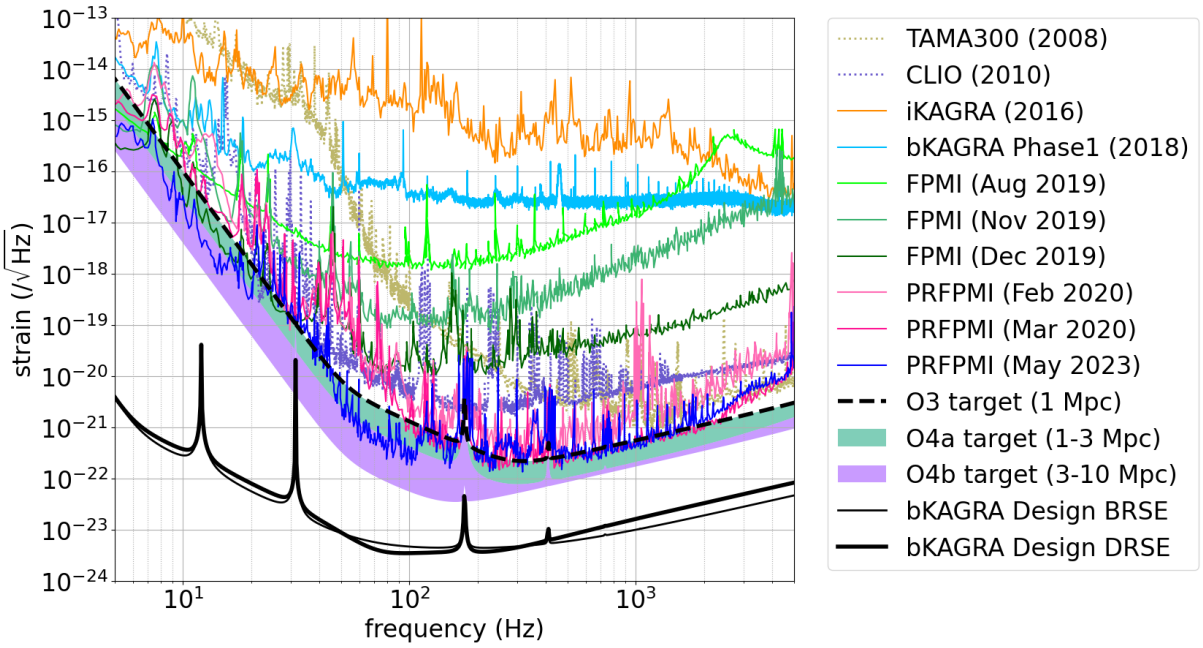

Fig. 2. KAGRA strain sensitivity improvement towards O3, according to date and the interferometer configurations. The sensitivities of TAMA300 and CLIO which are the proto-types for KAGRA are also listed as one of the references. The sensitivity in O4a and the target sensitivity for O3(Black bold dashed line), O4a(Grenn area), and O4b(Violet area) are also references. Two ultimate sensitivities of KAGRA are listed assuming broadband resonant sideband extraction (BRSE) case and detuned RSE case(DRSE).

conditions caused by a low-pressure system passing through Japan around April 13th and 14th. While the quiet underground environment of KAGRA provides advantages in the operation of the instrument, KAGRA is not completely free from the effects of bad weather. The nearest coastline is approximately 40 km away. Ocean waves crashing on the shoreline constantly excite ground vibrations around 0.2 Hz, which becomes about one order of magnitude stronger during storms, and it becomes difficult to operate the interferometer.

Following the joint run, the vibration isolation control system has been improved, and additional environmental monitors and the wavefront sensor system have been installed. The duty cycle of KAGRA was improved after that.

Fig.3 represents the noise amplitude spectral density of GEO (black) and KAGRA (yellow) during the O3GK run. Narrow peaks in the spectra are due to such sources as resonances of the suspension system (violin modes) and harmonics of the electrical grid frequency (50 Hz for GEO and 60 Hz for KAGRA). Fig.4 represents the detectable distance of the inspiral of binary neutron stars (BNS).

Overview of the results of data analysis

Several GW event searches were performed. Those include all-sky searches for binary neutron star coalescences by using the GstLAL pipeline, all-sky searches for unmodeled short-duration burst waves with the coherent WaveBurst pipeline, targeted Compact Binary Coalescence (CBC) searches associated with short Gamma Ray Bursts (GRBs) by using pyGRB pipeline, and targeted un-modeled burst searches associated with short and long GRBs by using X-pipeline. No candidate GW events were identified.

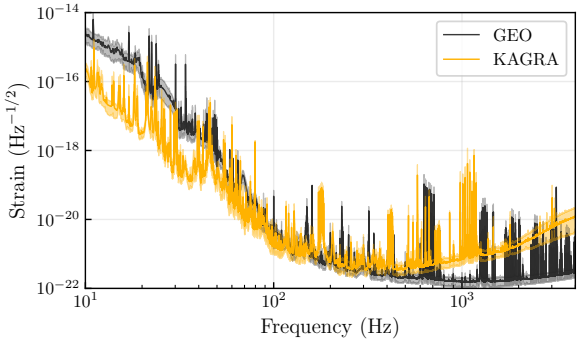

Fig. 3. Noise amplitude spectral density of GEO (black) and KAGRA (yellow) during O3GK run.

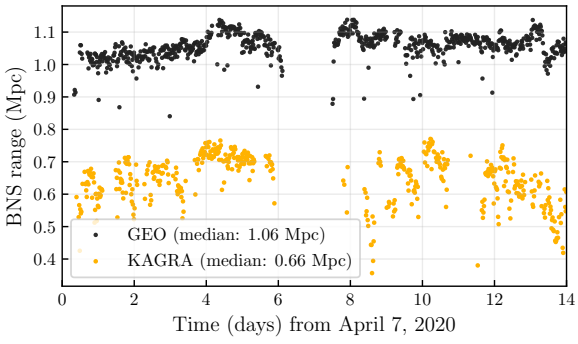

Fig. 4. BNS inspiral ranges for GEO and KAGRA during O3GK run.

Table 1. GRBs observed during O3GK run times when both detectors were taking science-quality data.

GRB Name	Data Source	Type	Analysis
200412A	*Fermi*-GBM	Long	`X-Pipeline`
200415A	*Fermi*-GBM, IPN	Short	`X-Pipeline` & `PyGRB`
200418A	*Fermi*-GBM	Long	`X-Pipeline`
200420A	*Fermi*-GBM	Short	`X-Pipeline` & `PyGRB`

The GRB events analyzed are listed in Table 1. Among them, a short GRB, GRB 200415A, was subsequently associated with a magnetar giant flare in the nearby galaxy NGC253 at 3.5 Mpc based on its sky position, temporal and spectral properties, and its inferred energy, and it was especially interesting to search for GW signals associated with this GRB. However, we could not constrain the progenitor of this GRB from the analysis of the O3GK data.

The lack of detected events in this observing run is expected given the sensitivity of the GEO–KAGRA network at the time. However, the sensitivity of KAGRA is expected to improve by more than two orders of magnitude later in this decade, becoming comparable to that of the LIGO and Virgo detectors. Our analyses have demonstrated the ability to incorporate KAGRA data into standard transient search pipelines that have been used to detect GWs in LIGO and Virgo data.

These results were published in PTEP[56]. The O3GK data was publicly released at the GWOSC site (`https://doi.org/10.7935/38s2-7g84`).

Commissioning for O4 and O4 Observation

Commissioning

After the O3GK, almost all vacuum chambers were vented and the suspensions were upgraded to solve problems we learned from the commissioning before O3GK. Room temperature suspensions (named Type-A tower) of ETMY were once deconstructed and reinstalled to tune the vertical vibration isolation filters. In addition, new accelerometers for inertial damping controls are installed on the top of the Type-A towers to improve the stability of lock acquisition and observation. New optical sensors are installed on cryogenic sapphire mirror suspensions (called cryogenic payload[26]) to improve the sensitivity. Actuators of the cryogenic payloads are newly designed to improve the stability of the interferometer. Since we adapted PRFPMI for the interferometer configuration in the fourth LVK international observing run (O4), the SRM mirror was swapped to the anti-reflection coating mirror to avoid the loss of GW signals, while it was 70% reflection mirror during O3GK.

Other than the suspension upgrades, we newly installed baffles (named mid-size baffles) in front of the mirrors at the corner station to mitigate the scattered light noise. In addition, some beam dumpers were also additionally installed to dump the unwanted stray lights. Characterization and installation of a new high-power laser for increasing laser power injected into the interferometer have proceeded though the new high-power laser was not used during O4. The mirrors of OMC were replaced with new ones to improve the performance of OMC. A phase noise cancellation system was newly installed into the auxiliary locking system to improve the stability of lock acquisition of the interferometer.

A mirror cooling scheme was also established during the commissioning period to cool the sapphire mirrors to below 100 K without severe frosting which significantly reduced arm finesse and disturbed interferometer locking. Vacuum evacuation continued for over 3 weeks with turbo molecular pumps to reduce the residual water molecules inside the cryostat. Duct shield cooling was initiated and continued until the duct shields were completely cooled. After the duct shield cooling, the radiation shields were cooled to further trap the residual gas molecules such as water, nitrogen, and oxygen. Thanks to the new schemes, ETMX can maintain the temperature of 90 K for more than one year without any significant degradation of the X-arm cavity finesse. In addition, the vibration of cryostats was also investigated at the cryogenic temperature for better noise budgets in the KAGRA sensitivity[61, 66].

FPMI was recovered with the upgraded hardware in August 2022, and PRFPMI was restored in February 2023. After recovery of the interferometer, control optimization, feedforward, and environmental noise reduction were performed to improve the sensitivity as was done during the O3 commissioning. After the known noise hunting, Alignment Sensing and Control (ASC) was implemented to stabilize the interferometer. Wave Front Sensing (WFS) was implemented to control BS, ETMX, and ETMY, but it was difficult in O3GK. Alignment Dither System (ADS) was implemented for PRM and IMMT2 to better maintain of PRMI alignment. In addition, we implemented Beam Position Control (BPC) to PR2, ITMX, and ITMY to keep the beam spot on PR2, ETMX, and ETMY. For the OMC alignment, a new alignment scheme (called Beacon WFS control) was established and it improved the KAGRA's sensitivity and stability. Thanks to these ASCs, 1.5 Mpc of BNS range sensitivity was achieved in May 2023.

In parallel, the frequency-dependent squeezing demonstration using the 300m Fabry-Perot cavity as a filter cavity in TAMA300 at NAOJ was successfully done[55] for the future KAGRA upgrade.

O4a Observation

Observation Status

O4 started from 15:00 (UTC) on May 24th, 2023. O4 is divided into two periods with a two-month commissioning break between them. The former period is named O4a and the latter O4b. KAGRA joined the observation as O4a from the first[99]. Although other detectors continued observing run until the end of O4a (16:00 (UTC) on the 16 of January 2024), KAGRA stopped the observing run at 23:00 (UTC) on 20 June 20, 2023 in order to restart the commissioning to improve the sensitivity toward O4b.

The average BNS range of KAGRA during O4a is 1.3 ± 0.1 Mpc, which is two times better than that in O3GK. The duty factor of KAGRA in O4a is 82%, which is significantly higher than that during O3GK (53%). Fig.5 shows the BNS range and the duty factors during the KAGRA observing run in O4a. The longest lock duration is 21.5 hours and the main

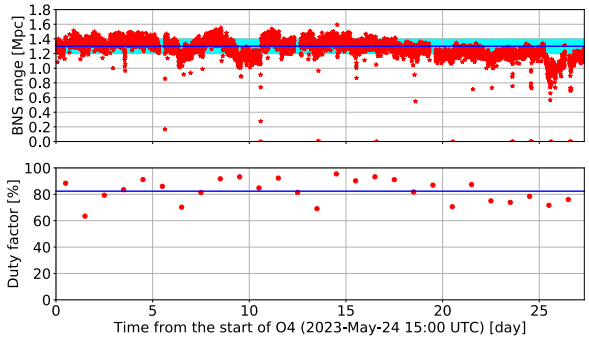

Fig. 5. BNS range (top) and duty factor (bottom) during KAGRA observing run in O4a. The blue line in each graph shows the average of the BNS range and the duty factor. The Cyan area shows the uncertainty of the averaged BNS range.

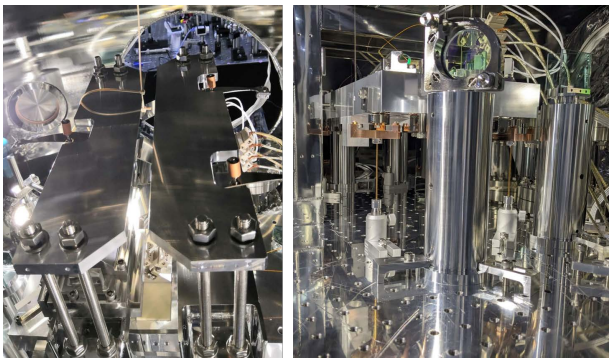

Fig. 6. Photos of newly installed eddy current dampers. The left photo shows the damper on the OMC suspension to damp the bounce mode of the blade spring. The right photo shows the damper below the OMC suspension to damp the pendulum mode of the OMC suspension.

reason for the observation downtime was caused by the earthquakes. Compared with O3GK, the interferometer condition is significantly improved.

O4 KAGRA detection paper

The expected observable distance of BNS by KAGRA at O4b is at most 10 Mpc, and the event rate is not large. However, if we use the information of BBH events observed by LIGO and Virgo, like coalescence time and masses, the probability of finding BBH signals in KAGRA data can be increased significantly. Thus, there might be some possibilities that we can observe the signature of nearby BBH events in KAGRA data during O4b with such a strategy. We have already proposed the O4 KAGRA detection paper as one of the LVK full-collaboration paper plans in O4. A dedicated pipeline that uses a Bayesian method and aims the detection of signals in KAGRA data has been developed. It has been demonstrated with simulated data that the detection efficiency of this new pipeline is better than the usual matched filtering method. We will finalize the development and test of the new pipeline soon and will proceed to the code review and will be stand-by for the O4b observing run of KAGRA.

When KAGRA joins the LVK detector network, we expect that parameter estimation accuracy, especially the accuracy of source localization will be improved. Thus, parameter estimation is also an important data analysis task. We plan to use `Bilby` pipeline which is the current main parameter estimation pipeline of LVK. We have already analyzed 3 BBH events that were observed by LIGO and were also involved in the KAGRA operation time during the KAGRA O4a run and checked whether we had any improvement of the sky-localization when we added KAGRA data to LIGO data. We plan to perform the same analysis for O4b data.

Post O4a commissioning

After O4a, noise budgeting of the interferometer was performed. All payload control noise was projected into the KAGRA sensitivity, and it was confirmed that the longitudinal local damping control of ITMX and ETMX and the angular damping control of BS and SR3 limited the sensitivity at low frequencies. It was also confirmed that the axial Length Sensing and Control (LSC), power recycling cavity, and Michelson interferometer length controls, are coupled to the KAGRA sensitivity at low frequency. The laser intensity noise, frequency noise, PD dark noise, and shot noise were also projected into the KAGRA sensitivity, and it was confirmed that the PD dark noise, shot noise, and frequency noise limited the sensitivity at high frequencies. On the other hand, the laser intensity noise was well below the sensitivity during O4a, Vibration analysis at several locations in KAGRA was also performed by acoustic injection and it was revealed that the KAGRA sensitivity were sensitive to the vibration around OMC, which limited the sensitivity around 100 Hz. Thermal noise, which was estimated from the quality factors of sapphire mirrors and fibers in practical sapphire mirror suspensions, was also projected into the KAGRA sensitivity.

After completing the noise budget during O4a, ASC of both arms was updated. The WFS signals were fed back to the Differential HARD (DHARD) and Common HARD (CHARD), while the SOFT modes [1] of both arms were controlled independently with the DC Quadrant Photo Detector(QPD)s on both transmission ports. Thanks to the new ASC scheme, intracavity power became more stable and PRFPMI lock with 5 W IMC output could be achieved with RF signals to reduce the shot noise and PRCL/MICH control noise. In addition, the OMC vacuum tank was opened once, and stray light dumpers were installed. In addition, eddy current dampers for the OMC suspensions were newly installed on and below the OMC suspension to reduce the vibration coupling around OMC (Fig. 6).

*[1] An interferometric GW detector has two orthogonal arms, each equipped with an optical cavity consisting of two mirrors. If the mirror tilts, the cavity's internal optical axis exhibits translational(SOFT mode) or tilt(HARD mode) motions. So, the optical axis motion can be considered angular degrees of freedom. Since the interferometer output naturally separates into common and differential modes, angular degrees of freedom are conventionally expressed using the common and differential modes of the optical axis motion (tilt and translation). In KAGRA, the mode where the light reflected from the two arms converges at the same position on the beam splitter is called common, while the mode where it converges at different positions is called differential.

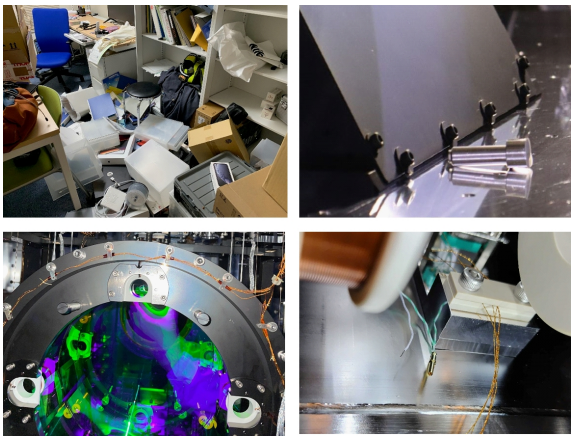

Fig. 7. Damages by the Noto-Peninsula Earthquake. Top-left: Scattering in a room in the KAGRA Data Analysis Building. Top-right: Dropped-off magnet in PRM vacuum tank, Bottom-left: All magnets dropped off from Y end test mass, Bottom-right: Wire cut due to collision among components in the suspension.

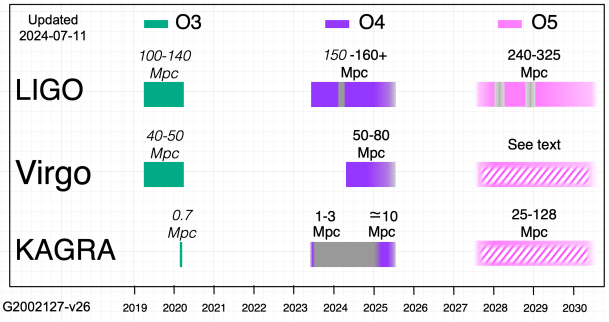

Fig. 8. LVK Observation Run Plans.

Recovery from the Noto-Peninsula earthquake

On January 1st, 2024, a 7.6 magnitude earthquake struck near the KAGRA site, marking the most significant seismic tremor in the area of the KAGRA site in the past century. According to the data of Geophysical Information Authority of Japan, the whole mountain that housed KAGRA was measured to move towards the north-northwest (roughly along the Y-arm of KAGRA) by 2∼3 cm. The X-arm of KAGRA was estimated to be shrunk by ∼0.3 mm, while the Y-arm extended by ∼1.6 mm. The angle between X and Y arms was estimated to decrease by 5×10^{-7} rad from 90 degrees.

Although the Japanese earthquake scale of five minus on the surface in the Hida-city area was attenuated to three at the underground area of KAGRA, 10 of 20 mirror suspension and seismic noise isolation systems were damaged, and we needed to vent and open all vacuum chambers and ducts, except for both 3-km arm parts. Most of the damage was the drop-off of magnets from mirrors (Fig. 7). Some cuts of cables due to strikes by suspension components were found. We also noticed large relative alignment changes of suspended parts inside the suspension maybe due to slipping of suspending wires at their clamping positions. Glitches in some photo-sensors' signals were also observed maybe because of kink-like damages in the thin signal cables by shakings. The recovery works started just after the disaster in January 2024. Finally, repair for the mechanical part in all seismic noise isolators was completed in July 2024, and we started the recovery of the PRFPMI configuration for commissioning.

LVK Observing Run Plans

Fig. 8 shows the LVK observation run plans including the 5th Observing run(O5). Although O5 is planned to start in 2027, the actual start will depend on the preparation status of LVK in the future. KAGRA plans to start O5 with LV with the BNS range sensitivity of 25 Mpc∼128 Mpc. For O5, KAGRA has several upgrade plans. One is the replacement of ITMs that have less birefringence and equal reflectances. Especially, the equal reflectances will contribute to a better common mode reduction ratio(CMMR), resulting in a smaller laser frequency noise contribution, etc. Another is replacing the seismic noise isolation structure for OMC with a better one. More upgrade plans are also being discussed for O5. In addition, a 10-year plan is also being discussed in KAGRA.

KAGRA Collaboration

Institute	Country	(*)
ICRR, Univ. of Tokyo(UT)	Japan	38
NAOJ	Japan	26
KEK	Japan	12
School of Science, UT	Japan	23
Univ. of Toyama	Japan	18
Earthquake Research Inst., UT	Japan	2
Kavli IPMU, UT	Japan	2
School of Arts and Science, UT	Japan	2
Osaka Metropolitan Univ.	Japan	17
Niigata Univ.	Japan	10
Tokyo Inst. of Technology	Japan	13
Univ. of Electro-Communications	Japan	3
Tokyo City Univ.	Japan	2
National Defense Academy	Japan	1
JAXA	Japan	1
National Inst. of Advanced Industrial and Science Tech.	Japan	1
National Inst. of Information and Communications Tech.	Japan	1
Inst. of Statistical Mathematics	Japan	1
Aoyama Univ.	Japan	15
Sokendai	Japan	1
Hosei Univ.	Japan	1
Waseda Univ.	Japan	1
Toho Univ.	Japan	1
Nihon Univ.	Japan	1
Chiba Inst. of Technology	Japan	1
RIKEN	Japan	3
Univ. of Tsukuba	Japan	1
Shinshu Univ.	Japan	1
Inst. for Molecular Science	Japan	1
Nagoya Univ.	Japan	3
National Inst. for Fusion Science	Japan	1
Osaka Univ.	Japan	2
Osaka Inst. of Technology	Japan	1
Kyoto Univ.	Japan	5
Ryukoku Univ.	Japan	1
Hiroshima Univ.	Japan	2
Fukuoka Univ.	Japan	4
Hirosaki Univ.	Japan	1
Univ. of the Ryukyus	Japan	2
Kanazawa Medical Univ.	Japan	1
National College of Tech., Nagaoka	Japan	2
National College of Tech., Fukui	Japan	1
Universite catholique de Louvain	Belgium	1
Beijing Normal Univ.	China	21
APM, Chinese Academy of Sci.	China	9
Chinese Academy of Sciences	China	8
NAO, Chinese Academic of Sci.	China	7
Wuhan Univ.	China	6
Peking Univ.	China	4
The Chinese Univ. of Hong Kong	China	4
Shanghai Normal Univ.	China	2
Shanxi Datong Univ.	China	1
Duke Kunshan Univ.	China	1
Sun Yat-sen Univ.	China	1
Univ. of Chinese Academy of Sci.	China	1
Universite Paris Cite	France	2
Laboratoire d'Annecy de Physique des Particules	France	1
Univ. of Sannio	Italy	5
Univ. of Salerno	Italy	3
Sapienza Universita di Roma	Italy	2
Istituto Nazionale di Fisica Nucleare	Italy	1
Univ. of Perugia	Italy	1
Camerino Univ.	Italy	1
Scuola Normale Superiore Pisa	Italy	1
Univ. of Trento	Italy	1
Univ. of Padova	Italy	1
Univ. of Guadalajara	Mexico	1
Warsaw Univ. of Technology	Poland	1
Korea Astronomy and Space Science Inst.	Korea	9
Ulsan National Inst. of Science and Technology	Korea	4
Myongji Univ.	Korea	3
Chungnam National Univ.	Korea	3
Sejong Univ.	Korea	2
Ewha Womans Univ.	Korea	1
Hanyang Univ.	Korea	1
Inje Univ.	Korea	1
Pusan National Univ.	Korea	1
Yonsei Univ.	Korea	1
Korea Inst. of Science and Technology Information	Korea	1
National Inst. for Mathematical Sciences	Korea	1
National Tsing Hua Univ.	Taiwan	22
National Yang Ming Chiao Tung Univ.	Taiwan	9
National Cheng Kung Univ.	Taiwan	7
Tamkang Univ.	Taiwan	5
Academia Sinica	Taiwan	4
National Taiwan Normal Univ.	Taiwan	2
National Applied Research Laboratories	Taiwan	1
Industrial Tech. Research Inst.	Taiwan	1
National Central Univ.	Taiwan	1
Universidad Autonoma de Madrid	Spain	2
Cardiff Univ.	UK	1
California Inst. of Technology	USA	3
Univ. of Notre Dame	USA	2
LIGO Hanford Observatory	USA	1
Syracuse Univ.	USA	1
Univ. of Washington	USA	1
Univ. of Virginia	USA	1
Collaborator Total		405
Institute & University Total		97

(*) means 2024 data.

Members

Professor

Takaaki Kajita, Distinguished Prof., KAGRA PI,
Shinji Miyoki, KAGRA Observatory Director,
Masatake Ohashi, Hideyuki Tagoshi, Norikatsu Mio (Project),

Associate Professor

Takashi Uchiyama, Osamu Miyakawa, Takafumi Ushiba, Takahiro Sawada,

Assistant Professor

Takahiro Yamamoto, Soichiro Morisaki, Takaaki Yokozawa, Shoichi Oshino (Project), Tatsuya Narikawa (Project), Hirotaka Yuzurihara (Project),

Postdoctoral Fellows

Nami Uchikata, Darkhan Tuyenbayev, Kenta Tanaka,

Project Staff

Nobuhiro Kimura,

Past Staff

Keiko Kokeyama, Assist. Prof., to Jan. 2021
Kyohei Kawaguchi, Assist. Prof., Mar. 2018 to Mar. 2024
Yuzuru Yoshii, Project Prof., to Mar. 2022
Eiichi Hirose, Project Assist., to Mar. 2019
Yoshio Saito, Project Prof., to Mar. 2020
Yoshio Saito, Senior, Fellow, Apr. 2020 to Mar. 2022
Toshikazu Suzuki, Senior Fellow, to Mar. 2022
Ken-ichi Oohara, Senior Fellow, Apr. 2021 to Mar. 2022
Lucia Trozz, Postdoc. Fellow, Jul. 2018 to Jul. 2020
Koki Okutomi, Postdoc. Fellow, Apr. 2019 to Apr. 2020
Fabian Pena Arellano, Postdoc. Fellow, Jul. 2018 to Jul. 2021
Satoshi Tanioka, Postdoc. Fellow, Apr. 2021 to Jul. 2021
Jishnu Suresh, Postdoc. Fellow, Feb. 2019 to Sep. 2021
Miyo Koseki, Postdoc. Fellow, Apr. 2020 to Dec. 2021
Yuhang Zhao, Postdoc. Fellow, Apr. 2021 to Dec. 2022

Graduate Students

6 students were awarded doctorate degrees and 16 students earned master's degrees from 2018 to 2024, supervised by ICRR staff members.

Bibliography

[1] "On the stability of a superspinar", Ken-ichi Nakao, Pankaj S. Joshi, Jun-Qi Guo, Prashant Kocherlakota, Hideyuki Tagoshi, Tomohiro Harada, Mandar Patil, Andrzej Krolak, Physics Letters B 780, 410–413 (2018), DOI: 10.1016/j.physletb.2018.03.014

[2] "Demonstration for a two-axis interferometric tilt sensor in KAGRA", Keiko Kokeyama, June Gyu Park, Kyuman Cho, Shin Kirii, Tomotada Akutsu, Masayuki Nakanoa, Shogo Kambara, Kunihiko Hasegawa, Naoko Ohishi, Kohei Doi, Seiji Kawamura, Physics Letters A 382, 1950–1955 (2018), DOI:10.1016/j.physleta.2018.05.004

[3] "Multiwindow Nonharmonic Analysis Method for Gravitational Waves", Dongbao Jia, Kenta Yanagisawa, Yuta Ono, Kanna Hirobayashi, Masaya Hasegawa, Shigeki Hirobayashi, Hideyuki Tagoshi, Tatsuya Narikawa, Nami Uchikata, Hirotaka Takahashi, IEEE Access., 6, 48645 - 48655 (2018), DOI:10.1109/ACCESS.2018.2867494

[4] "Time–frequency-based non-harmonic analysis to reduce line-noise impact for LIGO observation system", D.Jia, K. Yanagisawa, M. Hasegawa, S. Hirobayashi, H. Tagoshi, T. Narikawa, N. Uchikata, H. Takahashi, Astronomy and Computing 25, 238–246 (2018), DOI:10.1016/j.ascom.2018.10.003

[5] "Molecular adsorbed layer formation on cooled mirrors and its impacts on cryogenic gravitational wave telescopes", Kunihiko Hasegawa, Tomotada Akutsu, Nobuhiro Kimura, Yoshio Saito, Toshikazu Suzuki, Takayuki Tomaru, Ayako Ueda, and Shinji Miyoki, Phys. Rev. D 99, 022003 (2019), DOI:10.1103/PhysRevD.99.022003

[6] "Vibration isolation system with a compact damping system for power recycling mirrors of KAGRA", Y.Akiyama et al. (KAGRA Collaboration), Class. Quantum Grav. 36 095015(2019), DOI:10.1088/1361-6382/ab0fcb

[7] "A time–frequency analysis of gravitational wave signals with non-harmonic analysis", Kenta Yanagisawa, Dongbao Jia, Shigeki Hirobayashi, Nami Uchikata, Tatsuya Narikawa, Koh Ueno, Hirotaka Takahashi, and Hideyuki Tagoshi, Prog. Theor. Exp. Phys. 2019, 063F01 (2019), DOI:10.1093/ptep/ptz043

[8] "First cryogenic test operation of underground km-scale gravitational-wave observatory KAGRA", T.Akutsu et al. (KAGRA Collaboration), Class. Quantum Grav. 36 165008(2019), DOI:10.1088/1361-6382/ab28a9

[9] "Stochastic gravitational wave background map-making using regularized deconvolution", S. Panda, S. Bhagwat, Jishnu Suresh, and S. Mitra, PHYSICAL REVIEW D 100, 043541 (2019), DOI:10.1103/PhysRevD.100.043541

[10] “Searching for black hole echoes from the LIGO-Virgo Catalog GWTC-1”, Nami Uchikata, Hiroyuki Nakano, Tatsuya Narikawa, Norichika Sago, Hideyuki Tagoshi, and Takahiro Tanaka, Phys. Rev. D 100, 062006 (2019), DOI:10.1103/PhysRevD.100.062006

[11] “Design and experimental demonstration of a laser modulation system for future gravitational-wave detectors”, Kohei Yamamoto, Keiko Kokeyama, Yuta Michimura, Yutaro Enomoto, Masayuki Nakano, Gui-Guo Ge, Tomoyuki Uehara, Kentaro Somiya, Kiwamu Izumi, Osamu Miyakawa, Takahiro Yamamoto, Takaaki Yokozawa, Yuta Fujikawa, Nobuyuki Fujii and Takaaki Kajita, Class. Quantum Grav. 36 205009 (2019), DOI:10.1088/1361-6382/ab4489

[12] “Discrepancy in tidal deformability of GW170817 between the Advanced LIGO twin detectors”, Tatsuya Narikawa, Nami Uchikata, Kyohei Kawaguchi, Kenta Kiuchi, Koutarou Kyutoku, Masaru Shibata, and Hideyuki Tagoshi, Phys. Rev. Research 1, 033055 (2019), DOI:10.1103/PhysRevResearch.1.033055

[13] “An arm length stabilization system for KAGRA and future gravitational-wave detectors”, T.Akutsu et al. (KAGRA Collaboration), Class. Quantum Grav. 37 035004(2020), DOI:10.1088/1361-6382/ab5c95

[14] “Application of the independent component analysis to the iKAGRA data”, T.Akutsu et al. (KAGRA Collaboration), Prog. Theor. Exp. Phys. 2020, 053F01 (2020) , DOI:10.1093/ptep/ptaa056

[15] ”Prospects for improving the sensitivity of the cryogenic gravitational wave detector KAGRA”, Yuta Michimura, Kentaro Komori, Yutaro Enomoto, Koji Nagano, Atsushi Nishizawa, Eiichi Hirose, Matteo Leonardi, Eleonora Capocasa, Naoki Aritomi, Yuhang Zhao, Raffaele Flaminio, Takafumi Ushiba, Tomohiro Yamada, Li-Wei Wei, Hiroki Takeda, Satoshi Tanioka, Masaki Ando, Kazuhiro Yamamoto, Kazuhiro Hayama, Sadakazu Haino, and Kentaro Somiya, PHYSICAL REVIEW D 102, 022008 (2020), DOI:10.1103/PhysRevD.102.022008

[16] “Overview of KAGRA : KAGRA science”, T Akutsu, et al.(KAGRA collaboration), Prog. Theor. Exp. Phys. 2020, 05A103 (2020), DOI:10.1093/ptep/ptaa120

[17] “Overview of KAGRA: Detector design and construction history”, T. Akutsu et al.(KAGRA collaboration), Prog. Theor. Exp. Phys. 2020, 05A101 (2020) , DOI:10.1093/ptep/ptaa125

[18] “Prospects for observing and localizing gravitational-wave transients with Advanced LIGO, Advanced Virgo and KAGRA”, B. P. Abbott, R. Abbott, et al., KAGRA Collaboration, LIGO Scientific Collaboration and Virgo Collaboration (full author paper), Living Rev Relativ 23, 3 (2020), DOI:10.1007/s41114-020-00026-9

[19] “Reanalysis of the binary neutron star mergers GW170817 and GW190425 using numerical-relativity calibrated waveform models”, Tatsuya Narikawa, Nami Uchikata, Kyohei Kawaguchi, Kenta Kiuchi, Koutarou Kyutoku, Masaru Shibata, and Hideyuki Tagoshi, Phys. Rev. Research 2, 043039 (2020), DOI:10.1103/PhysRevResearch.2.043039

[20] “Reducing orbital eccentricity in initial data of black hole–neutron star binaries in the puncture framework”, Koutarou Kyutoku, Kyohei Kawaguchi, Kenta Kiuchi, Masaru Shibata, Keisuke Taniguchi, PHYSICAL REVIEW D 103, 023002 (2021), DOI:10.1103/PhysRevD.103.023002

[21] “Radiative Cooling of the Thermally Isolated System in KAGRA Gravitational Wave Telescope”, Tomohiro Yamada and on behalf of the KAGRA collaboration, J. Phys.: Conf. Ser. 1857 012002(10th ACASC/2nd Asian-ICMC/CSSJ Joint Conference) (2020), DOI:10.1088/1742-6596/1857/1/012002

[22] “Overview of KAGRA: Calibration, detector characterization, physical environmental monitors, and the geophysics interferometer”, T. Akutsu et al. (KAGRA collaboration), Prog. Theor. Exp. Phys. 2021, 05A102 (2021), DOI:10.1093/ptep/ptab018

[23] “Demographic Landscape of the KAGRA collaboration”, Keiko Kokeyama, Chunglee Kim, Joseph M. Fedrow, and Ayaka Shoda, AIP Conference Proceedings, Volume 2319, Issue 1, 150001 (2021), DOI:10.1063/5.0036998

[24] “Vibration isolation systems for the beam splitter and signal recycling mirrors of the KAGRA gravitational wave detector”, T. Akutsu et al. (KAGRA Collaboration), Class. Quantum Grav. 38 065011(2021), DOI:10.1088/1361-6382/abd922

[25] “Demonstration of a dual-pass differential Fabry-Perot interferometer for future interferometric space gravitational wave antennas”, Koji Nagano, Hiroki Takeda, Yuta Michimura, Takashi Uchiyama and Masaki Ando, Class. Quantum Grav. 38 085018 (2021), DOI:10.1088/1361-6382/abed60

[26] “Cryogenic suspension design for a kilometer-scale gravitational-wave detector”, Takafumi Ushiba, Tomotada Akutsu, Sakae Araki, Rishabh Bajpai, Dan Chen, Kieran Craig, Yutaro Enomoto, Ayako Hagiwara, Sadakazu Haino, Yuki Inoue, Kiwamu Izumi, Nobuhiro Kimura, Rahul Kumar, Yuta Michimura, Shinji Miyoki, Iwao Murakami, Yoshikazu Namai, Masayuki Nakano, Masatake Ohashi, Koki Okutomi, Takaharu Shishido, Ayaka Shoda, Kentaro Somiya, Toshikazu Suzuki, Suguru Takada, Masahiro Takahashi, Ryutaro Takahashi, Shinichi Terashima, Takayuki Tomaru, Flavio Travasso, Ayako Ueda, Helios Vocca, Tomohiro Yamada, Kazuhiro Yamamoto, and Simon Zeidler, Class. Quantum Grav. 38, 085013 (2021), DOI:10.1088/1361-6382/abe9f3

[27] “A nonparametric method to assess the significance of events in the search for gravitational waves with false discovery rate”, Yuzurihara Hirotaka et al., J. Phys.: Conf. Ser. 1468 012222(TAUP2019) (2020), DOI:10.1088/1742-6596/1468/1/012222

[28] “KAGRA Cryogenic Suspension Control toward the Observation Run 3”, Tomohiro Yamada and on behalf of the KAGRA collaboration, J. Phys.: Conf. Ser. 1468 012217 (TAUP 2019) (2020), DOI:10.1088/1742-6596/1468/1/012217

[29] “Global control using a laser strainmeter for KAGRA”, Koseki Miyo on behalf of the KAGRA Collaboration, J. Phys.: Conf. Ser. 1468 012221 (TAUP 2019) (2020), DOI:10.1088/1742-6596/1468/1/012221

[30] “Unified mapmaking for an anisotropic stochastic gravitational wave background”, Jishnu Suresh, Anirban Ain, and Sanjit Mitra, Phys. Rev. D 103, 083024 (2021), DOI:10.1103/PhysRevD.103.083024

[31] “Gravitational wave physics and astronomy in the nascent era”, M.Arimoto et al., Prog. Theor. Exp. Phys. 2023, 10A103 (2021), DOI:10.1093/ptep/ptab042

[32] “Method for environmental noise estimation via injection tests for ground-based gravitational wave detectors”, T. Washimi, T. Yokozawa, T. Tanaka, Y. Itoh, J. Kume, J. Yokoyama, Class. Quantum Grav. 38 125005 (2021), DOI:10.1088/1361-6382/abf89a

[33] “Diving below the spin-down limit: Constraints on gravitational waves from the energetic young pulsar PSR J0537-6910”, R. Abbott et al,(LIGO Scientific Collaboration, Virgo Collaboration, and KAGRA Collaboration, NICER), ApJL 913 L27 (2021), DOI:10.3847/2041-8213/abffcd

[34] “High Performance Heat Conductor with Small Spring Constant for Cryogenic Applications”, Tomohiro Yamada, Takayuki Tomaru, Toshikazu Suzuki, Takafumi Ushiba, Nobuhiro Kimura, Suguru Takada, Yuki Inoue, Takaaki Kajita, Cryogenics, 116, 103280 (2021), DOI:10.1016/j.cryogenics.2021.103280

[35] “Constraints on cosmic strings using data from the third Advanced LIGO-Virgo observing run”, R. Abbott et al. (LIGO Scientific Collaboration, Virgo Collaboration, and KAGRA Collaboration), Phys. Rev. Lett. 126, 241102 (2021), DOI:10.1103/PhysRevLett.126.241102

[36] “Observation of Gravitational Waves from Two Neutron Star–Black Hole Coalescences”, R. Abbott et al. (LIGO Scientific Collaboration, Virgo Collaboration, and KAGRA Collaboration), 2021 ApJL 915 L5 (2021), DOI:10.3847/2041-8213/ac082e

[37] “Prospects for estimating parameters from gravitational waves of superspinar binaries”, Nami Uchikata, Tatsuya Narikawa, Phys. Rev. D 104, 024059 (2021), DOI:10.1103/PhysRevD.104.024059

[38] “Effects of lightning strokes on underground gravitational waves observatories”, T. Washimi, T. Yokozawa, M. Nakano, T. Tanaka, K. Kaihotsu, Y. Mori, T. Narita, 2021 JINST 16 P07033 (2021), DOI:10.1088/1748-0221/16/07/P07033

[39] “Local Hurst exponent computation of data from triaxial seismometers monitoring KAGRA”, A. Longo, S. Bianchi, W. Plastinao, K. Miyo, T. Yokozawa, T. Washimi, A. Araya, Pure Appl. Geophys. 178, 3461–3470 (2021), DOI:10.1007/s00024-021-02810-2

[40] “Upper Limits on the Isotropic Gravitational-Wave Background from Advanced LIGO’s and Advanced Virgo’s Third Observing Run”, R. Abbott et al. (LIGO Scientific Collaboration, Virgo Collaboration, and KAGRA Collaboration), Phys. Rev. D 104, 022004 (2021), DOI:10.1103/PhysRevD.104.022004

[41] “Search for anisotropic gravitational-wave backgrounds using data from Advanced LIGO’s and Advanced Virgo’s first three observing runs”, R. Abbott et al. (LIGO Scientific Collaboration, Virgo Collaboration, and KAGRA Collaboration), Phys. Rev. D 104, 022005 (2021), DOI:10.1103/PhysRevD.104.022005

[42] “The KAGRA underground environment and lessons for the Einstein Telescope”, Francesca Badaracco, Jan Harms, Camilla De Rossi, Irene Fiori, Kouseki Miyo, Taiki Tanaka, Takaaki Yokozawa, Federico Paoletti, and Tatsuki Washimi, Phys. Rev. D 104, 042006 (2021), DOI:10.1103/PhysRevD.104.042006

[43] “Gravitational-wave constraints on the GWTC-2 events by measuring the tidal deformability and the spin-induced quadrupole moment”, Tatsuya Narikawa, Nami Uchikata, Takahiro Tanaka, Phys. Rev. D 104, 084056 (2021), DOI:10.1103/PhysRevD.104.084056

[44] “Application of the Hilbert-Huang transform for analyzing standing-accretion-shock-instability induced gravitational waves in a core-collapse supernova”, M. Takeda, Y. Hiranuma, N. Kanda ,K. Kotake, T. Kuroda, R. Negishi, K. Oohara, K. Sakai, Y. Sakai, T. Sawada, H. Takahashi, S. Tsuchida, Y. Watanabe, T. Yokozawa, Phys. Rev. D 104, 084063 (2021), DOI:10.1103/PhysRevD.104.084063

[45] “All-sky search for continuous gravitational waves from isolated neutron stars in the early O3 LIGO data”, R. Abbott et al. (LIGO Scientific Collaboration, Virgo Collaboration, and KAGRA Collaboration), Phys. Rev. D 104, 082004 (2021), DOI:10.1103/PhysRevD.104.082004

[46] “Investigation of crackling noise in the vibration isolation systems of the KAGRA gravitational wave detector”, Y Zhao, S Kirii, Y Liu, T Uchiyama, R Takahashi, S Kawamura, Physics Letters A 416, 127664 (2021), DOI:10.1016/j.physleta.2021.127664

[47] “Constraints from LIGO O3 data on gravitational-wave emission due to r-modes in the glitching pulsar PSR J0537-6910”, R. Abbott et al. (LIGO Scientific Collaboration, Virgo Collaboration, and KAGRA Collaboration), ApJ 922 71 (2021), DOI:10.3847/1538-4357/ac0d52

[48] “Searches for Continuous Gravitational Waves from Young Supernova Remnants in the Early Third Observing Run of Advanced LIGO and Virgo”, R. Abbott et al. (LIGO Scientific Collaboration, Virgo Collaboration, and KAGRA Collaboration), ApJ 921 80 (2021), DOI:10.3847/1538-4357/ac17ea

[49] “All-sky search for long-duration gravitational-wave bursts in the third Advanced LIGO and Advanced Virgo run”, R. Abbott et al. (LIGO Scientific Collaboration, Virgo Collaboration, and KAGRA Collaboration), Phys. Rev. D 104, 102001(2021), DOI:10.1103/PhysRevD.104.102001

[50] “A nonparametric method to assess the significance of events in the search for gravitational waves with false discovery rate”, Hirotaka Yuzurihara, Shuhei Mano, Hideyuki Tagoshi, Prog. Theor. Exp. Phys. 2021 123F01 (2021), DOI:10.1093/ptep/ptab137

[51] “All-sky search for short gravitational-wave bursts in the third Advanced LIGO and Advanced Virgo run”, R. Abbott et al. (The LIGO Scientific Collaboration, the Virgo Collaboration, and the KAGRA Collaboration), Phys. Rev. D 104, 122004 (2021), DOI:10.1103/PhysRevD.104.122004

[52] “Search for continuous gravitational waves from 20 accreting millisecond x-ray pulsars in O3 LIGO data”, R. Abbott et al. (LIGO Scientific Collaboration, Virgo Collaboration, and KAGRA Collaboration), Phys. Rev. D 105, 022002 (2021), DOI:10.1103/PhysRevD.105.022002

[53] “Constraints on dark photon dark matter using data from LIGO’s and Virgo’s third observing run”, R. Abbott et al. (LIGO Scientific Collaboration, Virgo Collaboration, and KAGRA Collaboration), Phys. Rev. D 105, 063030 (2022), Erratum Phys. Rev. D 109, 089902 (2024), DOI:10.1103/PhysRevD.105.063030, 10.1103/PhysRevD.109.089902

Phys. Rev. D 105, 063030 (2022), Erratum Phys. Rev. D 109, 089902 (2024) 10.1103/PhysRevD.105.063030, 10.1103/PhysRevD.109.089902

[54] “Search for intermediate-mass black hole binaries in the third observing run of Advanced LIGO and Advanced Virgo”, R. Abbott et al. (LIGO Scientific Collaboration, Virgo Collaboration, and KAGRA Collaboration), A & A 659, A84 (2022), DOI:10.1051/0004-6361/202141452

[55] “Improving the stability of frequency-dependent squeezing with bichromatic control of filter cavity length, alignment, and incident beam pointing”, Yuhang Zhao, Eleonora Capocasa, Marc Eisenmann, Naoki Aritomi, Michael Page, Yuefan Guo, Eleonora Polini, Koji Arai, Yoichi Aso, Martin van Beuzekom, Yao-Chin Huang, Ray-Kuang Lee, Harald Lück, Osamu Miyakawa, Pierre Prat, Ayaka Shoda, Matteo Tacca, Ryutaro Takahashi, Henning Vahlbruch, Marco Vardaro, Chien-Ming Wu, Matteo Leonardi, Matteo Barsuglia, Raffaele Flaminio, Phys. Rev. D 105, 082003 (2022), DOI:10.1103/PhysRevD.105.082003

[56] “First joint observation by the underground gravitational-wave detector KAGRA with GEO 600”, Abbott R, Others (LIGO-Virgo-KAGRA collaboration), Prog. Theor. Exp. Phys. 2022 063F01 (2022), DOI:10.1093/ptep/ptac073

[57] “Search for Gravitational Waves Associated with Gamma-Ray Bursts Detected by Fermi and Swift during the LIGO-Virgo Run O3b”, Abbott R, Others (LIGO-Virgo-KAGRA collaboration), 2022 ApJ 928 186 (2022), DOI:10.3847/1538-4357/ac532b

[58] “The Current Status and Future Prospects of KAGRA, the Large-Scale Cryogenic Gravitational Wave Telescope Built in the Kamioka Underground”, H Abe et al (KAGRA collaboration), Galaxies 2022, 10(3), 63 (2022), DOI:10.3390/galaxies10030063

[59] “All-sky search for gravitational wave emission from scalar boson clouds around spinning black holes in LIGO O3 data”, Abbott R, Others (LIGO-Virgo-KAGRA collaboration), PhysRevD.105.102001 (2022), DOI:10.1103/PhysRevD.105.102001

[60] “Searches for Gravitational Waves from Known Pulsars at Two Harmonics in the Second and Third LIGO-Virgo Observing Runs”, Abbott R, Others (LIGO-Virgo-KAGRA collaboration), ApJ 935 1 (2022), DOI:10.3847/1538-4357/ac6acf

[61] “A laser interferometer accelerometer for vibration sensitive cryogenic experiments”, Rishabh Bajpai, Takayuki Tomaru, Kazuhiro Yamamoto, Takfumi Ushiba, Nobuhiro Kimura, Toshikazu Suzuki, Tomohiro Yamada, Tohru Honda, Meas. Sci. Technol. 33 085902 (2022), DOI:10.1088/1361-6501/ac6d46

[62] “Narrowband Searches for Continuous and Long-duration Transient Gravitational Waves from Known Pulsars in the LIGO-Virgo Third Observing Run”, Abbott R, Others (LIGO-Virgo-KAGRA collaboration), ApJ 932 133 (2022), DOI:10.3847/1538-4357/ac6ad0

[63] “All-sky, all-frequency directional search for persistent gravitational waves from Advanced LIGO’s and Advanced Virgo’s first three observing runs”, Abbott R, Others (LIGO-Virgo-KAGRA collaboration), Phys. Rev. D 105, 122001 (2022), DOI:10.1103/PhysRevD.105.122001

[64] “Unsupervised learning architecture for classifying the transient noise of interferometric gravitational-wave detectors”, Yusuke Sakai, Yousuke Itoh, Piljong Jung, Keiko Kokeyama, Chihiro Kozakai, Katsuko T. Nakahira, Shoichi Oshino, Yutaka Shikano, Hirotaka Takahashi, Takashi Uchiyama, Gen Ueshima, Tatsuki Washimi, Takahiro Yamamoto, and Takaaki Yokozawa, Scientific Reports, 12:9935 (2022) , DOI:10.1038/s41598-022-13329-4

[65] “Mass-spin reparametrization for a rapid parameter estimation of inspiral gravitational-wave signals”, Eunsub Lee, Soichiro Morisaki, and Hideyuki Tagoshi, Phys. Rev. D 105, 124057 (2022), DOI:10.1103/PhysRevD.105.124057

[66] “Vibration analysis of KAGRA cryostat at cryogenic temperature”, Rishabh Bajpai, Takayuki Tomaru, Nobuhiro Kimura, Takafumi Ushiba, Kazuhiro Yamamoto, Toshikazu Suzuki, Tohru Honda, Class. Quantum Grav. 39 165004 (2022), DOI:10.1088/1361-6382/ac7cb5

[67] “Search for continuous gravitational wave emission from the Milky Way center in O3 LIGO-Virgo data”, Abbott R, Others (LIGO-Virgo-KAGRA collaboration), Phys. Rev. D 106, 042003 (2022), DOI:10.1103/PhysRevD.106.042003

[68] “Search for Subsolar-Mass Binaries in the First Half of Advanced LIGO’s and Advanced Virgo’s Third Observing Run”, Abbott R, Others (LIGO-Virgo-KAGRA collaboration), Phys. Rev. Lett. 129, 061104(2022), DOI:10.1103/PhysRevLett.129.061104

[69] “Search for gravitational waves from Scorpius X-1 with a hidden Markov model in O3 LIGO data”, Abbott R,Others (LIGO-Virgo-KAGRA collaboration), Phys. Rev. D 106, 062002 (2022), DOI:10.1103/PhysRevD.106.062002

[70] “Response of the underground environment of the KAGRA observatory against the air pressure disturbance from the Tonga volcano eruption on January 15th, 2022”, Tatsuki Washimi, Takaaki Yokozawa, Akiteru Takamori, Akito Araya, Sota Hoshino, Yousuke Itoh, Yuichiro Kobayashi, Jun’ya Kume, Kouseki Miyo, Masashi Ohkawa, Shoichi Oshino, Takayuki Tomaru, Jun’ichi Yokoyama, Hirotaka Yuzurihara, Prog. Theor. Exp. Phys. 2022 113H02 (2022), DOI:10.1093/ptep/ptac128

[71] “All-sky search for continuous gravitational waves from isolated neutron stars using Advanced LIGO and Advanced Virgo O3 data”, Abbott R, Others (LIGO-Virgo-KAGRA collaboration), Phys. Rev. D 106, 102008 (2022), DOI:10.1103/PhysRevD.106.102008

[72] “Follow-up analyses of the binary-neutron-star signals GW170817 and GW190425 by using post-Newtonian waveform models”, Tatsuya Narikawa, Nami Uchikata, Phys. Rev. D 106, 103006 (2022), DOI:10.1103/PhysRevD.106.103006

[73] “Thermal Performance of a Cryogenic Parallel Heat Pipe System”, Ramnarong Wanison, Nobuhiro Kimura, Masahide Murakami, Hirotaka Nakai, and Suguru Takada, Cryogenics Vol.128, 103589 (2022), DOI:10.1016/j.cryogenics.2022.103589

[74] “Model-based Cross-correlation Search for Gravitational Waves from the Low-mass X-Ray Binary Scorpius X-1 in LIGO O3 Data”, Abbott R, Others (LIGO-Virgo-KAGRA collaboration), ApJL 941 L30 (2022), DOI:10.3847/2041-8213/aca1b0

[75] “Input optics systems of the KAGRA detector during O3GK”, T Akutsu et al (KAGRA collaboration), Prog. Theor. Exp. Phys. 2023 023F01(2022), DOI:10.1093/ptep/ptac166

[76] “Noise subtraction from KAGRA O3GK data using Independent Component Analysis”, H Abe et al (KAGRA collaboration), Class. Quantum Grav. 40 085015 (2023), DOI:10.1088/1361-6382/acc0cb

[77] “Search for subsolar-mass black hole binaries in the second part of Advanced LIGO’s and Advanced Virgo’s third observing run”, Abbott R, Others (LIGO-Virgo-KAGRA collaboration), MNRAS 524, 5984–5992 (2023), DOI:10.1093/mnras/stad588

[78] “Rapid hierarchical inference of neutron star equation of state from multiple gravitational wave observations of binary neutron star coalescences”, Anarya Ray, Michael Camilo, Jolien Creighton, Shaon Ghosh, Soichiro Morisaki, Phys. Rev. D 107, 043035 (2023), DOI:10.1103/PhysRevD.107.043035

[79] “Population of Merging Compact Binaries Inferred Using Gravitational Waves through GWTC-3”, Abbott R,Others (LIGO-Virgo-KAGRA collaboration), Phys. Rev. X 13, 011048 (2023), DOI:10.1103/PhysRevX.13.011048

[80] “Fixed-target charmonium production and pion parton distributions”, Wen-Chen Chang, Jen-Chieh Peng, Stephane Platchkov, and Takahiro Sawada, Phys. Rev. D 107, 056008 (2023), DOI:10.1103/PhysRevD.107.056008

[81] “Constraints on the Cosmic Expansion History from GWTC–3”, Abbott R, Others (LIGO-Virgo-KAGRA collaboration), ApJ 949 76 (2023), DOI:10.3847/1538-4357/ac74bb

[82] “Ground strains induced by the 2022 Hunga-Tonga volcanic eruption, observed by a 1500-m laser strainmeter at Kamioka, Japan”, Akiteru Takamori, Akito Araya, Kouseki Miyo, Tatsuki Washimi, Takaaki Yokozawa, Hideaki Hayakawa, Masatake Ohashi, Earth Planets Space 75, 98 (2023), DOI:10.1186/s40623-023-01857-w

[83] “Open Data from the Third Observing Run of LIGO, Virgo, KAGRA, and GEO”, Abbott R, Others (LIGO-Virgo-KAGRA collaboration), ApJS 267 29 (2023), DOI:10.3847/1538-4365/acdc9f

[84] “Pion PDFs confronted by fixed-target charmonium production”, Wen-Chen Chang, Chia-Yu Hsieh, Yu-Shiang Lian, Jen-Chieh Peng, Stephane Platchkov, Takahiro Sawada, AAPPS Bull. 33, 15 (2023), DOI:10.1007/s43673-023-00085-4

[85] “Localization of binary neutron star mergers with a single cosmic explorer”, Pratyusava Baral, Soichiro Morisaki, Ignacio Magaña Hernandez, Jolien Creighton, Phys. Rev. D 108, 043010 (2023), DOI:10.1103/PhysRevD.108.043010

[86] “Binary tree approach to template placement for searches for gravitational waves from compact binary mergers”, Chad Hanna, Soichiro Morisaki et al., Phys. Rev. D 108, 042003 (2023), DOI:10.1103/PhysRevD.108.042003

[87] “Improved ranking statistics of the GstLAL inspiral search for compact binary coalescences”, Leo Tsukada , Soichiro Morisaki, et al., Phys. Rev. D 108, 043004 (2023), DOI:10.1103/PhysRevD.108.043004

[88] “Overview of KAGRA: Data transfer and management”, Akutsu T, Others KAGRA Collaboration, Prog. Theor. Exp. Phys. 2023 10A102 (2023), DOI:10.1093/ptep/ptad112

[89] “Multipole tidal effects in the post-Newtonian gravitational-wave phase of compact binary coalescences”, Tatsuya Narikawa, Phys. Rev. D 108, 063029 (2023), DOI:10.1103/PhysRevD.108.063029

[90] “Measurement of flavor asymmetry of the light-quark sea in the proton with Drell-Yan dimuon production in p+p and p+d collisions at 120 GeV”, J. Dove, T. Sawada et al., Phys. Rev. C 108, 035202 (2023), DOI:10.1103/PhysRevC.108.035202

[91] “Search for Gravitational Waves Associated with Fast Radio Bursts Detected by CHIME/FRB during the LIGO-Virgo Observing Run O3a”, Abbott R, Others (LIGO-Virgo-KAGRA collaboration), ApJ 955 155 (2023), DOI:10.3847/1538-4357/acd770

[92] “First results of axion dark matter search with DANCE”, Yuka Oshima, Hiroki Fujimoto, Jun’ya Kume, Soichiro Morisaki, Koji Nagano, Tomohiro Fujita, Ippei Obata, Atsushi Nishizawa, Yuta Michimura, Masaki Ando, Phys. Rev. D 108, 072005 (2023), DOI:10.1103/PhysRevD.108.072005

[93] “Probing the Solar Interior with Lensed Gravitational Waves from Known Pulsars”, Ryuichi Takahashi, Soichiro Morisaki, Teruaki Suyama, ApJ 957 52 (2023), DOI:10.3847/1538-4357/acfa93

[94] “Performance of the KAGRA detector during the first joint observation with GEO600 (O3GK)”, H. Abe et al. KAGRA Collaboration, Prog. Theor. Exp. Phys. 2023 10A101 (2023), DOI:10.1093/ptep/ptac093

[95] “Searching for gravitational wave echoes from black hole binary events in the third observing run of LIGO, Virgo, and KAGRA collaborations”, Nami Uchikata, Tatsuya Narikawa, Hiroyuki Nakano, Norichika Sago, Hideyuki Tagoshi, and Takahiro Tanaka, Phys. Rev. D 108, 104040 (2023), DOI:10.1103/PhysRevD.108.104040

[96] “Stochastic effects on observation of ultralight bosonic dark matter”, Hiromasa Nakatsuka, Soichiro Morisaki, Tomohiro Fujita, Jun’ya Kume, Yuta Michimura, Koji Nagano, Ippei Obata, Phys. Rev. D 108, 092010 (2023), DOI:10.1103/PhysRevD.108.092010

[97] “Upper limit on scalar field dark matter from LIGO-Virgo third observation run”, Koki Fukusumi, Soichiro Morisaki, Teruaki Suyama, Phys. Rev. D 108, 095054(2023), DOI:10.1103/PhysRevD.108.095054

[98] “GWTC-2.1: Deep extended catalog of compact binary coalescences observed by LIGO and Virgo during the first half of the third observing run”, Abbott R, Others (LIGO-Virgo-KAGRA collaboration), Phys. Rev. D 109, 022001 (2023), DOI:10.1103/PhysRevD.109.022001

[99] “Status of the underground gravitational wave detector KAGRA”, T. Ushiba on behalf of the KAGRA Collaboration, PoS TAUP2023, 116 (2024), DOI:10.22323/1.441.0116

[100] “Rapid localization and inference on compact binary coalescences with the Advanced LIGO-Virgo-KAGRA gravitational-wave detector network”, Soichiro Morisaki, Rory Smith, Leo Tsukada, Surabhi Sachdev, Simon Stevenson, Colm Talbot, and Aaron Zimmerman, Phys. Rev. D 108, 123040 (2023), DOI:10.1103/PhysRevD.108.123040

[101] “GWTC-3: Compact Binary Coalescences Observed by LIGO and Virgo during the Second Part of the Third Observing Run”, Abbott R, Others (LIGO-Virgo-KAGRA collaboration), Phys. Rev. X 13, 041039 (2023), DOI:10.1103/PhysRevX.13.041039

[102] “A Joint Fermi-GBM and Swift-BAT Analysis of Gravitational-wave Candidates from the Third Gravitational-wave Observing Run”, Fletcher C, Others (LIGO-Virgo-KAGRA collaboration), 2024 ApJ 964 149 (2024), DOI: 10.3847/1538-4357/ad1eed

OBSERVATIONAL COSMOLOGY GROUP

Introduction

We study early galaxy formation and evolution, which is a missing piece in our understanding of cosmic history. The outstanding scientific questions include the formation of first stars and galaxies, and the structural/dynamical/chemical evolutions of galaxies during the early epoch of cosmic history. Our basic strategy is to carry out deep surveys using the largest telescope facilities such as Subaru, ALMA, and James Webb Space Telescope (JWST), which have the sensitivity required to probe the distant universe. The main results based on our research activities from April 2018 to March 2024 are summarized as follows.

Summary from 2018 to 2024

- Based on the Subaru Hyper Suprime-Cam (HSC) survey, we have constructed extensive samples of high-z galaxies at $z \sim 2$–7, allowing for statistical analysis of their physical properties. Our findings have revealed a significant excess in the number densities of bright galaxies compared to the Schechter function, suggesting inefficient active galactic nucleus (AGN) feedback for star formation at $z \sim 4$–7. Additionally, we have obtained nearly constant star formation efficiency from $z \sim 2$–6, with the cosmic star formation rate (SFR) density evolution driven by changes in the halo number density and accretion rate. Furthermore, intensity mapping of Lyα emitters (LAEs) indicates extended diffuse Lyα emission beyond the virial radius $R_{\rm vir}$ of a dark matter halo with a mass of $10^{11} M_\odot$, powered by resonant scattering in the circumgalactic medium (CGM) and intergalactic medium (IGM).

- We have initiated a Subaru intensive program, EMPRESS, for local extremely metal-poor galaxies (EMPGs) using Subaru/HSC, identifying candidates with a machine-learning classifier and confirming some with follow-up spectroscopy, revealing star-forming galaxies with low metallicity. Additionally, deep Subaru near-infrared (NIR) spectroscopy for EMPGs has provided new measurements of primordial helium abundance ($Y_{\rm P}$), contributing to constraints on cosmological parameters, including the effective number of neutrino species ($N_{\rm eff}$) and baryon-to-photon ratio (η), suggesting potential lepton asymmetry and implications for the Hubble tension.

- Leveraging deep JWST data taken in multiple programs, we have spectroscopically confirmed UV luminosity functions and cosmic star formation rates from 25 galaxies at $z = 8.61$–13.20, finding high star formation efficiency and significant contributions from star-forming galaxies at these high redshifts. Chemical abundance analyses of 70 star-forming galaxies at $z = 4$–10 have revealed unique C/N and N/O ratios, suggesting enrichment by the CNO cycle, and indicating connections to globular cluster formation. Additionally, we have identified the first statistical sample of faint type-1 AGNs at $z > 4$, showing a substantial AGN population at high redshifts and revealing their contribution to cosmic reionization.

The details are described in what follows.

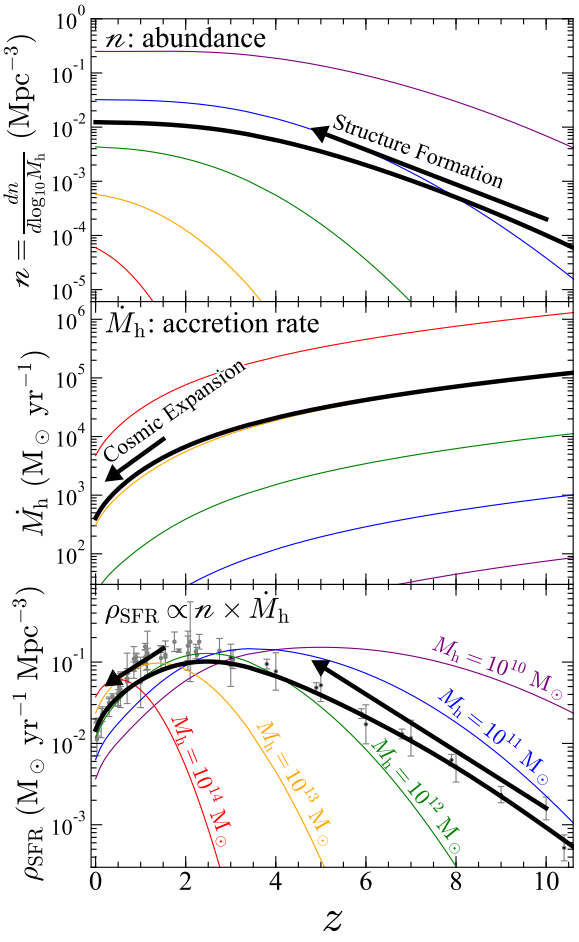

Fig. 1. Mechanism of the cosmic SFR density evolution. **Top panel:** the purple, blue, green, orange, and red curves indicate the number density of halos whose masses are $M_{\rm h} = 10^{10}, 10^{11}, 10^{12}, 10^{13}$, and $10^{14} M_\odot$, respectively. The black curve represents a weighted number density. **Middle panel:** same as the top panel but for the dark matter accretion rate. **Bottom panel:** same as the top panel but for the cosmic SFR density. The gray circles are observed cosmic SFR densities in the literature. Since the cosmic SFR density at a given halo mass is proportional to the galaxy (halo) number densities and SFRs (accretion rates), the redshift evolution of the cosmic SFR density is made by the monotonic steep increase of the halo number density from $z \sim 10$ to $z \sim 4$ and the monotonic decrease of the accretion rate from $z \sim 2$ to $z \sim 0$, resulting in a peak of the SFR density around $z \sim 2$–3.

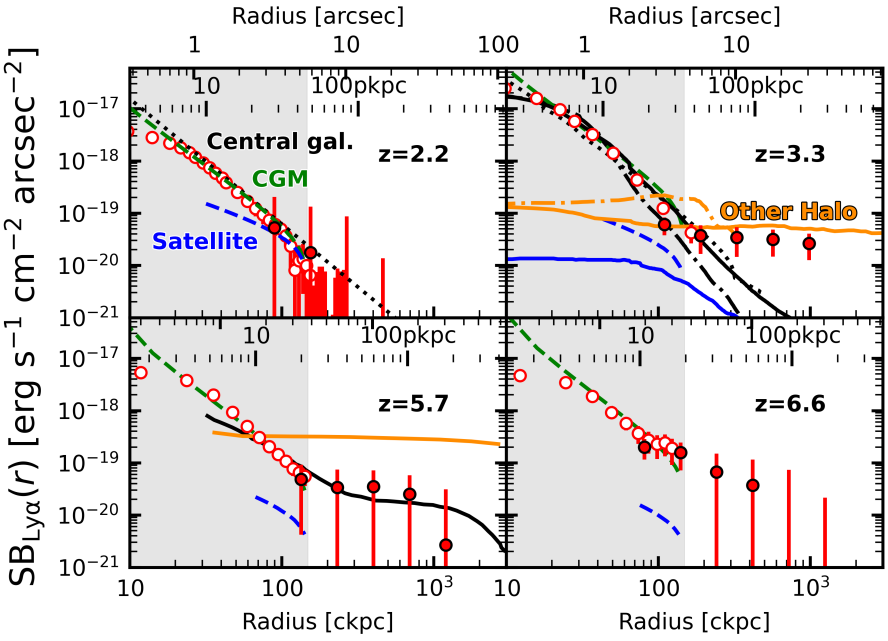

Fig. 2. Comparison of the $SB_{Ly\alpha}$ radial profiles between the observational and theoretical studies at $z = 2.2$ (top left), 3.3 (top right), 5.7 (bottom left), and 6.6 (bottom right). The filled red circles depict the observational results taken from our *all* sample ($z = 2.2$–6.6), while the open red circles show the results from previous observational work. We represent the theoretical work with the lines, whose colors indicate the origins of the Lyα emission: the central galaxy (black), CGM (green), satellite galaxies (blue), and other halos (orange). We normalize the $SB_{Ly\alpha}$ profiles from the model predictions such that the central galaxy ($r \lesssim 1''$) has a $L_{Ly\alpha}$ value similar to that observed at each redshift. The gray shaded area illustrates the regions inside the R_{vir} of a dark matter halo with $M_{halo} = 10^{11}\,M_\odot$.

Subaru Hyper Suprime-Cam Survey

In [99], we have presented new measurements of rest-UV luminosity functions and angular correlation functions from 4,100,221 galaxies at $z \sim 2$–7 identified in the Subaru/HSC survey and CFHT Large Area U-band Survey. The obtained luminosity functions at $z \sim 4$–7 cover a very wide UV luminosity range of ~ 0.002–$2000L^*_{UV}$ combined with previous studies, confirming that the dropout luminosity function is a superposition of the AGN luminosity function dominant at $M_{UV} \lesssim -24$ mag and the galaxy luminosity function dominant at $M_{UV} \gtrsim -22$ mag, consistent with galaxy fractions based on 1037 spectroscopically identified sources. Galaxy luminosity functions estimated from the spectroscopic galaxy fractions show the bright-end excess beyond the Schechter function at $\gtrsim 2\sigma$ levels, possibly made by inefficient mass quenching, low dust obscuration, and/or hidden AGN activity. By analyzing the correlation functions at $z \sim 2$–6 with HOD models, we have found a weak redshift evolution (within 0.3 dex) of the ratio of the SFR to the dark matter accretion rate, $SFR/\dot{M}_h$, indicating the almost constant star formation efficiency at $z \sim 2$–6, as suggested by our earlier work at $z \sim 4$–7. Meanwhile, the ratio gradually increases with decreasing redshift at $z < 5$ within 0.3 dex, which quantitatively reproduces the cosmic SFR density evolution (Figure 1), suggesting that the redshift evolution is primarily driven by the increase of the halo number density due to the structure formation, and the decrease of the accretion rate due to the cosmic expansion. Extrapolating this calculation to higher redshifts assuming the constant efficiency suggests a rapid decrease of the SFR density at $z > 10$ with $\propto 10^{-0.5(1+z)}$, which will be directly tested with the James Webb Space Telescope.

In [140], we have presented 20,567 LAEs at $z = 2.2$–7.3 that are photometrically identified by the SILVERRUSH program in a large survey area up to 25 deg^2 with deep images of five broadband filters (*grizy*) and seven narrowband filters targeting Lyα lines at $z = 2.2, 3.3, 4.9, 5.7, 6.6, 7.0$, and 7.3 taken by the HSC Subaru Strategic Program (SSP) and the Cosmic HydrOgen Reionization Unveiled with Subaru (CHORUS) survey. We have selected secure $> 5\sigma$ sources showing narrowband color excesses via Lyα break screening, taking into account the spatial inhomogeneity of limiting magnitudes. After removing spurious sources by careful masking and visual inspection of coadded and multi-epoch images obtained over the 7 yr of the surveys, we have constructed LAE samples consisting of 6995, 4641, 726, 6124, 2058, 18, and 5 LAEs at $z = 2.2, 3.3, 4.9, 5.7, 6.6, 7.0$, and 7.3, respectively, although the $z = 7.3$ candidates are tentative. Our LAE catalogs contain 289 spectroscopically confirmed LAEs at the expected redshifts from previous work. We have demonstrated that the number counts of our LAEs are consistent with previous studies with similar LAE selection criteria. The LAE catalogs will be made public on our project webpage with detailed descriptions of the content and ancillary information about the masks and limiting magnitudes.

In [107], we have conducted intensity mapping to probe for extended diffuse Lyα emission around LAEs at $z \sim 2$–7, exploiting very deep (~ 26 mag at 5σ) and large-area (~ 4.5 deg^2) Subaru/HSC narrowband (NB) images and large LAE catalogs consisting of a total of 1540 LAEs at $z = 2.2, 3.3, 5.7$, and 6.6 obtained by the HSC-SSP and CHORUS projects. We have calculated the spatial correlations of these LAEs with $\sim$ 1–2 billion pixel flux values of the NB images, deriving

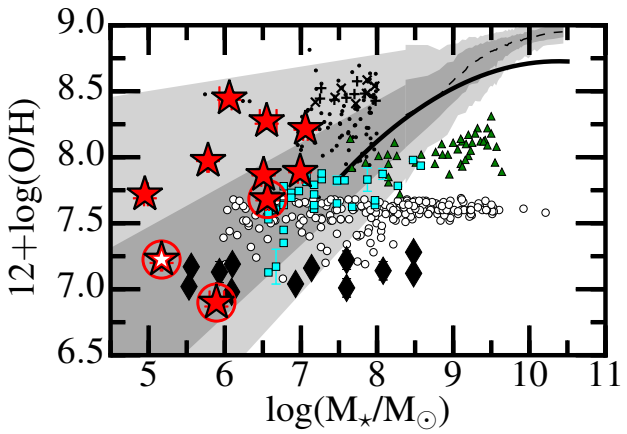

Fig. 3. Mass-metallicity relation of our metal-poor galaxies. Galaxies that satisfy the EMPG condition in our metal-poor galaxy sample are marked with a large circle. The open star indicates a galaxy whose metallicity is obtained with the empirical relation not with the direct method because of the non-detection of [O III]λ4363 and [O II]$\lambda\lambda$7320,7330 emission lines. For comparison, low-metallicity objects at low redshifts from the literature are plotted with green triangles, cyan squares, and open circles. With diamonds, we show representative metal-poor galaxies (or clumps of them) with $12+\log(\mathrm{O/H}) \sim 7.0$–$7.2$. The solid and dashed lines indicate averaged local star-forming galaxies (SFGs) obtained in the literature. The dark gray and light gray shaded regions represent the 68th and 95th percentile distributions of SFGs in previous work, although the extrapolation is applied below $\log(M_\star/M_\odot) = 8.4$. We also show relatively metal-enriched dwarfs from SDSS with crosses and pluses, as well as galaxies from the DEEP2 survey with dots in the stellar-mass range of $\log(M_\star/M_\odot) < 8.0$. The typical metallicity error of our metal-poor galaxies is $\Delta(\mathrm{O/H}) \sim 0.01$ dex.

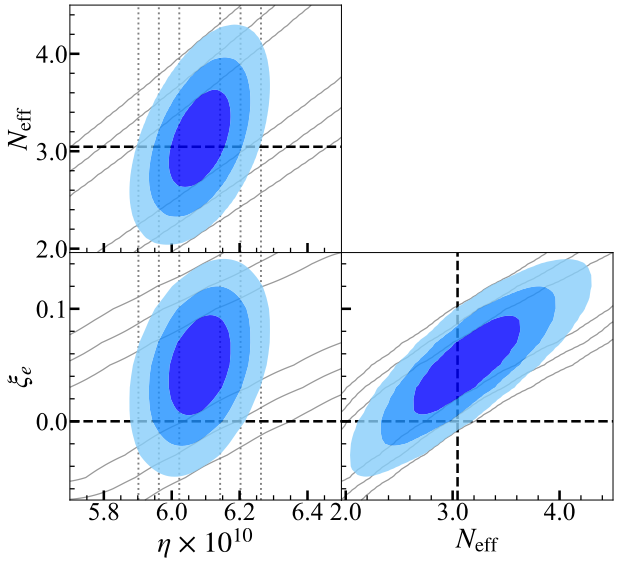

Fig. 4. Constraints on $N_{\rm eff}$, η, and $\xi_{\rm e}$. The solid gray contours show the constraint from our $Y_{\rm P}$ value and the $D_{\rm P}$ measurement in the literature. The vertical dotted lines represent the Planck Collaboration constraint on η. The constraint combining with the $Y_{\rm P}$, $D_{\rm P}$, and η measurements is shown with blue contours. These contours show the 1σ, 2σ, and 3σ confidence limits. The Standard Model values of $N_{\rm eff} = 3.046$ and $\xi_{\rm e} = 0$ are represented with black dashed lines.

the average Lyα surface brightness ($\mathrm{SB_{Ly\alpha}}$) radial profiles around the LAEs. By carefully estimating systematics such as fluctuations of sky background and point-spread functions, we have detected Lyα emission at 100–1000 comoving kpc around $z = 3.3$ and 5.7 LAEs at the 3.2σ and 3.7σ levels, respectively, and tentatively (2.0σ) at $z = 6.6$. The emission is as diffuse as $\sim 10^{-20}$–10^{-19} erg s^{-1} cm^{-2} arcsec^{-2} and extended beyond the virial radius of a dark matter halo with a mass of 10^{11} $M_\odot$. While the observed $\mathrm{SB_{Ly\alpha}}$ profiles have similar amplitudes at $z = 2.2$–6.6 within the uncertainties, the intrinsic $\mathrm{SB_{Ly\alpha}}$ profiles (corrected for the cosmological dimming effect) increase toward high redshifts. This trend may be explained by increasing hydrogen gas density due to the evolution of the cosmic volume. Comparisons with theoretical models suggest that extended Lyα emission around an LAE is powered by resonantly scattered Lyα photons in the CGM and IGM that originate from the inner part of the LAE and/or neighboring galaxies around the LAE (Figure 2).

Subaru Intensive Program EMPRESS

In [59], we have initiated a new survey for local EMPGs with Subaru/HSC large-area ($\sim$500 deg^2) optical images reaching a 5σ limit of $\sim$26 mag, about 100 times deeper than the Sloan Digital Sky Survey (SDSS). To select $Z/Z_\odot < 0.1$ EMPGs from $\sim$40 million sources detected in the Subaru images, we have first developed a machine-learning (ML) classifier based on a deep neural network algorithm with a training data set consisting of optical photometry of galaxy, star, and QSO models. We have tested our ML classifier with SDSS objects having spectroscopic metallicity measurements and confirm that our ML classifier accomplishes 86% completeness and 46% purity EMPG classifications with photometric data. Applying our ML classifier to the photometric data of the Subaru sources, as well as faint SDSS objects with no spectroscopic data, we have obtained 27 and 86 EMPG candidates from the Subaru and SDSS photometric data, respectively. We have conducted optical follow-up spectroscopy for 10 of our EMPG candidates with Magellan/LDSS-3+MagE, Keck/DEIMOS, and Subaru/FOCAS and find that the 10 EMPG candidates are star-forming galaxies at $z = 0.007$–0.03 with large Hβ equivalent widths of 104–265Å, stellar masses of $\log(M_*/M_\odot)$ = 5.0–7.1, and high specific star formation rates of $\sim$300 Gyr^{-1}, which are similar to those of early galaxies at $z \gtrsim 6$ reported recently. We have spectroscopically confirmed that 3 out of 10 candidates are truly EMPGs with $Z/Z_\odot < 0.1$, one of which is HSC J1631+4426, the most metal-poor galaxy, with $Z/Z_\odot = 0.016$, ever reported (Figure 3).

In [118], the primordial He abundance $Y_{\rm P}$ is a powerful probe of cosmology. Currently, $Y_{\rm P}$ is best determined by observations of metal-poor galaxies, while there are only a few known local EMPGs having reliable He/H measurements with He Iλ10830 NIR emission. Here we have presented deep Subaru NIR spectroscopy for 10 EMPGs. Combining the existing optical data, He/H values of 5 out of the 10 EMPGs are reliably derived by the Markov chain Monte Carlo algorithm. Adding the existing 3 EMPGs and 51 moderately

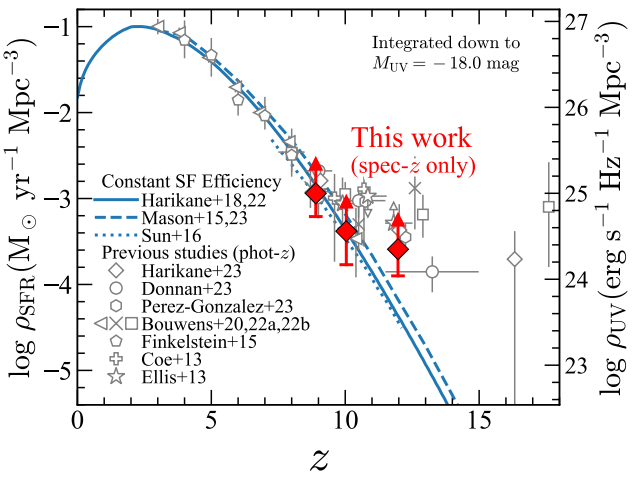

Fig. 5. Cosmic SFR density evolution. The red diamonds represent the spectroscopic constraints on the cosmic SFR densities obtained in this study integrated down to $M_{\rm UV} = -18.0$ mag (corresponding to $\rm SFR_{UV} = 0.8 M_\odot\,yr^{-1}$, based on the Salpeter IMF with a conversion factor of $\rm SFR/L_{UV} = 1.15\times10^{-28} M_\odot\,yr^{-1}/(erg\,s^{-1}\,Hz^{-1})$). These measurements are firm lower limits because (1) only spectroscopically confirmed galaxies without AGN signatures are used, and (2) the measurements are not corrected for dust extinction. The error includes both the 1σ Poisson error and the cosmic variance. The blue curves are predictions of the constant star formation (SF) efficiency models. The obtained lower limit of the SFR density at $z\sim12$ is higher than the model predictions. The gray open symbols are estimates of previous studies using photometric samples. Our spectroscopic constraints are consistent with these photometric estimates.

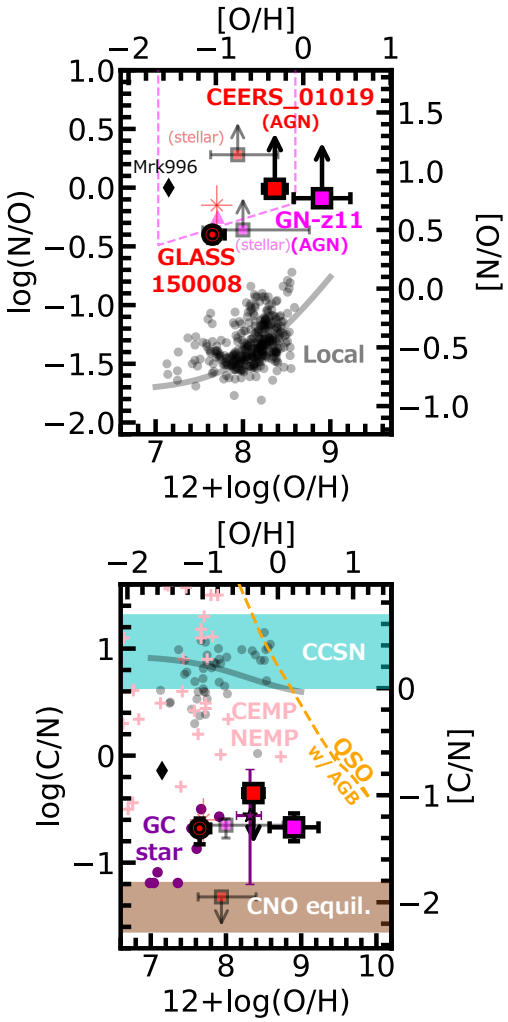

Fig. 6. N/O (top) and C/N (bottom) as a function of 12 + log(O/H). The double red circle denotes the measurements of GLASS_150008 based on the stellar photoionization model. The measurements of CEERS_01019 (red square) and GN-z11 (magenta square) are based on the AGN photoionization models, while those based on the stellar photoionization models are shown by the semitransparent red and magenta squares, respectively. The semitransparent magenta dashed lines, magenta triangle, and red crosses are the abundance measurements of GN-z11 and CEERS_01019 in the literature. The double circles correspond to the measurements with T_e determinations. Mrk996, a WR galaxy, is represented by the black diamonds and Galactic H II regions are shown by the gray dots, while the gray curves are the empirical relation of the Galactic stars. The purple circles are dwarf stars in a globular cluster (GC) NGC6752. The purple stars show abundance ratio distributions of dwarf stars in a metal-rich GC 47 Tuc. The pink crosses are carbon-enhanced metal-poor (CEMP) stars and nitrogen-enhanced metal-poor (NEMP) stars. The cyan and brown shaded regions indicate yields of CCSN and the equilibrium value of the CNO cycle, respectively. The orange dashed line shows a chemical evolution model that reproduces emission-line ratios of quasars, while nitrogen enrichment in the model is mainly caused by asymptotic giant branch (AGB) stars.

metal-poor (0.1–$0.4Z_\odot$) galaxies with reliable He/H estimates, we have obtained $Y_{\rm P} = 0.2370^{+0.0034}_{-0.0033}$ by linear regression in the (He/H) – (O/H) plane, where we increase the number of EMPGs from three to eight anchoring He/H of the most metal-poor gas in galaxies. Although our $Y_{\rm P}$ measurement and previous measurements are consistent, our result is slightly ($\sim1\sigma$) smaller due to our EMPGs. Including the existing primordial deuterium $D_{\rm P}$ measurement, we have constrained the effective number of neutrino species $N_{\rm eff}$ and the baryon-to-photon ratio η showing $\gtrsim$ 1–2σ tensions with the Standard Model and the Planck Collaboration results. Motivated by the tensions, we have allowed the degeneracy parameter of the electron neutrino $\xi_{\rm e}$, as well as $N_{\rm eff}$ and η, to vary. We obtain $\xi_{\rm e} = 0.05^{+0.02}_{-0.03}$, $N_{\rm eff} = 3.11^{+0.31}_{-0.34}$, and $\eta\times10^{10} = 6.08^{+0.06}_{-0.06}$ from the $Y_{\rm P}$ and $D_{\rm P}$ measurements with a prior of η taken from the Planck Collaboration results (Figure 4). Our constraints suggest a lepton asymmetry and allow for a high value of $N_{\rm eff}$ within the 1σ level, which could mitigate the Hubble tension.

Programs with JWST

In [153], we have presented pure spectroscopic constraints on the UV luminosity functions and cosmic SFR densities from 25 galaxies at $z_{\rm spec} = 8.61$–13.20. By reducing the JWST/NIRSpec spectra taken in multiple programs of Early Release Observation, Early Release Science, General Observer, and Director's Discretionary Time observations with our analysis technique, we independently confirm 16 galaxies at $z_{\rm spec} = 8.61$–11.40, including new redshift determinations, and a bright interloper at $z_{\rm spec} = 4.91$ that was claimed as a photometric candidate at $z\sim16$. In conjunction with nine galaxies at redshifts up to $z_{\rm spec} = 13.20$ in the literature, we have made a sample of 25 spectroscopically confirmed galaxies in total and carefully derive the best estimates and lower

limits of the UV luminosity functions. These UV luminosity function constraints are consistent with the previous photometric estimates within the uncertainties and indicate mild redshift evolution toward $z \sim 12$, showing tensions with some theoretical models of rapid evolution. With these spectroscopic constraints, we have obtained firm lower limits of the cosmic SFR densities and spectroscopically confirm a high SFR density at $z \sim 12$ beyond the constant star formation efficiency models, which supports earlier claims from the photometric studies. While there are no spectroscopically confirmed galaxies with very large stellar masses violating the ΛCDM model due to the removal of the bright interloper, we have confirmed star-forming galaxies at $z_{\rm spec} = 11$–13 with stellar masses much higher than model predictions (Figure 5). Our results indicate possibilities of high star formation efficiency ($> 5\%$), a hidden active galactic nucleus, a top-heavy initial mass function (possibly with Population III), and large scatter/variance. Having these successful and unsuccessful spectroscopy results, we have suggested observational strategies for efficiently removing low-redshift interlopers for future JWST programs.

In [148], we have presented chemical abundance ratios of 70 star-forming galaxies at $z \sim 4$–10 observed by the JWST/NIRSpec Early Release Observations, GLASS, and CEERS programs. Among the 70 galaxies, we have pinpointed two galaxies, CEERS_01019 at $z = 8.68$ and GLASS_150008 at $z = 6.23$, with extremely low C/N ([C/N]$\lesssim -1$), evidenced with C III]$\lambda\lambda$1907,1909, N III]λ1750, and N IV]$\lambda\lambda$1483,1486, which show high N/O ratios ([N/O]$\gtrsim 0.5$) comparable with the one of GN-z11, regardless of whether stellar or active galactic nucleus radiation is assumed (Figure 6). Such low C/N and high N/O ratios found in CEERS_01019 and GLASS_150008 (additionally identified in GN-z11) are largely biased toward the equilibrium of the CNO cycle, suggesting that these three galaxies are enriched by metals processed by the CNO cycle. On the C/N versus O/H plane, these three galaxies do not coincide with Galactic H II regions, normal star-forming galaxies, and nitrogen-loud quasars with asymptotic giant branch stars, but with globular-cluster (GC) stars, indicating a connection with GC formation. We have compared the C/O and N/O of these three galaxies with those of theoretical models and find that these three galaxies are explained by scenarios with dominant CNO-cycle materials, i.e., Wolf-Rayet (WR) stars, supermassive (10^3–$10^5 M_\odot$) stars, and tidal disruption events, interestingly with a requirement of frequent direct collapses. For all the 70 galaxies, we have presented measurements of Ne/O, S/O, and Ar/O, together with C/O and N/O. We identify four galaxies with very low Ne/O, log(Ne/O)< -1.0, indicating abundant massive ($\gtrsim 30 M_\odot$) stars.

In [146], we have presented the first statistical sample of faint type 1 AGNs at $z > 4$ identified by JWST/NIRSpec deep spectroscopy. Among the 185 galaxies at $z_{\rm spec} = 3.8$–8.9 confirmed with NIRSpec, our systematic search for broad-line emission reveals 10 type 1 AGNs at $z = 4.015$–6.936 whose broad component is only seen in the permitted Hα line and not in the forbidden [O III]λ5007 line that is detected with greater significance than Hα. The broad Hα line widths of FWHM$\simeq$1000–6000 km s^{-1} suggest that the AGNs have low-mass black holes with $M_{\rm BH} \sim 10^6$–$10^8 M_\odot$, remarkably lower than those of low-luminosity quasars previously identified at $z > 4$ with ground-based telescopes. JWST and Hubble Space Telescope high-resolution images reveal that the majority of them show extended morphologies indicating significant contribution to the total lights from their host galaxies, except for three compact objects two of which show red spectral energy distributions, probably in a transition phase from faint AGNs to low luminosity quasars. Careful AGN-host decomposition analyses show that their host's stellar masses are systematically lower than the local relation between the black hole mass and the stellar mass, implying a fast black hole growth consistent with predictions from theoretical simulations. A high fraction of the broad-line AGNs ($\sim 5\%$), higher than $z \sim 0$, indicates that the number density of such faint AGNs is higher than an extrapolation of the quasar luminosity function, implying a large population of AGNs in the early universe. Such faint AGNs contribute to cosmic reionization, while the total contribution is not large, up to $\sim 50\%$ at $z \sim 6$, because of their faint nature.

On-Going Projects and Future Prospects

We will conduct observational studies utilizing JWST and large ground-based telescopes such as Subaru and ALMA, which are engaged in extensive surveys. Additionally, aiming for world-leading research, we will use the Prime Focus Spectrograph (PFS) on Subaru and the wide-area imaging instrument on the Rubin Observatory, which are set to begin observations in 2025, to work on cosmology studies focusing on primordial helium abundance and σ_8 measurements as well as galaxy and supermassive black hole studies at high redshifts including the epoch of cosmic reionization. Along with observations of high-z objects using NASA Roman Space Telescope, slated to start in 2026–2027, by organically combine diverse data, we will undertake collaborative research to address new challenges, such as the potential tension with the Standard Model/lepton asymmetry, discrepancies in the ΛCDM model and structure formation, the physical origin of high N/O ratios, and early galaxy/black hole formation mechanisms. The observational results will be explained through the development of theoretical models, including numerical simulations, aiming to resolve these issues. Additionally, by identifying contradictions through comparisons with theoretical models, we will uncover new scientific challenges previously unknown. The PFS galaxy formation research has been underway since around 2010, with Professor Masami Ouchi serving as one of the co-chairs, and through the analysis of trial observational data, we have proposed PFS SSP observations. The construction of the Rubin Observatory is progressing smoothly, with observations expected to begin in 2025. Preparations for observations with the Roman Space Telescope are also underway, and Professor Masami Ouchi is leading the preparatory research on galaxy formation to which Japan is contributing.

Institute	Country	(*)
ICRR, Univ. of Tokyo	Japan	15
Kavli IPMU, U. of Tokyo	Japan	24
School of Science, U. of Tokyo	Japan	28
NAOJ	Japan	47
JAXA	Japan	6
Tohoku Univ.	Japan	10
Tsukuba Univ.	Japan	1
Kyoto Univ.	Japan	1
Osaka Univ.	Japan	2
Nagoya Univ.	Japan	8
Hokkaido Univ.	Japan	1
Hiroshima Univ.	Japan	4
Ehime Univ.	Japan	12
Tokyo Univ. of Science	Japan	3
Others	Japan	17
ASIAA	Taiwan	23
NCU	Taiwan	9
NTHU	Taiwan	6
Princeton Univ.	USA	27
Stanford Univ.	USA	1
JHU	USA	1
Univ. of Penn.	USA	1
Univ. of Geneva	Switzerland	1
ETH Zurich	Switzerland	1
SJTU	China	1
KIAA	China	1
Saint Mary's Univ.	Canada	1
ESO	Germany	1
SRON	Netherlands	1
Total		254

(*) Number of participants as of March 2023.

Members

Staff

Masami Ouchi, Professor, July 2010 to the present
Yoshiaki Ono, Assist. Professor, April 2012 to the present
Yuichi Harikane, Assist. Professor, June 2020 to the present

Postdoctoral Fellows

Jun Toshikawa, April 2017 to March 2021
Ken Mawatari, April 2018 to March 2021
Hideki Umehata, October 2021 to March 2022
Shohei Aoyama, April 2020 to July 2023
Yongming Liang, October 2022 to the present

Graduate Students

Nine students were awarded a doctor degree and ten students earned a master degree during FY 2018–2023, supervised by Masami Ouchi.

Bibliography

After April 2018

Papers in Refereed Journals

[1] "SPLASH-SXDF Multi-wavelength Photometric Catalog", Mehta, Vihang, et al., ApJS, 235, 36 (2018). **Cited 43 times**.

[2] "Large-scale Environment of a $z = 6.61$ Luminous Quasar Probed by Lyα Emitters and Lyman Break Galaxies", Ota, Kazuaki, et al., ApJ, 856, 109 (2018). **Cited 44 times**.

[3] "The onset of star formation 250 million years after the Big Bang", Hashimoto, Takuya, et al., Nature, 557, 392 (2018). **Cited 290 times**.

[4] "SILVERRUSH. V. Census of Lyα, [OIII]λ5007, Hα, and [CII]158μm Line Emission with $\sim$1000 LAEs at $z = 4.9$–7.0 Revealed with Subaru/HSC", Harikane, Yuichi, et al., ApJ, 859, 84 (2018). **Cited 111 times**.

[5] "SILVERRUSH. VI. A simulation of Lyα emitters in the reionization epoch and a comparison with Subaru Hyper Suprime-Cam survey early data", Inoue, Akio K., et al., PASJ, 70, 55 (2018). **Cited 69 times**.

[6] "Subaru High-z Exploration of Low-Luminosity Quasars (SHELLQs). III. Star formation properties of the host galaxies at $z \gtrsim 6$ studied with ALMA", Izumi, Takuma, et al., PASJ, 70, 36 (2018). **Cited 62 times**.

[7] "ALMA 26 Arcmin^2 Survey of GOODS-S at One Millimeter (ASAGAO): Average Morphology of High-z Dusty Star-forming Galaxies in an Exponential Disk ($n \simeq 1$)", Fujimoto, Seiji, et al., ApJ, 861, 7 (2018). **Cited 47 times**.

[8] "Subaru High-z Exploration of Low-luminosity Quasars (SHELLQs). IV. Discovery of 41 Quasars and Luminous Galaxies at $5.7 \leq z \leq 6.9$", Matsuoka, Yoshiki, et al., ApJS, 237, 5 (2018). **Cited 97 times**.

[9] "RELICS: Strong Lensing Analysis of the Galaxy Clusters Abell S295, Abell 697, MACS J0025.4-1222, and MACS J0159.8-0849", Cibirka, Nathália, et al., ApJ, 863, 145 (2018). **Cited 28 times**.

[10] "RELICS: A Candidate $z \sim 10$ Galaxy Strongly Lensed into a Spatially Resolved Arc", Salmon, Brett, et al., ApJL, 864, L22 (2018). **Cited 64 times**.

[11] "Detectability of the 21-cm signal during the epoch of reionization with 21-cm Lyman α emitter cross-correlation - I", Kubota, Kenji, et al., MNRAS, 479, 2754 (2018). **Cited 27 times**.

[12] "CHORUS. II. Subaru/HSC Determination of the Lyα Luminosity Function at $z = 7.0$: Constraints on Cosmic Reionization Model Parameter", Itoh, Ryohei, et al., ApJ, 867, 46 (2018). **Cited 54 times**.

[13] "The distribution and physical properties of high-redshift [OIII] emitters in a cosmological hydrodynamics simulation", Moriwaki, Kana, et al., MNRAS, 481, L84 (2018). **Cited 37 times**.

[14] "Subaru High-z Exploration of Low-luminosity Quasars (SHELLQs). V. Quasar Luminosity Function and Contribution to Cosmic Reionization at $z = 6$", Matsuoka, Yoshiki, et al., ApJ, 869, 150 (2018). **Cited 177 times**.

[15] "ALMA twenty-six arcmin^2 survey of GOODS-S at one millimeter (ASAGAO): Source catalog and number counts", Hatsukade, Bunyo, et al., PASJ, 70, 105 (2018). **Cited 86 times**.

[16] "The infrared-luminous progenitors of high-z quasars", Ginolfi, M., et al., MNRAS, 483, 1256 (2019). **Cited 10 times**.

[17] "Discovery of the First Low-luminosity Quasar at $z >$ 7", Matsuoka, Yoshiki, et al., ApJL, 872, L2 (2019). **Cited 133 times**.

[18] "Morphologies of $\sim$190,000 Galaxies at $z = 0$–10 Revealed with HST Legacy Data. III. Continuum Profile and Size Evolution of Lyα Emitters", Shibuya, Takatoshi, et al., ApJ, 871, 164 (2019). **Cited 52 times**.

[19] "Near-infrared Survey and Photometric Redshifts in the Extended GOODS-North Field", Hsu, Li-Ting, et al., ApJ, 871, 233 (2019). **Cited 7 times**.

[20] "Detection of the Far-infrared [OIII] and Dust Emission in a Galaxy at Redshift 8.312: Early Metal Enrichment in the Heart of the Reionization Era", Tamura, Yoichi, et al., ApJ, 874, 27 (2019). **Cited 176 times**.

[21] "Enhancement of HI absorption associated with the $z =$ 3.1 large-scale proto-cluster and characteristic structures with AGNs sculptured over Gpc scale in the SSA22 field", Hayashino, T., et al., MNRAS, 484, 5868 (2019). **Cited 10 times**.

[22] "Environmental impacts on molecular gas in protocluster galaxies at $z \sim 2$", Tadaki, Ken-ichi, et al., PASJ, 71, 40 (2019). **Cited 48 times**.

[23] "RELICS: High-resolution Constraints on the Inner Mass Distribution of the $z = 0.83$ Merging Cluster RXJ0152.7-1357 from Strong Lensing", Acebron, Ana, et al., ApJ, 874, 132 (2019). **Cited 21 times**.

[24] "The dominant origin of diffuse Lyα halos around Lyα emitters explored by spectral energy distribution fitting and clustering analysis", Kusakabe, Haruka, et al., PASJ, 71, 55 (2019). **Cited 11 times**.

[25] "Long Gamma-Ray Burst Rate at Very High Redshift", Kinugawa, Tomoya, et al., ApJ, 878, 128 (2019). **Cited 14 times**.

[26] "ALMA 26 arcmin^2 Survey of GOODS-S at 1 mm (ASAGAO): Near-infrared-dark Faint ALMA Sources", Yamaguchi, Yuki, et al., ApJ, 878, 73 (2019). **Cited 59 times**.

[27] "The Brightest UV-selected Galaxies in Protoclusters at $z \sim 4$: Ancestors of Brightest Cluster Galaxies?", Ito, Kei, et al., ApJ, 878, 68 (2019). **Cited 17 times**.

[28] "Fluorescent CII*1335Å emission spectroscopically resolved in a galaxy at $z = 5.754$", Bosman, Sarah E. I., et al., MNRAS, 487, L67 (2019). **Cited 3 times**.

[29] "How Do Galaxies Trace a Large-scale Structure? A Case Study around a Massive Protocluster at $z = 3.13$", Shi, Ke, et al., ApJ, 879, 9 (2019). **Cited 34 times**.

[30] "The absence of [CII]158μm emission in spectroscopically confirmed galaxies at $z > 8$", Laporte, N., et al., MNRAS, 487, L81 (2019). **Cited 57 times**.

[31] "SILVERRUSH. VII. Subaru/HSC Identifications of Protocluster Candidates at $z \sim$ 6–7: Implications for Cosmic Reionization", Higuchi, Ryo, et al., ApJ, 879, 28 (2019). **Cited 66 times**.

[32] "Big Three Dragons: A $z = 7.15$ Lyman-break galaxy detected in [OIII]88μm, [CII]158μm, and dust continuum with ALMA", Hashimoto, Takuya, et al., PASJ, 71, 71 (2019). **Cited 213 times**.

[33] "A Giant Green Pea Identified in the Spectroscopy of Spatially Extended [OIII] Sources", Yuma, Suraphong, et al., ApJ, 882, 17 (2019). **Cited 6 times**.

[34] "Lack of close-in, massive planets of main-sequence A-type stars from Kepler", Sabotta, Silvia, et al., MNRAS, 489, 2069 (2019). **Cited 8 times**.

[35] "Subaru High-z Exploration of Low-luminosity Quasars (SHELLQs). X. Discovery of 35 Quasars and Luminous Galaxies at $5.7 \leq z \leq 7.0$", Matsuoka, Yoshiki, et al., ApJ, 883, 183 (2019). **Cited 91 times**.

[36] "SILVERRUSH. VIII. Spectroscopic Identifications of Early Large-scale Structures with Protoclusters over 200 Mpc at $z \sim$ 6–7: Strong Associations of Dusty Star-forming Galaxies", Harikane, Yuichi, et al., ApJ, 883, 142 (2019). **Cited 83 times**.

[37] "RELICS: Reionization Lensing Cluster Survey", Coe, Dan, et al., ApJ, 884, 85 (2019). **Cited 172 times**.

[38] "Balmer breaks in simulated galaxies at $z > 6$", Binggeli, Christian, et al., MNRAS, 489, 3827 (2019). **Cited 14 times**.

[39] "Fast Outflows Identified in Early Star-forming Galaxies at $z =$ 5–6", Sugahara, Yuma, et al., ApJ, 886, 29 (2019). **Cited 43 times**.

[40] "Detections of [OIII]88μm in two quasars in the reionization epoch", Hashimoto, Takuya, et al., PASJ, 71, 109 (2019). **Cited 35 times**.

[41] "Second data release of the Hyper Suprime-Cam Subaru Strategic Program", Aihara, Hiroaki, et al., PASJ, 71, 114 (2019). **Cited 363 times**.

[42] "Planck Far-infrared Detection of Hyper Suprime-Cam Protoclusters at $z \sim 4$: Hidden AGN and Star Formation Activity", Kubo, Mariko, et al., ApJ, 887, 214 (2019). **Cited 27 times**.

[43] "First Identification of 10 kpc [CII]158μm Halos around Star-forming Galaxies at $z = 5$–7", Fujimoto, Seiji, et al., ApJ, 887, 107 (2019). **Cited 113 times**.

[44] "Discovery of Protoclusters at $z \sim 3.7$ and 4.9: Embedded in Primordial Superclusters", Toshikawa, Jun, et al., ApJ, 888, 89 (2020). **Cited 15 times**.

[45] "Evidence for a Highly Opaque Large-scale Galaxy Void at the End of Reionization", Kashino, Daichi, et al., ApJ, 888, 6 (2020). **Cited 28 times**.

[46] "Stellar Properties of $z \gtrsim 8$ Galaxies in the Reionization Lensing Cluster Survey", Strait, Victoria, et al., ApJ, 888, 124 (2020). **Cited 38 times**.

[47] "Rest-frame UV properties of luminous strong gravitationally lensed Lyα emitters from the BELLS GALLERY Survey", Marques-Chaves, R., et al., MNRAS, 492, 1257 (2020). **Cited 13 times**.

[48] "Balmer Break Galaxy Candidates at $z \sim 6$: A Potential View on the Star Formation Activity at $z \gtrsim 14$", Mawatari, Ken, et al., ApJ, 889, 137 (2020). **Cited 28 times**.

[49] "CHORUS. III. Photometric and Spectroscopic Properties of Lyα Blobs at $z = 4.9$–7.0", Zhang, Haibin, et al., ApJ, 891, 177 (2020). **Cited 17 times**.

[50] "Truth or Delusion? A Possible Gravitational Lensing Interpretation of the Ultraluminous Quasar SDSS J010013.02+280225.8 at $z = 6.30$", Fujimoto, Seiji, et al., ApJ, 891, 64 (2020). **Cited 18 times**.

[51] "ALMA uncovers the [CII] emission and warm dust continuum in a $z = 8.31$ Lyman break galaxy", Bakx, Tom J. L. C., et al., MNRAS, 493, 4294 (2020). **Cited 111 times**.

[52] "Early Low-mass Galaxies and Star-cluster Candidates at $z \sim$ 6–9 Identified by the Gravitational-lensing Technique and Deep Optical/Near-infrared Imaging", Kikuchihara, Shotaro, et al., ApJ, 893, 60 (2020). **Cited 64 times**.

[53] "Deep multiredshift limits on Epoch of Reionization 21 cm power spectra from four seasons of Murchison Widefield Array observations", Trott, Cathryn M., et al., MNRAS, 493, 4711 (2020). **Cited 157 times**.

[54] "The role of galaxies and AGN in reionizing the IGM - III. IGM-galaxy cross-correlations at $z \sim 6$ from eight quasar fields with DEIMOS and MUSE", Meyer, Romain A., et al., MNRAS, 494, 1560 (2020). **Cited 40 times**.

[55] "Large Population of ALMA Galaxies at $z > 6$ with Very High [OIII]88μm to [CII]158μm Flux Ratios: Evidence of Extremely High Ionization Parameter or PDR Deficit?", Harikane, Yuichi, et al., ApJ, 896, 93 (2020). **Cited 130 times**.

[56] "Three-dimensional Distribution Map of HI Gas and Galaxies around an Enormous Lyα Nebula and Three QSOs at $z = 2.3$ Revealed by the HI Tomographic Mapping Technique", Mukae, Shiro, et al., ApJ, 896, 45 (2020). **Cited 16 times**.

[57] "RELICS: A Very Large ($\theta_{\rm E} \sim 40''$) Cluster Lens — RXC J0032.1+1808", Acebron, Ana, et al., ApJ, 898, 6 (2020). **Cited 12 times**.

[58] "The UV Luminosity Function of Protocluster Galaxies at $z \sim 4$: The Bright-end Excess and the Enhanced Star Formation Rate Density", Ito, Kei, et al., ApJ, 899, 5 (2020). **Cited 17 times**.

[59] "Extremely Metal-poor Representatives Explored by the Subaru Survey (EMPRESS). I. A Successful Machine-learning Selection of Metal-poor Galaxies and the Discovery of a Galaxy with $M_{\rm star} < 10^6\ M_\odot$ and $0.016\ Z_\odot$", Kojima, Takashi, et al., ApJ, 898, 142 (2020). **Cited 56 times**.

[60] "A Wide and Deep Exploration of Radio Galaxies with Subaru HSC (WERGS). III. Discovery of a $z = 4.72$ Radio Galaxy with the Lyman Break Technique", Yamashita, Takuji, et al., AJ, 160, 60 (2020). **Cited 14 times**.

[61] "Observations of the Lyman-α Universe", Ouchi, Masami, et al., ARA&A, 58, 617 (2020). **Cited 127 times**.

[62] "A Detailed Study of Massive Galaxies in a Protocluster at $z = 3.13$", Shi, Ke, et al., ApJ, 899, 79 (2020). **Cited 18 times**.

[63] "Dual Supermassive Black Holes at Close Separation Revealed by the Hyper Suprime-Cam Subaru Strategic Program", Silverman, John D., et al., ApJ, 899, 154 (2020). **Cited 39 times**.

[64] "ALMA twenty-six arcmin^2 survey of GOODS-S at one millimeter (ASAGAO): Millimeter properties of stellar mass selected galaxies", Yamaguchi, Yuki, et al., PASJ, 72, 69 (2020). **Cited 11 times**.

[65] "The Mass-Metallicity Relation at $z \simeq 8$: Direct-method Metallicity Constraints and Near-future Prospects", Jones, Tucker, et al., ApJ, 903, 150 (2020). **Cited 51 times**.

[66] "Testing an indirect method for identifying galaxies with high levels of Lyman continuum leakage", Yamanaka, Satoshi, et al., MNRAS, 498, 3095 (2020). **Cited 10 times**.

[67] "The Subaru HSC Galaxy Clustering with Photometric Redshift. I. Dark Halo Masses versus Baryonic Properties of Galaxies at $0.3 \leq z \leq 1.4$", Ishikawa, Shogo, et al., ApJ, 904, 128 (2020). **Cited 18 times**.

[68] "The Faint End of the Quasar Luminosity Function at $z \sim 5$ from the Subaru Hyper Suprime-Cam Survey", Niida, Mana, et al., ApJ, 904, 89 (2020). **Cited 46 times**.

[69] "Faint Quasars Live in the Same Number Density Environments as Lyman Break Galaxies at $z \sim 4$", Uchiyama, Hisakazu, et al., ApJ, 905, 125 (2020). **Cited 6 times**.

[70] "Broadband Selection, Spectroscopic Identification, and Physical Properties of a Population of Extreme Emission-line Galaxies at $3 < z < 3.7$", Onodera, Masato, et al., ApJ, 904, 180 (2020). **Cited 19 times**.

[71] "CHORUS. I. Cosmic HydrOgen Reionization Unveiled with Subaru: Overview", Inoue, Akio K., et al., PASJ, 72, 101 (2020). **Cited 16 times**.

[72] "Statistical Correlation between the Distribution of Lyα Emitters and Intergalactic Medium HI at $z \sim 2.2$ Mapped by the Subaru/Hyper Suprime-Cam", Liang, Yongming, et al., ApJ, 907, 3 (2021). **Cited 24 times**.

[73] "Subaru High-z Exploration of Low-luminosity Quasars (SHELLQs). XII. Extended [CII] Structure (Merger or Outflow) in a $z = 6.72$ Red Quasar", Izumi, Takuma, et al., ApJ, 908, 235 (2021). **Cited 16 times**.

[74] "A puzzling non-detection of [OIII] and [CII] from a $z \approx 7.7$ galaxy observed with ALMA", Binggeli, C., et al., A&A, 646, A26 (2021). **Cited 5 times**.

[75] "FIR-luminous [CII] Emitters in the ALMA-SCUBA-2 COSMOS Survey (AS2COSMOS): The Nature of Submillimeter Galaxies in a 10 Comoving Megaparsec-scale Structure at $z \sim 4.6$", Mitsuhashi, I., et al., ApJ, 907, 122 (2021). **Cited 12 times**.

[76] "RELICS-DP7: Spectroscopic Confirmation of a Dichromatic Primeval Galaxy at $z \sim 7$", Pelliccia, Debora, et al., ApJL, 908, L30 (2021). **Cited 11 times**.

[77] "ALMA Lensing Cluster Survey: An ALMA Galaxy Signposting a MUSE Galaxy Group at $z = 4.3$ Behind "El Gordo"", Caputi, K. I., et al., ApJ, 908, 146 (2021). **Cited 35 times**.

[78] "ALMA Lensing Cluster Survey: Bright [CII]158μm Lines from a Multiply Imaged Sub-L* Galaxy at $z = 6.0719$", Fujimoto, Seiji, et al., ApJ, 911, 99 (2021). **Cited 44 times**.

[79] "Accelerated Galaxy Growth and Environmental Quenching in a Protocluster at $z = 3.24$", Shi, Ke, et al., ApJ, 911, 46 (2021). **Cited 24 times**.

[80] "Faint LAEs near $z > 4.7$ CIV absorbers revealed by MUSE", Díaz, C. G., et al., MNRAS, 502, 2645 (2021). **Cited 25 times**.

[81] "RELICS: Properties of $z \geq 5.5$ Galaxies Inferred from Spitzer and Hubble Imaging, Including A Candidate $z \sim 6.8$ Strong [OIII] emitter", Strait, Victoria, et al., ApJ, 910, 135 (2021). **Cited 30 times**.

[82] "SILVERRUSH X: Machine Learning-aided Selection of 9318 LAEs at $z = 2.2$, 3.3, 4.9, 5.7, 6.6, and 7.0 from the HSC SSP and CHORUS Survey Data", Ono, Yoshiaki, et al., ApJ, 911, 78 (2021). **Cited 21 times**.

[83] "EMPRESS. II. Highly Fe-enriched Metal-poor Galaxies with $\sim$1.0 $(\mathrm{Fe/O})_\odot$ and 0.02 $(\mathrm{O/H})_\odot$: Possible Traces of Supermassive ($>$300 $M_\odot$) Stars in Early Galaxies", Kojima, Takashi, et al., ApJ, 913, 22 (2021). **Cited 26 times**.

[84] "Probing Feedback via IGM tomography and the Lyα Forest with Subaru PFS, TMT/ELT, and JWST", Nagamine, Kentaro, et al., ApJ, 914, 66 (2021). **Cited 26 times**.

[85] "SILVERRUSH. IX. Lyα Intensity Mapping with Star-forming Galaxies at $z = 5.7$ and 6.6: A Possible Detection of Extended Lyα Emission at $\gtrsim$100 Comoving Kiloparsecs around and beyond the Virial-radius Scale of Galaxy Dark Matter Halos", Kakuma, Ryota, et al., ApJ, 916, 22 (2021). **Cited 21 times**.

[86] "ALMA Lensing Cluster Survey: a strongly lensed multiply imaged dusty system at $z \geq 6$", Laporte, N., et al., MNRAS, 505, 4838 (2021). **Cited 25 times**.

[87] "Subaru High-z Exploration of Low-luminosity Quasars (SHELLQs). XIV. A Candidate Type II Quasar at $z = 6.1292$", Onoue, Masafusa, et al., ApJ, 919, 61 (2021). **Cited 15 times**.

[88] "EMPRESS. III. Morphology, Stellar Population, and Dynamics of Extremely Metal-poor Galaxies (EMPGs): Are EMPGs Local Analogs of High-z Young Galaxies?", Isobe, Yuki, et al., ApJ, 918, 54 (2021). **Cited 17 times**.

[89] "Optical Spectroscopy of Dual Quasar Candidates from the Subaru HSC-SSP program", Tang, Shenli, et al., ApJ, 922, 83 (2021). **Cited 21 times**.

[90] "Subaru/FOCAS IFU revealed the metallicity gradient of a local extremely metal-poor galaxy", Kashiwagi, Yuri, et al., PASJ, 73, 1631 (2021). **Cited 2 times**.

[91] "First HETDEX Spectroscopic Determinations of Lyα and UV Luminosity Functions at $z = 2$–3: Bridging a Gap between Faint AGNs and Bright Galaxies", Zhang, Yechi, et al., ApJ, 922, 167 (2021). **Cited 24 times**.

[92] "SILVERRUSH. XI. Constraints on the Lyα Luminosity Function and Cosmic Reionization at $z = 7.3$ with Subaru/Hyper Suprime-Cam", Goto, Hinako, et al., ApJ, 923, 229 (2021). **Cited 27 times**.

[93] "The Hobby-Eberly Telescope Dark Energy Experiment (HETDEX) Survey Design, Reductions, and Detections", Gebhardt, Karl, et al., ApJ, 923, 217 (2021). **Cited 71 times**.

[94] "FOREVER22: galaxy formation in protocluster regions", Yajima, Hidenobu, et al., MNRAS, 509, 4037 (2022). **Cited 29 times**.

[95] "A Wide and Deep Exploration of Radio Galaxies with Subaru HSC (WERGS). VI. Distant Filamentary Structures Pointed Out by High-z Radio Galaxies at $z \sim 4$", Uchiyama, Hisakazu, et al., ApJ, 926, 76 (2022). **Cited 6 times**.

[96] "Galaxy morphologies revealed with Subaru HSC and super-resolution techniques. I. Major merger fractions of $L_{\rm UV} \sim 3$–$15L^*_{\rm UV}$ dropout galaxies at $z \sim 4$–7", Shibuya, Takatoshi, et al., PASJ, 74, 73 (2022). **Cited 16 times**.

[97] "EMPRESS. IV. Extremely Metal-poor Galaxies Including Very Low-mass Primordial Systems with $M_* = 10^4$–$10^5 M_\odot$ and 2%–3% (O/H): High (Fe/O) Suggestive of Metal Enrichment by Hypernovae/Pair-instability Supernovae", Isobe, Yuki, et al., ApJ, 925, 111 (2022). **Cited 28 times**.

[98] "CHORUS. IV. Mapping the Spatially Inhomogeneous Cosmic Reionization with Subaru HSC", Yoshioka, Takehiro, et al., ApJ, 927, 32 (2022). **Cited 10 times**.

[99] "GOLDRUSH. IV. Luminosity Functions and Clustering Revealed with 4,000,000 Galaxies at $z \sim 2$–7: Galaxy-AGN Transition, Star Formation Efficiency, and Implication for Evolution at $z > 10$", Harikane, Yuichi, et al., ApJS, 259, 20 (2022). **Cited 133 times**.

[100] "Subaru High-z Exploration of Low-luminosity Quasars (SHELLQs). XVI. 69 New Quasars at $5.8 < z < 7.0$", Matsuoka, Yoshiki, et al., ApJS, 259, 18 (2022). **Cited 37 times**.

[101] "EMPRESS. VI. Outflows Investigated in Low-mass Galaxies with $M_* = 10^4$–$10^7 M_\odot$: Weak Feedback in Low-mass Galaxies?", Xu, Yi, et al., ApJ, 929, 134 (2022). **Cited 18 times**.

[102] "Surface Brightness Profile of Lyman-α Halos out to 320 kpc in HETDEX", Lujan Niemeyer, Maja, et al., ApJ, 929, 90 (2022). **Cited 22 times**.

[103] "A Search for H-Dropout Lyman Break Galaxies at $z \sim$ 12–16", Harikane, Yuichi, et al., ApJ, 929, 1 (2022). **Cited 85 times**.

[104] "Third data release of the Hyper Suprime-Cam Subaru Strategic Program", Aihara, Hiroaki, et al., PASJ, 74, 247 (2022). **Cited 185 times**.

[105] "EMPRESS. VII. Ionizing Spectrum Shapes of Extremely Metal-poor Galaxies: Uncovering the Origins of Strong He II and the Impact on Cosmic Reionization", Umeda, Hiroya, et al., ApJ, 930, 37 (2022). **Cited 25 times**.

[106] "MUSUBI (MegaCam Ultra-deep Survey: u*-band Imaging) Data for the COSMOS and SXDS Fields", Wang, Wei-Hao, et al., ApJS, 260, 54 (2022). **Cited 0 times**.

[107] "SILVERRUSH. XII. Intensity Mapping for Lyα Emission Extending over 100–1000 Comoving Kpc around $z \sim 2$–7 LAEs with Subaru HSC-SSP and CHORUS Data", Kikuchihara, Shotaro, et al., ApJ, 931, 97 (2022). **Cited 12 times**.

[108] "CLASSY III. The Properties of Starburst-driven Warm Ionized Outflows", Xu, Xinfeng, et al., ApJ, 933, 222 (2022). **Cited 38 times**.

[109] "Are the newly-discovered $z \sim 13$ drop-out sources starburst galaxies or quasars?", Pacucci, Fabio, et al., MNRAS, 514, L6 (2022). **Cited 27 times**.

[110] "The ALMA-ALPINE [CII] survey. The star formation history and the dust emission of star-forming galaxies at $4.5 < z < 6.2$", Burgarella, D., et al., A&A, 664, A73 (2022). **Cited 11 times**.

[111] "The COS Legacy Archive Spectroscopy Survey (CLASSY) Treasury Atlas", Berg, Danielle A., et al., ApJS, 261, 31 (2022). **Cited 62 times**.

[112] "Bridging Optical and Far-infrared Emission-line Diagrams of Galaxies from Local to the Epoch of Reionization: Characteristic High [OIII]88μm/SFR at $z > 6$", Sugahara, Yuma, et al., ApJ, 935, 119 (2022). **Cited 16 times**.

[113] "First Identification of a CMB Lensing Signal Produced by 1.5 Million Galaxies at $z \sim 4$: Constraints on Matter Density Fluctuations at High Redshift", Miyatake, Hironao, et al., PhRvL, 129, 061301 (2022). **Cited 15 times**.

[114] "EMPRESS. V. Metallicity Diagnostics of Galaxies over 12 + log(O/H) $\simeq$ 6.9–8.9 Established by a Local Galaxy Census: Preparing for JWST Spectroscopy", Nakajima, Kimihiko, et al., ApJS, 262, 3 (2022). **Cited 48 times**.

[115] "A Lower Bound of Star Formation Activity in Ultra-high-redshift Galaxies Detected with JWST: Implications for Stellar Populations and Radiation Sources", Inayoshi, Kohei, et al., ApJL, 938, L10 (2022). **Cited 57 times**.

[116] "CLASSY. II. A Technical Overview of the COS Legacy Archive Spectroscopic Survey", James, Bethan L., et al., ApJS, 262, 37 (2022). **Cited 21 times**.

[117] "The discovery and characterization of (594913) 'Ayló'chaxnim, a kilometre sized asteroid inside the orbit of Venus", Bolin, Bryce T., et al., MNRAS, 517, L49 (2022). **Cited 15 times**.

[118] "EMPRESS. VIII. A New Determination of Primordial He Abundance with Extremely Metal-poor Galaxies: A Suggestion of the Lepton Asymmetry and Implications for the Hubble Tension", Matsumoto, Akinori, et al., ApJ, 941, 167 (2022). **Cited 52 times**.

[119] "Discovery of 24 radio-bright quasars at $4.9 \leq z \leq 6.6$ using low-frequency radio observations", Gloudemans, A. J., et al., A&A, 668, A27 (2022). **Cited 19 times**.

[120] "ALMA Observations of CO Emission from Luminous Lyman-break Galaxies at $z = 6.0293$–6.2037", Ono, Yoshiaki, et al., ApJ, 941, 74 (2022). **Cited 4 times**.

[121] "ALMA Lensing Cluster Survey: Hubble Space Telescope and Spitzer Photometry of 33 Lensed Fields Built with CHArGE", Kokorev, V., et al., ApJS, 263, 38 (2022). **Cited 46 times**.

[122] "A Wide and Deep Exploration of Radio Galaxies with Subaru HSC (WERGS). IX. The most overdense region at $z \sim 5$ inhabited by a massive radio galaxy", Uchiyama, Hisakazu, et al., PASJ, 74, L27 (2022). **Cited 3 times**.

[123] "Extreme value statistics of the halo and stellar mass distributions at high redshift: are JWST results in tension with ΛCDM?", Lovell, Christopher C., et al., MNRAS, 518, 2511 (2023). **Cited 102 times**.

[124] "HETDEX Public Source Catalog 1: 220 K Sources Including Over 50 K Lyα Emitters from an Untargeted Wide-area Spectroscopic Survey", Mentuch Cooper, Erin, et al., ApJ, 943, 177 (2023). **Cited 17 times**.

[125] "The Gas and Stellar Content of a Metal-poor Galaxy at $z = 8.496$ as Revealed by JWST and ALMA", Heintz, K. E., et al., ApJL, 944, L30 (2023). **Cited 31 times**.

[126] "A Comprehensive Study of Galaxies at $z \sim 9$–16 Found in the Early JWST Data: Ultraviolet Luminosity Functions and Cosmic Star Formation History at the Pre-reionization Epoch", Harikane, Yuichi, et al., ApJS, 265, 5 (2023). **Cited 300 times**.

[127] "ALMA detection of 321 GHz water maser emission in the radio galaxy NGC 1052", Kameno, Seiji, et al., PASJ, 75, L1 (2023). **Cited 4 times**.

[128] "Stellar Initial Mass Function (IMF) Probed with Supernova Rates and Neutrino Background: Cosmic-average IMF Slope Is $\simeq$ 2–3 Similar to the Salpeter IMF", Aoyama, Shohei, et al., ApJ, 946, 69 (2023). **Cited 4 times**.

[129] "The SSA22 HI Tomography Survey (SSA22-HIT). I. Data Set and Compiled Redshift Catalog", Mawatari, Ken, et al., AJ, 165, 208 (2023). **Cited 0 times**.

[130] "A solar metallicity galaxy at $z > 7$? Possible detection of the [NII]122μm and [OIII]52μm lines", Killi, Meghana, et al., MNRAS, 521, 2526 (2023). **Cited 8 times**.

[131] "The Stellar Mass-Black Hole Mass Relation at $z \sim 2$ down to $M_{\rm BH} \sim 10^7 M_\odot$ Determined by HETDEX", Zhang, Yechi, et al., ApJ, 948, 103 (2023). **Cited 7 times**.

[132] "Quasar Luminosity Function at $z = 7$", Matsuoka, Yoshiki, et al., ApJL, 949, L42 (2023). **Cited 25 times**.

[133] "Morphologies of Galaxies at $z \gtrsim 9$ Uncovered by JWST/NIRCam Imaging: Cosmic Size Evolution and an Identification of an Extremely Compact Bright Galaxy at $z \sim 12$", Ono, Yoshiaki, et al., ApJ, 951, 72 (2023). **Cited 57 times**.

[134] "EMPRESS. IX. Extremely Metal-poor Galaxies are Very Gas-rich Dispersion-dominated Systems: Will the James Webb Space Telescope Witness Gaseous Turbulent High-z Primordial Galaxies?", Isobe, Yuki, et al., ApJ, 951, 102 (2023). **Cited 7 times**.

[135] "Cosmological-scale Lyα Forest Absorption around Galaxies and AGNs Probed with the HETDEX and SDSS Spectroscopic Data", Sun, Dongsheng, et al., ApJ, 951, 25 (2023). **Cited 1 times**.

[136] "Big Three Dragons: Molecular Gas in a Bright Lyman-break Galaxy at $z = 7.15$", Hashimoto, Takuya, et al., ApJ, 952, 48 (2023). **Cited 6 times**.

[137] "EMPRESS. XI. SDSS and JWST Search for Local and $z \sim 4$–5 Extremely Metal-poor Galaxies (EMPGs): Clustering and Chemical Properties of Local EMPGs", Nishigaki, Moka, et al., ApJ, 952, 11 (2023). **Cited 5 times**.

[138] "The Spitzer Coverage of HSC-Deep with IRAC for Z studies (SHIRAZ). I. IRAC Mosaics", Annunziatella, Marianna, et al., AJ, 166, 25 (2023). **Cited 3 times**.

[139] "Photometric IGM tomography with Subaru/HSC: the large-scale structure of Ly α emitters and IGM transmission in the COSMOS field at $z \sim 5$", Kakiichi, Koki, et al., MNRAS, 523, 1772 (2023). **Cited 1 times**.

[140] "SILVERRUSH. XIII. A Catalog of 20,567 Lyα Emitters at $z = 2$–7 Identified in the Full-depth Data of the Subaru/HSC-SSP and CHORUS Surveys", Kikuta, Satoshi, et al., ApJS, 268, 24 (2023). **Cited 4 times**.

[141] "ALMA FIR View of Ultra-high-redshift Galaxy Candidates at $z \sim 11$–17: Blue Monsters or Low-z Red Interlopers?", Fujimoto, Seiji, et al., ApJ, 955, 130 (2023). **Cited 37 times**.

[142] "Plausible association of distant late M dwarfs with low-frequency radio emission", Gloudemans, A. J., et al., A&A, 678, A161 (2023). **Cited 1 times**.

[143] "No strong radio absorption detected in the low-frequency spectra of radio-loud quasars at $z > 5.6$", Gloudemans, A. J., et al., A&A, 678, A128 (2023). **Cited 1 times**.

[144] "Redshift Evolution of Electron Density in the Interstellar Medium at $z \sim$ 0–9 Uncovered with JWST/NIRSpec Spectra and Line-spread Function Determinations", Isobe, Yuki, et al., ApJ, 956, 139 (2023). **Cited 40 times**.

[145] "FOREVER22: the first bright galaxies with Population III stars at redshifts $z \simeq$ 10–20 and comparisons with JWST data", Yajima, Hidenobu, et al., MNRAS, 525, 4832 (2023). **Cited 29 times**.

[146] "A JWST/NIRSpec First Census of Broad-line AGNs at $z = 4$–7: Detection of 10 Faint AGNs with $M_{\rm BH} \sim 10^6$–$10^8 M_\odot$ and Their Host Galaxy Properties", Harikane, Yuichi, et al., ApJ, 959, 39 (2023). **Cited 154 times**.

[147] "Constraint on the event rate of general relativistic instability supernovae from the early JWST deep field data", Moriya, Takashi J., et al., MNRAS, 526, 2400 (2023). **Cited 1 times**.

[148] "JWST Identification of Extremely Low C/N Galaxies with [N/O] $\gtrsim$ 0.5 at $z \sim$ 6–10 Evidencing the Early CNO-cycle Enrichment and a Connection with Globular Cluster Formation", Isobe, Yuki, et al., ApJ, 959, 100 (2023). **Cited 32 times**.

[149] "JWST Census for the Mass-Metallicity Star Formation Relations at $z = 4$–10 with Self-consistent Flux Calibration and Proper Metallicity Calibrators", Nakajima, Kimihiko, et al., ApJS, 269, 33 (2023). **Cited 129 times**.

[150] "An enhanced abundance of bright galaxies in protocluster candidates at $z \sim$ 3–5", Toshikawa, Jun, et al., MNRAS, 527, 6276 (2024). **Cited 3 times**.

[151] "MAMMOTH-Subaru. V. Effects of Cosmic Variance on Lyα Luminosity Functions at $z = 2.2$–2.3", Ma, Ke, et al., ApJ, 961, 102 (2024). **Cited 3 times**.

[152] "MAMMOTH-Subaru. III. Lyα Halo Identified by Stacking $\sim$3300 Lyα Emitters at $z = 2.2$–2.3", Zhang, Haibin, et al., ApJ, 961, 63 (2024). **Cited 7 times**.

[153] "Pure Spectroscopic Constraints on UV Luminosity Functions and Cosmic Star Formation History from 25 Galaxies at $z_{\rm spec} = 8.61$–13.20 Confirmed with JWST/NIRSpec", Harikane, Yuichi, et al., ApJ, 960, 56 (2024). **Cited 98 times**.

[154] "SHARPEST: the atmospheric turbulence profiling experiment using Shack-Hartmann sensor at the Subaru telescope", Ogane, Hajime, et al., MNRAS, 527, 1831 (2024). **Cited 0 times**.

[155] "EMPRESS. XII. Statistics on the Dynamics and Gas Mass Fraction of Extremely Metal-poor Galaxies", Xu, Yi, et al., ApJ, 961, 49 (2024). **Cited 5 times**.

[156] "EMPRESS. XIII. Chemical Enrichment of Young Galaxies Near and Far at $z \sim$ 0 and 4–10: Fe/O, Ar/O, S/O, and N/O Measurements with a Comparison of Chemical Evolution Models", Watanabe, Kuria, et al., ApJ, 962, 50 (2024). **Cited 18 times**.

Papers in Conference Proceedings

[157] "The University of Tokyo Atacama Observatory 6.5m telescope: On-sky performance of the near-infrared instrument SWIMS on the Subaru telescope", Konishi, Masahiro, et al., Proceedings of the SPIE, 11447, 114475H (2020).

[158] "A machine learning software to estimate morphological parameters of distant galaxies", Umayahara, Takuya, et al., Proceedings of the SPIE, 11452, 1145223 (2020).

[159] "Innovative astronomical applications with a new-generation relational database", Furusawa, Junko, et al., Proceedings of the SPIE, 11452, 1145226 (2020).

[160] "Unbiased surveys of dust-enshrouded galaxies using ALMA", Kohno, Kotaro, et al., Proceedings of the 7th Chile-Cologne-Bonn Symposium: Physics and Chemistry of Star Formation, 16 (2023).

THEORY GROUP

Theory Group

[Principal Investigator: Masahiro Kawasaki]

Introduction

The primary focus of the theory group is on particle physics phenomenology and particle cosmology. The collaboration between cosmology and particle physics has created significant synergy, enhancing our understanding of the fundamental laws governing the universe.

The theory group, led by Kawasaki and Ibe, has made substantial contributions to the field. Since 2018, the group has hosted eight postdoctoral researchers, leading to the publication of 135 papers in refereed journals, one paper in conference proceedings, and three papers currently under review.

In addition to research, the group is actively involved in graduate education in collaboration with the Department of Physics. Since 2018, the group has accepted twenty-three graduate students, eleven of them have successfully earned their Ph.D. degrees.

Research Highlights

The research activities of the theory group cover a broad range of particle physics and cosmology. Research highlights of the theory group after 2018 are;

- Precise estimation of the Wino/Higgsino decay rate [115, 133].
- Proposal for new types of grand unified theories with seemingly complete SU(5) multiplets [39, 107].
- Constraints on dark matter self-interaction cross sections using ultra-faint dwarf galaxies [69].
- Constraints on dark photon mass based on its impact on the effective number of neutrinos, $N_{\rm eff}$ [54].
- Investigation into the implications of the revised primordial helium abundance Y_p [104, 105, 129, 135].
- Studies of various extended objects, including an analytic derivation of the decay rate for I-balls/oscillons [30, 45].
- Investigation of primordial black hole (PBH) formation [4, 12, 18, 41, 91, 125, 132, 138]
- Exploration of potential sources for the stochastic gravitational wave background detected by Pulsar Timing Array experiments [131, 134].

Research Activities

The discovery of the Higgs boson at the LHC in 2012 provided strong validation for the Standard Model of particle physics. However, the absence of compelling evidence for physics beyond the Standard Model at the LHC has heightened the importance of collaboration between particle physics and cosmology in the quest for new discoveries. As a result, the distinction between particle phenomenology and particle cosmology is becoming increasingly blurred.

Supersymmetry

Supersymmetry has long been a leading candidate for physics beyond the Standard Model, allowing a large separation between low and high energy scales, such as the Planck scale. The precise unification of gauge coupling constants at the grand unified theory (GUT) scale also strongly supports the minimal supersymmetric standard model (MSSM). The MSSM is consistent with the properties of the Higgs boson's elementary scalar field.

Among the new particles predicted by the MSSM, Higgsinos and Winos are prime dark matter candidates due to their weak interactions. When other superparticles are heavy, mass differences between their charged (charginos) and neutral components (neutralinos) become degenerate, leading to long-lived charginos. For Winos, this mass difference is around 165 MeV across much of the parameter space, resulting in chargino decay into the lightest neutralino and a charged pion. Higgsinos, however, can have mass differences ranging from 0.1 GeV to 1 GeV, leading to various hadronic decay channels. In Refs. [115, 133], we analyzed Winos and Higgsinos, focusing on decay signatures through leptonic and hadronic modes. Using the latest experimental data, we studied decay rates, including hadronic modes, to assess their impact on chargino lifetimes (Fig. 1). Additionally, we performed next-to-leading order (NLO) calculations for leptonic decay modes, applicable to more general fermionic electroweak multiplets, such as quintuplet dark matter.

In 2021, the Muon $g-2$ experiment at Fermilab reported that the measured value of the muon anomalous magnetic moment, $g-2$, deviated from the Standard Model's conventional prediction by 4.2σ. While ongoing reconsiderations of the Standard Model's theoretical predictions are still underway, the explanation of this discrepancy through new physics remains a topic of active discussion. In Ref. [85], we present a gauge-mediated supersymmetry breaking model that simultaneously explains the muon $g-2$ anomaly and the Higgs boson mass without introducing CP violation, a common issue in such models. The model is consistent with current experimental constraints and provides a clear prediction for the LHC, where the discovery of light Winos and Higgsinos would be a significant confirmation.

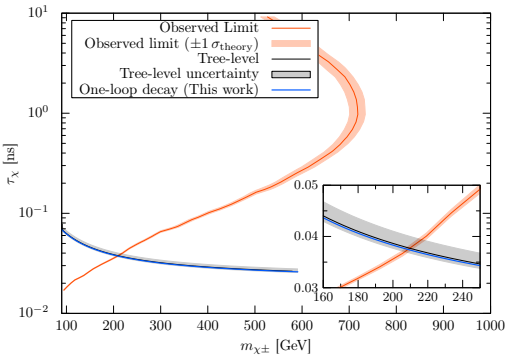

Fig. 1. The LHC constraint on the charged Higgsino mass and lifetime based on the disappearing charged track search, where $\Delta m_{\pm} \sim$300 MeV. The red solid line shows the 95%. limit by the ATLAS experiment(Eur.Phys.J.C82(2022)606). The red band shows $\pm 1\,\sigma$ uncertainty of the production cross section of the Higgsino. The upper-left region of the red line has been excluded. The blue solid line is the lifetime based on the NLO decay rate for the pure Higgsino, which decays into χ_1^0 and χ_2^0. The gray band shows the tree-level prediction with its uncertainty.

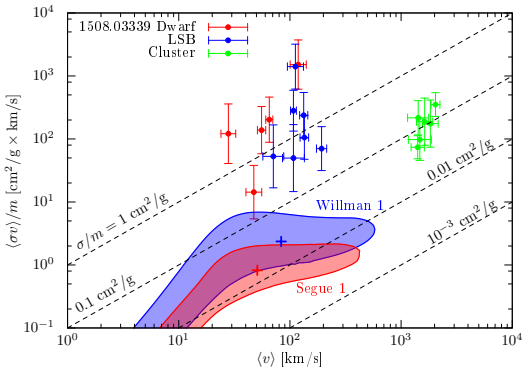

Fig. 2. The 1σ parameter estimation of $\langle v\rangle$-$\langle\sigma v\rangle/m$. for Segue 1 and Willman 1 with the Plummer profile. We also show the SIDM cross section which are favored by the dwarf irregular galaxies (red), low surface brightness galaxies (blue) and clusters (green).

Higgs Properties

The discovery of the Higgs boson was a monumental milestone in particle physics. This discovery solidified the Standard Model as a successful theory of particle interactions. However, recent developments, such as the de Sitter swampland conjecture, challenge the completeness of the Standard Model within the context of quantum gravity, which excludes the scalar potential of the Higgs field with a local maximum.

To make the Standard Model consistent with this conjecture, a quintessence field Q has been proposed to modify the Higgs potential. In Ref. [20], however, we found that such a modification leads to a Q-dependent Higgs vacuum expectation value (VEV), resulting in a long-range force between fermions and a time-dependent VEV, both of which conflict with experimental constraints. These conflicts require fine-tuning which is not justified by the conjecture itself. We further showed that, even if such an unjustified fine tuning condition is imposed at the tree level, radiative corrections upset it. Consequently, we concluded that most of the habitable vacua in the string landscape are in tension with the phenomenological constraints. Our point of view prompted a reconsideration of the de Sitter swampland conjecture and made an important contribution to the search for consistency between quantum gravity and low energy effective theory.

Grand Unified Theory

It is remarkable that the matter fields in the Standard Model are fully unified into the SU(5) representations. A straightforward explanation of this fact is to embed all the Standard Model gauge groups into a simple group containing SU(5), i.e., the grand unified theory (GUT). The road to the unified theory is, however, not as straightforward as it appears. A closer look at the renormalization group evolution (RGE) has revealed that the unification of the three gauge coupling constants is not very precise. The grand unification scale indicated by the RGE also results in too rapid proton decay.

In Ref. [39, 107], we discuss another possibility, dubbed as "Fake GUT", which explains why the Standard Model matter fields form the complete SU(5) multiplets. In Fake GUT, the apparent matter unification can be explained by a chiral gauge group G, G=SU(5)$\times H$, with three copies of $\bar{\mathbf{5}} \oplus \mathbf{10}$ chiral fermions of SU(5). We emphasize that the SM matter fields are not necessarily embedded into the chiral representations to explain the apparent unification. The novel phenomenological prediction of the fake GUT is more variety of the nucleon decay modes than the conventional GUT. For example, it is even possible that the decay rate of the $p \to \mu^+ + \pi^0$ mode is larger than that of the $p \to e^+ + \pi^0$ mode, which is not expected in the conventional GUT.

Dark Matter

The existence of dark matter has been established by a wide range of cosmological and astrophysical observations. Nevertheless, its nature remains elusive. Identification of the nature of DM is one of the most important challenges of modern particle physics. In theory group, we have proposed many new models of dark matter which are interrelated to physics beyond the Standard Model. We are also studying various phenomenological properties of dark matter such as self-interactions and also studying how to identify dark matter experimentally through direct/indirect detection experiments.

The self-interacting dark matter (SIDM) model which has gained attention as a potential solution to discrepancies between observed galactic structures and predictions made by the collisionless cold dark matter (CDM) model, particularly at small scales. In Ref. [69], we investigated the SIDM model by analyzing the stellar kinematics of 23 ultra-faint dwarf (UFD) galaxies—systems dominated by dark matter with minimal baryonic interference. Our results indicate that none of the UFDs strongly support non-zero self-interaction, with two galaxies, Segue 1 and Willman 1, providing particularly stringent upper limits on the self-interacting cross-section (Fig. 2). Our findings challenge the simple SIDM model, suggesting that these galaxies are consistent with collisionless dark matter and highlighting the need for further investigation into the dynamical evolution of SIDM.

Dark Photon

The dark photon is a massive gauge boson associated with a new U(1) gauge symmetry that arises in extensions of the

Standard Model of particle physics, particularly in theories involving dark matter. Theoretical motivations for the existence of the dark photon are compelling. For example, the U(1) symmetry can be responsible for the stability of dark matter and can provide dark matter self-interactions, which may address the small-scale structure problems in collisionless dark matter scenarios. Additionally, the dark photon could act as a portal, transferring excess entropy from the dark sector to the Standard Model sector.

In Ref. [54], we investigate the cosmological constraints on the MeV-scale dark photon through its impact on the effective number of neutrino species, $N_{\rm eff}$. Observations of the cosmic microwave background (CMB) place stringent constraints on $N_{\rm eff}$. If the dark photon exists in the thermal bath around the neutrino decoupling temperature, i.e., $T = \mathcal{O}(1)$ MeV, its decay and annihilation would heat the electron-photon plasma, leading to a reduction in $N_{\rm eff}$. By solving the momentum-dependent Boltzmann equation for the dark photon, we found that dark photon masses below 8.5 MeV are excluded by current Planck data. Furthermore, future CMB Stage-IV experiments are expected to be sensitive to dark photon masses up to 17 MeV. Our results apply to a broad range of models involving dark photons, although we assume that the dark photon couples minimally to the Standard Model sector through kinetic mixing with the QED photon. In Ref. [101], we also analyzed similar constraints on a dark scalar particle (Fig. 3).

In Refs. [110, 127, 128, 139], we further explored constraints on various dark photon models using data from FASER, FASER2, DUNE, the ILC beam dump experiment, and the T2K Off-Axis Near Detector. Since the interactions of the dark photon with Standard Model fermions depend on their U(1) charges, it is crucial to combine various experimental channels, including existing constraints from Orsay, Nomad, PS191, KEK, LSND, and CHARM experiments, to comprehensively explore the dark photon parameter space.

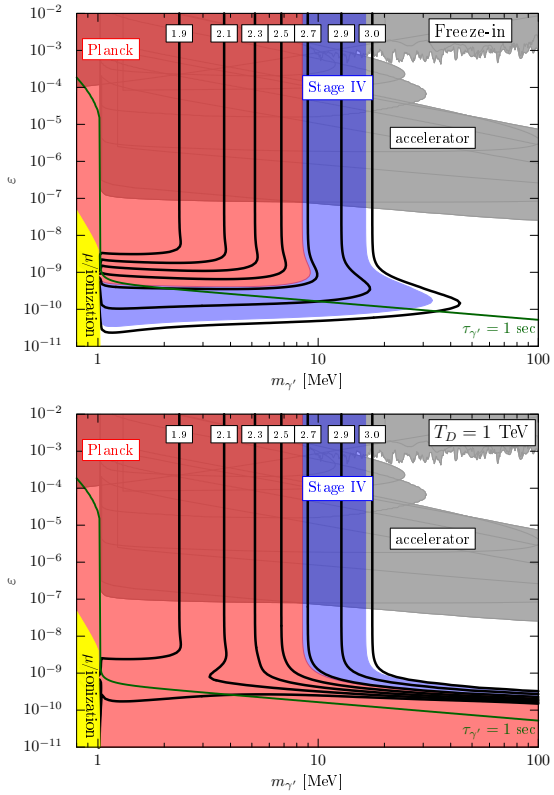

Fig. 3. The contour plots of $N_{\rm eff}$ on the dark photon mass ($m_{\gamma'}$) and kinetic mixing parameter (ε) plane. The upper panel corresponds to the freeze-in scenario, while the lower panel to the early decoupled scenario. The red region shows the present Planck constraint $N_{\rm eff} = 2.99^{+0.34}_{-0.33}$ (95%). The blue region shows that the sensitivity of the stage-IV CMB experiment $\delta N_{\rm eff} = 0.06$. The green line corresponds to the parameters where the lifetime of the dark photon is $\tau_{\gamma'} = 1$ sec. The gray shaded region is the compilation of the constraints from the beam dump and the collider experiments iand the electron $g-2$ constraint.

Big Bang Nucleosynthesis and Lepton Asymmetry

The predicted abundances of the light elements in Big Bang Nucleosynthesis (BBN) are sensitive to the cosmological scenario of the early universe. Recently, in Ref. [105], we presented a new determination of the primordial helium abundance (Y_P) using observations from extremely metal-poor galaxies (EMPGs), which serve as a powerful probe for understanding the early universe. The resultant primordial helium abundance is $Y_P = 0.2370^{+0.0034}_{-0.0033}$, which is lower than previous measurements, which suggests the universe has a large lepton asymmetry.

Motivated by the newly determined Y_p, we studied the Affleck-Dine (AD) mechanism for lepton number generation and subsequent Q-ball formation in Ref. [104]. In this scenario, the generated lepton number is confined in Q-balls and is protected from being converted to a baryon number through the sphaleron processes. We found that the universe with large lepton asymmetry suggested by the new ^{4}He measurement can be successfully realized. In this scenario, Q-balls dominate the universe and realize the sharp transition from an early matter-dominated era to a radiation-dominated era at the Q-ball decay, which enhances the production of gravitational waves (GWs) through a second-order effect of the scalar perturbations (Poltergeist mechanism [37, 59]). In Refs. [116, 129] we investigated the GW enhancement and found that the resultant GW spectrum can be consistent with the recent PTA experiment results. Furthermore, in Ref. [135] we studied the resonant production of sterile neutrinos in the universe with a large lepton asymmetry and showed that sterile neutrinos with mass $\gtrsim 20$ keV can account for the dark matter without contradicting X-ray and Lyman-α constraints.

Extended Objects

In physics beyond the Standard model, various types of the extended objects (solitons) are predicted which are localized stable solutions to nonlinear field equations. They come in two main types: topological and non-topological solitons. Topological solitons, like magnetic monopoles and cosmic strings, are stabilized by a topological charge, preventing them from decaying. Non-topological solitons, such as Q-balls, achieve stability through energy conservation and nonlinear interactions rather than topological constraints. Both types are crucial for exploring the non-perturbative aspects of field theories and understanding complex structures in the universe.

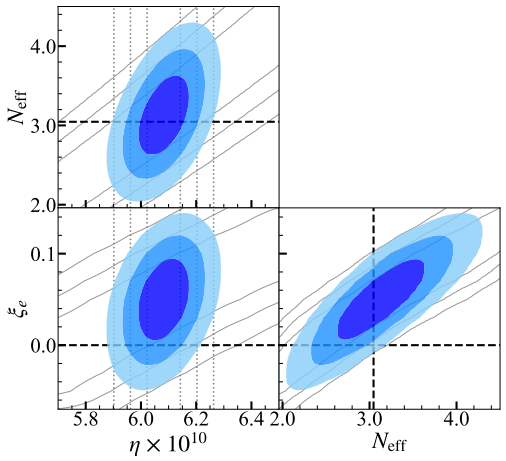

Fig. 4. Constraints on the effective number of neutrino species $N_{\rm eff}$, the baryon-to-photon ratio η and the lepton asymmetry ξ_e. The solid gray contours show the constraint with our $Y_{\rm P}$ value and the $D_{\rm P}$ measurement. The vertical dotted lines represent the Planck constraint on η. The constraint combining with the $Y_{\rm P}$, $D_{\rm P}$, and η measurements is shown with blue contours. These contours show $1\sigma, 2\sigma$ and 3σ confidence limits. The standard model values of $N_{\rm eff} = 3.046$ and $\xi_e = 0$ are represented with black dashed lines.

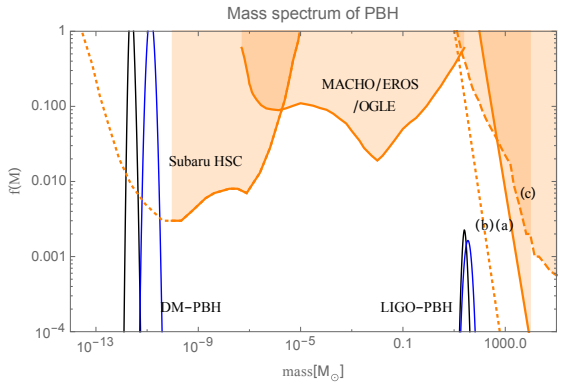

Fig. 5. PBH mass spectra $f(M)$ explaining dark matter (around $10^{-12}M_\odot$) and LIGO-Virgo-KAGRA events (around $30M_\odot$) for the delta-function window (black lines) and top-hat window function (blue lines). The shaded regions are excluded from observations.

I-ball/oscillon is one-type of non-topological solitons are produced in various contexts of the early universe in, such as, the inflaton evolution and the axion evolution. However, their decay process has long been unclear. In Ref. [30], we derive an analytic formula of the decay rate of the I-balls/oscillons within the classical field theory. In our approach, we calculate the Poynting vector of the perturbation around the I-ball/oscillon profile by solving a relativistic field equation, with which the decay rate of the I-ball/oscillon is obtained. We also performed a classical lattice simulation and confirmed the validity of our analytical formula of the decay rate numerically. In Ref. [45], we also examined the stability of a special type of I-ball/oscillon, the "exact" I-ball/oscillon, whose adiabatic invariant is exactly conserved. We show that the exact I-ball/oscillon is stable in classical field theory, but not stable against small perturbations depending on the value of its adiabatic invariant. Accordingly, the exact I-ball/oscillon breaks up in the presence of the fluctuations with corresponding instability modes. We also confirmed the fragileness of the exact I-ball/oscillon by the classical lattice simulation. Our studies clarified the decay mechanism of the I-ball/oscillon. Furthermore,

We also studied various types of extended objects including a new type of cosmic strings with long-range force between them ([48, 61]), a composite objects connecting magnetic monopole and comic strings ([93, 121]). We also discussed how the superconducting current inside a cosmic string leaks out from the superconducting cosmic strings ([84]). Although there is a long history of research on extended objects, there are still many unanswered questions regarding their detailed dynamics. Through these studies, extended objects may lead to new probes of the early universe.

Formation of Primordial Black Holes

Primordial black holes (PBHs) are black holes produced from large density fluctuations in the early universe. Gravitational waves from the coalescence of binary black holes were first detected by the Laser Interferometer Gravitational-Wave Observatory (LIGO) in 2015. Since then, many gravitational wave events have been detected. One of the promising candidates for BHs causing the gravitational wave events is PBHs with mass $\sim \mathcal{O}(10)M_\odot$. PBHs are also a good candidate for dark matter in the universe if they have masses between $10^{-13}M_\odot$ and $10^{-10}M_\odot$. Furthermore, it is known that supermassive black holes (SMBHs) reside in the centers of almost all massive galaxies. The recent observation by the James Webb Space Telescope suggests the existence of SMBHs with masses of $10^6M_\odot$ to $10^{10}M_\odot$ at redshift $z \sim 10$. Those SMBHs can be formed from the seed PBHs with mass $\sim 10^4M_\odot$. Therefore, we studied the formation of PBHs that explain gravitational events, dark matter, and seeds of SMBHs.

In Ref. [12] we studied PBH formation in an axionlike curvaton model with a coupling to inflation, which leads to a sharp peak in the power spectrum of the curvature perturbations. We also evaluated the non-Gaussianity effect of the curvaton and uncertainty from the choice of the window functions. It was found that the axionlike curvaton model produces enough PBHs to explain the black hole binaries ($\sim \mathcal{O}(10)M_\odot$) observed in the LIGO-Virgo-KAGRA Collaboration or PBHs as dark matter ($\sim 10^{-12}M_\odot$) (Fig. 5).

In Ref. [34] we investigated the effect of the nonlinear relation between density and curvature perturbations on the formation of PBHs. When the compaction function is used as a criterion for PBH formation, the required curvature perturbation for the PBH formation increases due to the nonlinearity. We found that the nonlinear effect slightly suppresses the PBH formation and the suppression is comparable to that expected if the primordial curvature perturbation would have the local form of non-Gaussianity with nonlinear parameter $f_{\rm NL} \sim -1$.

In Refs. [4, 18, 41] we proposed a novel PBH formation scenario based on the Affleck-Dine mechanism for baryogenesis. In this scenario, PBHs with mass $\gtrsim \mathcal{O}(10)M_\odot$ are formed from high baryon-density bubbles produced by the Affleck-Dine mechanism, which accounts for the gravitational

events caused by the coalescence of binary black holes or the seeds for SMBHs. Furthermore, in Ref. [91] we studied the clustering of PBHs formed by the Affleck-Dine mechanism and found that formed PBHs show a strong clustering due to the stochastic dynamics of the AD field. Taking the clustering effect into account, we estimated the merger rate and isocurvature perturbations of PBHs and found that they show significant deviations from those without clustering. In Ref. [109] we proposed an alternative scenario where the AD leptogenesis results in the inhomogeneous formation of Q-balls with lepton charges, which collapse into PBHs. This model can avoid large inhomogeneity in baryon distribution that could spoil the success of BBN. It was found that the PBH formation model for seeds of SMBHs by the AD mechanism causes strong clustering that is inconsistent with the observed angular correlation of quasars. Thus, in Ref. [138] we proposed a modified model that can significantly reduce the PBH clustering on large scales by considering a time-dependent Hubble-induced mass during inflation. This model can suppress the quasar angular correlation sufficiently and can successfully explain the seeds of SMBHs.

Gravitational Wave Signals

The Pulsar Timing Array (PTA) experiment is a method for detecting the background gravitational waves that permeate the universe by observing the arrival times of signals from multiple pulsars over extended periods. PTA is particularly sensitive to low-frequency gravitational waves in the nanohertz range. Recently, strong indications of background gravitational waves have been observed in PTA experiments such as NANOGrav and EPTA. These experiments have detected a specific angular correlation, Hellings-Downs curve, which is considered strong evidence for the existence of background gravitational waves. However, the exact sources of these background gravitational waves remain unresolved, leaving open questions about their origins. This discovery is expected to provide new insights into the structure and evolution of the universe.

In Ref. [131], we studied the production of stochastic gravitational waves induced by curvature perturbations in the axionlike curvaton model for PBH formation [12]. The axionlike curvaton model can produce large curvature perturbations with a significant non-Gaussianity. We showed that the axion curvaton model can successfully explain the gravitational waves detected by the PTA experiments and avoid PBH overproduction at the same time (Fig. 6). We also showed that the peak mass of the PBH spectrum can be around $\mathcal{O}(0.1-1)M_\odot$ in the model that explains the PTA results. Furthermore, we found it difficult to relate the PTA results to PBHs with $\mathcal{O}(10)M_\odot$ for the BHs detected by the LIGO-Virgo-KAGRA collaborations because the PTA results favor the blue-tilted power spectrum on the PTA scales.

Cosmic strings are also considered to be one of the prime candidates for the origin of the background gravitational waves. Cosmic strings are a type of topological soliton which is formed at the phase transition of U(1) gauge symmetry in the early universe. Long cosmic strings reconnect at intersection and produce string loops which disappear by emitting gravitational waves (see e.g. Ref. [44]). Intriguingly, observed

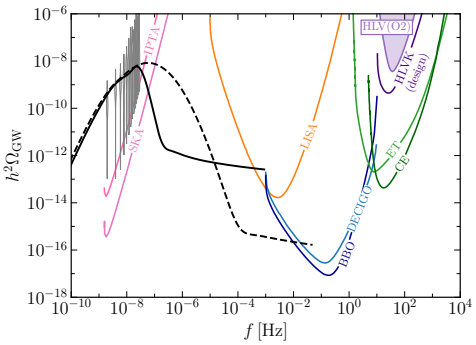

Fig. 6. The power spectrum of the stochastic gravitational wave background in the cases of the sharp peak (black solid) and the broad peak (black dashed). The sensitivity curves for various GW detectors are also shown, and the shaded region with HLV(O2) is already excluded. The gray violins are from the NANOGrav result.

gravitational wave spectrum is well fitted by the gravitational wave from the metastable cosmic strings. In Ref. [134], we revisited the decay rate of metastable cosmic strings, which emerge in models with a two-step symmetry breaking process. Traditionally, the decay rate has been estimated using an infinitely thin string approximation, assuming a large hierarchy between the symmetry-breaking scales. In this paper, we took a new approach that considers the finite sizes of both the cosmic string and the monopole, leading to a more reliable lower limit on the tunneling factor even in scenarios where the conventional estimate fails. The findings suggest that this refined method is crucial for interpreting the gravitational wave signals detected by PTA experiments, by those from the metastable strings.

Members

Staff

Masahiro Kawasaki, Professor, 2004–present
Masahiro Ibe, Assoc. Professor, 2011–present

Postdoctoral Fellows

Yutaro Shoj, 2016-2018
Ryo Nagai, 2018-2019
Ippei Obata 2018-2020
Kohei Hayashi 2018-2020
Hiramatsu Takashi, 2019-2020
Tomohiro Fujita 2020-2021
Kento Asai, 2022-present
Koki Tokeshi, 2024-present

Graduate Students

Eleven students were awarded doctor degrees and nineteen students earned master degrees during 2018–2024, supervised by ICRR staff members.

Bibliography

The symbol ∗ indicates the authors belonging to ICRR. Nine papers, [10], [17], [20], [32], [34], [60], [65], [66], [77], [80], are cited more than fifty times. Seven papers, [8], [15], [28], [37], [38], [50], [59], are cited more than a hundred times.

Papers in Refereed Journals (after April 2018)

[1] M. Ibe* K. Ichikawa, S. i. Horigome, M. N. Ishigaki, S. Matsumoto, M. Ibe*, H. Sugai and K. Hayashi, Mon. Not. Roy. Astron. Soc. **479**, no.1, 64-74 (2018) doi:10.1093/mnras/sty1387 [arXiv:1706.05481 [astro-ph.GA]].

[2] A. Agrawal, T. Fujita* and E. Komatsu, Phys. Rev. D **97**, no.10, 103526 (2018) doi:10.1103/PhysRevD.97.103526 [arXiv:1707.03023 [astro-ph.CO]].

[3] M. Kawasaki* and E. Sonomoto*, Phys. Rev. D **97**, no.8, 083507 (2018) doi:10.1103/PhysRevD.97.083507 [arXiv:1710.07269 [hep-ph]].

[4] F. Hasegawa* and M. Kawasaki*, Phys. Rev. D **98**, no.4, 043514 (2018) doi:10.1103/PhysRevD.98.043514 [arXiv:1711.00990 [astro-ph.CO]].

[5] K. Ando*, K. Inomata*, M. Kawasaki*, K. Mukaida and T. T. Yanagida, Phys. Rev. D **97**, no.12, 123512 (2018) doi:10.1103/PhysRevD.97.123512 [arXiv:1711.08956 [astro-ph.CO]].

[6] J. P. Hong*, M. Kawasaki* and M. Yamazaki, Phys. Rev. D **98**, no.4, 043531 (2018) doi:10.1103/PhysRevD.98.043531 [arXiv:1711.10496 [astro-ph.CO]].

[7] M. Kawasaki*, E. Sonomoto* and T. T. Yanagida, Phys. Lett. B **782**, 181-184 (2018) doi:10.1016/j.physletb.2018.05.014 [arXiv:1801.07409 [hep-ph]].

[8] K. Ando*, K. Inomata* and M. Kawasaki*, Phys. Rev. D **97**, no.10, 103528 (2018) doi:10.1103/PhysRevD.97.103528 [arXiv:1802.06393 [astro-ph.CO]].

[9] H. Fukuda, M. Ibe*, M. Suzuki and T. T. Yanagida, JHEP **07**, 128 (2018) doi:10.1007/JHEP07(2018)128 [arXiv:1803.00759 [hep-ph]].

[10] S. Chigusa, T. Moroi and Y. Shoji*, Phys. Rev. D **97**, no.11, 116012 (2018) doi:10.1103/PhysRevD.97.116012 [arXiv:1803.03902 [hep-ph]].

[11] M. Ibe*, A. Kamada, S. Kobayashi* and W. Nakano*, JHEP **11**, 203 (2018) doi:10.1007/JHEP11(2018)203 [arXiv:1805.06876 [hep-ph]].

[12] K. Ando*, M. Kawasaki* and H. Nakatsuka*, Phys. Rev. D **98**, no.8, 083508 (2018) doi:10.1103/PhysRevD.98.083508 [arXiv:1805.07757 [astro-ph.CO]].

[13] T. Haga, K. Inomata*, A. Ota and A. Ravenni, JCAP **08**, 036 (2018) doi:10.1088/1475-7516/2018/08/036 [arXiv:1805.08773 [astro-ph.CO]].

[14] M. Ibe*, M. Suzuki and T. T. Yanagida, JHEP **08**, 049 (2018) doi:10.1007/JHEP08(2018)049 [arXiv:1805.10029 [hep-ph]].

[15] I. Obata*, T. Fujita* and Y. Michimura, Phys. Rev. Lett. **121**, no.16, 161301 (2018) doi:10.1103/PhysRevLett.121.161301 [arXiv:1805.11753 [astro-ph.CO]].

[16] K. Inomata*, M. Kawasaki*, A. Kusenko and L. Yang, JCAP **12**, 003 (2018) doi:10.1088/1475-7516/2018/12/003 [arXiv:1806.00123 [astro-ph.CO]].

[17] M. Kawasaki*, T. Sekiguchi, M. Yamaguchi and J. Yokoyama, PTEP **2018**, no.9, 091E01 (2018) doi:10.1093/ptep/pty098 [arXiv:1806.05566 [hep-ph]].

[18] F. Hasegawa* and M. Kawasaki*, JCAP **01**, 027 (2019) doi:10.1088/1475-7516/2019/01/027 [arXiv:1807.00463 [astro-ph.CO]].

[19] T. Hiramatsu*, S. Yokoyama, T. Fujita* and I. Obata*, Phys. Rev. D **98**, no.8, 083522 (2018) doi:10.1103/PhysRevD.98.083522 [arXiv:1808.08044 [astro-ph.CO]].

[20] K. Hamaguchi, M. Ibe* and T. Moroi, JHEP **12**, 023 (2018) doi:10.1007/JHEP12(2018)023 [arXiv:1810.02095 [hep-th]].

[21] M. Kawasaki* and V. Takhistov, Phys. Rev. D **98**, no.12, 123514 (2018) doi:10.1103/PhysRevD.98.123514 [arXiv:1810.02547 [hep-th]].

[22] K. Inomata* and M. Kamionkowski, Phys. Rev. Lett. **123**, no.3, 031305 (2019) doi:10.1103/PhysRevLett.123.031305 [arXiv:1811.04959 [astro-ph.CO]].

[23] K. Inomata* and M. Kamionkowski, Phys. Rev. D **99**, no.4, 043501 (2019) doi:10.1103/PhysRevD.99.043501 [arXiv:1811.04957 [astro-ph.CO]].

[24] M. Ibe*, M. Yamazaki and T. T. Yanagida, Class. Quant. Grav. **36**, no.23, 235020 (2019) doi:10.1088/1361-6382/ab5197 [arXiv:1811.04664 [hep-th]].

[25] M. Ibe*, A. Kamada, S. Kobayashi*, T. Kuwahara and W. Nakano*, JHEP **03**, 173 (2019) doi:10.1007/JHEP03(2019)173 [arXiv:1811.10232 [hep-ph]].

[26] T. Fujita*, R. Namba and I. Obata*, JCAP **04**, 044 (2019) doi:10.1088/1475-7516/2019/04/044 [arXiv:1811.12371 [astro-ph.CO]].

[27] I. Obata*, T. Fujita* and Y. Michimura, [arXiv:1811.12051 [physics.ins-det]].

[28] K. Inomata* and T. Nakama, Phys. Rev. D **99**, no.4, 043511 (2019) doi:10.1103/PhysRevD.99.043511 [arXiv:1812.00674 [astro-ph.CO]].

[29] M. B. Gavela, M. Ibe*, P. Quilez and T. T. Yanagida, Eur. Phys. J. C **79**, no.6, 542 (2019) doi:10.1140/epjc/s10052-019-7046-3 [arXiv:1812.08174 [hep-ph]].

[30] M. Ibe*, M. Kawasaki*, W. Nakano* and E. Sonomoto*, JHEP **04**, 030 (2019) doi:10.1007/JHEP04(2019)030 [arXiv:1901.06130 [hep-ph]].

[31] K. Hayashi* and I. Obata*, Mon. Not. Roy. Astron. Soc. **491**, no.1, 615-633 (2020) doi:10.1093/mnras/stz2950 [arXiv:1902.03054 [astro-ph.CO]].

[32] K. Nagano, T. Fujita*, Y. Michimura and I. Obata*, Phys. Rev. Lett. **123**, no.11, 111301 (2019) doi:10.1103/PhysRevLett.123.111301 [arXiv:1903.02017 [hep-ph]].

[33] M. Ibe*, M. Suzuki, T. T. Yanagida and N. Yokozaki, Eur. Phys. J. C **79**, no.8, 688 (2019) doi:10.1140/epjc/s10052-019-7186-5 [arXiv:1903.12433 [hep-ph]].

[34] M. Kawasaki* and H. Nakatsuka*, Phys. Rev. D **99**, no.12, 123501 (2019) doi:10.1103/PhysRevD.99.123501 [arXiv:1903.02994 [astro-ph.CO]].

[35] M. Ibe*, Y. Shoji* and M. Suzuki, JHEP **11**, 140 (2019) doi:10.1007/JHEP11(2019)140 [arXiv:1904.02545 [hep-ph]].

[36] R. Nagai*, M. Tanabashi, K. Tsumura and Y. Uchida, Phys. Rev. D **100**, no.7, 075020 (2019) doi:10.1103/PhysRevD.100.075020 [arXiv:1904.07618 [hep-ph]].

[37] K. Inomata*, K. Kohri, T. Nakama and T. Terada, Phys. Rev. D **100**, 043532 (2019) [erratum: Phys. Rev. D **108**, no.4, 049901 (2023)] doi:10.1103/PhysRevD.108.049901 [arXiv:1904.12879 [astro-ph.CO]].

[38] K. Inomata*, K. Kohri, T. Nakama and T. Terada, JCAP **10**, 071 (2019) [erratum: JCAP **08**, E01 (2023)] doi:10.1088/1475-7516/2019/10/071 [arXiv:1904.12878 [astro-ph.CO]].

[39] M. Ibe*, S. Shirai, M. Suzuki and T. T. Yanagida, Phys. Rev. D **100**, no.5, 055024 (2019) doi:10.1103/PhysRevD.100.055024 [arXiv:1906.02977 [hep-ph]].

[40] D. Hashimoto, O. Macias, A. J. Nishizawa, K. Hayashi*, M. Takada, M. Shirasaki and S. Ando, JCAP **01**, 059 (2020) doi:10.1088/1475-7516/2020/01/059 [arXiv:1906.06701 [astro-ph.CO]].

[41] M. Kawasaki* and K. Murai*, Phys. Rev. D **100**, no.10, 103521 (2019) doi:10.1103/PhysRevD.100.103521 [arXiv:1907.02273 [astro-ph.CO]].

[42] M. Ibe*, A. Kamada, S. Kobayashi*, T. Kuwahara and W. Nakano*, Phys. Rev. D **100**, no.7, 075022 (2019) doi:10.1103/PhysRevD.100.075022 [arXiv:1907.03404 [hep-ph]].

[43] M. Ibe*, S. Kobayashi*, R. Nagai* and W. Nakano*, JHEP **01**, 027 (2020) doi:10.1007/JHEP01(2020)027 [arXiv:1907.11464 [hep-ph]].

[44] J. A. Dror, T. Hiramatsu*, K. Kohri, H. Murayama and G. White, Phys. Rev. Lett. **124**, no.4, 041804 (2020) doi:10.1103/PhysRevLett.124.041804 [arXiv:1908.03227 [hep-ph]].

[45] M. Ibe*, M. Kawasaki*, W. Nakano* and E. Sonomoto*, Phys. Rev. D **100**, 125021 (2019) doi:10.1103/PhysRevD.100.125021 [arXiv:1908.11103 [hep-ph]].

[46] M. Ibe*, S. Kobayashi*, M. Suzuki and T. T. Yanagida, Phys. Rev. D **101**, no.3, 035029 (2020) doi:10.1103/PhysRevD.101.035029 [arXiv:1909.01604 [hep-ph]].

[47] M. Kawasaki*, W. Nakano* and E. Sonomoto*, JCAP **01**, 047 (2020) doi:10.1088/1475-7516/2020/01/047 [arXiv:1909.10805 [astro-ph.CO]].

[48] T. Hiramatsu*, M. Ibe* and M. Suzuki, JHEP **02**, 058 (2020) doi:10.1007/JHEP02(2020)058 [arXiv:1910.14321 [hep-ph]].

[49] Y. Michimura, Y. Oshima, T. Watanabe, T. Kawasaki, H. Takeda, M. Ando, K. Nagano, I. Obata* and T. Fujita*, J. Phys. Conf. Ser. **1468**, no.1, 012032 (2020) doi:10.1088/1742-6596/1468/1/012032 [arXiv:1911.05196 [physics.ins-det]].

[50] K. Inomata* and T. Terada, Phys. Rev. D **101**, no.2, 023523 (2020) doi:10.1103/PhysRevD.101.023523 [arXiv:1912.00785 [gr-qc]].

[51] M. Kawasaki* and H. Nakatsuka*, JCAP **04**, 017 (2020) doi:10.1088/1475-7516/2020/04/017 [arXiv:1912.06993 [hep-ph]].

[52] K. Nagano, I. Obata*, T. Fujita* and Y. Michimura, J. Phys. Conf. Ser. **1468**, no.1, 012027 (2020) doi:10.1088/1742-6596/1468/1/012027 [arXiv:1912.09123 [hep-ph]].

[53] M. Kawasaki*, H. Nakatsuka* and I. Obata*, JCAP **05**, 007 (2020) doi:10.1088/1475-7516/2020/05/007 [arXiv:1912.09111 [astro-ph.CO]].

[54] M. Ibe*, S. Kobayashi*, Y. Nakayama* and S. Shirai, JHEP **04**, 009 (2020) doi:10.1007/JHEP04(2020)009 [arXiv:1912.12152 [hep-ph]].

[55] S. Kasuya, M. Kawasaki*, F. Otani* and E. Sonomoto*, Phys. Rev. D **102**, no.4, 043016 (2020) doi:10.1103/PhysRevD.102.043016 [arXiv:2001.02582 [hep-ph]].

[56] Y. Hamada, M. Ibe*, Y. Muramatsu, K. y. Oda and N. Yokozaki, Eur. Phys. J. C **80**, no.5, 482 (2020) doi:10.1140/epjc/s10052-020-7922-x [arXiv:2001.05235 [hep-ph]].

[57] S. i. Horigome, K. Hayashi*, M. Ibe*, M. N. Ishigaki, S. Matsumoto and H. Sugai, Mon. Not. Roy. Astron. Soc. **499**, no.3, 3320-3337 (2020) doi:10.1093/mnras/staa2909 [arXiv:2002.04866 [astro-ph.GA]].

[58] K. Inomata*, K. Kohri, T. Nakama and T. Terada, J. Phys. Conf. Ser. **1468**, no.1, 012001 (2020) doi:10.1088/1742-6596/1468/1/012001

[59] K. Inomata*, M. Kawasaki*, K. Mukaida, T. Terada and T. T. Yanagida, Phys. Rev. D **101**, no.12, 123533 (2020) doi:10.1103/PhysRevD.101.123533 [arXiv:2003.10455 [astro-ph.CO]].

[60] G. B. Gelmini, M. Kawasaki*, A. Kusenko, K. Murai* and V. Takhistov, JCAP **09**, 051 (2020) doi:10.1088/1475-7516/2020/09/051 [arXiv:2005.06721 [hep-ph]].

[61] T. Hiramatsu*, M. Ibe* and M. Suzuki, JHEP **09**, 054 (2020) doi:10.1007/JHEP09(2020)054 [arXiv:2005.10421 [hep-ph]].

[62] S. Okano and T. Fujita*, JCAP **03**, 026 (2021) doi:10.1088/1475-7516/2021/03/026 [arXiv:2005.13833 [astro-ph.CO]].

[63] M. Kawasaki*, K. Kohri, T. Moroi, K. Murai* and H. Murayama, JCAP **12**, 048 (2020) doi:10.1088/1475-7516/2020/12/048 [arXiv:2006.14803 [hep-ph]].

[64] K. Ando* and V. Vennin, Phys. Rev. A **102**, no.5, 052213 (2020) doi:10.1103/PhysRevA.102.052213 [arXiv:2007.00458 [quant-ph]].

[65] P. Lu, V. Takhistov, G. B. Gelmini, K. Hayashi*, Y. Inoue and A. Kusenko, Astrophys. J. Lett. **908**, no.2, L23 (2021) doi:10.3847/2041-8213/abdcb6 [arXiv:2007.02213 [astro-ph.CO]].

[66] K. Hayashi*, M. Chiba and T. Ishiyama, Astrophys. J. **904**, no.1, 45 (2020) doi:10.3847/1538-4357/abbe0a [arXiv:2007.13780 [astro-ph.GA]].

[67] M. Ibe*, S. Kobayashi*, Y. Nakayama* and S. Shirai, JHEP **12**, 004 (2020) doi:10.1007/JHEP12(2020)004 [arXiv:2007.16105 [hep-ph]].

[68] T. Fujita*, I. Obata*, T. Tanaka and K. Yamada, Class. Quant. Grav. **38**, no.4, 045010 (2021) doi:10.1088/1361-6382/abce49 [arXiv:2008.02764 [gr-qc]].

[69] K. Hayashi*, M. Ibe*, S. Kobayashi*, Y. Nakayama* and S. Shirai, Phys. Rev. D **103**, no.2, 023017 (2021) doi:10.1103/PhysRevD.103.023017 [arXiv:2008.02529 [astro-ph.CO]].

[70] T. Fujita*, Y. Minami, K. Murai* and H. Nakatsuka*, Phys. Rev. D **103**, no.6, 063508 (2021) doi:10.1103/PhysRevD.103.063508 [arXiv:2008.02473 [astro-ph.CO]].

[71] T. Hiramatsu*, K. Murai*, I. Obata* and S. Yokoyama, JCAP **03**, 047 (2021) doi:10.1088/1475-7516/2021/03/047 [arXiv:2008.03233 [astro-ph.CO]].

[72] Y. Michimura, T. Fujita*, S. Morisaki, H. Nakatsuka* and I. Obata*, Phys. Rev. D **102**, no.10, 102001 (2020) doi:10.1103/PhysRevD.102.102001 [arXiv:2008.02482 [hep-ph]].

[73] K. D. Nakamura, K. Miuchi, S. Kazama, Y. Shoji*, M. Ibe* and W. Nakano*, PTEP **2021**, no.1, 013C01 (2021) doi:10.1093/ptep/ptaa162 [arXiv:2009.05939 [physics.ins-det]].

[74] J. L. Evans, M. Ibe* and T. T. Yanagida, Phys. Rev. D **103**, no.3, 035009 (2021) doi:10.1103/PhysRevD.103.035009 [arXiv:2009.11448 [hep-ph]].

[75] M. Kawasaki*, W. Nakano*, H. Nakatsuka* and E. Sonomoto*, JCAP **01**, 061 (2021) doi:10.1088/1475-7516/2021/01/061 [arXiv:2010.09311 [astro-ph.CO]].

[76] M. Kawasaki*, W. Nakano*, H. Nakatsuka* and E. Sonomoto*, doi:10.1088/1475-7516/2021/04/019 [arXiv:2010.13504 [astro-ph.CO]].

[77] K. Inomata*, M. Kawasaki*, K. Mukaida and T. T. Yanagida, Phys. Rev. Lett. **126**, no.13, 131301 (2021) doi:10.1103/PhysRevLett.126.131301 [arXiv:2011.01270 [astro-ph.CO]].

[78] S. Morisaki, T. Fujita*, Y. Michimura, H. Nakatsuka* and I. Obata*, Phys. Rev. D **103**, no.5, L051702 (2021) doi:10.1103/PhysRevD.103.L051702 [arXiv:2011.03589 [hep-ph]].

[79] M. Kawasaki* and S. Ueda*, JCAP **04**, 049 (2021) doi:10.1088/1475-7516/2021/04/049 [arXiv:2011.10397 [hep-ph]].

[80] T. Fujita*, K. Murai*, H. Nakatsuka* and S. Tsujikawa, Phys. Rev. D **103**, no.4, 043509 (2021) doi:10.1103/PhysRevD.103.043509 [arXiv:2011.11894 [astro-ph.CO]].

[81] S. Eijima*, M. Shaposhnikov and I. Timiryasov, JCAP **04**, no.04, 049 (2022) doi:10.1088/1475-7516/2022/04/049 [arXiv:2011.12637 [hep-ph]].

[82] K. Ando* and V. Vennin, JCAP **04**, 057 (2021) doi:10.1088/1475-7516/2021/04/057 [arXiv:2012.02031 [astro-ph.CO]].

[83] M. Kawasaki* and H. Nakatsuka*, JCAP **05**, 023 (2021) doi:10.1088/1475-7516/2021/05/023 [arXiv:2101.11244 [astro-ph.CO]].

[84] M. Ibe*, S. Kobayashi*, Y. Nakayama* and S. Shirai, JHEP **05**, 217 (2021) doi:10.1007/JHEP05(2021)217 [arXiv:2102.05412 [hep-ph]].

[85] M. Ibe*, S. Kobayashi*, Y. Nakayama* and S. Shirai, JHEP **07**, 098 (2021) doi:10.1007/JHEP07(2021)098 [arXiv:2104.03289 [hep-ph]].

[86] Y. Oshima, H. Fujimoto, M. Ando, T. Fujita*, Y. Michimura, K. Nagano, I. Obata and T. Watanabe, [arXiv:2105.06252 [hep-ph]].

[87] M. Ibe*, S. Kobayashi* and K. Watanabe*, JHEP **07**, 220 (2021) doi:10.1007/JHEP07(2021)220 [arXiv:2105.07642 [hep-ph]].

[88] H. Fujimoto, Y. Oshima, M. Ando, T. Fujita*, Y. Michimura, K. Nagano and I. Obata, [arXiv:2105.08347 [physics.ins-det]].

[89] M. Kawasaki*, H. Nakatsuka*, K. Nakayama and T. Sekiguchi, JCAP **12**, no.12, 015 (2021) doi:10.1088/1475-7516/2021/12/015 [arXiv:2105.08334 [astro-ph.CO]].

[90] K. Nagano, H. Nakatsuka*, S. Morisaki, T. Fujita*, Y. Michimura and I. Obata, Phys. Rev. D **104**, no.6, 062008 (2021) doi:10.1103/PhysRevD.104.062008 [arXiv:2106.06800 [hep-ph]].

[91] M. Kawasaki*, K. Murai* and H. Nakatsuka*, JCAP **10**, 025 (2021) doi:10.1088/1475-7516/2021/10/025 [arXiv:2107.03580 [astro-ph.CO]].

[92] T. Fujita*, K. Murai*, I. Obata and M. Shiraishi, JCAP **01**, no.01, 007 (2022) doi:10.1088/1475-7516/2022/01/007 [arXiv:2109.06457 [astro-ph.CO]].

[93] T. Hiramatsu*, M. Ibe*, M. Suzuki and S. Yamaguchi, JHEP **12**, 122 (2021) doi:10.1007/JHEP12(2021)122 [arXiv:2109.12771 [hep-ph]].

[94] T. Fujita*, K. Mukaida, K. Murai* and H. Nakatsuka*, Phys. Rev. D **105**, no.10, 103519 (2022) doi:10.1103/PhysRevD.105.103519 [arXiv:2110.03228 [hep-ph]].

[95] K. Imagawa*, M. Kawasaki*, K. Murai*, H. Nakatsuka* and E. Sonomoto*, JCAP **02**, 024 (2023) doi:10.1088/1475-7516/2023/02/024 [arXiv:2110.05790 [hep-ph]].

[96] Y. Oshima, H. Fujimoto, M. Ando, T. Fujita*, J. Kume, Y. Michimura, S. Morisaki, K. Nagano, H. Nakatsuka* and A. Nishizawa, *et al.* J. Phys. Conf. Ser. **2156**, no.1, 012042 (2021) doi:10.1088/1742-6596/2156/1/012042 [arXiv:2110.10607 [physics.ins-det]].

[97] S. Hashiba, K. Kamada and H. Nakatsuka*, JCAP **04**, no.04, 058 (2022) doi:10.1088/1475-7516/2022/04/058 [arXiv:2110.10822 [hep-ph]].

[98] M. Kawasaki*, H. Nakatsuka* and K. Nakayama, JCAP **03**, no.03, 061 (2022) doi:10.1088/1475-7516/2022/03/061 [arXiv:2110.12620 [astro-ph.CO]].

[99] Y. Michimura, T. Fujita*, J. Kume, S. Morisaki, K. Nagano, H. Nakatsuka*, A. Nishizawa and I. Obata, J. Phys. Conf. Ser. **2156**, no.1, 012071 (2021) doi:10.1088/1742-6596/2156/1/012071 [arXiv:2111.00420 [hep-ph]].

[100] M. Kawasaki*, K. Miyazaki*, K. Murai*, H. Nakatsuka* and E. Sonomoto*, JCAP **08**, 066 (2022) doi:10.1088/1475-7516/2022/08/066 [arXiv:2112.10464 [astro-ph.CO]].

[101] M. Ibe*, S. Kobayashi*, Y. Nakayama* and S. Shirai, JHEP **03**, 198 (2022) doi:10.1007/JHEP03(2022)198 [arXiv:2112.11096 [hep-ph]].

[102] T. Fujita*, H. Nakatsuka*, I. Obata and S. Young, JCAP **09**, 017 (2022) doi:10.1088/1475-7516/2022/09/017 [arXiv:2202.02401 [astro-ph.CO]].

[103] T. Fujita*, K. Murai* and R. Namba, Phys. Rev. D **105**, no.10, 103518 (2022) doi:10.1103/PhysRevD.105.103518 [arXiv:2203.03977 [hep-ph]].

[104] M. Kawasaki* and K. Murai*, JCAP **08**, no.08, 041 (2022) doi:10.1088/1475-7516/2022/08/041 [arXiv:2203.09713 [hep-ph]].

[105] A. Matsumoto, M. Ouchi, K. Nakajima, M. Kawasaki, K. Murai, K. Motohara, Y. Harikane, Y. Ono, K. Kushibiki and S. Koyama, *et al.* Astrophys. J. **941**, no.2, 167 (2022) doi:10.3847/1538-4357/ac9ea1 [arXiv:2203.09617 [astro-ph.CO]].

[106] T. Fujita*, K. Imagawa* and K. Murai*, JCAP **07**, no.07, 046 (2022) doi:10.1088/1475-7516/2022/07/046 [arXiv:2203.15273 [astro-ph.CO]].

[107] M. Ibe*, S. Shirai, M. Suzuki, K. Watanabe* and T. T. Yanagida, JHEP **07**, 087 (2022) doi:10.1007/JHEP07(2022)087 [arXiv:2205.01336 [hep-ph]].

[108] H. Nakatsuka*, S. Morisaki, T. Fujita*, J. Kume, Y. Michimura, K. Nagano and I. Obata, Phys. Rev. D **108**, no.9, 092010 (2023) doi:10.1103/PhysRevD.108.092010 [arXiv:2205.02960 [astro-ph.CO]].

[109] K. Kasai*, M. Kawasaki* and K. Murai*, JCAP **10**, 048 (2022) doi:10.1088/1475-7516/2022/10/048 [arXiv:2205.10148 [astro-ph.CO]].

[110] K. Asai*, A. Das, J. Li, T. Nomura and O. Seto, Phys. Rev. D **106**, no.9, 095033 (2022) doi:10.1103/PhysRevD.106.095033 [arXiv:2206.12676 [hep-ph]].

[111] S. Eijima*, O. Seto and T. Shimomura, Phys. Rev. D **106**, no.10, 103513 (2022) doi:10.1103/PhysRevD.106.103513 [arXiv:2207.01775 [hep-ph]].

[112] K. Murai*, F. Naokawa, T. Namikawa and E. Komatsu, Phys. Rev. D **107**, no.4, L041302 (2023) doi:10.1103/PhysRevD.107.L041302 [arXiv:2209.07804 [astro-ph.CO]].

[113] K. Asai*, Y. Sakai, J. Sato, Y. Takanishi and M. Yamanaka, Phys. Lett. B **836**, 137627 (2023) doi:10.1016/j.physletb.2022.137627 [arXiv:2209.08257 [hep-ph]].

[114] T. Araki, K. Asai*, H. Otono, T. Shimomura and Y. Takubo, JHEP **01**, 145 (2023) doi:10.1007/JHEP01(2023)145 [arXiv:2210.12730 [hep-ph]].

[115] M. Ibe*, M. Mishima*, Y. Nakayama* and S. Shirai, JHEP **01**, 017 (2023) doi:10.1007/JHEP01(2023)017 [arXiv:2210.16035 [hep-ph]].

[116] S. Kasuya, M. Kawasaki* and K. Murai*, JCAP **05**, 053 (2023) doi:10.1088/1475-7516/2023/05/053 [arXiv:2212.13370 [astro-ph.CO]].

[117] M. Ibe*, JPS Conf. Proc. **39**, 011007 (2023) doi:10.7566/JPSCP.39.011007

[118] K. Asai*, S. Iwamoto, M. Perelstein, Y. Sakaki and D. Ueda, JHEP **02**, 129 (2024) doi:10.1007/JHEP02(2024)129 [arXiv:2301.03816 [hep-ph]].

[119] Y. Oshima, H. Fujimoto, J. Kume, S. Morisaki, K. Nagano, T. Fujita*, I. Obata, A. Nishizawa, Y. Michimura and M. Ando, Phys. Rev. D **108**, no.7, 072005 (2023) doi:10.1103/PhysRevD.108.072005 [arXiv:2303.03594 [hep-ex]].

[120] S. Eijima*, M. Ibe* and K. Murai*, JHEP **05**, 010 (2023) doi:10.1007/JHEP05(2023)010 [arXiv:2303.09751 [hep-ph]].

[121] A. Chitose* and M. Ibe*, Phys. Rev. D **108**, no.3, 035044 (2023) doi:10.1103/PhysRevD.108.035044 [arXiv:2303.10861 [hep-ph]].

[122] J. R. Eskilt, L. Herold, E. Komatsu, K. Murai*, T. Namikawa and F. Naokawa, Phys. Rev. Lett. **131**, no.12, 121001 (2023) doi:10.1103/PhysRevLett.131.121001 [arXiv:2303.15369 [astro-ph.CO]].

[123] M. Kawasaki* and T. T. Yanagida, JHEP **11**, 106 (2023) doi:10.1007/JHEP11(2023)106 [arXiv:2304.10100 [hep-ph]].

[124] K. Asai*, J. Sato, R. Suda, Y. Takanishi and M. J. S. Yang, JHEP **11**, 213 (2023) doi:10.1007/JHEP11(2023)213 [arXiv:2305.01421 [hep-ph]].

[125] K. Kasai*, M. Kawasaki*, N. Kitajima, K. Murai, S. Neda* and F. Takahashi, JCAP **10**, 049 (2023) doi:10.1088/1475-7516/2023/10/049 [arXiv:2305.13023 [astro-ph.CO]].

[126] M. Kawasaki* and T. T. Yanagida, JCAP **01**, 014 (2024) doi:10.1088/1475-7516/2024/01/014 [arXiv:2306.14579 [hep-ph]].

[127] K. Asai*, A. Das, J. Li, T. Nomura and O. Seto, Phys. Rev. D **109**, no.7, 075026 (2024) doi:10.1103/PhysRevD.109.075026 [arXiv:2307.09737 [hep-ph]].

[128] T. Araki, K. Asai*, T. Iizawa, H. Otono, T. Shimomura and Y. Takubo, JHEP **11**, 056 (2023) doi:10.1007/JHEP11(2023)056 [arXiv:2308.01565 [hep-ph]].

[129] M. Kawasaki* and K. Murai*, JCAP **01**, 050 (2024) doi:10.1088/1475-7516/2024/01/050 [arXiv:2308.13134 [astro-ph.CO]].

[130] K. Asai*, T. Asano, J. Sato and M. J. S. Yang, PTEP **2024**, no.7, 073E01 (2024) doi:10.1093/ptep/ptae094 [arXiv:2309.01162 [hep-ph]].

[131] K. Inomata*, M. Kawasaki*, K. Mukaida and T. T. Yanagida, Phys. Rev. D **109**, no.4, 043508 (2024) doi:10.1103/PhysRevD.109.043508 [arXiv:2309.11398 [astro-ph.CO]].

[132] K. Kasai*, M. Kawasaki*, N. Kitajima, K. Murai*, S. Neda* and F. Takahashi, JCAP **05**, 092 (2024) doi:10.1088/1475-7516/2024/05/092 [arXiv:2310.13333 [astro-ph.CO]].

[133] M. Ibe*, Y. Nakayama* and S. Shirai, JHEP **03**, 012 (2024) doi:10.1007/JHEP03(2024)012 [arXiv:2312.08087 [hep-ph]].

[134] A. Chitose*, M. Ibe*, Y. Nakayama*, S. Shirai and K. Watanabe*, JHEP **04**, 068 (2024) doi:10.1007/JHEP04(2024)068 [arXiv:2312.15662 [hep-ph]].

[135] K. Kasai*, M. Kawasaki* and K. Murai*, JCAP **08**, 008 (2024) doi:10.1088/1475-7516/2024/08/008 [arXiv:2402.11902 [hep-ph]].

[136] S. Kasuya, M. Kawasaki* and N. Tsuji, Phys. Rev. D **109**, no.8, 083039 (2024) doi:10.1103/PhysRevD.109.083039 [arXiv:2403.01675 [hep-ph]].

[137] T. Aokii*, M. Ibei*, S. Shirai and K. Watanabei*, JHEP **07**, 269 (2024) doi:10.1007/JHEP07(2024)269 [arXiv:2404.19342 [hep-ph]].

[138] K. Kasaii*, M. Kawasakii*, K. Muraii* and S. Nedai*, [arXiv:2405.09790 [astro-ph.CO]].

[139] T. Araki, K. Asai*, Y. Nakashima and T. Shimomura, [arXiv:2406.17760 [hep-ph]].

FACILITIES

KAMIOKA OBSERVATORY

1. Introduction

There are four operating bodies for the underground site in Kamioka: 1) Kamioka Observatory, Institute for Cosmic Ray Research (ICRR), the University of Tokyo; 2) Tohoku University Research Center for Neutrino Science; 3) Kamioka Satellite, Kavli Institute for the Physics and Mathematics of the Universe (Kavli IPMU), the University of Tokyo; 4) KAGRA Observatory, ICRR, the University of Tokyo (listed in order of foundation). These institutions cooperate in various aspects, including safety issues and sharing some maintenance costs for the common underground environments. However, they remain independent entities, operating different facilities with separate budgets.

The underground laboratory is located 1,000 meters underground (equivalent to 2,700 meters of water) in the Kamioka Mine, Gifu prefecture, approximately 200 km west of Tokyo. Established in 1995 primarily to house and operate the Super-Kamiokande (SK) detector, the observatory has expanded its role to include operating XMASS direct dark matter search experiment. In 2020, construction officially began on the Hyper-Kamiokande (HK) detector, which is located about 8 km south of SK.

Additionally, the observatory accommodates experiments by external research institutions based on proposals; notable projects include CANDLES and AXEL, double beta decay experiments using ^{48}Ca and ^{136}Xe, led by Osaka University and Tohoku University, respectively. NEWAGE is another dark matter experiment led by Kobe University aimed at detecting recoil nuclei directions.

2. Brief History and Major Achievements

The construction budget for SK was approved in 1991, initiating a five-year construction project. SK is a 50,000-ton water Cherenkov detector with an inner volume of 32,000 tons of water optically separated from an outer layer of anti-counters with an average thickness of 2 meters. In 1992, an US group joined the project to construct and operate the anti-counters. SK was designed to address unresolved problems from Kamiokande experiment, specifically atmospheric neutrino anomalies and solar neutrino problems. It also aimed to detect neutrino bursts from supernovae and proton decay.

In 1994, a ground-level computer building was constructed and it accommodates computer system. In 1995, the Kamioka Observatory was officially founded to operate the SK detector.

In 1996, the construction of SK detector was completed and its data taking has been started. In 1998, SK discovered the up-down asymmetry in the zenith angle distribution of the atmospheric muon neutrinos, providing clear evidence for neutrino oscillation independent of the flux calculation.

The first long baseline neutrino oscillation experiment on an earth scale, K2K, commenced in 1999. It involved injecting man-made neutrinos produced at KEK PS to SK, located 250 km away from the neutrino source. The experiment concluded in 2004 with observations confirming neutrino oscillations based on the detection of 112 muon events, fewer than 156 expected without oscillation.

In June 2001, SK published the 1256 days of data for solar neutrino observations. On the same day, SNO announced their first result on charged current interactions. The comparison between SK's electron scattering data and SNO's charged current data indicated a significant effect (3.6σ), suggesting non-electron type neutrinos are present in solar neutrinos detected on Earth, marking the first evidence for solar neutrino oscillation.

In 2009, T2K, a new long baseline neutrino oscillation experiment, was started to explore the yet undetermined mixing angle of θ_{13}. An intense neutrino beam from J-PARC was directed toward SK located 295 km away. In 2011, T2K presented evidence for a non-zero θ_{13}, namely first observation of electron-neutrino appearance in muon-neutrino beam. This observation of oscillations from muon-neutrinos to electron-neutrinos opened the way to experimentally reveal leptonic CP asymmetry and search for the origin of baryon asymmetry in the universe.

3. Operation

Kamioka Observatory employs three technical staff members dedicated to daily maintenance of the underground laboratory and one additional staff member focused on safety management concerning chemicals and high-pressure gasses. Experiments and related equipment are primarily operated by scientists from each collaborating institution. For HK construction, five dedicated technical staff members support civil works and detector construction.

The observatory has a full-time scientific staff comprising 24 members (3 professors, 6 associate professors, and 15 research associates) along with four administrative staff members, including a promotions staff member and a university research administrator. These personnel manage SK operations, HK construction efforts, and research activities while also overseeing facility-related matters for approximately 5,000 visiting scientists annually.

Safety management for onsite and visiting researchers is critical and requires enhancement as HK construction progresses based on the very large international collaboration.

4. Procedure of approving experiments in Kamioka Observatory

Each year, ICRR receives experimental proposals not only for underground experiments but also for all relevant projects associated with ICRR. A program assessment committee, including external members, evaluates these proposals based primarily on scientific merit. Following approval by this committee, the Kamioka steering committee assesses whether ap-

proved proposals align with underground laboratory capabilities.

Typically, the observatory provides space and facilities such as electricity and water while users supply all necessary equipment. Before final decisions are made regarding experiments' feasibility in underground settings or potential new cavity requirements, experimental collaborations negotiate with observatory representatives. Once approved, observatory management ensures compliance with safety regulations; for instance, using liquid scintillator requires permission from local fire authorities along with adherence to numerous rules. The observatory sometimes ask the experimental group to change a design by taking into account those regulations.

5. Facilities

5.1. Underground Facilities

The entrance to underground facilities is approximately a ten-minute drive from ground office buildings. A horizontal access tunnel approximately 1.7 km long allows users access to underground facilities at any time since the Kamioka mine is no longer operational. The map of the facility area is shown in Fig. 1.

SK and KamLAND (Tohoku University) are shown in circles. CLIO and Laser strain meter are placed at the L-shape laboratory and the length of each arm is 100 m. Labs A to H are under the supervision by Kamioka Observatory and Labs 1 and 2 are the Kavli IPMU laboratories.

- **Lab.A**: Backyard of SK housing an electron LINAC for the calibration for SK and low background test equipments.
- **Lab.B**: L-shape laboratory; the length of each arm is 20 m. NEWAGE is operating at the end of one arm and the other arm was used by the Super-Conductive Gravity meter until 2016. The crossing area is used for various test experiments and preparations.
- **Lab.C**: Hall (15 m wide and 20 m long) for XMASS.
- **Lab.D**: Houses CANDLES.
- **Lab.E**: Contains a 200-ton EGADS water tank, which was built for testing the feasibility of the SK-Gd project.
- **Lab.F**: Houses computer clusters and hydrostatic test equipment.
- **Lab.G**: Houses a Gd dissolving system and a Gd-loaded water recirculation system, both of which have been in operation since 2020.
- **Lab.H**: Contains resin tanks designed to remove Gd from Super-K water during drainage.
- **Lab.1**: Equipped with devices for detecting radioactive contaminations, impurities and so on. Among them are two high purity Germanium detectors, Gas analyzer, Particle counters, Scanning Electron Microscope and so on.
- **Lab.2**: Houses computer clusters.

All the laboratories are within 400 m distances.

5.2. Environmental Backgrounds

The deep underground environment provides low radioactivity and low seismic noise and gives good opportunities to perform physics experiments requiring such experimental conditions.

At the depth of 2,700 m water equivalence, the cosmic ray muon flux, about 250 muons/m^2/day, is $\sim$1/100,000 of the surface flux.

The environmental gamma ray backgrounds from the wall depend upon locations and energy. It ranges from 0.1$\sim$0.2 /MeV/cm^2/sec at around 1 MeV and 0.01$\sim$0.02 /MeV/cm^2/sec at around 2 MeV.

The thermal and non-thermal neutron fluxes in Kamioka Observatory are measured to be

$$\phi_n^{thermal} = 8.3\pm0.6\times10^{-6}\mathrm{cm}^{-2}\mathrm{s}^{-1} \quad \text{and}$$
$$\phi_n^{non-thermal} = 1.2\pm0.1\times10^{-5}\mathrm{cm}^{-2}\mathrm{s}^{-1} \quad ,$$

respectively. In order to reduce those environmental γ and neutron backgrounds, water shields are most effective and commonly used in Kamioka. There are 2 to 3 m water layers surrounding the inner volume of SK which would effectively reduce those backgrounds. The 800 tons water tank for the XMASS experiment provides 10^{-7} reduction for neutrons.

The Rn concentration of the mine air varies $\sim$100 Bq/m^3 to $\sim$2000 Bq/m^3 depending on the season of the year. To reduce the exposure of workers and experiments, fresh air from outside of the mine is brought into the experimental areas. 100 m^3 of fresh air per minutes is brought through a 1.8 km pipe. Rn concentration of the fresh air is $\leq$50 Bq/m^3 and the Rn concentration of the experimental areas are always kept $<$ 100 Bq/m^3. To further reduce the effects of Rn for experiments, so called "Rn-free air" generation system which is based on charcoal filters is installed in the mine. The Rn concentration of "Rn-free air" is $<$ 1 mBq/m^3 and 18 m^3 per hour of flow is available for purging detectors and buffer tanks for the ultra pure water system. The U/Th and K contamination in the rocks in the mine are $\sim$1.0 ppm for U, $\sim$3.2 ppm for Th and 1.6% for K at a typical location.

To study and establish low background environment, we have ICP-MASS spectrometer, GAS MASS spectrometer, and low background Ge detectors in the underground laboratory. Those are available for the users of the underground observatory.

An electron LINAC of which energy ranges 5 MeV to 15 MeV is set up near the SK detector for the purpose of the low energy calibration. The energy of the LINAC covers exactly the energy range of the detectable solar neutrinos in SK. The DT neutron generator can also be used to produce ^{16}N in the water as a calibration source. Other radioactive calibration sources are available in the underground laboratory.

5.3. Ground Facilities

The office buildings for both Kamioka Observatory (ICRR) and Kamioka Satellite (Kavli IPMU) are adjacent and interconnected via a passageway. The observatory operates a dormitory offering accommodation by eighteen single rooms,

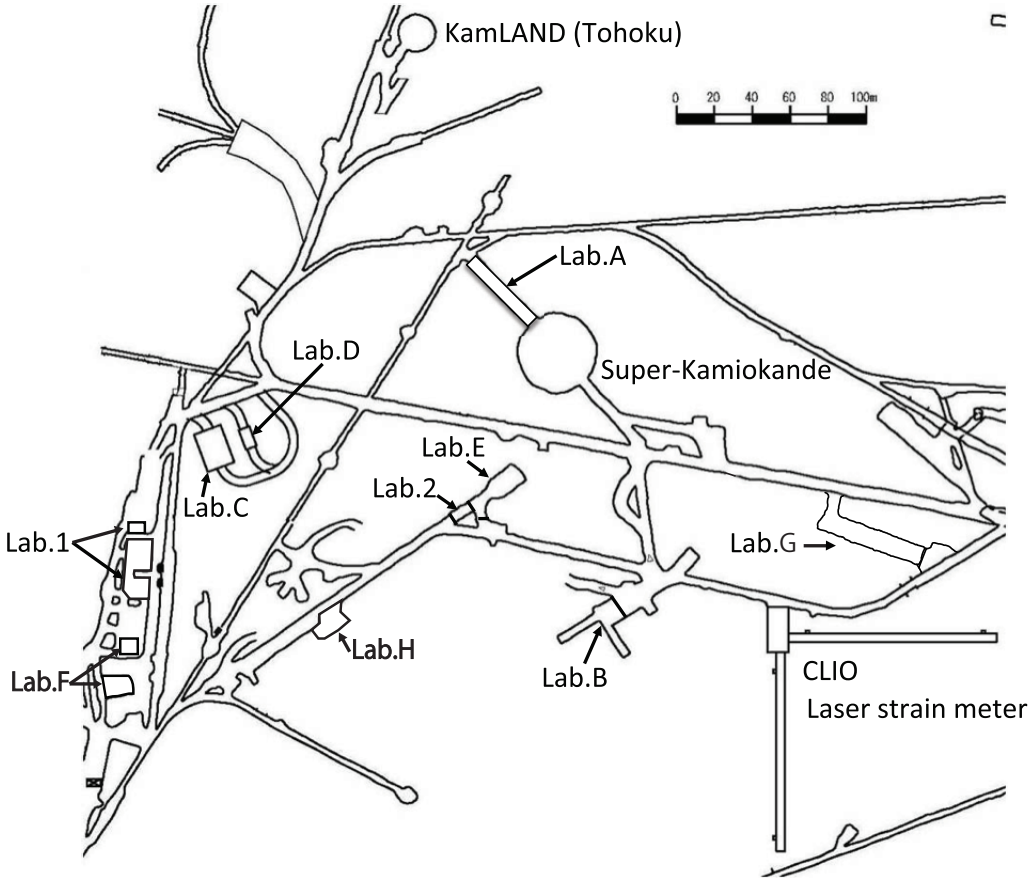

Fig. 1. Layout of Kamioka Observatory

one twin room, and one traditional tatami room. Three meals served daily upon reservation. The observatory also manages computer systems alongside electronics and chemical workshops within its office building. The computer system consists of 2632 cores with 2.60 GHz and the memory size is 4 GB/core. Disk space available is 15 PB and the access speed is greater than 8 GB/s in total. We also have a tape backup system with 4.8 PB. This system primarily supports data storage from SK experiments accessible internationally.

KAGRA OBSERVATORY

Overview

The KAGRA observatory was established in 2016 to operate Large-scale Cryogenic Gravitational Wave Telescope (nicknamed KAGRA). The buildings of KAGRA observatory are located on the foot of Ikenoyama-mountain at the border between Gifu and Toyama prefecture, about 35 km south of Toyama city in Japan. KAGRA Observatory has the data analysis building(DAB)(Fig. 1) and the rental space in the community center of Hida City. DAB and the Atotsu entrance of the KAGRA GW telescope are about 5 km away from each other. KAGRA gravitational wave telescope has an L-shape tunnel facility, and it is located more than 200 m under the mountain surface. The corner station of KAGRA GW telescope is accessible through a 500 m access tunnel from the Atotsu area (Fig. 2).

Fig. 1. KAGRA Data Analysis Building(DAB). The community center of Hida city is beside DAB.

Site Operation

KAGRA on-site members are listed in Table1. The facility maintenance in KAGRA is mainly done by two technical staff and four academic support staff. Also, one technical staff and three academic support staff contribute to the digital control system and analog electronics production in KAGRA. One academic staff manages public affairs. The KAGRA office staff manages general affairs and the dormitory operation on the 4th floor in the newly built Kamioka Research Complex building. The KAGRA safety control office, consisting of the ICRR on-site faculty staff controls safety affairs at the site.

Scientific Goal and History

KAGRA project aims to observe several gravitational waves per year with its designed sensitivity as one of the observatories of the world GW detection network including Advanced-LIGO, Advanced-Virgo, and planned LIGO-India. The KAGRA project was partially approved in 2010 as one of Leading-edge Research Infrastructure Program and also supported by the program for Promoting Large-scale Science Projects, Subsidy for Facilities Expenses, and Grants-in-Aid for Scientific Research from the Ministry of Education, Culture, Sports, Science and Technology (MEXT). In October 2019, MoU signed with LIGO and Virgo on data sharing and network detection of GWs. In June 2024, the statement of the collaboration for Einstein Telescope project between KAGRA and INFN, Italy was made.

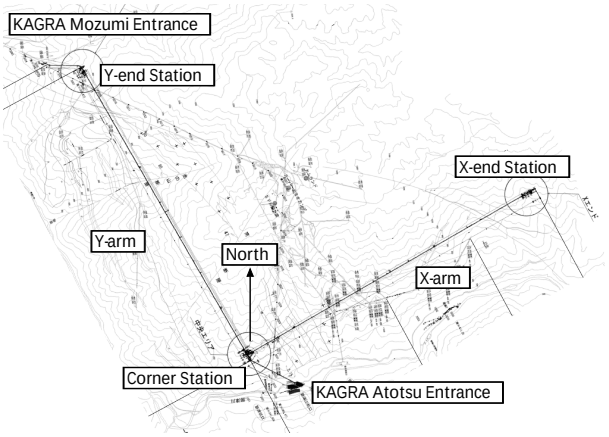

Fig. 2. KAGRA tunnel alignment. The corner station has a 500 m access tunnel from the Atotsu area, while the Y-end station has a 900 m access tunnel from the Mozumi area. The Y-arm tunnel is rotated to the east direction by about 27 degrees from the north direction.

Table 1. On-site members of ICRR and NAOJ. (*) means the member from NAOJ

Position		Position	
Prof.	2	Technical Staff	3
Assoc. Prof.	4	Office Staff	3
Assist. Prof.	4(2)	Academic Support Staff	7(2)
Postdoc Fellows	2	Technical Support Staff	3
Project Staff	1	Custodian Support Staff	4
Graduate Students	4		

Collaboration

In the KAGRA project, Institute for Cosmic Ray Research plays the role of a host promoting institute, and National Astronomical Observatory of Japan (NAOJ) and High Energy Accelerator Research Organization (KEK) are the main support organizations. Toyama University is also significantly contributing as the nearest university to the KAGRA site. More than 400 researchers in 97 institutes and universities in the world are collaborating for the construction, commissioning, sensitivity enhancement, and data analysis of KAGRA. Two Face-to-Face meetings mainly in Japan and a KAGRA International Workshop in collaborators' countries were held every year.

GW Observation

Almost all interferometer components were installed to complete the KAGRA observatory which adopts a power-recycled Fabry-Perot Michelson type interferometer with resonant sideband extraction technique until 2019 Spring. After the commissioning from May 2019 to March 2020, the KAGRA sensitivity reached 1Mpc in March 2020. Although the O3 LVK observation was not realized because of the COVID-19 pandemic, KAGRA performed international gravitational wave network observation with GEO600 as O3GK in April 2020. After more commissioning, repair, and upgrade work during the COVID-19 pandemic, KAGRA started the O4 LVK observation in May 2023 for 4 weeks (Fig. 3, Fig. 4). Unfortunately, the Noto-Peninsula earthquakes destroyed 10 of 20 seismic noise isolators in KAGRA on January 1st, 2024. The recovery work started just after this disaster, and mechanical repair was finished in July 2024.

Fig. 3. KAGRA Control Room in the Data Analysis Building during O4a. The observation status of KAGRA with 1.4 Mpc was displayed.

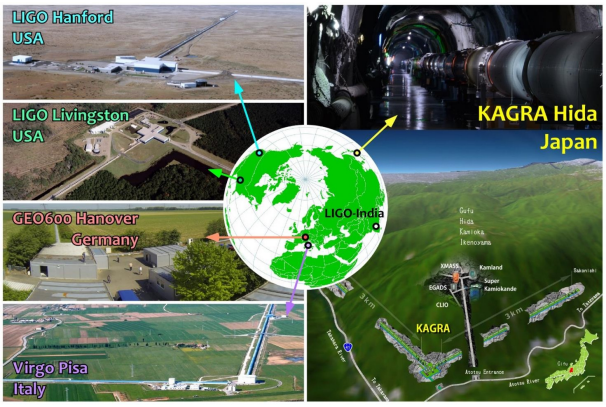

Fig. 4. International Gravitational Wave Detection Network.

Other Researches at the KAGRA site

One is the 1500-m laser strain meter(ST) operation by Earthquake Research Institute, The University of Tokyo (Fig. 5). ST was set along the X-arm vacuum ducts of KAGRA to monitor the ground motion of the Earth with the resolution in the order of 10^{-12}. ST is not only for geophysics but also for the best baseline motion reference for KAGRA. We expect to predict and mitigate the feedback signals to KAGRA mirrors and their suspension towers for the very low-frequency ranges to keep 3 km Fabry-Perot cavities' resonance by using the data from ST. ST(X500)'s front end is approximately 500 m from the KAGRA corner station, and its other end (X2000) is 1500 m from X500. ST covers wide frequency and spatial ranges. It regularly observes the tidal strains with amplitudes of the order of 10^{-8} and microseisms where the amplitude strongly relates to the weather condition of the Sea of Japan (in the range of 10^{-11} to 10^{-10} around 200 mHz), as well as regional earthquakes that induce large strain fluctuations of the order of 10^{-7} without saturating. One of the outputs of ST was detecting ground motion generated by the Hunga-Tonga volcanic eruption in 2022. It demonstrated that strain and atmospheric pressure were correlated, resulting in a regression coefficient of $-(2.3 \sim 3.7) \times 10^{-10}$ strain/hPa.

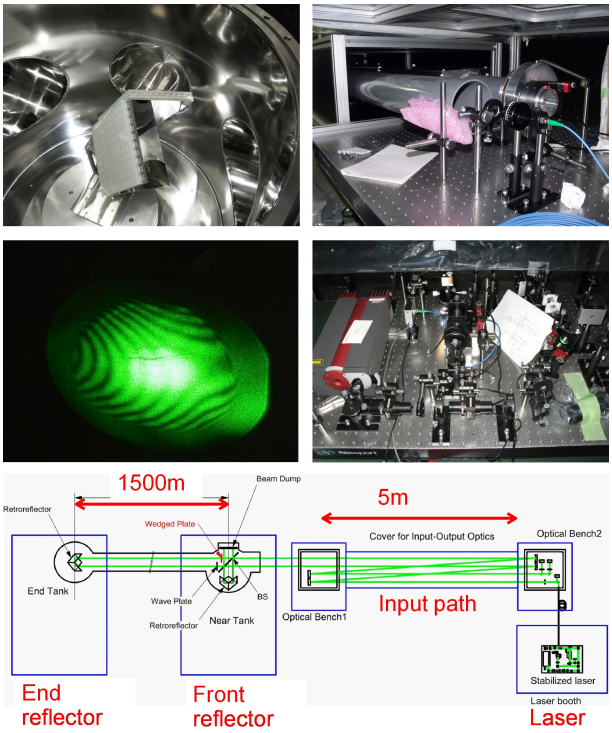

Fig. 5. 1500-m Laser Strain Meter. Left-top: 30 cm corner cube reflector. Right-top: Green laser injection point to the ST interferometer. Bottom-left: Interfered beam. Bottom-right: Frequency stabilization system for the green laser.

Another research is the ultralight vector dark matter(DM) search using KAGRA by RESCEU, The University of Tokyo. The laser interferometric gravitational wave detectors have the potential to detect ultralight vector DM by measuring the oscillating length changes in the optical cavities. Because KAGRA has the unique feature of having different substrates as a silica beam splitter and sapphire input test masses, the signal of vector DM can be enhanced in the length change in the auxiliary cavities compared to LIGO and Virgo GW telescopes. The first result of a search for U(1)B-L gauge boson DM using the KAGRA data during the first joint observation run together with GEO600(O3GK) was reported. The upper bounds on the U(1)B-L gauge coupling are obtained for DM masses around 10^{-13} eV to 10^{-12} eV.

High Energy Astrophysics Facility in Canarias

1. High Energy Astrophysics Facility in Canarias

High Energy Astrophysics Facility in Canarias, established on April 1, 2019, in La Palma, Canary Islands, Spain, is the actual base of international collaborations on the Cherenkov Telescope Array Observatory (CTAO) project cohosted by the CTAO group at ICRR (Fig. 1).

CTAO is the next-generation ground-based observatory for gamma-ray astronomy at very high energies, and more than 1500 researchers from 25 countries participate. With more than 70 telescopes in the northern and southern hemispheres, CTAO will be the world's largest and most sensitive high-energy gamma-ray observatory. The CTAO-Japan consortium significantly contributes to constructing large-sized telescopes (LSTs). Four of these telescopes are planned to be built in the northern hemisphere site in La Palma. The first of these, LST-1, was completed, and the first light was achieved at the end of December 2018.

Establishing the local corporation assets was needed for daily activities such as local procurement and employment to manage and operate the site. High Energy Astrophysics Facility in Canarias was established as a room inside the building of CALP (The Centro de Astrofísica en La Palma), a branch of IAC (Instituto de Astrofisca de Canarias) (Fig. 2).

Fig. 1. High Energy Astrophysics Facility in Canarias (top), which is inside the building of CALP (The Centro de Astrofísica en La Palma) at an altitude of 215 m (bottom), a branch of IAC (Instituto de Astrofisca de Canarias).

2. MAGIC telescopes

Many of the Cherenkov Cosmic Gamma Ray group at ICRR and the international collaborators operate the MAGIC Telescopes (Fig. 2) in La Palma, Canary Islands, through the ICRR Inter-University Research Program. Joint observations with the CTAO LST-1 and MAGIC were also conducted to take the cross-calibration and improve the gamma-ray detection sensitivity.

Fig. 2. CTAO LSTs and MAGIC telescopes are located at an altitude of about 2200 m, near the mountaintop of the Roque de los Muchachos in La Palma, Canary Islands (credit: Jelena Striskovic) (top). MAGIC Stereo System with two Cherenkov telescopes of 17 m diameters. Two telescopes are located at a distance of 85 m (bottom).

In 2004, the MAGIC Collaboration built the first large atmospheric imaging Cherenkov telescope, MAGIC-I, with a mirror surface of 236 m^2 and photomultiplier tubes. In 2009, a second telescope with the same characteristics, MAGIC-II, was installed at 85 m from MAGIC-I. The energy threshold achieved so far by the stereo observation is 25 GeV. The Japanese group (10 persons at ICRR and 21 persons outside ICRR in Chiba Univ., Hiroshima Univ., Konan Univ., Nagoya Univ., NAOJ, Osaka Univ., Osaka Metropolitan Univ., Tokai Univ., Yokohama National Univ., as of August 2024) has joined the MAGIC collaboration (about 300 persons in 13 countries) since 2010, and contributed to the operation (about ten onsite-shifters from the Japan group annually) and data analyses. They use the High Energy Astrophysics Facility in Canarias.

The highlights from MAGIC, which were published in journals after April 2018, are (1) The first detection of the Gamma Ray Burst GRB 190114C, (2) The first detection of gamma rays from the Nova RS Ophiuchi, (3) Detection of sub-TeV gamma rays from the IceCube 170922A [1]. The detailed results of (1) and (2) that the MAGIC Japan group significantly contributed are described below.

Gamma Ray Burst 190114C

In January 2019, the MAGIC telescopes, for the first time, detected the Gamma-Ray Burst (GRB) 190114C with a redshift of 0.42 [2]. MAGIC telescopes started observing the GRB at T_0 + 57 seconds after receiving the alert from the SWIFT-BAT satellite. The observation shows a 100 times higher flux of gamma rays than the Crab Nebula at T_0 + 80 sec and the resultant statistical significance of gamma rays was more than 50 sigma. The highest-energy photon reaches above 1 TeV, and the observed spectrum after the Extragalactic Background Light (EBL) de-absorption did not show any roll-off feature in the energy spectrum [2]. This observation shows the new gamma-ray emission mechanism in the GRB to explain the TeV emission, possibly the inverse Compton emission. The light curve shows the power-law decay $t^{-1.6}$, which is surprisingly parallel to the X-ray lightcurve measured by XRT [3]. It is worth mentioning that the energetics of the TeV emission is comparable with that of the X-ray emission. The two bump structures in the spectral energy distribution can be fit consistently with the Synchrotron Self Compton model as shown in Fig. 3 [3].

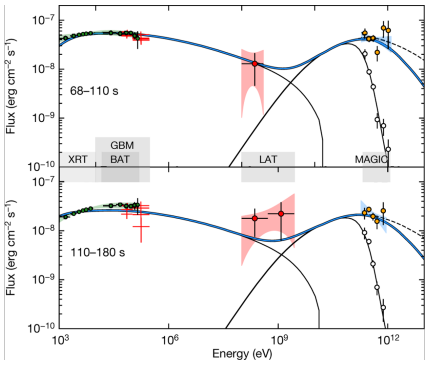

Fig. 3. Modelling of the broadband spectra in the time intervals 68-110 s and 110-180 s for GRB 190114C [3].

Recurrent Nova: RS Ophiuchi

Novae are luminous eruptions triggered by a thermonuclear runaway on a white dwarf surface when the white dwarf accretes a critical amount of matter from its stellar companion. Though novae have been revealed to be high-energy gamma-ray emitters through observations by Fermi-LAT, their gamma-ray emission mechanism remained unclear.

RS Ophiuchi (Oph) is a symbiotic system where a white dwarf is embedded in a red giant companion. It is well known as a recurrent nova with a recurrence time scale of ∼15 years. In August 2021, RS Oph was reported to be in a new burst state through optical and gamma-ray observations. In response to these alerts, MAGIC promptly started observations of RS Oph, only one day after the burst onset [4]. During the first four days after the eruption, MAGIC detected very high-energy (VHE) gamma rays from RS Oph at a statistical significance of 13.2σ in the energy range between 60 GeV and 250 GeV, contemporaneously with the Fermi-LAT and optical peaks. This is the first detection of VHE gamma rays from a nova, which is also achieved by H.E.S.S. and CTA LST-1 concurrently. The contemporaneous gamma-ray spectrum measured by Fermi-LAT and MAGIC suggests a common single component between 50 MeV and 250 GeV, as shown in Fig. 4.

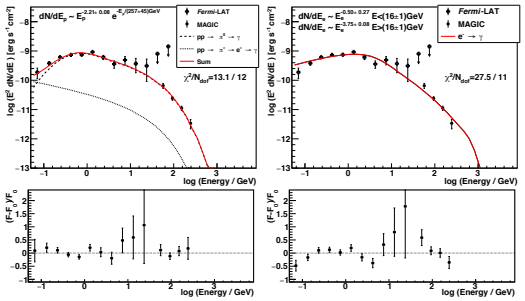

Fig. 4. Spectral energy distribution of gamma-ray emission from the 2021 outburst of RS Oph measured with Fermi-LAT and MAGIC. The hadronic (*left*) and leptonic (*right*) models are tested.

Though both protons and electrons may be accelerated in the nova shock and radiate gamma rays, the data strongly suggest a hadronic origin of the gamma-ray emission for the following reasons. First, the leptonic model needs an unnaturally sharp break in the intrinsic electron spectrum. In contrast, the hadronic model can describe the data with a natural proton distribution of a power law with an exponential cut-off. Second, the hadronic model fits the data statistically better than the leptonic model. Lastly, the data suggest an increase in the particle's maximum energy over time, which is in line with the absence of fast cooling in the hadronic model, while electrons are expected to be subject to substantial energy losses due to inverse Compton scattering.

The detection of VHE gamma rays from RS Oph revealed that the gamma-ray emission in this nova has a hadronic origin. However, it remains an open question whether the acceleration and radiation mechanisms observed in RS Oph are shared among all novae, including classical novae, or are unique to recurrent symbiotic novae. Further detection of novae in the VHE gamma-ray regime is needed to address this question.

Bibliography

[1] "Multimessenger observations of a flaring blazar coincident with high-energy neutrino IceCube-170922A", IceCube, Fermi-LAT, MAGIC, AGILE, ASAS-SN, HAWC, H.E.S.S, INTEGRAL, Kanata, Kiso, Kapteyn, Liverpool telescope, Subaru, Swift/NuSTAR, VERITAS, VLA/17B-403 teams, Science, Science.eaat1378 (2018).

[2] "Teraelectronvolt emission from the γ-ray burst GRB 190114C", MAGIC collaboration, Nature 575, 455 (2019).

[3] "Observation of inverse Compton emission from a long γ-ray burst", MAGIC collaboration et al., Nature 575, 459 (2019).

[4] "Proton acceleration in thermonuclear nova explosions revealed by gamma rays", MAGIC collaboration et al., Nature Astronomy, 689 (2022).

RESEARCH CENTER FOR COSMIC NEUTRINOS

The Research Center for Cosmic Neutrinos (RCCN) was established in 1999 with the aim of conducting research on neutrino and related topics.

Members of this center are participating in the Super-Kamiokande experiment, exploring the properties of neutrinos using data of atmospheric neutrinos and accelerator neutrinos, and search for neutrino emissions from high-energy celestial objects in the universe. we have provided the occasion to discuss theoretical ideas and experimental results on neutrino physics. Additionally, we are involved in the project of next-generation neutrino experiment, Hyper-Kamiokande, conducting research and development on the 50-cm diameter photomultiplier tube, and advancing preparations for the construction of the detector scheduled for 2026, with the ongoing goal of advancing neutrino research into the future.

The center also plays a role in the joint research program of ICRR. In addition to accepting research on neutrinos, as the facility utilization, in collaboration with the Computer Committee, the center manages a large-scale computer system used for joint research at this research institute by cosmic ray researchers nationwide (Fig 1). This computer system has a total of approximately 3,300 CPU cores, 9 petabytes of large capacity disk, and data transfer performance of 18 gigabytes per second. It is capable of analyzing large amounts of data obtained from cosmic ray observation experiments and generating simulation data that require high CPU capability. Every researchers, who are accepted for the research program, are able to have the computing account and utilize the computing resources. The system also provides several servers of system control, networking, internet services such as web, mail, online storage, etc. The system has been upgraded in every 6 years in order to have the benefits of the evolution of the latest computer performance. Since its update in the fiscal year 2020, it has been operated stably. The overall efficiency of providing the computing resources is greater than 95% at present (as of year 2024). The next upgrade of the system is planned in 2026.

Additionally, the center serves as the acceptance for joint research program by primary cosmic ray group, and operates the low-background experimental laboratory underground. The underground laboratory is equipped with four Germanium detectors (Fig. 2), mainly utilized for the measurements of cosmic radioactive isotopes. The scientific activities which have been made by using this laboratory are described in other section.

The center also supports outreach activities for the general public regarding cosmic ray research. Since 2009, ICRR has jointly held public lecture events twice a year in spring and summer with the Kavli Institute for the Physics and Mathematics of the Universe (Kavli IPMU). Specifically, for the spring event, the center collaborates with the public relations office to plan and implement it. The list of the public lectures, held between 2013 and 2018, is shown in Table 1.

Fig. 1. ICRR computering system managed by RCCN and ICRR computer committee.

Fig. 2. Low-background underground laboratory in Kashiwa campus.

RCCN has been accepting several applications of the joint-use research programs of ICRR, especially for the low background radioisotope measurement in the underground laboratory of the Kashiwa campus, and the simulation researches using the ICRR computing system. Furthermore, it accepts joint research solely for computer usage and research meetings related to future plans, among other activities. Table 2 shows the number of the accepted joint-use research applications accepted by the center from domestic and international researchers.

Table 1. List of public lectures organized by RCCN and ICRR Public Relation Office. These lectures are co-hosted by ICRR and Kavli IPMU.

	Date	Lecturers
1	April 13, 2019	Masahiro Kawasaki (ICRR)
		Hajime Sugai (Kavli IPMU)
2	August 8, 2020	Koji Noda (ICRR)
		Takeo Higuchi (Kavli IPMU)
3	April 10, 2021	Yoichi Asaoka (ICRR)
		Satoshi Murayama (Kavli IPMU)
4	April 9, 2022	Yuichi Harikane (ICRR)
		Naoki Yoshida (Kavli IPMU)
5	April 22, 2023	Masato Takita (ICRR)
		Shin-ichiro Takeda (Kavli IPMU)
6	April 20, 2024	Atsushi Takeda (ICRR)
		Yukari Itoh (Kavli IPMU)

Table 2. Number of accepted joint-use research applications by RCCN from domestic and international researchers for each fiscal year.

Fiscal Year	Domestic	International
2018	9	–
2019	11	0
2020	8	0
2021	6	0
2022	9	3
2023	9	2

Members

Staff

Takaaki Kajita,	Professor (till Mar. 2024)
Kimihiro Okumura,	Assoc. Professor
Fuyuki Tonakai,	Visiting Professor (from Apr. 2018)
Masanobu Shinohara,	Technical Staff (till Mar. 2023)
Shohei Aoyama,	Technical Staff (from Aug. 2023)
Yasuhiro Nishimura,	Research Associate (till Mar. 2019)
Takuya Tashiro,	Project Research Associate (from Oct. 2019)

NORIKURA OBSERVATORY

Introduction

The Norikura Observatory (36.10°N and 137.55°E) was founded in 1953 and attached to ICRR in 1976. It is located at 2770 m above sea level, and is the highest altitude manned laboratory in Japan (Fig. 1). Experimental facilities of the laboratory are made available to all the qualified scientists in the field of cosmic ray research and associated subjects. The AC electric power is generated by the dynamo and supplied throughout the observatory. The observatory can be accessed easily by car and public bus in summer (July-September). The 70th anniversary of the Norikura Observatory was celebrated in 2023.

Fig. 1. Norikura Observatory

The Norikura Observatory gave manned operation to the observations by the qualified scientists all the year until the year 2003. However, in order to reduce maintenance and labor costs without causing serious inconveniences for the researches, the feasibility of the automatic operation of the observatory during winter period has been tested since winter 2004. A long-distance (∼40km) wireless LAN system (11M bps) was set up in 2003. Two new easy-to-handle and easy-to-maintain dynamos of 115 KVA each, as shown in Fig. 2 were installed in 2004 as well. The unmanned operation of the observatory in winter, during which the battery backed-up solar panels keeps supplying the electricity to the wireless LAN and on-going cosmic-ray experiments, has been established.

Present major scientific interests of the laboratory is focused on the modulation of high energy cosmic rays in the interplanetary space associated with the solar activity, the generation of energetic particles by the solar flares, and the particle acceleration mechanism in thunderclouds, all of which require long-term observation. These researches have been carried out by the group of user universities, where ICRR provides them with laboratory facility. A part of the facility has been open for the environmental studies at high altitude such as aerosol-related mechanism in the atmosphere, observation

Fig. 2. A dynamo of 115KV.

of total ozone and UV solar radiation, for botanical study in the high-altitude environment.

Cosmic Ray Physics

Space weather observation using muon hodoscope [represented by Chihiro Kato, Shinshu University]

Mt. Norikura muon hodoscope has started its operation in 1998 aiming to observe a precursory signature of the interplanetary shock approaching the Earth. The detector succeeded for the first time to observe a loss-cone signature which is an intensity deficit within a narrow cone around the interplanetary magnetic field (IMF). The observation of the loss-cone precursor gives us unique information for the space weather forecast and for understanding the interplanetary disturbances in near Earth space [1]. Then, we started the Global Muon Detector Network (GMDN) observation in 2006 including another detector system at Syowa station in the Antarctic in 2018 to expand the covering area. The experiences at Mt. Norikura station was quite a help to start observation under severe environment in the Antarctic. A few space weather events were analyzed with this new GMDN. We found an interesting variations suggesting adiabatic acceleration in the flux rope. We also reported results of the integrated analysis in [9][10][11][12].

Solar neutron observation [represented by Yutaka Matsubara, Chubu University]

We have studied the acceleration mechanism of solar energetic particles by observing neutrons (>100 MeV) produced by the interaction between high energy ions and the solar atmosphere. The 64 m^2 solar neutron telescope at the Norikura observatory played the central role of the world-wide network. The achievements so far obtained are summarized as followings. The acceleration mechanism of solar energetic particles is stochastic if neutrons are produced at the same time as the

electromagnetic waves [2][3]. At least in one event neutrons are produced longer than hard X-rays [4]. The total energy which neutrons obtain during one solar flare does not exceed 0.1% of the energy of soft X-rays [5]. The observation of solar neutrons at Norikura has ceased in the summer of 2022. There are two stations which continue observing solar neutrons. One is at Sierra Negra (4,560 m) in Mexico. Another is at Chacaltaya (5,250 m) in Bolivia. The final puzzle of the acceleration mechanism of solar energetic particles is expected to be solved by the observation of these two stations. Recent progresses are reported in [13][14][15].

A new study for high precision measurement of muons [represented by Tasumi Koi, Chubu University]

We are conducting a research to repurpose the proportional counter section of the solar neutron telescope previously operated by Nagoya University at the Norikura Observatory into a hodoscope-type high-precision muon telescope.

Observational research on particle acceleration and cosmic-ray shower in thunderstorm electric fields via citizen science "Thundercloud Project" [represented by Teruaki Enoto, Kyoto University]

Our citizen science "Thundercloud Project" is a multi-site radiation monitoring of gamma rays from winter thunderclouds (gamma-ray glows) and high-energy radiation from lightning. For this project, we developed a portable radiation monitor called Compact Gamma-ray monitor (CoGaMo), which works only at the touch of a button, and installed it at about 70 locations around Kanazawa City with citizen supporters. The CoGaMo detectors have already succeeded in detecting several gamma-ray glows from thunderclouds [16]. We are also planning to distribute CoGaMo detectors at Mt. Norikura. Furthermore, in this project, we newly developed a special board for radiation measurement called "PENGUIN," which can be used in combination with a Sony board-type computer "Spresense". With this board, a two-channel portable radiation monitor can be made and used for future observations.

Study of Secondary Cosmic Rays from Thundercloud [represented by Atsushi Shiomi, Nihon University]

To study the relativistic electron acceleration mechanism by a thundercloud-derived electric field and the relation between thunder and cosmic-ray air showers, we started an experiment in 2015, mainly using gamma-ray detectors at the Norikura Observatory. The experiment consists of gamma-ray detectors, a lightning sensor, an electric field meter, a weather monitor, and an air shower array consisting of five scintillation detectors. Gamma-ray detectors using three crystals, NaI, CsI, and BGO, cover a total energy range of more than three orders of magnitude from 70 keV to 120 MeV.

Research on annual variations of ^{14}C concentration in *Pinus pumila* [represented by Fuyuki Tokanai, Yamagata University]

Solar activities and the extremely intense cosmic-ray events in the past have been investigated by measuring the ^{14}C concentration in the annual tree rings of old wood. However, since the amount of CO_2 in the atmosphere is affected by the global carbon cycle, the ^{14}C concentration in tree annual rings shows a delayed and attenuated response from the rate of the production. Thus, it is important to investigate the dependence of ^{14}C concentration in the plant using modern samples for which the number of sunspots and the amount of secondary cosmic rays are accurately observed. Since 2018, we have been continuously collecting cones and leaves of *Pinus pumila* that live in the alpine zone of Mt. Norikura and Mt. Zao, and measuring ^{14}C concentrations using a high-sensitivity accelerator mass spectrometer at Yamagata University. In addition, samples were collected from urban areas in Tokyo and Tendo city, Yamagata Prefecture. It is found that the Δ^{14}C values in *P. densiflora* samples from Tendo city were lower of Δ^{14}C in all years than those from Mt. Norikura and Mt. Zao, and no dependence on collection year was observed. *P. densiflora* samples from Tokyo showed the lowest Δ^{14}C values in all years among the samples collected, which also showed a decreasing trend from 2019 onwards. We plan to continue collecting data [17][18][19][20][21].

Test experiment of the Fuel cell [represented by Tasumi Koi, Chubu University]

The Norikura Observatory is currently unmanned in the winter season and a combination of solar panels and lead-acid batteries supplies power to detectors. The motivation for research lies in utilizing environmentally friendly fuel cells to provide electricity more reliably for the period. Upon consultation with fuel cell system vendors and investigation of the operational performance of a small-scale fuel cell experimentally which experienced failures within a few years, several issues related to the observatory's location have emerged. Taking these factors into account, it has been concluded that, for the time being, efforts should be directed towards enhancing the stability of the conventional solar panel and battery system, with fuel cells serving a supplementary role.

Environmental Study

Monitoring the cloud water quality for evaluation of the SO_2 in-cloud oxidation process [represented by Nagayoshi Katsuta, Gifu University]

In East Asia, the rapid economic growth has increased the fuel consumption, and the associated emissions from fossil fuels have risen since the 1980s [22]. The atmospheric SO_2 emitted from thermal power plants and factories progressively increased since 1980 and turned to decline from 2006. This is because the Chinese government has set a restrictive target on SO_2 reduction and implemented flue-gas desulfurization (FGD) system. It is well known that gaseous SO_2 is highly dissolved into cloud droplets and the subsequent oxidation brings formation of H_2SO_4. In the 1960-1990s, clouds of strong acid (pH = 3 to 4) were observed near the summit

of Mt. Norikura [6][7][8]. Therefore, we have monitored the cloud water quality in this site to assess in-cloud oxidation (acidification) of gaseous SO_2 during summertime in 1999-2000 and 2022-2023. As a result, the cloud pH increased from 4.0 to 4.7 during the past 20 years, while the NO_3^- and SO_4^{2-} concentrations of cloud water reduced to less than one-fifth, suggesting that cloud water is neutralized and purified. However, the cloud water H_2O_2 and O_3, the most important oxidant for gaseous SO_2 oxidation, were approximately the same level as 20 years ago [23][24][25][26].

Seasonal and diurnal variations in soil respiration rates at a treeline ecotone [represented by Koichi Takahashi, Shinshu University]

This study examined the seasonal and diurnal variations in soil respiration rates (R_S) during a growing season at the treeline ecotone (2800 m) on a volcanic mountain in Japan, using an automated measurement equipment. The aboveground biomass, the total R_S during the growing season, and the R_S per day during the growing season were low at 2800 m. Seasonal R_S variations positively correlated with those of soil and air temperatures. The mean volumetric soil water content (W_S) during the growing season was much low because of the scoria substrate. The monthly mean diel cycle of R_S was positively correlated with the soil temperature every month. The R_S decreased during the daytime especially in August, despite no changes in the W_S. Seasonal and diurnal R_S variations could be reproduced from soil and air temperatures, and W_S. Estimating soil respiration rate from these variables will help understand the future carbon budget of forests due to global warming. Recent progresses are reported in [27][28][29][30][31][32][33].

Bibliography

Before Year 2018

[1] K. Munakata, T. Kuwabara, S. Yasue, C. Kato, S. Akahane, M. Koyama, Y. Ohashi, A. Okada, T. Aoki, H. Kojima and J. W. Bieber, "A "loss-cone" precursor of an approaching shock observed by a cosmic-ray muon hodoscope on October 28, 2003", Geophys. Res. Lett., 32, L03S04-1 4, doi:10.1029/2004GL021469, 2005 (January 11).

[2] Watanabe, K., et al., Astrophys. J., 592, 590-596, 2003

[3] Watanabe, K., et al., Astrophys. J., 636, 1135-1141, 2006.

[4] Sako, T., et al., Astrophys. J. Lett., 651, L69-L72, 2006.

[5] Lopez, D., et al., Astropart. Phys., 76, 19-28, 2016.

[6] Okita, T.(1968). Concentration of sulfate and other inorganic metals in fog and cloud water and in aerosol. Journal of Meteorological Society Japan 46: 120-127.

[7] Minami Y. and Ishizaka Y. (1996). Evaluation of chemical composition in fog water near the summit of a high mountain in Japan. Atmospheric Environment 30: 3363-3376.

[8] Watanabe, K., Ishizaka, Y. and Takenaka, C. (1999). Chemical composition of Fog water near the summit of Mt. Norikura in Japan. Journal of Meteorological Society Japan 77: 997-1006.

After Year 2018

[9] K. Munakata, M. Kozai, C. Kato, Y. Hayashi, R. Kataoka, A. Kadokura, M. Tokumaru, R. R. S. Mendonça, E. Echer, A. Dal Lago, M. Rockenbach, N. J. Schuch, J. V. Bageston, C. R. Braga, H. K. Al Jassar, M. M. Sharma, M. L. Duldig, J. E. Humble, I. Sabbah, P. Evenson, P. S. Mangeard, T. Kuwabara, D. Ruffolo, A. Sáiz, W. Mitthumsiri, W. Nuntiyakul, and J. Kóta. Large-amplitude Bidirectional Anisotropy of Cosmic-Ray Intensity Observed with Worldwide Networks of Ground-based Neutron Monitors and Muon Detectors in 2021 November. ApJ, 938(1):30, October 2022.

[10] W. Kihara, K. Munakata, C. Kato, R. Kataoka, A. Kadokura, S. Miyake, M. Kozai, T. Kuwabara, M. Tokumaru, R. R. S. Mendonça, E. Echer, A. Dal Lago, M. Rockenbach, N. J. Schuch, J. V. Bageston, C. R. Braga, H. K. Al Jassar, M. M. Sharma, M. L. Duldig, J. E. Humble, P. Evenson, I. Sabbah, and J. Kóta. A Peculiar ICME Event in August 2018 Observed With the Global Muon Detector Network. Space Weather, 19(3):e02531, March 2021.

[11] C. Kato, W. Kihara, Y. Ko, A. Kadokura, R. Kataoka, P. Evenson, S. Uchida, S. Kaimi, Y. Nakamura, H. A. Uchida, K. Murase, and K. Munakata. New cosmic ray observations at Syowa Station in the Antarctic for space weather study. Journal of Space Weather and Space Climate, 11:31, January 2021.

[12] R. R. S. Mendonça, C. Wang, C. R. Braga, E. Echer, A. Dal Lago, J. E. R. Costa, K. Munakata, H. Li, Z. Liu, J. P. Raulin, T. Kuwabara, M. Kozai, C. Kato, M. Rockenbach, N. J. Schuch, H. K. Al Jassar, M. M. Sharma, M. Tokumaru, M. L. Duldig, J. E. Humble, P. Evenson, and I. Sabbah. Analysis of Cosmic Rays' Atmospheric Effects and Their Relationships to Cutoff Rigidity and Zenith Angle Using Global Muon Detector Network Data. Journal of Geophysical Research (Space Physics), 124(12):9791–9813, December 2019.

[13] Matsubara, Y., Gound level observation of solar neutrons (Japanese), RADIOISOTOPES, 68, 907-915, 2019.

[14] Muraki, Y., et al., Possible detection of solar gamma-rays by ground-level detectors in solar flares on 2011 March 7, Publ. Astron. Soc. Jpn, 72, 1-17, 2020.

[15] Newton-Bosch, J., et al., Atmospheric electric field effects on cosmic rays detected by the solar neutron telescope at Sierra Negra, J. Atmos. and S.-T. Phys., 253, 106156, 2023.

[16] Tsurumi, Enoto, Ikkatai, et al., "Citizen Science Observation of a Gamma-Ray Glow Associated With the Initiation of a Lightning Flash", Geophysical Research Letters, Volume 50, Issue 13, e2023GL103612 (2023).

[17] M. Takeyama, T. Moriya, H. Sakurai, H. Miyahara, F. Tokanai, Research of annual variations of ^{14}C concentrations in pinus pumila V, Extended Abstracts of the 84th JSAP Autumn Meeting, 20a-A310-3 (2023).

[18] M. Takeyama, T. Moriya, H. Sakurai, H. Miyahara, F. Tokanai, Research of annual variations of ^{14}C concentrations in pinus pumila IV, Extended Abstracts of the 83rd JSAP Autumn Meeting, 22a-C205-3 (2022).

[19] M. Takeyama, T. Moriya, H. Sakurai, H. Miyahara, F. Tokanai, Research of annual variations of ^{14}C concentrations in pinus pumila III, Extended Abstracts of the 82nd JSAP Autumn Meeting, 11a-N402-7 (2021).

[20] M. Takeyama, T. Moriya, H. Sakurai, H. Miyahara, F. Tokanai, Research of annual variations of ^{14}C concentrations in pinus pumila II, Extended Abstracts of the 81st JSAP Autumn Meeting, 8a-Z25-10 (2020).

[21] M. Takeyama, T. Moriya, H. Sakurai, H. Miyahara, F. Tokanai, Research of annual variations of ^{14}C concentrations in pinus pumila, Extended Abstracts of the 67th JSAP Spring Meeting, 14p-D209-4 (2020).

[22] Ohara,T. and Kurokawa, J. (2018) Long-term variation of emissions of air pollutants related to atmospheric aerosol in Asia, China and Japan. Earozoru Kenkyu 33: 95-101 (in Japanese).

[23] Kagawa, M., Katsuta, N. and Ishizaka, Y. (2021) Chemical characteristics of cloud water and the sulfate production under excess hydrogen peroxide in a high mountains region of central Japan. Water, Air, and Soil Pollution 237:177.

[24] Kagawa, M., Katsuta, N. and Ishizaka, Y. (2022) Selenite and selenate in clouds at a high-altitude mountain location in Central Japan. Atmospheric Research 276:106253.

[25] Kagawa, M., Katsuta, N., Naito, S., Masuki, Y., Yoshimizu, C., Chiba, H. and Tayasu, I. (2023) Sample pretreatment effects on isotopic compositions of oxygen and sulfur in $BaSO_4$ derived from atmospheric sulfate. Rapid Communications in Mass Spectrometry 37: e9659.

[26] Masako Kagawa (2023) Study of the dynamics of selenium in relation to the transport and oxidation of sulfur compounds in the atmosphere. The united graduate school of agricultural science, Gifu University. Doctor of Agriculture No.165.

[27] Takahashi, K., Otsubo, S. & Kobayashi, H. (2018) Comparison of photosynthetic traits of codominating subalpine conifers Abies veitchii and A. mariesii in central Japan. Landscape and Ecological Engineering 14: 91–97.

[28] Tateno, R., Tatsumi, C., Nakayama, M., Takahashi, K., Kerfahi, D. & Adams, J. (2019) Temperature effects on the first three years of soil ecosystem development on volcanic ash. Catena 172: 1–10.

[29] Takeda, S. & Takahashi, K. (2020) Elevational variation in abundance of coarse woody debris in subalpine forests, central Japan. Forest Ecology and Management 473: 118295.

[30] Takahashi, K. (2021) Productivity does not decrease at the climate extremes of tree ranges in the Japanese archipelago. Oecologia 197:259–269.

[31] Shimada, R. & Takahashi, K. (2022) Diurnal and seasonal variations in photosynthetic rates of dwarf pine Pinus pumila at the treeline in central Japan. Arctic, Antarctic, and Alpine Research 54:1–12.

[32] Takeda, S., Majima, R., Makita, N. & Takahashi, K. (2023) Five-year measurement data along a 1200 m elevational gradient reveals that global warming increases soil respiration. Frontiers in Forest and Global Change 6: 1145474.

[33] Takeda, S., Makita, N. & Takahashi, K. (2024) Seasonal and diurnal variations in soil respiration rates at a treeline ecotone and a lower distribution limit of subalpine forests. Journal of Plant Research.

AKENO OBSERVATORY

Introduction

Akeno Observatory is located in Akeno, Hokuto City, 20 km northwest of Kofu City and 130 km west of central Tokyo. The location is at the longitude of 138.5°E and the latitude of 35.8°N. The altitude is about 900 m above sea level. It was established in 1977 as a research center for air shower studies in the very high energy region, and it has been administered by ICRR as a facility of the joint research of ICRR.

The Akeno Air Shower experiment started in 1979 with an array covering 1 km^2 area. The array coverage was enlarged to 20 km^2 in 1984 and was gradually expanded to Akeno Giant Air Shower Array (AGASA) of approximately 100 km^2 area by 1990. AGASA was built to study ultra-high energy cosmic rays (UHECRs) in the energy range of 10^{20} eV.

Scientific Activities since 2018

The study of UHECRs by AGASA in Akeno was succeeded by the Telescope Array (TA) experiment in Utah, USA since 2008. After the shutdown of AGASA in 2004, all the AGASA detectors were dismantled and Akeno Observatory has been used for small-scale cosmic ray experiments, astrophysical observations and as a test/assembly/R&D facility of TA and other experiments by ICRR and university researchers[1]. As of 2024, there is the main campus of approximately ten thousand square meters (Fig. 1), one small site of the MITSuME telescope, three small sites each of a muon house, and one small site of an unused muon house. One assistant technical staff member works twice a week to maintain Akeno Observatory.

Fig. 1. The main campus of Akeno Observatory. The large experimental hall and the research building are from the left to the right.

Research and development for the Telescope Array project in Utah by the TA collaboration: The Telescope Array experiment is a hybrid cosmic ray detector that uses 507 surface detectors (SDs) and 38 atmospheric fluorescence detectors (FDs) to cover an area of approximately 700 km^2. Since then, the Telescope Array collaboration has been promoting the TA Low energy Extension (TALE) project[2] to expand the energy range of observations and the TAx4 project[3] to expand the detection area. Akeno Observatory is being used as a research and development site for the TA experiment and its extensions.

For example, in 2018, the time accuracy of all GPS modules for the SDs used in the TAx4 and TALE experiments were tested. A test bench was built at Akeno Observatory to measure the relative individual differences in GPS 1pps, and it was confirmed that the individual differences were a maximum of 19.3 ns, which is about half of the expected value.

In 2021, 50 SDs were manufactured at Akeno Observatory to be installed to lower the energy threshold to $10^{15.5}$ eV (Fig. 2). The manufactured SDs were transported to the TA site in Utah, USA, in 2022, and have been in stable operation as the TALE-infill air shower array covering 0.36 km^2 since 2023.

Fig. 2. Assembly of a plastic scintillator counter at the large experimental hall of Akeno Observatory

Observation by the multi-color imager for transients, survey and monstrous explosions (MITSuME) by N. Kawai, Y. Yatsu (Institute of Science Tokyo), et al.: One of the two MITSuME robotic telescopes was installed in Akeno Observatory in 2003 on the roof of the concrete muon detector site (Fig. 3).

The telescope has an aperture of 50 cm, an FOV of 28' × 28' and is equipped with a tricolor CCD camera capable of $g' : 400-550\,nm, R_c : 570-730\,nm, I_c : 730-850\,nm$ bands photometry. It is operated remotely from Science Tokyo. Upon receiving a GRB alert from Swift or Fermi, it quickly directs the telescope (9°/s maneuverability) toward the GRB direction, and makes a prompt observation of the GRB and its

*1 In the Japanese Fiscal Year (JFY) 2024, 10 proposals that included the usage of Akeno Observatory was accepted for the ICRR joint research program.

*2 S. Ogio et al., PoS(ICRC2019)375 (2019)

*3 R.U. Abbasi et al., NIM A, 1019 (2021) 165726

Fig. 3. The dome in which the MITSuME telescope was installed in Akeno.

afterglow. Since 2018, follow-up observations have been carried out on 231 GRBs, and 26 optical counterparts have been detected (See Fig. 4 for an example[4]).

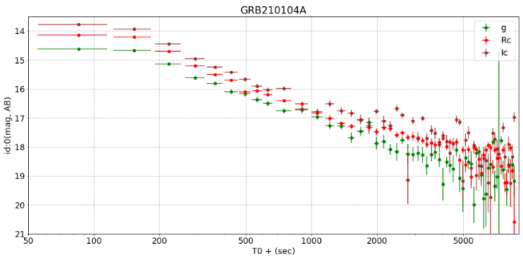

Fig. 4. The light curve of GRB 210104A, as observed by the 50cm MITSuME telescope at Akeno Observatory

It has also joined "The Optical and Infrared Synergetic Telescopes for Education and Research (OISTER) project consists of nine Japanese universities" exploring multi-messenger astronomy research and education. More than 20 supernova afterglows, X-ray binaries, and other objects have been observed in collaboration, and the team has achieved results[5].

MITSuME is a member of J-GEM and GROWTH and involves joint follow-up observations of gravitational wave events. MITSuME participated in the follow-up observations of the O3 observation period by LIGO/Virgo, which began in April 2019 and reported the results of 10 observations to GCNC[6].

Observation of galactic cosmic rays by large area muon telescope by A. Oshima (Chubu University), et al.: To clarify the interaction between the cosmic magnetic field and cosmic rays and establish observation methods for fluctuations in cosmic ray intensity (space weather) in interplanetary space between 0.3 and 1 AU, the team simultaneously observes fluctuations in intensity and anisotropy of 100 GeV region cosmic rays from multiple directions using muon telescopes in the GRAPES-3 experiment at Ooty, India, and Akeno Observatory. The muon telescope, consisting of four layers of proportional counters with 25 m^2 areas, was installed in each of the three muon houses, called M1, M5, and M8, in Akeno (Fig.5), and cosmic ray muons have been measured since 2003. The mode energy of primary cosmic rays is approximately 25 GeV corresponding to about 2-m thick concrete ceiling of the muon house and the latitude of Akeno Observatory. The redevelopment of the equipment has been partially completed, and the muon telescope at the M5 station has been operating stably since 2018. In 2021, an electric field meter for detecting lightning was installed, and the backend circuit (in JFY2022) and data acquisition circuit (in JFY2023) were completed, to resume stable and remote operation of the M1 and M8 stations from JFY2024.

Even while carrying out these upgrades to the equipment, interesting phenomena were detected, for example, the simultaneous detection of the Forbush Decrease accompanying the solar flare event (M1 class) by GRAPES-3 and the Akeno muon telescopes (1st November 2021) was reported at ICRC2023[7].

Fig. 5. One of the three muon detector housings with concrete shielding.

Research and development for a small atmospheric Cherenkov telescope by T. Yoshikoshi (ICRR, U. Tokyo), et al.: A small alt-azimuth telescope with a three-meter aperture was set up on the main campus of the Akeno Observatory for prototype testing with atmospheric Cherenkov light observations. This telescope is the only one in Japan dedicated to observing atmospheric Cherenkov light emitted from air showers. The refurbishment of the telescope control system, along with the assembly of the segment mirrors and optics, was completed in 2010 and 2011.

In JFY 2016, an atmospheric Cherenkov light event was observed for the first time with this telescope. The team also observed optical light signals from the Crab pulsar between 2020 and 2022 with this telescope, to precisely measure the dispersion measure fluctuations of the Crab pulsar signal from simultaneous observations with radio telescopes and to gain new insights into particle acceleration in the Crab nebula surrounding the pulsar. As a result, they detected a peak of approximately 4.5σ in a phase that is consistent with the main radio pulse of the Crab pulsar. Additionally, the phase distribution showed signs of the inter pulse in addition to the main pulse[8](Fig. 7).

R&D of a next-generation atmospheric fluorescence detec-

*4 N. Kawai et al., 2020 Inter University Research C03
*5 T. Yoshitake et al., PASJ 74 4 (2022) 805
*6 M. Sasada et al., PTEP 2021 5 (2021) 05A104

*7 A. Oshima et al., PoS(ICRC2023)1313 (2023)
*8 T. Yoshikoshi et al., 2023 Inter University Research C01

Fig. 6. The Akeno atmospheric Cherenkov telescope displayed during a tour of the 40th-anniversary events at the Akeno Observatory.

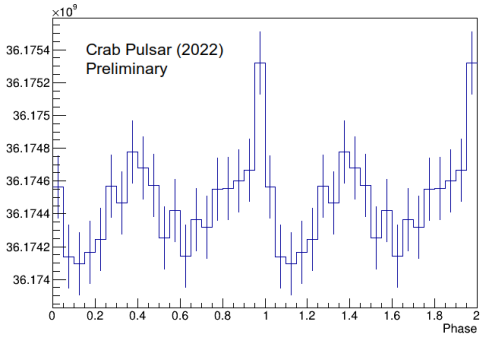

Fig. 7. The light curve of the optical Crab pulsar observed with the Akeno Cherenkov telescope.

tor by Y. Tameda (OECU), et al.: Akeno Observatory is also used as a research and development platform for next-generation cosmic ray instruments. One example of this is the development for the Comic Ray Air Fluorescence Fresnel lens Telescope (CRAFFT) project. The CRAFFT telescope is a next-generation atmospheric fluorescence telescope for use in the "Global Cosmic-ray Observatory (GCOS)" project, with an effective detection area more than 10 times that of the TAx4 and Auger, and features an inexpensive, simple structure aimed at mass production and ease of installation and operation. At Akeno Observatory, the optics of the CRAFFT telescope were tested from 2017 to 2018. Since then, the development base has been moved to the TA site, including simultaneous observations with the TA FDs (Fig. 8) [9].

Fig. 8. (Left) The camera with 12 PMTs mounted, (Centre) the CRAFFT telescope with an electric shutter attached, (Right) the waveform obtained from a test observation with TA FD trigger.

Study of fast moving dark matters and meteoroids using high sensitivity CMOS camera system by F. Kajino (Konan U.), et al.: Using multiple ultra-sensitive CMOS cameras to capture the trajectories of meteors in three dimensions, the speed and direction of objects entering the atmosphere can be determined, and their mass can be determined from their brightness[10]. From this, they search for Nuclearites, which are candidates for dark matter, and meteoroids originating from outside the solar system. Since 2017, observations have been carried out at several locations in Japan, including Akeno Observatory (Fig. 9), and in 2022, four cameras were moved to the TA site in Utah, USA, where observations will be continued until JFY2024[11].

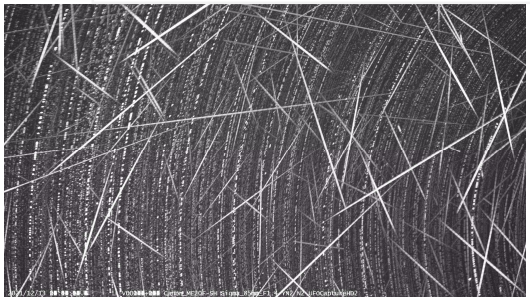

Fig. 9. Composite picture of the Geminids meteor shower observed at the Akeno Observatory on the night of 13 December 2021

In addition to the research mentioned above, Akeno Observatory is also used for various other research projects, such as research on geoid measurement technology using astronomical plumb deviation measurement (Y. Yatsu (Institute of Science Tokyo), et al.), research into methods of measuring atmospheric transparency using cooled CCD cameras (S. Udo (Kanagawa U.), et al.), development of new surface detectors for observing ultra-high energy cosmic rays (T. Nonaka (ICRR, U. Tokyo), et al.), and preparations for air shower observation for high energy gamma ray and cosmic ray detections at the Chacaltaya Cosmic Ray Observatory in Bolivia (Y. Tsunesada (OMU), et al.).

*9 Y. Tameda et al., PoS(ICRC2023)329 (2023), Y. Tameda et al., 2023 Inter University Research F07

*10 F. Kajino et al., 2021 Inter University Research F30

*11 F. Kajino et al., 2023 Inter University Research F18

LOW-LEVEL RADIOISOTOPE MEASUREMENT FACILITY

A low-level radioisotope measurement facility (LLRMF) was built at Kashiwa Campus in 2000 with the relocation of ICRR from Tanashi Campus in Tokyo. Historically, the facilities originated from Nokogiri-yama laboratory set up under Mt. Nokogiri-yama approximately 45 years ago, and the initial objectives were to count and investigate low-level cosmogenic nuclides in extraterrestrial materials such as cosmic dust falling down to the Earth's surface and/or the oceans. The new laboratory at Kashiwa Campus is located in a basement 23 m from the surface. The floor space is approximately 47 m^2 and all of the walls are painted with "MINEGUARD", which is a special paint that blocks radon gas from penetrating the reinforced concrete.

In this laboratory, four high-purity germanium (HPGe) detectors are installed to measure the natural radioactivity of various types of sample by gamma ray spectroscopy (Fig. 1).

Fig. 1. HPGe detectors installed in the underground laboratory at Kashiwa Campus

All the HPGe detectors are of the well type with U-style cryostats. Each HPGe detector is surrounded by an ultralow background shield with a 15 cm thick low-background lead. The specifications of these detectors are shown in Table 1. The data acquisition for the HPGe detectors is controlled by a computer, and the identification of radioisotopes is automated. In addition, environmental data of the laboratory such as temperature, humidity, atmospheric pressure, radon concentration, weights of liquid nitrogen vessels for cooling HPGe detectors, are monitored and logged by the network data logging system.

Table 1. Specifications of HPGe detectors.

HPGe No.	Well Diameter (mm)	Volume (cc)	Installed Year
1	10	190	1997
2	16	170	1997
3	16	116	1986
4	16	160	2005

The oxygen-density-meter is continuously monitored by a TV camera and displayed at the entrance-level floor. Before entering the underground laboratory, we are obliged to determine whether (1) ventilator is working, and (2) oxygen density is not lower than 20.9%. This facility has been utilized for the low-level counting of cosmogenic and environmental radioisotopes in various samples.

Theme 1: Detection of time variation of cosmogenic ^{7}Be by Fuyuki Tokanai (Yamagata Univ.) et al.

The temporal variation of the ^{7}Be concentrations in atmosphere has been measured in Yamagata, located in the mid-latitudes, over a 24-year period beginning in 2000 as shown in Fig. 2. This corresponds to the period from the solar maximum of the 23th solar cycle to almost the maximum of the 25th cycle. The yearly profile of the ^{7}Be concentration indicates the variation in galactic cosmic rays owing to solar modulation because ^{7}Be is produced by spallation of the air elements due to cosmic rays. The yearly profile of the ^{7}Be concentration showed a clear anticorrelation with that of the number of sunspots. Furthermore, ^{7}Be concentrations correlated well with 24 years of neutron monitoring data, with a Pearson correlation coefficient of 0.83 in a linear regression of the two. This indicates that the variation in the ^{7}Be concentration can quantitatively reflect the variability of solar activity, even in different solar cycles. However, the range of variation in ^{7}Be concentration is about three times larger than that of the neutron monitor data, suggesting a complex formation process of ^{7}Be in the atmosphere. To observe the latitudinal concentrations of cosmogenic nuclides, daily changes in ^{7}Be concentrations have been measured in Iceland, located at polar latitudes, since 2003 and in Bangkok, located at low latitudes, since 2014. The average ^{7}Be concentrations in Iceland and Bangkok after 2017 were approximately 37% and 51% of the Yamagata, respectively, suggesting the influence of global air mass motion in the atmosphere [1,2].

Theme 2: Time profile of radioactive Cs concentration and its aerosol size distribution in local area by Fuyuki Tokanai (Yamagata Univ.) et al.

The Fukushima Daiichi Nuclear Power Station (F1NPS), destroyed by the 2011 off the Pacific coast of Tohoku Earthquake, released large amounts of radioactive Cs over a wide area. Yamagata University, located 100 km northwest of the F1NPS, has continuously observed ^{137}Cs concentrations in the surface air since the accident on March 11, 2011, and has investigated changes in environmental radioactivity over time in the local area. This investigation is important not only for understanding the behavior of radioactive aerosols in the atmosphere, but also as a contribution to society. The daily profile of ^{137}Cs concentrations for the 13 years to 2023 show a rapid decay of about one year, followed by a very gradual de-

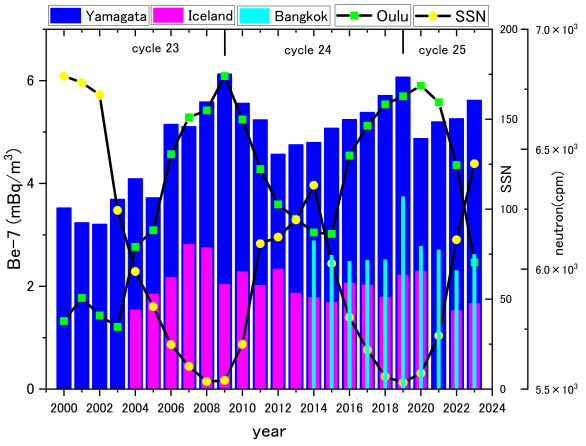

Fig. 2. Annual ^{7}Be concentration profiles for the 24 years since 2000. Blue, pink, and light blue bars indicate ^{7}Be concentrations in Yamagata, Iceland, and Bangkok, respectively. Solid yellow circles and solid green squares on the black line indicate the number of sun spots and Oulu neutron monitor data, respectively.

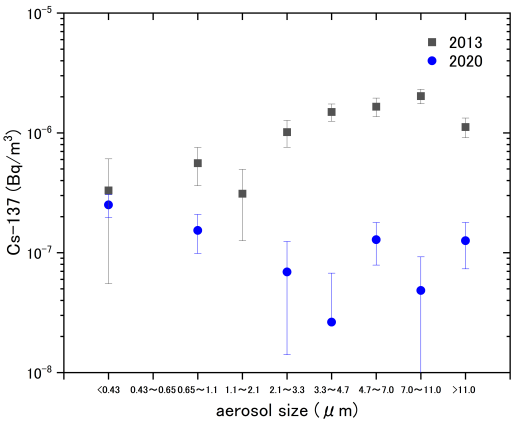

Fig. 4. Particle size distribution of ^{137}Cs in atmospheric aerosols in Yamagata in 2013 and 2020

cay including seasonal variations as shown in Fig. 3. The particle size distribution of ^{137}Cs in atmospheric aerosols was further investigated using the Andersen Cascade Impactor from 2013. Aerosols were separated into eight particle size levels ranging from 0.43 to 11 μm. As shown in Fig. 4, the average ^{137}Cs concentration above 2 μm is 3.6 times higher than the ^{137}Cs concentration below 2 μm in 2013, whereas the ratio is 0.4 times lower in 2020. These results indicate that the amount of ^{137}Cs attached to aerosols larger than 2 μm in size has decreased over the years, suggesting that the ^{137}Cs separated from the primary fallout is resuspended [3].

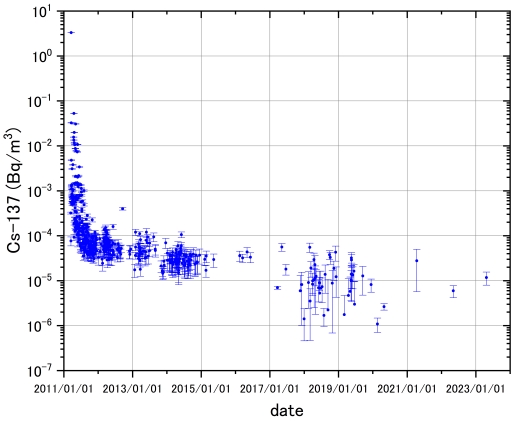

Fig. 3. Daily profile of atmospheric137 Cs concentrations in Yamagata City for 13 years from March 16, 2011

Theme 3: Research on the dynamics of radionuclides in the marine environment by Shigeyoshi Otosaka (Univ. of Tokyo) et.al

After the accident at the Fukushima Daiichi Nuclear Power Plant, the distribution of accident-derived radionuclides in the environment have investigated. However, especially in the coastal areas, there were still uncertainties regarding the impact of radionuclides on organisms immediately after the accident and the medium- to long-term migration process of radionuclides to ecosystems near the seafloor. In this project, we measured the concentration of small amounts of radionuclides that are difficult to measure at regular facilities using the low background radioactivity measurement laboratory at the ICRR, and conducted analysis on the following items.

(1) Behavior of radiocesium near the seafloor: We analyzed the ^{137}Cs concentration in seawater, seabed sediments, and pore water collected at a total of 40 stations in the coastal areas around Fukushima to assess the regulating factors controlling the radiocesium concentration in seabed sediment. Over the five years since 2016, the ^{137}Cs concentration in the seabed sediments had decreased by about 20%, with an average annual decrease rate of 4%. Although this rate was faster than the decay due to radioactive decay of ^{137}Cs radioactivity, it was found to be slower than the decrease rate from 2011 to 2015 (about 30% per year) (Fig. 5). The factors that reduce the radiocesium concentration in the surface sediments are thought to be (1) dilution due to vertical mixing of sediments, (2) transport of sediment particles to the offshore, and (3) desorption from sediments. While the dynamic processes of (1) and (2) were predominant immediately after the accident, it was suggested that the contribution of (3) has relatively increased after 2016. The supply of ^{137}Cs from land also increases the ^{137}Cs concentration in the marine sediments, and it is necessary to pay close attention to how this balance will change in the future [4,5,6,7].

(2) Monitoring radioactivity in biological samples by analysis of bivalve shells: Bivalves are known to record environmental information about their habitat in their shells. In this study, subsamples were taken along the growth direction from bivalve (*Margaritifera laevis*) shells collected in June 2011, three months after the accident, and the ^{137}Cs concentration in each subsample was measured by a HP Ge detector. For the four specimens, 1.4-5.6 Bq/kg of ^{137}Cs was detected in

the whole shell. The two specimens with high whole Cs concentrations ($>$ 5 Bq/kg) contained higher concentrations of ^{137}Cs in the shell skin scraped from the shell surface. On the other hand, no traces of ^{137}Cs were detected in the shell skin of the two specimens with low whole ^{137}Cs concentrations. Although the scraped shell skin accounted for less than 1% of the total shell weight, up to 50% of ^{137}Cs was present. This suggests that the ^{137}Cs concentration in the *Margaritifera laevis* shell records the variations in particulate radiocesium concentrations in the environment [8].

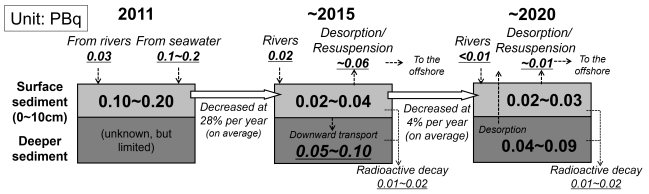

Fig. 5. Major processes affecting decrease in inventory of radiocaesium in the coastal region and estimated mass balance of ^{137}Cs (updated with Fig. 6.12 in Otosaka, 2023). Underlined values indicate the change of the ^{137}Cs inventory from the previous time step.

Theme 4: Measurement of the intrinsic radioisotopes in electron-tracking Compton telescopes for studying the radiation mechanism of extragalactic diffuse gamma-rays by Atsushi Takada (Kyoto Univ.) et al.

Extragalactic diffuse gamma rays, which are the uniform background emission in MeV band, are already observed, but their origin is still puzzling. Hawking radiation from primordial black holes with a mass of 10^{16-17} g or annihilation of WIMPs with a mass in the MeV range are also candidates, while the far active galactic nuclei are influential candidates. In 2018, we performed a balloon experiment with an electron-tracking Compton camera (ETCC) to demonstrate the ability to observe the celestial objects in space (SMILE-2+). SMILE-2+ successfully detected Crab nebula and positronium emission in the Galactic Center region. On the other hand, since SMILE-2+ ETCC had a wide field of view of 3 sr, it had a large exposure at the high galactic latitude. Then we are able to obtain the energy spectrum of extragalactic diffuse gamma rays, if we perfectly understand the background events during the flight.

The background events of SMILE-2+ were composed of atmospheric gamma rays, extragalactic diffuse gamma rays, instrumental gamma rays produced by the interaction between cosmic rays and material on the gondola, and chance coincidence events. Since the radioisotopes (RIs) in the detector are expected to make a large contribution to the chance coincidence, we estimated the abundance of RIs based on the measurements with the Ge detector at LLRMF. The Ge detector at LLRMF significantly detected U/Th in the GSO scintillator and ^{40}K in the PMT window. Through the simulation studies considering the RI abundance estimation, we obtained the energy spectrum of the background events shown in Fig. 6 [9]. The sum of the simulated estimates is in good agreement with the experimental energy spectrum. Therefore, we found that the majority of the background events near the 1 MeV are the chance coincidence of alpha particles emitted by radioisotopes in the GSO scintillators and the interactions of atmospheric gamma rays inside of the gaseous electron tracker. Based on the abundance measurements of the raw material and the scintillator, the GSO scintillators are contaminated with U/Th during the manufacturing process. However, the contamination pathway has not yet been determined. For the next scientific balloon flight, we will measure the internal RIs of the all pixels (∼7k pixels), because we will reuse the GSO scintillators.

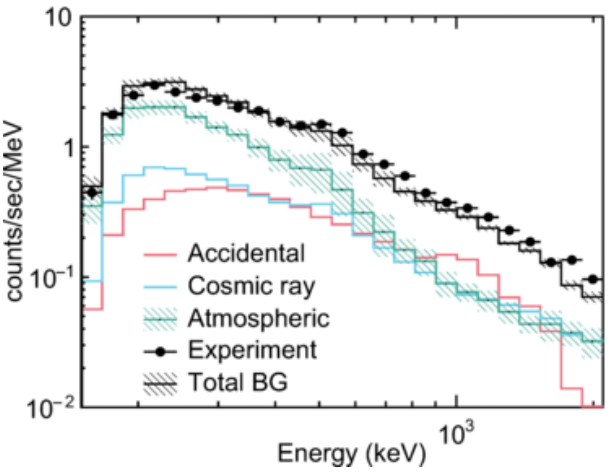

Fig. 6. Energy spectrum of the background events during SMILE-2+ level flight [9]. The sum of the simulated estimates is in good agreement with the measured energy spectrum. Near 1 MeV, the majority of the background events are chance events contributed by alpha particles emitted by the internal RIs (U/Th) in the GSO scintillators.

Reference

[1] H. Sakurai, F. Tokanai, et al., "Concentration of cosmogenic nuclide Be-7 in the surface atmosphere at the beginning of the 25th solar cycle", Japan Geoscience Union Meeting 2024 PEM11-P18 (Joint session with American Geophysical Union), 27th May (2024).

[2] H. Sakurai, F. Tokanai, et al., "Production rates of long-lived radionuclides ^{10}Be and ^{26}Al under direct muon-induced spallation in granite quartz and its implications for past high-energy cosmic ray fluxes", Phys. Rev. D 109, 102005 (2024).

[3] H. Sakurai, F. Tokanai, et al. "Temporal behavior of particle size distribution of ^{137}Cs-attached aerosols observed in Yamagata after the F1NPS accident", The 58th Annual Meeting on Radioisotopes and Radiation Researches 7th July (2021) (in Japanese).

[4] S. Otosaka, Y. Kamidaira, T. Ikenoue, H. Kawamura, "Distribution, dynamics, and fate of radiocesium derived from FDNPP accident in the ocean", J. Nucl. Sci. Technol. 59, 409-423, doi: 10.1080/00223131.2021.1994480 (2021).

[5] S. Otosaka,, S. Kambayashi, M. Fukuda, T. Tsuruta, T. Misonou, T. Suzuki, T. Aono. "Behavior of radiocesium in sediments in Fukushima coastal waters: Verification of desorption potential through the pore water",

Environmental Science and Technology 54, 13778-13785 (2020).

[6] S. Otosaka, M. Aoyama, D. Tsumune. ”Radiocaesium in the seabed sediments off Fukushima”, In Aoyama, M., Inomata, Y., Kaeriyama, H., Kumamoto, Y., Otosaka, S., Tateda, Y. and Tsumune, D. (eds). Radionuclides in the Marine Environment: Scientific view on the Fukushima Dai-ichi Nuclear Power Station Accident by 7 oceanographers. Tsukuba, Univ. of Tsukuba Press. ISBN 978-4-904074-77-0 (2023).

[7] C. Duffa, C. Bradshaw, S. Charmasson, Y. Kamidaira, S. Otosaka, O. Radakovitch, I. Senina, D. Tsumune, J. Vives i Batlle, ”Artificial Radionuclides in Coastal Marine Ecosystems” In Reference Module in Earth Systems and Environmental Sciences., Elsevier, doi: 10.1016/B978-0-323-90798-9.00029-9 (2023).

[8] N. Murakami-Sugihara, K. Shirai, H. Tazoe, K. Mizukawa, H. Takada, T. Yamagata, S. Otosaka, H. Ogawa, ”Spatiotemporal change of cesium-137 in the Pacific coast of Tohoku, Japan” The mussel watch approach. Mar. Poll. Bull. 168, 112413 (2021).

[9] T. Ikeda et al., ”Background contributions in the electron-tracking Compton camera aboard SMILE-2+”, Physical Review D, 108, 123013, DOI:10.1103/physrevd.108.123013 (2023).

APPENDIX

A.1: ORGANIZATION

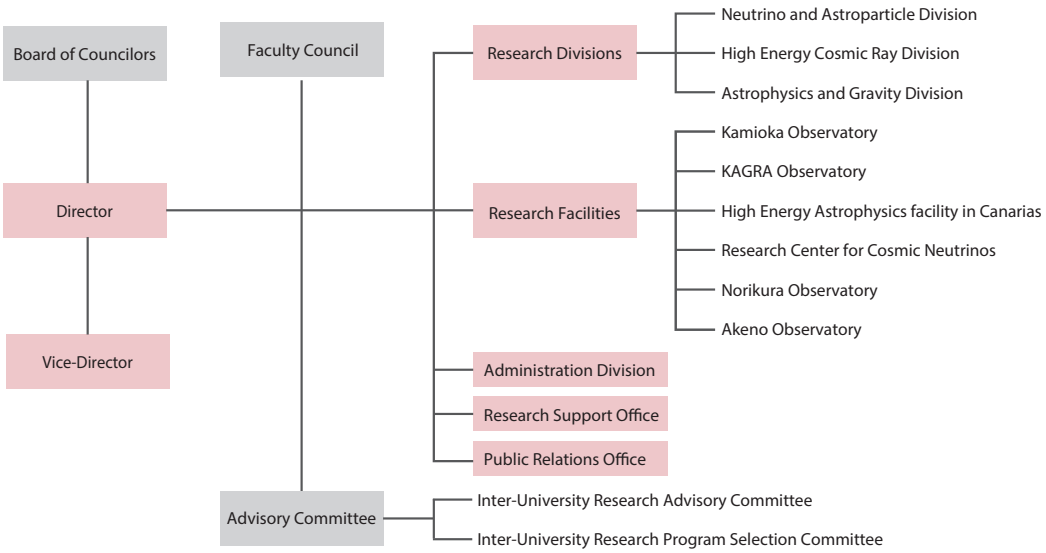

Fig. A.1-1 Organization of the Institute for Cosmic Ray Research as of April 2024.
(The external review panel has been organized every six years.)

A.2: ICRR STAFF (2024)

Due to the government's general austerity policy, universities have been required to reduce the number of faculty members, especially after the incorporation of national universities. To make effective use of human resources in response, the University of Tokyo has implemented a system of annually reviewing the number of faculty positions each faculty and institute can hire and reallocating the number of available faculty positions based on priority. As some projects expanded, ICRR continuously proposed reallocating new posts and, fortunately, obtained some. Namely, new posts of two research associates in 2018, one associate professor and one research associate in 2019, two research associates in 2020, and one research associate in 2021. After 2022, The University of Tokyo changed this "reallocation" system to a new allocation system without cuts. Then the ICRR got one professor in 2022.

We also proposed the organizational development of the Next-generation Neutrino Science Multi-Messenger Astronomy Organization, which was approved by MEXT in 2022. It is the alignment of four departments, such as the Graduate School of Science, KAVLI Institute for the Physics and Mathematics of the Universe, Earthquake Research Institute, and ICRR. The flagship facility "Hyper-Kamiokande" and other projects in ICRR aim to implement Multi-messenger Astronomy leveraging our strengths in cooperation with other institutes. For this alliance, we got new posts of one professor and one associate professor in 2023.

The Table below summarizes the staff of ICRR in 2024. The number of tenured researchers (Professors, Associate Professors, and Research Associates) in ICRR was slightly increased; it is 46 in 2024.

However, we need to note that re-allocated and newly allocated posts are time-limited to five years. Namely, ICRR will make continuous efforts to maintain these staff by allocating personnel expenses for retired or transferred staff, common expenses, large-scale project budgets, and so on.

Table A.2-1 Numbers of ICRR staff as of May 2024.

Professors	Associate Professors	Assistant Professors	Technical Staff[3]	Project Professors[1]	Project Associate Professors[1]	Project Assistant Professors[1]	Post-Doctoral Fellows[2]	Total
12	15	19	22	1	1	12	18	100

*1 Project Associate Professors and Project Research Associates have fixed terms.
*2 One JSPS researcher is included.
*3 Project Academic Specialists and Technical Assistants are included.

A.3: BUDGET (FY2018–2023)

Since the incorporation of national universities in 2004, the management expense grant has been gradually reduced. In the operation of university institutions, it is expected to acquire research funds not only from the management expense grant but also from external funds. The ICRR has been requesting the government for project budgets for each of the large-scale projects such as SK, KAGRA, CTA, and the operation of joint use/research center, separate from the allocated management expense grant essential for supporting core educational and research activities.

Table A.3-1 shows the expenditure settlement amount for each fiscal year. Those were expended from the management expense grant for supporting core educational and research activities and specific projects and external funds. In 2020, Supplies and Facilities declined because research activities were reduced due to activity restrictions caused by COVID-19. In 2021, the final year of the third six-year medium-term objective period, carry-over items were digested and so Supplies and Facilities increased. From 2022, a budget has been set up for the promotion of the HK project and so the total amount increased.

The external funds acquired for research promotion are shown in Table A.3-2. This varies depending on the research situation. Construction of HK started in FY2019. Table A.3-3 shows subsidies for the development of facilities for advanced research for it.

Table A.3-1 Annual Expenditures (in thousand yen).

	2018	2019	2020	2021	2022	2023
Personnel Expenses	823,000	872,000	898,000	898,000	1,048,000	1,068,000
Supplies and Facilities	1,729,000	1,611,000	1,173,000	2,078,000	1,990,000	1,974,000
Total	2,552,000	2,483,000	2,071,000	2,976,000	3,038,000	3,042,000

Table A.3-2 Amount of Grants-in-Aid for Scientific Research and Other External Funds (in thousand yen).

	2018	2019	2020	2021	2022	2023
Grants-in-Aid for Scientific Research(KAKENHI)	333,000	310,100	317,400	398,670	256,500	388,590
Trust Fund	0	1,966	340	231	0	0
Private Scholarship	1,960	3,387	1,600	0	0	3,180
Joint Research with Private Sector	0	0	0	0	47,871	283,128
Foundation	49,911	22,728	22,654	17,739	19,449	15,511
Total	384,871	338,181	341,994	416,640	323,820	690,409

Table A.3-3 Subsidy for Development of Facilities for Advanced Research (in thousand yen).

	2018	2019	2020	2021	2022	2023
HK Construction	0	3,129,000	3,323,000	4,402,552	6,105,727	4,267,000

B.1: AGREEMENTS OF INTERNATIONAL ACADEMIC COOPERATION

Table B.1-1 Academic cooperation agreements with overseas universities and research organizations.

Country	University/Institute	Year of Agreement
Bolivia	Universidad Mayor de 'San Andres'	1981
USA	College of Science, University of Utah	1995
USA	School of Physical Science, the University of California, Irvine	1995
USA	Graduate School of Arts and Sciences, Boston University	1995
Russia	Institute for Nuclear Research, Russian Academy of Science	2001
Australia	Faculty of Life and Physical Sciences, University of Western Australia	2001
USA	CIT LIGO Laboratory, California Institute of Technology	2009
Italy	European Gravitational Observatory/ Virgo Collaboration	2011
China	Shanghai United Center for Astrophysics, Shanghai Normal University	2011
UK	Institute for Gravitational Research, University of Glasgow	2011
Italy	University of Sannio at Benevento Department of Engineering	2012
China	National Astronomical Observatories, Chinese Academy of Sciences	2012
Spain	The Faculty Sciences, Autonomous University of Madrid	2013
Taiwan	Institute of Physics Academia Sinia	2017
Germany	Max Plank Institute for Physics	2017
Korea	Sungkyunkwan University, College of Science, Center for Cosmic Ray Research	2017
Poland	National Centre for Nuclear Research	2018
Spain	Instituto de Astrofisica de Canarias	2018
Canada	TRIUMF	2018
China	Tsinghua University	2018
China	Wuhan Institute of Physics and Mathematics, Chinese Academy of Sciences	2019
Taiwan	National Center for High-performance Computing(NCHC), National Applied Research Laboratories (NARLabs)	2019
Russia	Scobeltsyn Nuclear Physics Research Institute, Moscow State University	2020
France	The French National Centre for Scientific Research	2021
India	Tata Institute of Fundamental Research	2022
Mexico	Universidad de Guadalajara	2022
UK	Rutherford Appleton Laboratory	2023
Italy, Japan	The University of Perugia, National Astronomical Observatory of Japan	2023
Taiwan	National Yang Ming Chiao Tung University	2023

B.2: INTERNATIONAL MEETINGS

Table B.2-1 List of international meetings hosted or co-hosted by ICRR.

Date	Place	Symposium/Workshop Title	Participants
Mar. 5–7, 2018	Kashiwa	The first annual symposium innovative area ”Gravitational Wave Physics and Astronomy: Genesis”	99
Mar. 26–30, 2018	Tokyo	Tokyo Spring Cosmic Lyman Alpha Workshop	120
Jan. 11, 2019	Tokyo	1st Meeting of Hyper Kamiokande Financial Forum	50
Jun. 27, 2019	Tokyo	2nd Meeting of Hyper Kamiokande Financial Forum	45
Sep. 9–13, 2019	Toyama	Topics in Astroparticle and Underground Physics (TAUP2019)	540
Nov. 11–13, 2019	Chiba	Dark Matter Searches in the 2020s	117
Nov. 14–15, 2019	Chiba	The extreme Universe viewed in very-high-energy gamma rays 2019	83
Nov. 16–19, 2020	Online	KASHIWA DARK MATTER SYMPOSIUM	290
Dec. 18–20, 2020	Taiwan and Online	The 7th KAGRA International worcshop (KIW7)	240
Jan. 18–20, 2021	Chiba and Online	Black Hole Astrophysics with VLBI: Multi-Wavelength and Multi-Messenger Era	80
Nov. 29–Dec. 2, 2021	Online	KASHIWA DARK MATTER SYMPOSIUM	317
Feb. 7–9, 2022	Online	Black Hole Astrophysics with VLBI 2022	92
Feb. 2, 2022	Online	UTokyoNY Event ” Exploring the Universe with Multi-Messengers”	300
Mar. 14–17, 2022	USA	LIGO-Virgo-KAGRA collaboration meeting at Luisiana	808
Mar. 24–25, 2022	Chiba	Synergies at New Frontiers at Gamma-rays, Neutrinos and Gravitational Waves	70
Sep. 28–30, 2022	Gifu and Online	21st International Workshop on Next generation Nucleon Decay and Neutrino Detectors (NNN2022)	111
Mar. 6–11, 2023	Toyama and Online	Hyper-Kamiokande Collaboration meeting	223
Mar. 13–16, 2023	USA and Online	LIGO-Virgo-KAGRA collaboration meeting at Northwestern University	677
Jul. 26–Aug. 3. 2023	Nagoya and Online	38th International Cosmic Ray Conference (ICRC2023)	1429
Sep. 11–15, 2023	Toyama and Online	LIGO-Virgo-KAGRA collaboration meeting at Toyama	936
Oct. 23–28, 2023	Kamioka and Online	Hyper-Kamiokande Collaboration meeting	190

B.3: INTER-UNIVERSITY COLLABORATIVE RESEARCHES

As one of the "Joint Usage/Research Centers" in Japan, ICRR has been supporting inter-university collaborative research. MEXT newly established "International Joint Usage/Research Centers" in 2018, so ICRR applied for it and was approved as one of six. We appreciated the support letters sent by research communities overseas for our application. Because of this, ICRR has started strong support and collaboration for overseas researchers more than ever before.

Annually, ICRR issues calls for applications for collaborative research, and since 2019, it has also done so for overseas researchers. The following tables summarize the annual numbers of adopted proposals.

Table B.3-1 Annual numbers of applications for collaborative research programs.

Facilities		2018	2019	2020	2021	2022	2023	Subtotal
Kamioka Observatory	Domestic	40	44	46	45	43	41	259
	International		4	9	9	9	5	36
Akeno Observatory	Domestic	4	3	6	6	12	6	37
	International			2	2	1	0	5
Norikura Observatory		8	9	11	11	9	8	56
Low-Level Radioisotope Measurement Facility	Domestic	4	5	4	3	5	6	27
	International						1	1
KAGRA Observatory[1]	Domestic	15	18	22	22	23	25	125
	International		7	9	6	3	10	35
High Energy Astrophysics Facility in Canarias[2]	Domestic		10	11	11	10	14	56
	International		1	0	1	0	1	3
Laboratorial Facility in Kashiwa	Domestic	3	2	1	1	1	1	9
	International					3	2	5
Large-Scale Comping System in Kashiwa	Domestic	16	16	12	14	16	14	88
	International		2	2	1	6	1	12
Conference Facility in Kashiwa	Domestic	7	7	8	6	5	5	38
	International		6	3	1	0	0	10
Overseas Facilities[3]	Domestic	26	19	18	17	9	17	106
	International		5	4	5	1	6	21
Annual Sums	Domestic	123	133	139	136	133	137	801
	International		24	29	25	23	26	127

*1 The first laser interferometer using cryogenic mirrors developed in Kashiwa. KAGRA Observatory was established in 2016.

*2 The Large Scale Telescopes for the Cherenkov Telescope Array in La Palma developed in Kashiwa. High Energy Astrophysics Facility in Canarias was established in 2018.

*3 The Tibet ASγ Observatory, Observatory for Highest Energy Cosmic Rays in Utah, and Chacaltaya Observatory of Cosmic Physics. Applications for domestic activities corresponding to these overseas works are included here. The Cherenkov Telescope Array in La Palma was included in 2018.

Research Project Titles

1. Astroparticle physics using the Super-Kamiokande detector
2. Study of atmospheric neutrino flux and neutrino oscillations
3. Study of simulation for atmospheric neutrino
4. Study of flavor identification of atmospheric and beam neutrinos
5. Study of solar neutrino energy spectrum
6. Precise measurement of Day/Night effect for B8 solar neutrinos
7. Study for Supernova monitor
8. Study of Supernova Relic Neutrinos

9. Search for proton decay via $e^+\pi^0$ mode
10. Study of proton decay p $\rightarrow \nu K^+$
11. Study in upward-going muons and high energy neutrinos
12. Sidereal daily variation of $\sim$10TeV galactic cosmic ray intensity observed by the Super Kamiokande
13. Neutrino search associated with astronominal transient events
14. Measurement of charge ratio and polarization of cosmic ray muon using undergraund particle physics experiments
15. Tokai to Kamioka Long Baseline Experiment T2K
16. Neutrino interaction study using accelerator data
17. Study for improvement of neutrino oscillation measurement in T2K expriment
18. Energy calibration for Super-Kamiokande
19. Research and development of computer simulation of Super-Kamiokande detector
20. Development of low concentration radon detection system
21. Hyper-Kamiokande project
22. Development of the Large Aperture Photodetector for a next-generation neutrino detector
23. Development of software for the next generation neutrino detector
24. New Photogrammetry Calibration for Super-Kamiokande and Hyper-Kamiokande
25. Measurement of radon in underground laboratoried and evaluate of effects from radon to experiments
26. Study for lowering backgrounds of radioisotopes in large volume detectors
27. Development of a radioactivity assay system for underground experiments
28. Measurement of neutron flux at the Kamioka underground laboratory
29. Trace level measurements of radioactive impurities for undeground experiments, such as Super-Kamiokande with ICPMS
30. RI measurement for SK-Gd project with HPGe detector
31. Generation three direct dark matter search experiment
32. A Search for Dark Matter using Liquid Xenon Detector
33. Detector structure study for future direct dark matter search experiment
34. Improvement of ultra-low radioactivity molecular sieves and implementation in dark matter search experiment
35. Research and Development for XENONnT and future Dark Matter Searches
36. Direction-sensitive dark matter search
37. A study on the near-infrared emission of liquid xenon
38. Study of double beta decay of ^{48}Ca
39. Studies on the background evaluation using laser spectroscopy analysis
40. Searches for neutrinoless double beta decay with high-pressure Xenon gas detector
41. Strain, tilt, seismic measurement in Kamioka-mine
42. R & D for a Small Atmospheric Cherenkov Telescope in Akeno Observatory
43. Development of new surface detector for observation ultra high energy cosmic ray
44. Observation of the Galactic Cosmic Ray Intensities using the Large Area Muon Telescopes

45. Multi-Color Imager for Transients, Survey and Monstrous Explosions
46. Research on geoid measurement technology using astronomical plumb deviation measurement
47. Space weather observation using muon hodoscope at Mt. Norikura
48. Observation of cosmogenic nuclides concentrations at Mt. Norikura
49. Study of secondary cosmic rays from Thundercloud at Mt. Norikura
50. Investigation of alpine plants on Mt. Norikura
51. Atmospheric mercury speciation dynamics and mercury wet deposition monitoring at the high-altitude
52. Evaluation of atmospheric SO2 to cloud acidification at free troposhere through atmospheric observation at Mt. Norikura
53. A new study for high precision measurement of muons at Mt.Norikura
54. Citizen Science "Thundercloud Project" to elucidate the particle acceleration and interaction between cosmic rays and thunderclouds
55. Very-High-Energy Gamma-ray Observatory CTA Project
56. Development of Focal Plane Instruments for the CTA Large Sized Telescopes
57. Development of the readout system for the CTA large sized telescopes
58. Engineering runs of the first Large Size Telescope of CTA and construction of LST2-4 in La Palma Canary Islands, Spain
59. Commissioning and upgrade of the onsite data center for CTA North in La Palma, Spain
60. Development of SiPM modules for CTA-LST (3)
61. Development of the CTA/LST telescope control system
62. maintenance and operation of the optical and power systems in CTA LST
63. CTA-Japan Physics Research
64. Development of analysis method and initial observation with CTA Large-Sized Telescope
65. Development of camera for CTA small-sized telescopes
66. CTA Monte Carlo Simulation
67. Search for neutrino sources with the Large-Aperture Atmospheric Cherenkov Telescope
68. The extreme Universe viewed in very-high-energy gamma rays 2023
69. Study of High Energy Gamma-ray Objects with the MAGIC telescope
70. Kashiwa Dark Matter Symposium 2023
71. Development of a background reconstruction toolbox for the LST1 prototype and the upcoming CTA
72. Study of Extremely-high Energy Cosmic Rays by Telescope Array
73. R&D of the measurement of atmospheric transparency at the Telescope Array site
74. Study of very high energy cosmic rays around 10^{17} eV with the TALE hybrid experiment
75. Evaluation of optical characteristics of atmospheric fluorescence telescope by standard light source mounted on drone
76. Development and analysis of night cloud observation by CCD camera for automatic observation of air fluorescence detector
77. Observing ultrahigh-energy cosmic rays with new fluorescence detectors at Telescope Array site
78. Research and development of a Fresnel lens air fluorescence telescope for the next generation UHECR observation
79. Experimental Study of High-energy Cosmic Rays in the Tibet ASγ experiment

80. Sidereal daily variation of $\sim$10TeV galactic cosmic ray intensity observed by the Tibet air shower array
81. Study of the composition of cosmic-rays at the Knee
82. A study on variation of interplanetary magnetic field with the cosmic-ray shadow by the sun.
83. Air shower observation for high-energy gamma ray and cosmic ray detections at the Chacaltaya Cosmic Ray Observatory
84. Study of High Energetic Radiation from Thundercloud in the Altiplano
85. Study of solar magnetic fields using the cosmic-ray Sun's shadow observed at the southern hemishpere
86. Study of high-energy cosmic-ray anisotropy at the Chacaltaya Cosmic Ray Observatory
87. Development of an advanced Compton camera using SOI pixel semiconductor
88. Design study of a Compton camera for study of cosmic rays
89. Study of Fast Moving Dark Matters and Meteoroids using High Sensitivity CMOS Camera System
90. Study on High Energy Cosmic-ray Sources by Observations in Space with CALET
91. Comparative study of high energy astrophysical phenomena
92. Development of a new code for cosmic-ray air shower simulation
93. Cosmic ray interactions in the knee and the highet energy regions
94. Development of improvements and test observations for the elucidation of very-high energy particle emitting objects by NTA
95. Clear identification of very high energy particle sources by NTA
96. Project for make "Cosmic Ray" to a common word (Application of Virtual Reality technology)
97. Development of the data acquisition system for the extension of the TA$\times$4 surface detectors
98. YMAP symposium 2023
99. Observation of airshower fluorescence light at the TA-FD site by using an Imaging UV telescope
100. Investigating the gamma-ray signatures of feedback microphysics in star-forming environments
101. Search for UHECR sources considering the galactic magnetic field and the mass composition
102. Research of Large-scale Gravitational wave Telescope(XIII)
103. Study of Gravitational-wave by cryogenic laser interferometer CLIO in KAMIOKA Mine(VII)
104. Development of Monitor and Interlock System for KAGRA
105. Research on cryogenic payload for KAGRA
106. Development of conduction cooling schemes for KAGRA
107. R&D for the intensity stabilization of the laser system in KAGRA
108. Development of scattered light measurement technique and noise reduction for improving sensitivity in KAGRA IV
109. Development of optical cavity for ultranarrow stable lasers
110. Study of Environmental Noise Reduction in KAGRA
111. Study of the environmental noise of KAGRA detector by environmental injection
112. Noise characteristics analysis using machine learning and deep learning and its application to interferometer diagnosis (III)
113. Development of glitch data analysis system for improving gravitational detection
114. Search for poorly modeled gravitational wave signal using KAGRA

115. Reduction of Non-Stationary Noise in KAGRA
116. Development of a noise source identification tool for improving the sensitivity of KAGRA telescope
117. Development of a new caliabration method and sensitivity improvement for gravitational wave telescope based on thermal nosie
118. Numerical Simulation of Electro-Magnetic Wave Propagation in Gravitational wave Detector XI
119. Development of a high performance sapphire mirror suspension
120. Control and automatic operation for KAGRA
121. Construction of KAGRA data transfer and storage system (9)
122. Promotion of collaborative research to incorporate KAGRA data into the low latency international gravitational wave search network (3)
123. Construction of a diagnostic system for the gravitational wave detector
124. Test measurement of underground gravity measurement at micro-meter scale
125. Precise geophysical observation at the Kamioka underground site and modeling of crustal activities
126. Gravitational Wave Data Analysis
127. Cosmic Reionization and Galaxy Formation Probed with Large Optical Near-Infrared Telescopes
128. Evolution of the universe and particle physics
129. Detection of time variations for cosmogenic nucleid Be-7
130. Time profile of radioactive Cs concentration and its aerosol size distribution in local area
131. Development of new analysis techniques for supernova neutrino observation by Super Kamiokande
132. Behavior of radionuclides in the marine environment
133. Frontier of the planetary material science
134. Measurement of the intrinsic radioisotopes in electron-tracking Compton telescopes for studying the radiation mechanism of extragalactic diffuse gamma-rays
135. Water Purification System R&D for Precision Neutrino Detectors
136. Precise calculation of the atmospheric neutrino flux
137. CRC workshop for future plans in cosmic ray research
138. Light scattering measurement in the water using the Super-Kamiokande detector
139. Study of supernova neutrinos in Super-Kamiokande
140. Data Taking, Calibrations, Measurements and Analysis with Super-Kamiokande I – VI
141. Towards a multiphysics liquid Xe TPC with scintillation and charge multiplication readouts
142. Hyper-Kamiokande OD PMTs QA
143. Research and Development of the high-performance segment mirrors and the camera entrance windows for the CTA Large Size Telescopes
144. Ultra-high-energy cosmic-ray origin studies with the Telescope Array and TAx4 surface detector
145. Study of Anisotropy of Ultra High Energy Cosmic Rays with Telescope Array and TAx4
146. Study of high-energy cosmic rays at a high altitude in Tibet, China
147. Study for Galactic CR origin using the ALPACA air shower array in Bolivia
148. Constraining the nature of the emission in PeVatrons observed by Alpaca.

149. Bayesian analysis on the origin of ultra-high energy cosmic ray events collected by the TA experiment
150. Study of the signals and reconstruction of cosmic ray events via surface detectors from the Telescope Array and the Pierre Auger cosmic ray detectors
151. Synergies at new frontiers at gamma-rays, neutrinos and gravitatinal waves.
152. Filter cavity experiments for the frequency dependent squeezed light for KAGRA
153. Measuring the birefringence of the sapphire mirrors installed in the KAGRA detector
154. Position control system for silicon monolithic suspension in cryogenic gravitational waves detectors.
155. Implementing Sophisticated Data Analysis Methods on KAGRA Data
156. Applications of machine learning technique on gravitational wave detection
157. Study the Gravitational Wave with the Most Modern Technology
158. Noise Subtraction of KAGRA Data using Machine Learning Method: DeepClean
159. Developing a template-free method of searching gravitational wave signals with autoregressive modeling
160. Low-Latency Localization and Parameter Estimation of Gravitational Waves Using Probabilistic Deep Learning
161. Self interacting dark matter and gravitational waves
162. A water monitoring system for Hyper-Kamiokande
163. Constraining systematics at T2K and SuperKamiokande oscillation analyses using neutrino-nucleus interaction models

B.4: EDUCATIONAL ACTIVITIES

One of the important functions of ICRR is to educate graduate students directly at ICRR as a part of the Graduate School of Science, the University of Tokyo, and indirectly at graduate schools of domestic/foreign universities through collaborative research programs.

Table B.4-1 Annual numbers of accepted master/doctor theses.

	2018	2019	2020	2021	2022	2023	Subtotal
Master theses at ICRR	17	14	15	15	18	9	88
Master theses at domestic universities	33	32	41	49	31	40	226
Total numbers of master theses in Japan[1]	50	46	56	64	49	49	314
Doctor theses at ICRR	11	12	4	6	6	8	47
Doctor theses at domestic universities	8	5	5	6	5	9	38
Doctor theses at foreign universities	25	11	3	4	12	12	67
Total numbers of doctor theses	44	28	12	16	23	29	152

*[1] Since the numbers of master theses are not available for all the collaborating foreign universities, only the domestic numbers are tabulated.

B.5: PUBLIC RELATIONS

Overview

Four staff take charge of public relations; two of them are assigned in Kashiwa ICRR headquarters and each one in Kamioka Observatory and KAGRA Observatory. Under the supervision of ICRR director, Public Relations Committee, organized by these 4 staff, make plan and implement following public-relations activities.

1. Publications
2. Press Releases
3. Multimedia Contents
4. Exhibitions
5. Original Goods
6. Interactive Events

Publications

News Letter

ICRR News is published quarterly at Kashiwa headquarters, providing summary of the seasonal news topics with photos.

Brochure

ICRR Catalogue is published annually, offering a basic overview of every research group and ICRR management division.

Annual Report

ICRR Annual Report is also published annually, providing detailed information on scientific outcomes of every research group in ICRR.

Press Releases

ICRR publishes press releases about research outcomes and coming soon events towards media reporters of TV, newspaper and so on, 10-20 times a year so that they can be picked up by media to create public news. There were many research outcomes in these 5 years; First gamma ray burst detection by the ground-based Cherenkov Space Telescope "MAGIC" (December 2019), First detection of diffused gamma ray above 100TeV as the first proof of Pevatron in our Galaxy (April 2021), Starting observation by the gravitational wave telescope KAGRA (February 2020), A series of scientific discoveries on far distant galaxies by the James Webb Space Telescope (November and December 2023). Meanwhile, PR office intensified efforts in organizing press conference at UTokyo Hongo Campus in Tokyo, which surely improved stakeholder relationship.

Multimedia Contents

Websites

The official Website is administrated by PR office in ICRR headquarters and every research project in ICRR such as Super Kamiokande (SK) and KAGRA, has its own website to introduce an overview and topics of the project. On top of them, PR office recently created and began to administrate the official website of Next-Generation Neutrino Science and Multi-messenger Astronomy Organization (NNSO), reorganized from the Next-generation Neutrino Science Organization in October 2023. [Find more on https://www.nnso.u-tokyo.ac.jp/en/]

Videos

An 8-minutes-video which is edited in English with Japanese subtitles, introduces ICRR experimental facilities all over the world. Videos featuring Super-Kamiokande and KAGRA are also available from the ICRR portal site. [Find more on http://www.icrr.u-tokyo.ac.jp/en/medias/]

The 360° Panoramic Video for Virtual Reality(VR)

A goggle with a smartphone display on its glass top provides a chance to explore Super-Kamiokande, XMASS and KAGRA observatory as a VR experience. [Find more on http://www.icrr.u-tokyo.ac.jp/en/medias/4209/]

Exhibitions

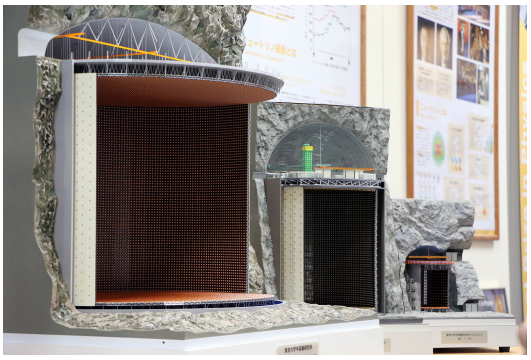

ICRR collaborates with other organizations to create new type of exhibitions. Main collaborators are as follows:

- National Museum of Nature and Science, Tokyo
- National Museum of Emerging Science and Innovation (Miraikan)
- Local government and universities located near ICRR experimental facilities (KamiokaLab)

Original Goods

ICRR creates several kinds of original goods for sale: jigsaw puzzle featuring SK, notebook, mug cup, calendar and so on. Furthermore, several shop owners in Hida city where ICRR Kamioka Observatory and KAGRA Observatory are located, have created goods with SK-photo-printed package under an agreement of our cooperation to the local area promotion. The purpose is to promote ICRR public relations and enhance support for our research activities. In fact, small portion of revenue goes to the fund such as “Supporting Young Researchers in ICRR”(UTokyo Foundation), which enable ICRR to employ young researchers as ICRR Fellows who can get extra research funds.

Interactive Events

Open Campus

Several thousand people visit ICRR headquarters every year on the Kashiwa Open Campus every year in October. They are attracted by science cafe, workshops, original goods sale and other entertainments which PR Committee coordinates with many students and researchers. One of the contents, a workshop of interferometer experiment “mini-KAGRA” is also offered to high school students who visit ICRR headquarters.

ICRR x Kavli IPMU Public Lecture

ICRR collaborates with Kavli Institute for the Physics and Mathematics of the Universe (Kavli IPMU) to organize public lectures in spring and fall every year. The number of people wishing to attend the lecture always exceeds capacity of the

venue. In the past, four hundred people who won the lottery enjoyed the lecture. But since the COVID-19, public-relation events including this public lecture has been held in Hybrid style; onsite with YouTube broadcasting. So, all of applicants can enjoy the event. In the spring of 2024, about 950 people enjoyed the lecture both onsite and online broadcasting with 10-day archive in YouTube.

Spring School

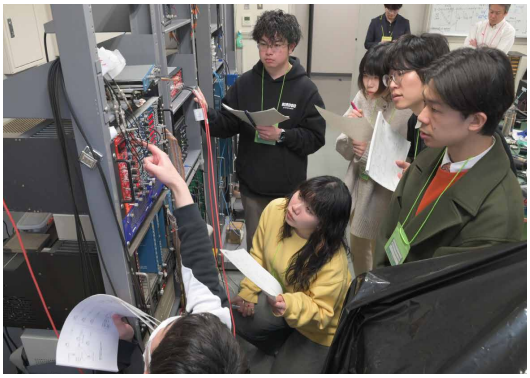

ICRR offers 30 university students from all over Japan to spend in ICRR for 5 days and 4 nights in March every year from 2012. This program, called ”Spring School”, provides lectures, experiments, data analysis, and students split in six groups to make presentations on each research topic. Students, tutors and also ICRR director who meet for the first time get along with each other and have a profitable experience under one roof.

Special Event for Female Students

Special event for female undergraduate students is co-organized annually by ISSP (Institute for Solid State Physics), Kavli IPMU and ICRR. It started about 10 years ago to encourage female students to study physics as their major in graduate schools, motivated by the fact that the number of female is so much small in this field in Japan. At this event, several female persons who established their careers with physics background are invited to make presentations and answer questions from participants who are eager to know their future prospect.